Geotechnical Field Reconnaissance: Gorkha (Nepal) Earthquake of April 25 2015 and Related Shaking Sequence

Geotechnical Extreme Event Reconnaissance

GEER Association Report No. GEER-040.

Version 1.1

August 7, 2015

Authors: Youssef M.A. Hashash (UIUC), Binod Tiwari (CSF), Robb E. S. Moss (CalPoly), Domniki Asimaki (Caltech), Kevin B. Clahan (LCI), D. Scott Kieffer (TUGraz), Doug S. Dreger (UCB), Amy Macdonald (TT), Chris M. Madugo (PG&E), H. Benjamin Mason (OSU), Menzer Pehlivan (MRCE), Deepak Rayamajhi (OSU), Indra Acharya (TU) and Basanta Adhikari (TU).

Contributors: Brian D. Collins (USGS), Randall Jibson (USGS), Eric M. Thompson (USGS), Sachindra Dahal (UIUC), Diwakar Khadka (MT), Sital Uprety (UIUC), Maja Bitenc (TUGraz), Mirjam Ziselsberger (TUGraz), Sanjib Basnet (TU), Sangita Rai (TU), Surendra Awasthi (TU) and Gerhard Lauk (TUGraz).

CalPoly: Cal Poly San Luis Obispo.
Caltech: California Institute of Technology
CSF: Cal State Fullerton
LCI: Lettis Consultants International, Inc.
MRCE Mueser Rutledge Consulting Engineers
OSU: Oregon State University
PG&E: Pacific Gas and Electric
TT: Thornton Tomasetti
TU: Tribhuvan University
TUGraz: Graz University of Technology
UCB: University of California, Berkeley
UIUC: University of Illinois at Urbana-Champaign
USGS: United States Geologic Survey
MT: Material Test Pvt. Ltd.

Executive Summary

The April 25, 2015 Gorkha (Nepal) Earthquake and its related aftershocks had a devastating impact on Nepal. The earthquake sequence resulted in nearly 9,000 deaths, tens of thousands of injuries, and has left hundreds of thousands of inhabitants homeless. With economic losses estimated at several billion US dollars, the financial impact to Nepal is severe and the rebuilding phase will likely span many years.

The Geotechnical Extreme Events Reconnaissance (GEER) Association assembled a reconnaissance team under the leadership of D. Scott Kieffer, Binod Tiwari and Youssef M.A. Hashash to evaluate geotechnical impacts of the April 25, 2015 Gorkha Earthquake and its related aftershocks. The focus of the reconnaissance was on time-sensitive (perishable) data, and the GEER team included a large group of experts in the areas of Geology, Engineering Geology, Seismology, Tectonics, Geotechnical Engineering, Geotechnical Earthquake Engineering, and Civil and Environmental Engineering. The GEER team worked in close collaboration with local and international organizations to document earthquake damage and identify targets for detailed follow up investigations.

The overall distribution of damage relative to the April 25, 2015 epicenter indicates significant ground motion directivity, with pronounced damage to the east and comparatively little damage to the west. In the Kathmandu Basin, characteristics of recorded strong ground motion data suggest that a combination of directivity and deep basin effects resulted in significant amplification at a period of approximately five seconds. Along the margins of Kathmandu Basin structural damage and ground failures are more pronounced than in the basin interior, indicating possible basin edge motion amplification. Although modern buildings constructed within the basin generally performed well, local occurrences of heavy damage and collapse of reinforced concrete structures were observed. Ground failures in the basin included cyclic failure of silty clay, lateral spreading and liquefaction.

Significant landsliding was triggered over a broad area, with concentrated activity east of the April 25, 2015 epicenter and between Kathmandu and the Nepal-China border. The distribution of concentrated landsliding partially reflects directivity in the ground motion. Several landslides have dammed rivers and many of these features have already been breached.

Hydropower is a primary source of electric power in Nepal, and several facilities were damaged due to earthquake-induced landsliding. Powerhouses and penstocks experienced significant damage, and an intake structure currently under construction experienced significant dynamic settlement during the earthquake. Damage to roadways, bridges and retaining structures was also primarily related to landsliding. The greater concentration of infrastructure damage along steep hillsides, ridges and mountain peaks offers a proxy for the occurrence of topographic amplification.

The lack of available strong motion records has severely limited the GEER team's ability to understand how strong motions were distributed and how they correlate to distributions of landsliding, ground failure and infrastructure damage. It is imperative that the engineering and scientific community continues to install strong motion stations so that such data is available for future earthquake events. Such information will benefit the people of Nepal through improved approaches to earthquake resilient design.

Acknowledgements

The work of the GEER Association, in general, is based upon work supported in part by the National Science Foundation through the Geotechnical Engineering Program under Grant No. CMMI-1266418. Any opinions, findings, and conclusions or recommendations expressed in this material are those of the authors and do not necessarily reflect the views of the NSF.

The GEER Association is made possible by the vision and support of the NSF Geotechnical Engineering Program Directors: Dr. Richard Fragaszy and the late Dr. Cliff Astill. GEER members also donate their time, talent, and resources to collect time-sensitive field observations of the effects of extreme events.

The Center of Disaster Studies at the Institute of Engineering of Tribhuvan University was the primary collaborator in managing access to sites and providing local professionals and students to accompany the GEER team.

Reconnaissance efforts such as this are a massive group effort and the authors would like to thank and acknowledge the following organizations for their support of the reconnaissance effort:

- EERI: Earthquake Engineering Research Institute
- BuildChange
- California State University Fullerton
- California Polytechnic State University San Luis Obispo
- California Institute of Technology (Caltech)
- Kadoori Agricultural Aid Association
- Kathmandu University
- Graz University of Technology
- Melamchi Water Supply Project
- Nepal Department of Electricity Development
- Nepal Department of Roads
- Nepal Geotechnical Engineering Society
- Nepal Department of Physical Infrastructure and Roads
- Nepal Department of Irrigation
- Nepal Department of Mines and Geology
- Nepal Electricity Authority
- NSET
- Oregon State University
- Pacific Gas and Electric (PG&E)
- Thornton Tomasetti
- Tribhuvan University, Institute of Engineering, Pulchowk Campus
- University of Illinois at Urbana-Champaign, CEE Rapid Response Grant
- USGS: United States Geological Survey
- USAID: U.S. Agency for International Development

The Partners of Mueser Rutledge Consulting Engineers (MRCE) have graciously supported this effort by providing engineering time and resources for the field work of Dr. Menzer Pehlivan. Lettis Consultants International, Inc. (LCI) has also graciously supported geologic

field reconnaissance and requisite reporting for Kevin Clahan as part of LCI's internal grants program. The support of MRCE and LCI in this mission and report is gratefully acknowledged..

Moreover, the authors would like to acknowledge the support of Prof. Jonathan Bray (UC Berkeley); Professor Tri Ratna Bajracharya (Tribhuvan University); Professor Nagendra Raj Sitoula (Tribhuvan University); Professor Gokarna Motra (Tribhuvan University); Tuk Lal Adhikari (Nepal Geotechnical Society); Gopal Basnet (Nepal Department of Electricity Development); Madhab Koirala (Rasuwagadi Hydroelectricity Project); Bigyan Shrestha (Upper Tamakoshi Hydroelectricity Project); Mohan Gautam (Upper Tamakoshi Hydroelectricity Project); Pradip Thike (Upper Tamakoshi Hydroelectricity Project); Arjun Jung Thapa (Department of Roads); Tulasi Sitoula (Ministry of Physical Infrastructure and Roads); Nawa Raj K.C. (Department of Roads); Narayan Gurung (Kadoori Agricultural Aid Association); Vijay Mahato (Department of Road); Monica Maharjan (Tokyo University of Technology); Rajendra Man Shrestha (All Round Travels and Tours); Hari Dhakal (Rising Star Cargo); Honorary Rishi Dhakal (Nepalese Consulate Los Angeles); Diego Melgar (University of California, Berkeley Seismological Laboratory); John-Phillip Avouac (California Institute of Technology, Department of Geology and Planetary Sciences, Pasadena, CA, and University of Cambridge, Department of Earth Sciences, Cambridge, UK) and many others who contributed to the GEER team in Nepal and USA. The authors thank Ms. Jiaxin Xu who is an undergraduate researcher at the University of Illinois for assisting in data compilation and report editing.

Table of Contents

List of Tables

List of Figures

1 Introduction

GEER (Geotechnical Extreme Event Reconnaissance) mobilized two teams to investigate the earthquake effects following the April 25th, 2015 M7.8 event in Nepal. Team A was in country from May 6th to May 22nd to start the broad initial assessment of earthquake effects. During that time the May 12th, 2015 M7.3 event occurred resulting in complex loading and more effects. Team B was in country from May 22nd to June 3rd to follow up on the initial investigations, acquire more perishable data, and to focus on the most important lessons to be learned from these events.

Observations and data were collected on:

- Spatial patterns of the ground shaking intensity due to the underlying rupture dynamics (e.g., directivity).
- Seismic induced landslides, rockfalls, slumps, avalanches, slide-dams, etc.
- Absence/presence of surface fault ruptures.
- Site response effects including basin edge effects and topographic effects.
- Damage to infrastructure such as highways, bridges, dams, roads, pipelines, tunnels, and hydro-facilities.
- Effects due to liquefaction and other ground failure mechanisms.
- Foundation damage and how that related to structural damage.

Team A was restricted to covering the affected area by car due to a ban on flying that followed a US helicopter crash, and a ban on UAV's (unmanned aerial vehicle) due to unauthorized use by others immediately following the earthquakes. Team A covered a broad region ranging from Pokhara in the West to Khurkot in the East, from Tibet boarder in the North to India border in the South (Figure 1-1).

By the time Team B1 was in country the flying ban was lifted and team members were able to get in the air via helicopter and UAV to observe regions that could not be accessed by car (Figure 1-2). They were able to access regions in the North and East that either don't have roads or they do have roads but they were blocked by slides. Team B1 also focused on some specific failures of importance in the Kathmandu Valley and the surrounding regions. Team B2 focused on site response effects in Kathmandu Valley and building stronger ties with local agencies to carry on the work started here.

The investigations presented in this report are the result of a wholly collaborative effort and required the participation of all team members and our in-country collaborators. The goal is to document as clearly as possible the earthquake effects to learn from this event and better prepare for future events.

Photos of most Team A and B members are shown in Figure 1-3 and Figure 1-4. Appendix A provides a detailed team itinerary. The Acknowledgements section provides a list of all collaborating organizations.

Technology continues to play an increasingly important role in field reconnaissance activities. This GEER team took full advantage of a range of tools. Smart phone GPS tagged photos provided high resolution images with location information even where no phone service is available. Smart phones were also used for field note taking, and continuous GPS track acquisition. GPS cameras proved to be significantly inferior to smart phones in terms of their ability to provide photo location information. Smart watches with GPS tracking were also

deployed and proved to be an alternative to handheld devices for acquiring continuous GPS tracks. The team also deployed a drone (Parrot Bepop drone from the University of Illinois, Figure 1-5), after obtaining appropriate official permissions, in documenting damage of hydropower projects. Action cameras (GoPro Hero, Figure 1-6) were mounted on the nose of the reconnaissance helicopter to capture video footage of landslides. Cloud file storage was used extensively for rapid exchange of data between the field and home teams.

Figure 1-1 All regional track logs of Team A (Locations of Mw7.8 main shock and Mw7.3 aftershock are presented with stars).

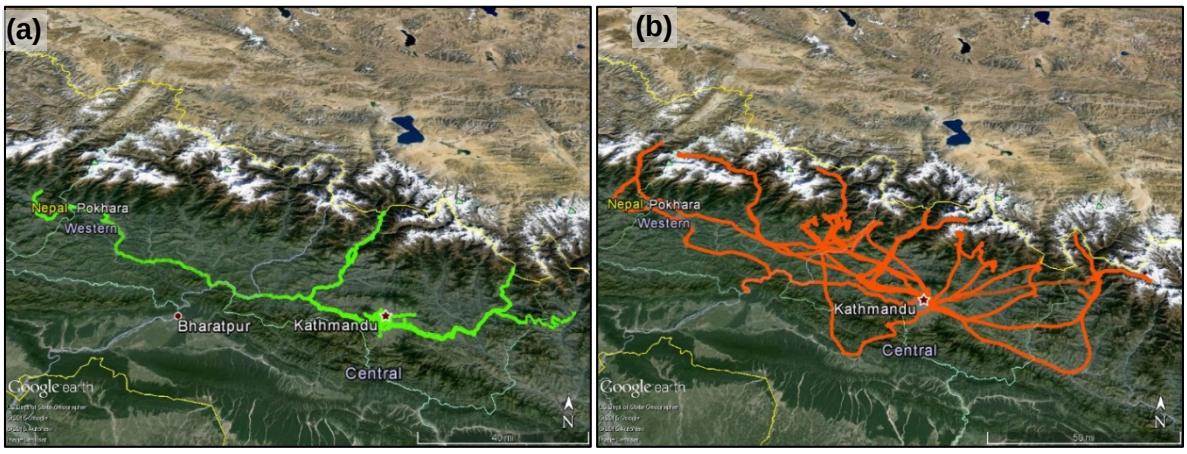

Figure 1-2 Regional Tracks logs of Team B: (a) ground reconnaissance tracks, (b) helicopter reconnaissance tracks.

Figure 1-3 Team A members (from left): Robb E.S. Moss, Kevin B. Clahan, Binod Tiwari, D. Scott Kieffer, Mirjam Ziselsberger, Maja Bitenc.

Figure 1-4 Team B members (from left): Randall Jibson, Amy Macdonald, Eric M. Thompson, Menzer Pehlivan, Chris M. Madugo, Binod Tiwari, Youssef M.A. Hashash, Brian D. Collins, Sital Uprety.

Figure 1-5 Flying Robot/Camera (Drone) used in field reconnaissance, 27^{O}45’45.3”N, 85^{O}52’22.8”E.

Figure 1-6 GoPro Hero Camera mounted on the nose of the reconnaissance helicopter, 27^{O}57’31.7”N, 85^{O}57’17.7”E.

2 Tectonic, Geologic, and Geomorphic Setting

2.1 Regional Tectonics

The April 25, 2015 M_W 7.8 Gorkha earthquake occurred in the actively deforming central Himalayan mountain range are approximately 80 km northwest of Kathmandu, Nepal. The Himalaya is the result of the collision of India and the Eurasia/Tibetan plate about 50 Ma (e.g., Powell and Conaghan, 1973). The initial India-Eurasia collision along the Indus-Tsangpo suture zone. The timing of the collision is marked by the transition from marine to non-marine sedimentation in the suture zone between 54 and 50 Ma (Rowley, 1996; Searle et al., 1997) and K-Ar dating (Ratschbacher et al., 1994) that assigned a 50 Ma age to southward obduction of the Indus-Tsangpo suture zone. The compressional tectonic regime of the Himalaya is generally framed by the sinistral transform Chaman fault in the west and the dextral Sagaing fault in the east. The collision of the Indian plate into Eurasia also resulted in the formation of the transform Altyn Tagh and Karakorum faults in central Asia that accommodate lateral escape to the east.

The geodynamics of the northward convergence of India beneath Eurasia generates high rates of seismicity that threaten millions of people in the mountainous regions of Nepal and within the Indian Gangetic plain. At present, the 40-50 mm/year of northward convergence of India relative to stable Eurasia (Patriat and Achache, 1984) is believed to be absorbed by a combination of horizontal shearing and crustal shortening. Crustal thickening, primarily under the Tibetan Plateau, has also been debated as a structural model for convergence. Across the Central Himalaya of Nepal nearly half of this convergence (estimated at about 2 cm/year) is absorbed by convergence across the plate boundary decollement, as shown from GPS geodetic campaigns (Avouac, 2003). Convergence is also manifested by recurring small to moderate, large, and great earthquakes, such as the great Bihar-Nepal earthquake of 1934 (M_s 8.2) or the large Kangra earthquake of 1905 (Ms 7.8) (Hough and Billam, 2008) and now the Gorkha earthquake (Mw 7.8) which are associated with large reverse faults.

Geophysical and structural studies of the Central Himalayas suggest that the three major thrust faults in the Nepal Himalaya, including the Main Central Thrust fault (MCT), the Main Boundary Thrust fault (MBT), and the Main Frontal thrust fault (MFT), from north to south, sole at depth into a single major shear zone, the Main Himalayan Thrust (MHT), along which the Indian crust is thrust under Eurasia (Seeber and Armbruster, 1981; DeCelles et al., 2002; Bollinger et al., 2006). Since continental convergence the basal MHT has restructured its surface expression to accommodate continued deformation along the rising rangefront. The active thrust ramp has migrated southward from the initial MCT to the MBT to its current surface expression, the MFT, as continued collision and structural stacking at depth take place (e.g., Gansser, 1964; Le Fort, 1975; Nakata, 1989; Yeats et al., 1992).

The MHT has a flat-ramp-flat geometry, where the lower flat is creeping, the upper flat is locked and the ramp itself is a transition zone. The general dip of the MHT is very shallow, typically less than 10° (Ader et al., 2012) with the flats dipping approximately 5° to 6° (Figure 2-1). The thrust ramp geometry of the MHT produces three primary types of Himalayan earthquakes: 1) Moderate earthquakes that occur within the vicinity of the ramp (clustered around the MHT) at the transition from fault creep at depth to stick slip behavior towards the ground surface; 2) Large blind earthquakes (1805, 1833, possibly 1905) that rupture from the top of the ramp toward the MFT, but don't extend to the surface; and 3) great earthquakes (1934, 1505, ~1400, 1255, possibly 1100) that extend to the surface, and likely down the ramp. Observations by

the GEER team and others have demonstrated that the April 25, 2015, Mw 7.8 Gorkha earthquake as well as the May 12, 2015, Mw 7.3 aftershock, fall into the second category of Himalayan earthquakes that are large but blind as they do not rupture the surface (Figure 2-1).

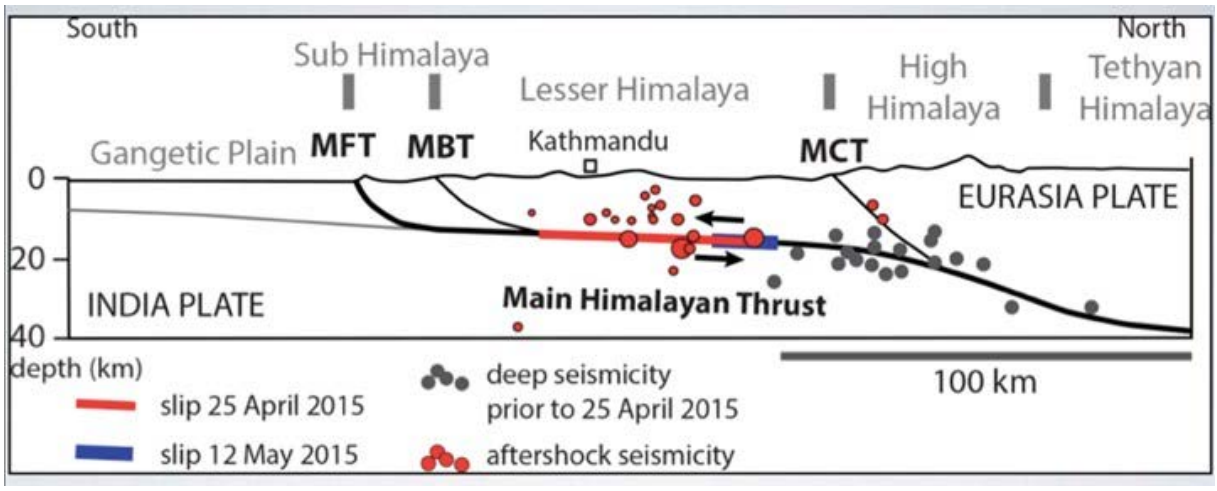

Figure 2-1 Generalized cross section through the Central Himalaya showing the flat-ramp-flat geometry of the MHT and the modelled slip of the Gorkha earthquake and May 12, 2015 aftershock (USGS, 2015).

Global Positioning System (GPS) measurements show that India and southern Tibet converge at 20 ± 3 mm/year (Larson et al., 1999). Geodetic convergence rates across the Central Himalaya have been estimated at 17.8 ± 0.5 mm/yr (Ader et al., 2012), and 19 ± 2.5mm/yr (Bettinelli et al., 2006). The MCT and MBT are known to be active in segments generally to the east and west of the central Himalaya, however, the MHT and MFT have been shown to accommodate most of the crustal shortening across the central Himalaya in Nepal (Cattin and Avouac, 2000; Lave and Avouac, 2000; Bollinger, Henry, and Avouac, 2006). The MFT has a slip rate estimated from uplifted Holocene terraces to be 21.5 ± 1.5 mm/yr in central Nepal (Lave and Avouac, 2000), seemingly accounting for the entire slip budget of the MHT at depth.

The most recent great earthquakes with a magnitude greater than eight include the 1897 (M_w 8.0-8.7), and 1950 (M_w 8.7) (Pandey and Molnar, 1988; Chander, 1989; Molnar, 1990; Bilham, 1995; Ambraseys and Bilham, 2000, Bilham and England, 2001). Historical observations regarding the damaging effects of earthquakes indicates that Kathmandu has been struck by numerous very large earthquakes throughout historical time (Rana, 1935; Pant, 2002). Significant earthquake attributed damage to Himalaya communities and the greater Kathmandu Valley was reported in the years 1100, 1223, 1225, 1344, 1408, 1505, 1555, 1681,1724, 1803, 1833, 2005, 1947, 2005 (Avouac, 2003; Bilham, 2004, 2009; Bilham et al., 2001) and are further discussed in Section 3.1 of this report.

Similar to the 2015 Gorkha earthquake, the 1934 Bihar-Nepal earthquake is believed to have ruptured the MHT to the southeast of Kathmandu, however, the 1934 Bihar-Nepal earthquake also ruptured to the ground surface along the MFT (Bolinger, et al., 2014) where the Gorkha earthquake did not. Macroseismic intensities and subsidence of the foreland revealed from leveling data suggest that the 1934 earthquake ruptured approximately 250–300 km along the Himalaya arc (Bilham et al., 1998). Recent work by Sapkota and others (2012) have documented evidence that the 1934 and 1255 earthquakes both ruptured the ground surface along the Main Frontal Thrust (MFT). In comparison, although seismological evidence suggests the hypocenter of the 2015 Gorkha earthquake was located along or near the

MHT/MFT fault plane, no evidence of surface ground rupture or ground deformation (ie. folding or warping) was identified following the 2015 Mw 7.8 Gorkha earthquake.

2.2 Geologic and Geomorphologic Setting

The large east-west trending Himalayan thrust faults separate areas of sharply contrasting geology. These differing bedrock units as well as long term slip along the faults controls the geomorphology of the Central Himalaya. North of the MCT, high-grade metamorphic units of the Higher Himalaya rise to elevations from around 1000 m to over 8000 m. These units consist of highly metamorphosed, amphibolite-grade schist with intrusive granitic plutons. These units most likely correspond to an accreted exotic terrane onto India in the early Paleozoic (Robinson et al., 2001). An abrupt break-in-slope along the MCT separates the High Himalayan units from the Lesser Himalaya.

The Lesser Himalaya geologic units are located between the MCT to the north and the MBT to the south in an area of sharp relief but relatively low elevations. These geologic units are predominantly folded, medium to low-grade metasediments originally deposited between about 16 and 21 Mya in the Himalaya foreland before being tectonically uplifted (DeCelles et. al., 2001). In the Kathmandu area a klippe composed of crystalline rocks accounts for some of the higher relief of the Lesser Himalaya in this region.

The sub-Himalaya consists of the Siwalik Hills which are bounded to the south by the MFT and to the north by the MBT (e.g., Delcaillau, 1986; Mugnier et al., 1999; Lave´ and Avouac, 2000). This area is generally characterized by relatively low elevation hills that are incised by the highly erosive drainages coming out of the Himalaya. The Siwaliks consist of several kilometers of Tertiary siltstones, sandstones, and conglomerates that have been scraped off the Precambrian Indian basement as a result of thin-skinned tectonics along the active deformation front of the advancing range. The material is easily erodible but forms steep reliefs which help demonstrate the active deformation associated with the MFT.

2.3 References

Ader, T., et al. (2012), Convergence rate across the Nepal Himalaya and interseismic coupling on the Main Himalayan Thrust: Implications for seismic hazard, J. Geophys. Res., 117, B04403, doi:10.1029/2011JB009071.

Ambraseys, N., and Bilham, R. (2000). A note on the Kangra earthquake of 4 April 1905. Curr. Sci. 79, 46–50.

Avouac, J. P., 2003, Mountain building, erosion, and the seismic cycle in the Nepal Himalaya, Adv. Geophys. 46, pp. 1–80.

Bettinelli, P., J.-P. Avouac, M. Flouzat, F. Jouanne, L. Bollinger, P. Willis, and G. Chitrakar, 2006, Plate motion of India and Interseismic strain in the Nepal Himalaya from GPS and DORIS measurements, J. Geod., 80, 567–589.

Bilham, R., 1995, Location and magnitude of the 1833 Nepal earthquake and its relation to the rupture zones of contiguous great Himalayan earthquakes. Curr. Sci. 69, 101–128.

Bilham, R., Blume, F., Bendick, R., and Gaur, V. K. (1998). Geodetic constraints on the translation and deformation of India: Implications for future great Himalayan earthquakes, Curr. Sci. 77, 213–229.

Bilham, R., Gaur, V.K., Molnar, P (2001) Himalayan seismic hazard. Science, 293, 1442–1444

Bilham, R., and England, P., 2001, Platean 'pop-up' in the great 1897 Assam earthquake, Nature 410 (6830), 806‑809.

Bilham, R (2004) Earthquakes in India and the Himalaya: tectonics, geodesy and history. Annals of Geophysics, 47 (2), 839-858.

Bilham, R (2009). The seismic future of cities. Bulletin of Earthquake Engineering, 7, 839–887.

Bollinger, L., Henry, P., and Avouac, J.P., 2006, Mountain building in the Nepal Himalaya: Thermal and kinematic model, Earth and Planetary Science Letters 244, 58–71

Bollinger, L., Sapkota, S.N., Tapponnier, P., Klinger, Y., Rizza, M., Van der Woerd, J., Tiwari, J.R., Pandey, R., Bitri, A., and Bes de Berc, S., 2014, Estimating the return times of great Himalayan earthquakes in eastern Nepal: Evidence from the Patu and Bardibas strands of the Main Frontal Thrust, J. Geophys. Res. SolidEarth, 119, doi:10.1002/2014JB010970.

Cattin, R., and Avouac, J. P., 2000, Modeling of mountain building and the seismic cycle in the Himalaya of Nepal. J. Geophys. Res. 105, 13389‑13407.

Chander, R. (1989). Southern limits of major earthquake ruptures along the Himalaya between longitudes 75_ and 90_E. Tectonophysics 170, 115‑123.

DeCelles, P. G., Robinson, D. M., Quade, J., Ojha, T. P., Garzione, C. N., Copeland, P., and Upreti, B. N., 2001, Stratigraphy, structure, and tectonic evolution of the Himalayan fold-thrust belt in western Nepal. Tectonics 20, 487‑509.

Delcaillau, B. (1986). Dynamique et. evolution structurale du piemont frontal de lmalaya: les Siwaliks du Ne´pal oriental. Rev. geol. dyn. geogr. phys. 27, 319‑337.

Gansser, A., 1964, Geology of the Himalayas, Interscience Publishers, London, 289 pp.

Hough, S.E., and Bilham, R., 2008, Site response of the Ganges basin inferred from re-evaluated macroseismic observations from the 1897 Shillong, 1905 Kangra, and 1934 Nepal earthquakes, *J. Earth Syst. Sci.* **117**, S2, pp. 773–782

Larson, K., Bürgmann, R., Bilham, R., Freymueller, J.T., 1999, Kinematics of the India–Eurasia collision zone from GPS measurements, J. Geophys. Res. 104, 1077–1093.

Lave, J., and Avouac, J. P., 2000, Active folding of fluvial terraces across the Siwaliks Hills, Himalayas of central Nepal. J. Geophys. Res. 105, 5735‑5770.

Le Fort, P., 1975, Himalaya: the collided range: Present knowledge of the continental arc, Am. J. Sci. 275A, 1‑44.

Molnar, P. (1990). A review of the seismicity and the rates of active underthrusting and deformation at the Himalaya. J. Him. Geol. 1, 131‑154.

Mugnier, J. L., Leturmy, P., Mascle, G., Huyghe, P., Chalaron, E., Vidal, G., Husson, L., and Delcaillau, B. (1999). The Siwaliks of western Nepal 1: Geometry and kinematics. J. Asian Earth Sci. 17, 629‐642.

Nakata, T. (1989). Active faults of the Himalaya of India and Nepal, In “Tectonics of the Western Himalayas”, L. L. Malinconico, Jr., and R. Lillie, eds. Geol. Soc. of America, pp. 243‐264.

Pandey, M. R., and Molnar, P., 1988, The distribution of intensity of the Bihar-Nepal earthquake of 15 January 1934 and bounds on the extent of the rupture zone. J. Nepal Geol. Soc. 5, 23‐45.

Pant, M. R., 2002, A step toward a historical seismicity of Nepal. Adarsa 2, 29‐60.

Patriat, P., and J. Achache, India-Eurasia collision chronology has implications for crustal shortening and driving mechanisms of plates, *Nature*, *311*, 615–621, 1984.

Powell, C. M. A., and Conaghan, P. J., 1973, Plate tectonics and the Himalayas, Earth Planetary Science Letters 20, 1–12.

Rana, B. S. J. B., 1935, ‘‘Nepalako mahabhukampa (1990 sala) Nepal’s Great Earthquake.’’

Ratschbacher, L., Frisch,W., Liu, G., and Chen, C., 1994, Distributed deformation in southern and western Tibet during and after India-Asia collision: Journal of Geophysical Research, v. 99, p. 19917–19945.

Robinson, D. M., DeCelles, P. G., Patchett, P. J., and Garzione, C. N., 2001, The kinematic evolution of the Nepalese Himalaya interpreted from Nd isotope. E.P.S.L. 192, 507–521.

Searle, M., Corfield, R. I., Stephenson, B., and McCarron, J., 1997a, Structure of the north Indian continental margin in the Ladakh-Zanskar Himalayas: Implications for the timing of obduction of the Spontang ophiolite, India-Asia collision and deformational events in the Himalaya: Geological Magazine, v. 134, p. 297–316.

Yeats, R. S., Nakata, T., Farah, A., Mizra, M. A., Pandey, M. R., and Stein, R. S., 1992, The Himalayan frontal fault system. Annales Tectonicae, Special Issue (Supp. to Vol. 6), pp. 85–98.

3 Seismological information and recorded ground motions

As discussed in Section 2.1, the compressional tectonic regime of the Himalaya generates high rates of seismicity that threaten millions of people in the mountainous regions of Nepal and India. Continued crustal shortening in the Himalaya is being accommodated by several major thrust faults which also separate distinctive geologic regions and geomorphologic provinces. Although abundant historical evidence of earthquake damage has been recorded, earthquake rupture parameters such as location, length, slip, and magnitude for distinct events remain largely uncertain. The following sections summarize the seismological aspects of the April 25, 2015 M_W 7.8 Gorkha earthquake.

3.1 Historical and Recent Earthquakes

Nepal has a long history of destructive earthquakes. At least ten major earthquakes (Chitrakar and Pandey, 1986) were recorded in the historical archives since the 13th century. This section summarizes anecdotal and documented evidence of these earthquakes, alongside their associated evidence of site effects.

- **1255 AD (June, 7)**: This is the oldest known event that severely damaged Kathmandu. The intensity of this major earthquake reached at least X (Rana et al., 2007). The magnitude of the earthquake is approximated to be around M7.8 in Richter scale. Historical records indicate that many houses and temples in Nepal collapsed after the 1255 Earthquake, and one-third of the population including the King, Abhaya Malla, was killed.
- **1260 AD**: Five years after the mega-earthquake of 1255 AD, once again caused collapse of many buildings and temples and severe damage in many more. Although limited information is available regarding this earthquake, it is known that this earthquake has caused many people casualties together with the subsequent widespread of epidemic and famine.
- **1408 AD** earthquake was another major earthquake that hit the Kathmandu Valley. This earthquake completely destroyed the Rato Matchendranath temple and caused severe damage and collapse of many other buildings and temples.
- **1681 AD** Earthquake hit Nepal and Kathmandu valley. Although limited information is available, heavy loss of lives and collapse and damage of many buildings including temples were noted.
- **1767 AD** Earthquake reported to cause twenty-one aftershocks in a twenty-four hour period. There are no available information regarding the loss and damage due these shocks.
- **1810 AD** Twenty-one shocks were reported to occur over a month period (May or June). The number of casualties caused by the 1810 shocks were relatively small. Some buildings and temples were destroyed and severely damaged.
- **1823 AD** Seventeen shocks with moderate magnitudes were felt in the Kathmandu valley. There was no documented loss of human life or livestock.
- **1833 AD** Kathmandu Valley was hit by two main shocks in the late summer, one in the afternoon, 6pm, and the other in the night, 11 pm. Most of the buildings, houses, public shelters, and temples had collapsed. The Tower of Dharahara was severely damaged. Thimi and Bakhtapur were completely destroyed. Records indicate 18,000 houses collapsed around the country, 4,214 of which were located in the Kathmandu Valley.

- **1834 AD** Four major shocks were reported during June and July. Although these shocks were not as strong as 1833 shocks, the flooding in Bagmati River due to excessive rain during the earthquakes caused damage to the bridges.
- **1934 AD (January, 15)** Earthquake, also known as Great Nepal Bihar Earthquake, is the strongest earthquake of the 20th century and this earthquake had caused the highest number of casualties ever recorded in Nepal. The epicenter of this moment magnitude Mw=8.1 (M8.4 in Richter scale) earthquake was located in eastern region, 9.5 km south of Mount Everest. The earthquake caused major damages at a widespread area, where the intensity of the earthquake varied from VII to X in Modified Mercalli scale (Figure 3-1a). Mercalli Intensity X extended in to Kathmandu Valley, Kathmandu Valley experienced an extreme damage, and most of the buildings were destroyed in the three main cities of the valley: Kathmandu, Bakhtapur, and Patan. Due to the 1934 Earthquake more than 8,500 people lost their lives, more than 126,000 houses were severely damaged, and more than 80,000 buildings were completely collapsed. Damage distribution reported during the 1934 event suggests that site effects must have played a major role in modifying the ground motion, particularly on the southern part of the Kathmandu basin (Dixit et al., 1998). One noteworthy phenomenon of this earthquake was that sand and water vents appeared throughout the central vents of the earthquake area. The ground around these sand fissures subsided, causing more damage. Extensive liquefaction of the ground took place over a length of 300 km (called the slump belt), in which many structures went afloat.
- **1980 AD** earthquake with M6.5 on Richter scale affected mostly the far western portion of Nepal. 125 people lost their lives, 248 were seriously injured. 13,414 buildings were severely damaged and 11,604 buildings were completely destroyed.
- **1988 AD (August, 21)** Also known as Udaipur Earthquake with M 6.9 affected mostly the eastern region of the country. Earthquake resulted in 721 deaths, 6553 serious injuries, and damages in more than 65000 buildings. Total direct loss due to the earthquake was reported to be 5 billion rupees.

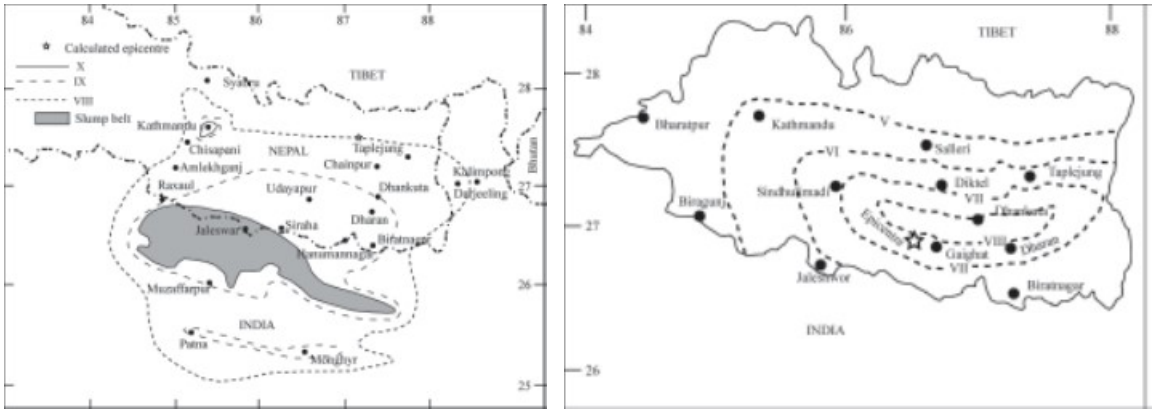

Figure 3-1 Intensity map for (a) 1934 Great Nepal-Bihar Earthquake and (b) 1988 Udiapur Earthquake (after Bhattarai et al., 2011)

- **1993 AD** earthquake affected the central and the mid-western regions of the country. Earthquake resulted in 1 death, 11 reported injuries, damages in 451 buildings, and collapse of 72 houses. Total direct loss due to earthquake was more than 48 million rupees.

- **1994 AD** earthquake affected the western regions of the country. Earthquake resulted in 12 reported injuries, damages in more than 84,000 buildings, and collapse of 623 houses. Total direct loss due to earthquake was around 16.35 million rupees.
- **1997 AD** earthquake affected the central and far-western regions of the country. Earthquake resulted in 1 reported injury, damages in more than 60 buildings, and collapse of 196 houses. Total direct loss due to earthquake was around 51.29 million rupees.
- **2011 AD (September, 18)** Earthquake with M6.9 earthquake with the epicenter 272 km east of Kathmandu and focal depth of 19.7 km caused widespread damage in the country. Earthquake was reported to be an intra-plate event within the upper Eurasian plate or the underlying Indian plate. This earthquake was mostly felt in the eastern and central Nepal, including Kathmandu. Although the earthquake caused extensive damage in several buildings, there were only 3 reported deaths due to this earthquake. Earthquake cause 164 injuries out of which 30 were critical, collapse of more than 6,000 houses, and damages in more than 14000 houses. (CUEE Report 2011-1)

3.2 Regional seismicity and recorded earthquakes

The April 25, 2015 M_W 7.8 Gorkha earthquake occurred on or close to the main Himalayan frontal thrust fault (Figure 3-2). This fault system is highly active with numerous large to great earthquakes occurring in the instrumental record as well as defined from pre-instrumental historical records. The extent of rupture inferred from aftershocks (Figure 3-2) and finite-source analyses (Figure 3-4 and Figure 3-5) indicate that it extended from the southern end of the great M_W 8.2 Central Himalayan Earthquake of 1505, to the northern edge of the great M_s 8.1 Kathamandu earthquake of 1934. In 1833 a M_s >= 7.7 earthquake occurred at the northern terminous of the 1934 event (Bilham, 1995). The geometrical relationship of these three events as well as possible events in 1669 and 1255 (Bilham, 1995) suggests structural discontinuity or segmentation of the frontal fault at this location. The rupture dimension of the Gorkha earthquake inferred from the aftershock distribution and from finite-source modeling indicates that the rupture spanned the boundary between the 1505 and 1934 earthquakes (Figure 3-3).

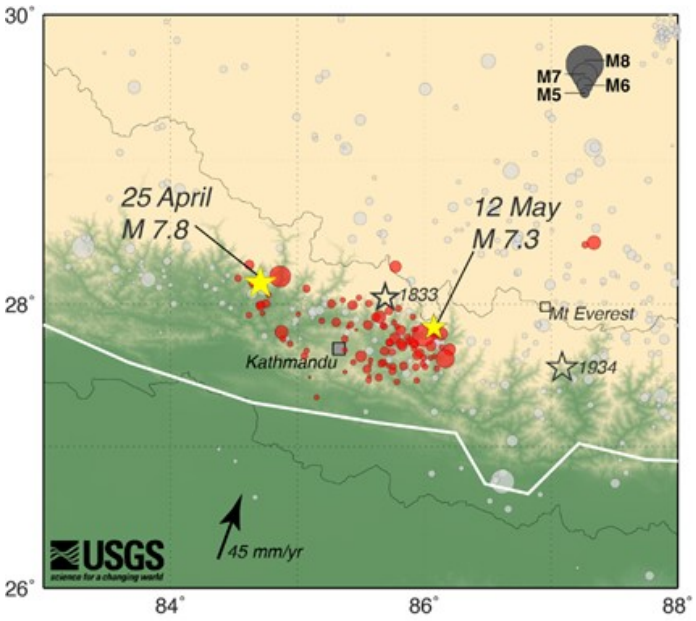

Figure 3-2 Aftershock seismicity map for the 25 April event prepared by Robertson and Koontz (USGS).

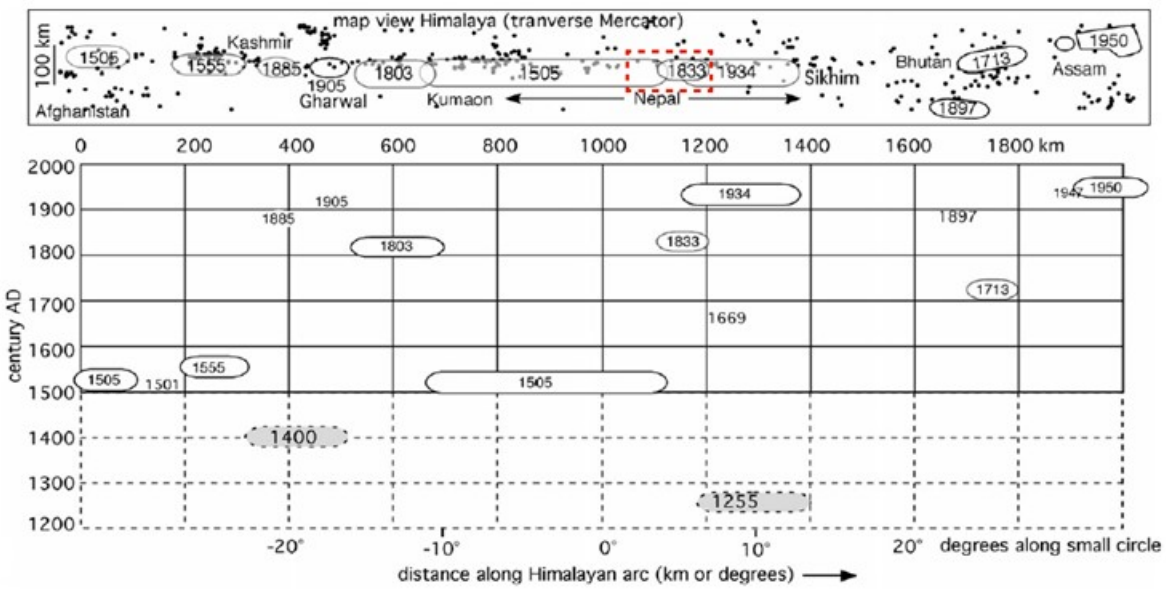

Figure 3-3 modified from Bilham (1995). Time position plot of large and great earthquakes along the Himalayan frontal thrust. The distances are along the small circle of the arc of the Himalayan frontal thrust. The red rectangle is 160 km long, and encompasses the aftershock seismicity (Figure 3-2). It is seen to span the rupture zones of the 1505, 1833 and 1934 earthquakes.

3.3 Foreshocks

The nearby 1833 event had two foreshocks (Bilham, 1995). A search of the ANSS catalog for M>= 2.0 events within a 400 km search radius centered at the mainshock epicenter turned up only three events that could possibly be short term foreshocks. These events, Mb 4.6 (April 2), 5.0 (April 21) and 4.4 (April 22) occurred 170, 240 and 228 km from the mainshock epicenter and despite the closeness in time to the mainshock due to their distance from the mainshock epicenter they are unlikely to be foreshocks.

3.4 April 25, 2015 M_w7.8 main event

The M_W 7.8 Gorkha earthquake occurred on April 25, 2015 at 06:11:26 UTC on or near the main Himalayan thrust fault at 28.1473 N latitude and 84.7079 E longitude with a hypocentral depth of 15 km. To date (June 14, 2015) there are 222 aftershocks listed in the ANSS catalog to Mb 3.4. There have been 5 aftershocks with M_W larger than 6.0, one of which was a M_W 7.3 event that occurred on May 12, 2015 approximately 140 km east of the mainshock epicenter.

Three moment tensor solutions are reported by the USGS (2015) for the mainshock using teleseismic body wave and surface wave data. The scalar seismic moment is well constrained and ranges from 5.44 to 7.76e20 Nm, corresponding to M_W 7.8-7.9. The centroid depth estimates range from 10-24 km, and all mechanisms show a low angle NNE dipping fault plane with strike 290-295, dip 7-11, and rake 101-108 degrees.

Finite-source models for the mainshock show unilateral rupture from the epicenter approximately 150 km to the ESE. Figure 3-4 shows the USGS (2015) model based on teleseismic P and SH body waves. The fault model is defined by a strike of 295 degrees with an 11 degree dip. Overall rupture dimensions are approximately 150 km along strike, and 120 km down dip. The average and peak slips are 0.65 and 3.10 m, respectively, and the peak

occurs approximately 80 km ESE from the epicenter near the Kathmandu basin. The scalar seismic moment is $8.1x10^{20}$ Nm corresponding to Mw 7.9. The majority of slip occurred within 65-70 seconds of the onset of the earthquake. The kinematic model suggests that the rupture initiated with a fast rupture velocity, slowing as it progressed into the high slip patch that extends from approximately 30 to 100 km from the epicenter although the spatial resolution of the model is very coarse.

A second kinematic finite-source model was obtained by Galetzka et al. (2015) from the inversion of ground deformation information from ALOS-2 InSAR scenes, three-component displacement time histories from seven high-rate, 5 Hz GPS stations (CHLM, KKN4, LAST, NAST, RMTE, SNDL), and a three-component strong-motion record located in Kathmandu (KATNP). Their model shown in Figure 3-5 has an along strike length of ~150 km similar to that in the USGS model, but a much narrower down-dip width of ~50 km. The two models are similar in the length and down-dip width of the large slip patch. The narrow slip distribution in the Galetzka model seems to be bounded by the locations of aftershocks (Figure 3-5**)**. The average and peak slips are 0.69 and 6.67 m, and the scalar moment is 6.68e20 Nm corresponding to M_W 7.8. The rupture in this model lasted 65 seconds similar to what was found from the teleseismic waveform data.

Leonard (2010) developed self-consistent empirical scaling relations for fault length, width and average slip for strike-slip, interplate dip-slip and earthquakes in stable continental regions. Given the range in scalar seismic moment from the moment tensor analysis, the Leonard (2010) relation estimates for fault length, width and average slip are 128-148 km, 44-49 km, and 0.26-0.28 m, respectively. Both the aftershock distribution and estimates of rupture extent from kinematic finite-source analysis yield rupture dimensions that are consistent with the Leonard (2010) scaling relations. The average slip from the finite-source models are larger than the average found by Leonard (2010) for interplate dip-slip events, and may indicate the Gorkha earthquake has a higher average stress drop. The average stress drop determined from the Galetzka et al. (2015) finite-source model is 2.6 MPa.

The fault slip lying entirely east of the hypocenter suggests that there could be a strong directivity effect in the shaking from the earthquake. Examination of the teleseismic SH body waveforms used in the USGS model indicates that stations located to the ESE have shorter duration than stations located to the NNW, consistent with eastward rupture directivity. However, it should be noted that for dip-slip events in which the slip direction is perpendicular to the strike of the fault that P-SV radiation lobes (direction of maximum radiation) are perpendicular to the fault strike, and SH radiation lobes are oriented 45 degrees to the fault strike. This radiation pattern leads to a more subdued directivity effect at local and regional distances as was observed for the 1999 Mw 7.6 Chi Chi, Taiwan earthquake (Aaagaard et al., 2004), and the 2004 Mw 6.5 San Simeon earthquake (Rolandone et al., 2006). Thus directivity modulation of the seismic wavefield was likely not strong in the Gorkha earthquake, though it is not possible to investigate this in detail with the local and regional data that is presently available.

Due to the shallow depth and low angle dip of the rupture plane all sites located north of the surface projection of the fault plane are on the hanging block. Observational evidence and simulations indicate that substantial amplification of seismic energy can occur at sites on the hanging block compared to sites the same distance from the surface projection of the fault on the foot block (Donahue et al., 2014). Four of the 5 Hz GPS sites (KKN4, NAST, CHLM, SNDL) and the strong motion station KATNP are located over the fault plane, and are likely affected

by hanging wall effects. In addition, these sites, particularly those over the large slip patch (Figure 3-5) are approximately 10 km from the rupture plane and substantial static deformation (intermediate-field) terms, “fling,” have likely contributed to the nature of the strong ground shaking. This is discussed in more detail in Section 3.6.

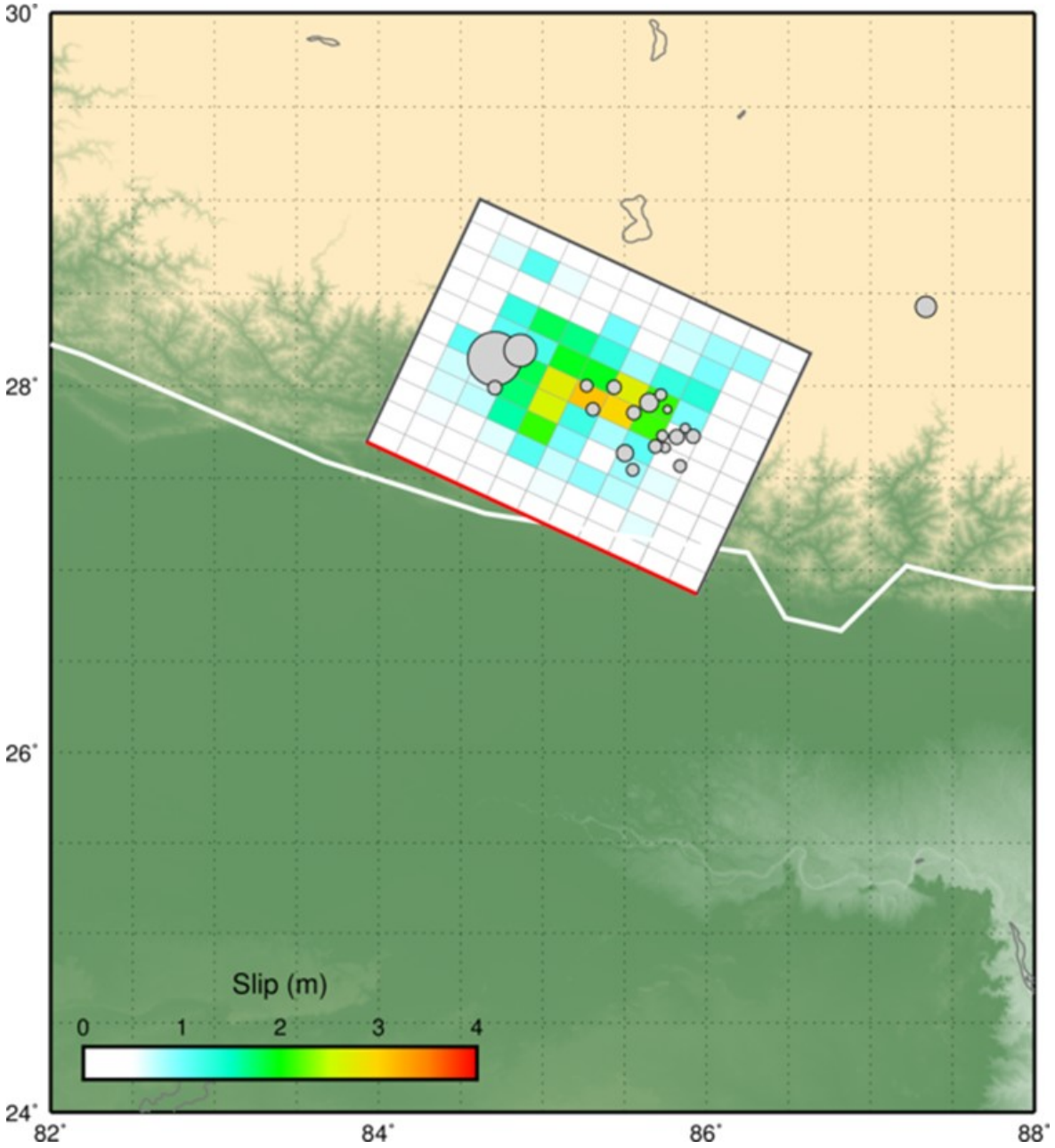

Figure 3-4 USGS (2015) finite-source model from the inversion of teleseismic body and surface waves.

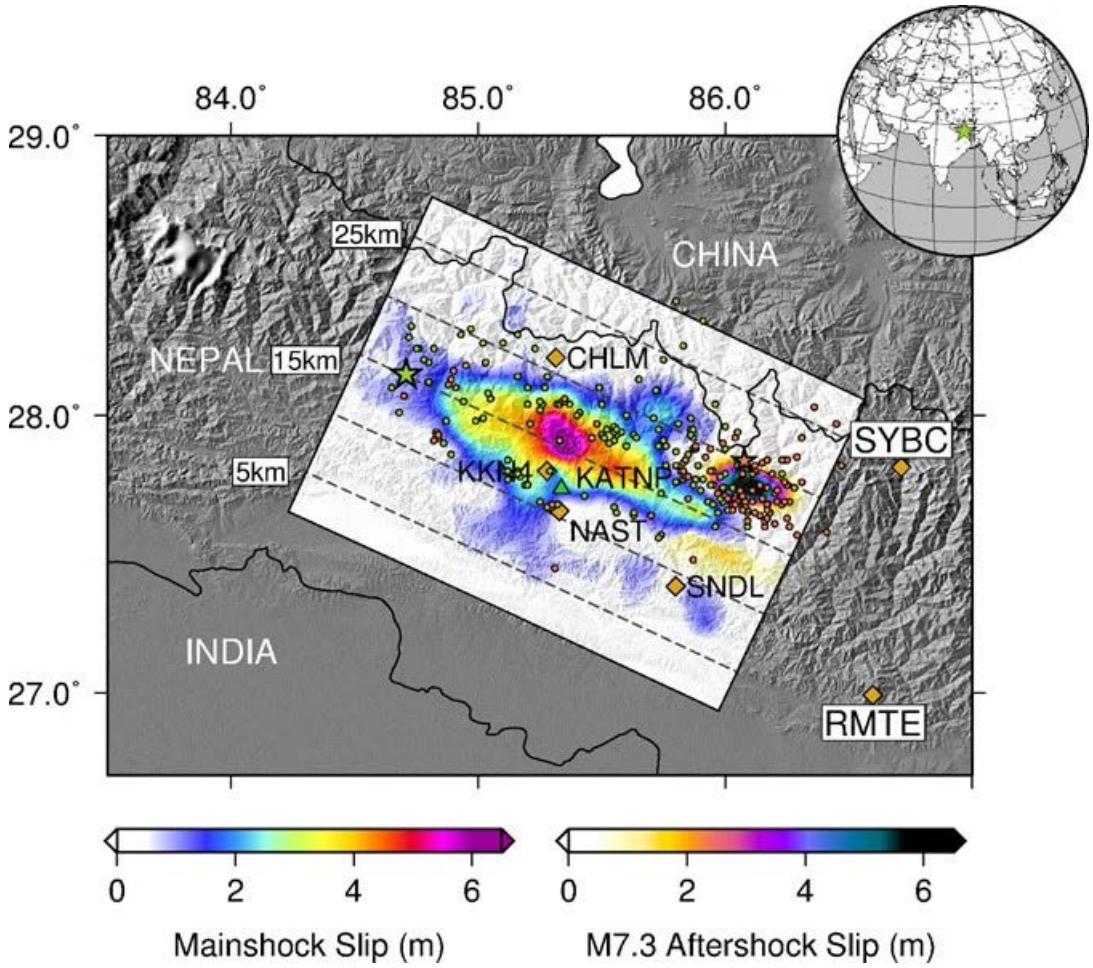

Figure 3-5 The Galetzka et al. (2015) slip model obtained from the inversion of Alos-2 InSAR data and ground motion time histories from five 5 Hz GPS sites (CHLM, KKN4, LAST, NAST, RMTE, SNDL), and a strong motion instrument in Kathmandu (KATNP). The green star shows the epicenter of the mainshock, and the orange star and adjacent slip for the M_w7.3 aftershock. The aftershock slip distribution was obtained by inverting only static InSAR data.

3.5 Aftershock Sequence

In the first two months following the event 222 M>4 aftershocks have been reported in the USGS ANSS catalog. Figure 3-6 shows the distribution of aftershocks spatially and in time. There were 130 M>4 aftershocks in the first week spanning the entire rupture area. Several events are located considerable distance from the mainshock fault and are likely triggered earthquakes. In week 2, 3 and 4-8 there were 17, 59 and 17 M>4 aftershocks. The increase in aftershock seismicity in week 3 is due to the aftershock sequence of the M7.3 event that occurred on May 12, 2015. These aftershocks are largely located at the eastern edge of the aftershock distribution delineated in week 1. As Figure 3-5 shows the slip inferred from InSAR static deformation for the M 7.3 aftershock (Lindsey et al., 2015) is located adjacent to the eastern edge of the mainshock slip.

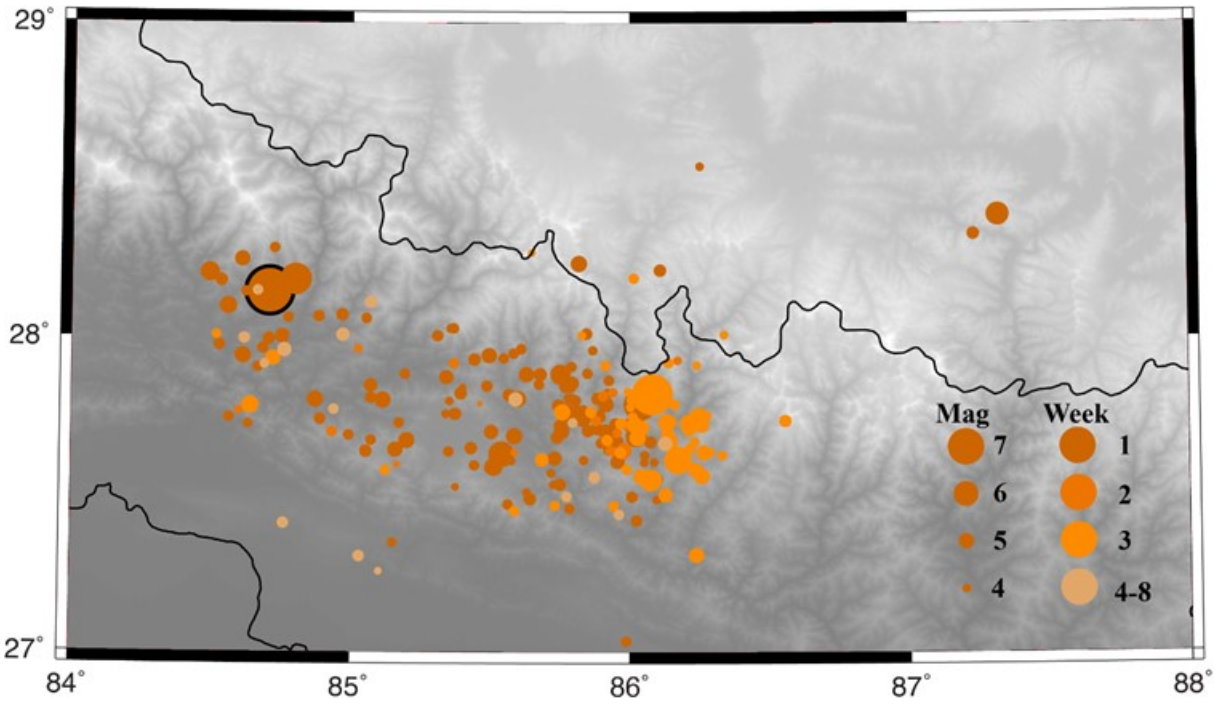

Figure 3-6 Spatial and temporal distribution of aftershocks.

3.6 Recorded ground motions

Despite the large magnitude of the M7.8 Gorkha earthquake, and the very short epicentral distance of downtown Kathmandu, the ground motions recorded in the middle of the basin (Figure 3-7) had a very low peak ground acceleration PGA = 0.16g and a very long period (5s) predominant pulse (Figure 3-8). Unfortunately, the earthquake sequence was poorly recorded, and only one strong motion instrument (KATNP) managed by the USGS has so far provided ground motion time-series over the bandwidth of engineering interest. As a consequence, the factors that shaped the amplitude and frequency content of the mainshock are still poorly understood, particularly in the short period range of engineering interest (>0.5 Hz). At longer periods, continuous GPS stations of the Caltech Tectonic Observatory provided an excellent approximation of the rock outcrop ground shaking, and have revealed the extent to which source and path effects contributed in shaping the amplitude and frequency characteristics of the strong motion record at KATNP. The data were used by JPL/ARIA and are archived at UNAVCO

Figure 3-7 shows the location of the USGS KATNP strong motion station (27°42'43.20"N, 85°18'57.60"E). As it will be shown in Chapter 4, KATNP is located on top of the thickest layer of the Katmandu lake deposits, estimated between 200-300m.

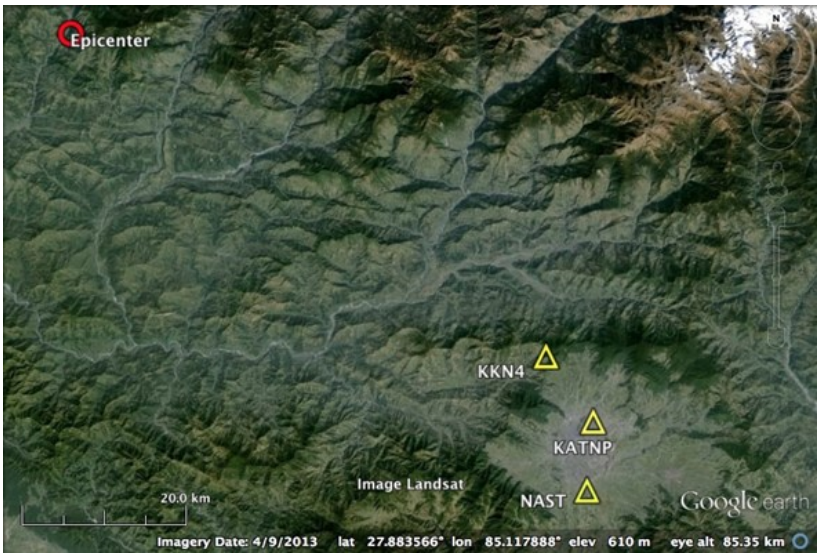

Figure 3-7 Location of the strong motion station KATNP (27.730 N, 85.336 E), the only instrument that has so far provided acceleration time series, and two nearby 5 Hz GPS sites KKN4 (27.8007 N, 85.2788 E) and NAST (27.6567 N, 85.3277 E).

In Figure 3-8 we show the 3-component acceleration time series of the mainshock at KATNP, where one can clearly see the long period predominant pulse of the two horizontal components; the comparatively higher frequency content of the vertical component; and what appears to be a very early aftershock at 270s (S. Hough, personal communication). In Figure 3-9, we next show the Fourier amplitude spectra of the series, which reveal that the vertical component also has significant energy at 0.25Hz, and a lower rate of high frequency decay compared to the horizontal components. To further analyze the evolution of frequency content of the strong motions as a function of time, we also plot in Figure 3-10 the spectrograms of the three mainshock components, where we can clearly see the long period 5sec pulse reverberating for several cycles (denoted by white dashed line on the vertical axis); and the secondary pulse that arrives approximately at 270s.

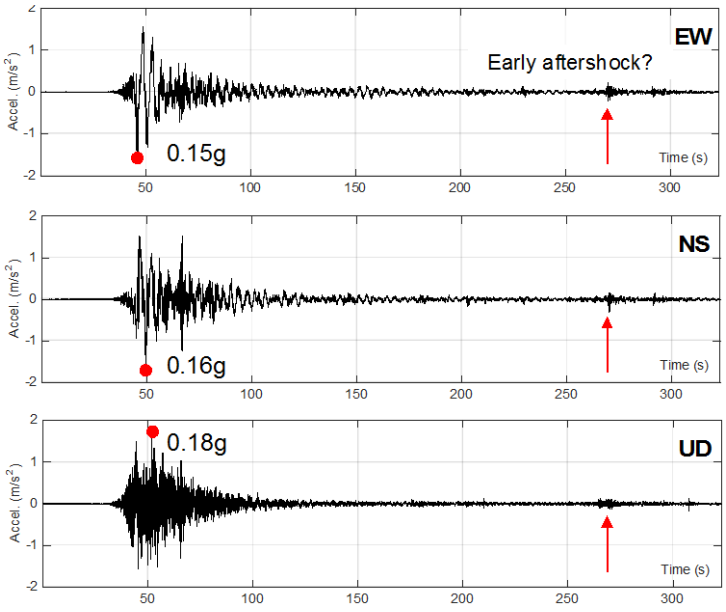

Figure 3-8 Strong motion time series of the 04/25/2015 M7.8 Gorkha mainshock recorded at KATNP.

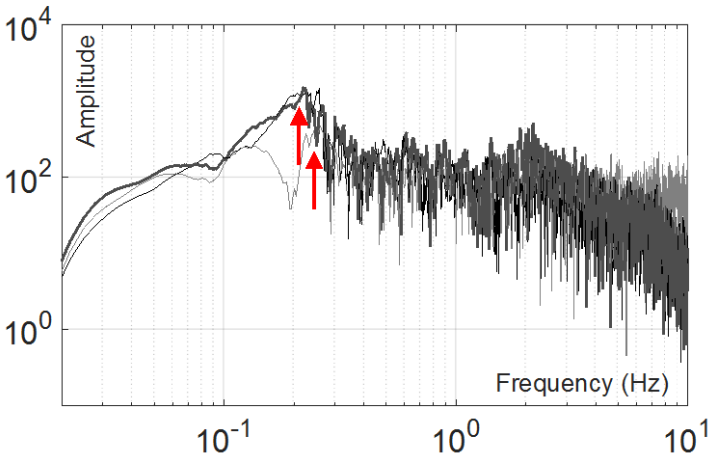

Figure 3-9 Acceleration Fourier spectra of the 04/25/2015 M7.8 Gorkha mainshock recorded at KATNP.

In Figure 3-11 we compare the response spectra of the mainshock, the M7.3 05/12/2015 aftershock, and the 6 next strongest aftershocks listed in Table 3-1. We here observe two features: (i) in the low period (high frequency) range of the response spectra, the mainshock peaks at 0.47s, the M7.3 aftershock at 0.43s and the weaker aftershocks within the range 0.2-0.3s, a period elongation suggestive of nonlinear site response; (ii) the horizontal components of the mainshock appear to be the only ones with energy in the 5s period range, while the aftershock long period peaks are at much shorter periods (1-3s). From the observation alone, one could assume that the 5s pulse is purely a source characteristic of the maishock. However, as we will show in Chapter 4, source and near-surface path (basin) effects most likely contributed to the frequency content of the mainshock, although further research is required to verify our hypothesis.

Table 3-1 Six aftershocks analyzed in Figure 3-11, in addition to the M_w7.8 mainshock and the strongest M_w7.3 aftershock.

2015-04-26_07-09-10_UTC_Mw6.7
2015-04-25_06-45-21_UTC_Mw6.6
2015-04-25_23-16-15_UTC_Mw5.6
2015-04-25_06-56-05_UTC_Mw5.5
2015-04-25_08-55-56_UTC_Mw5.3
2015-04-26_16-26-05_UTC_Mw5.3

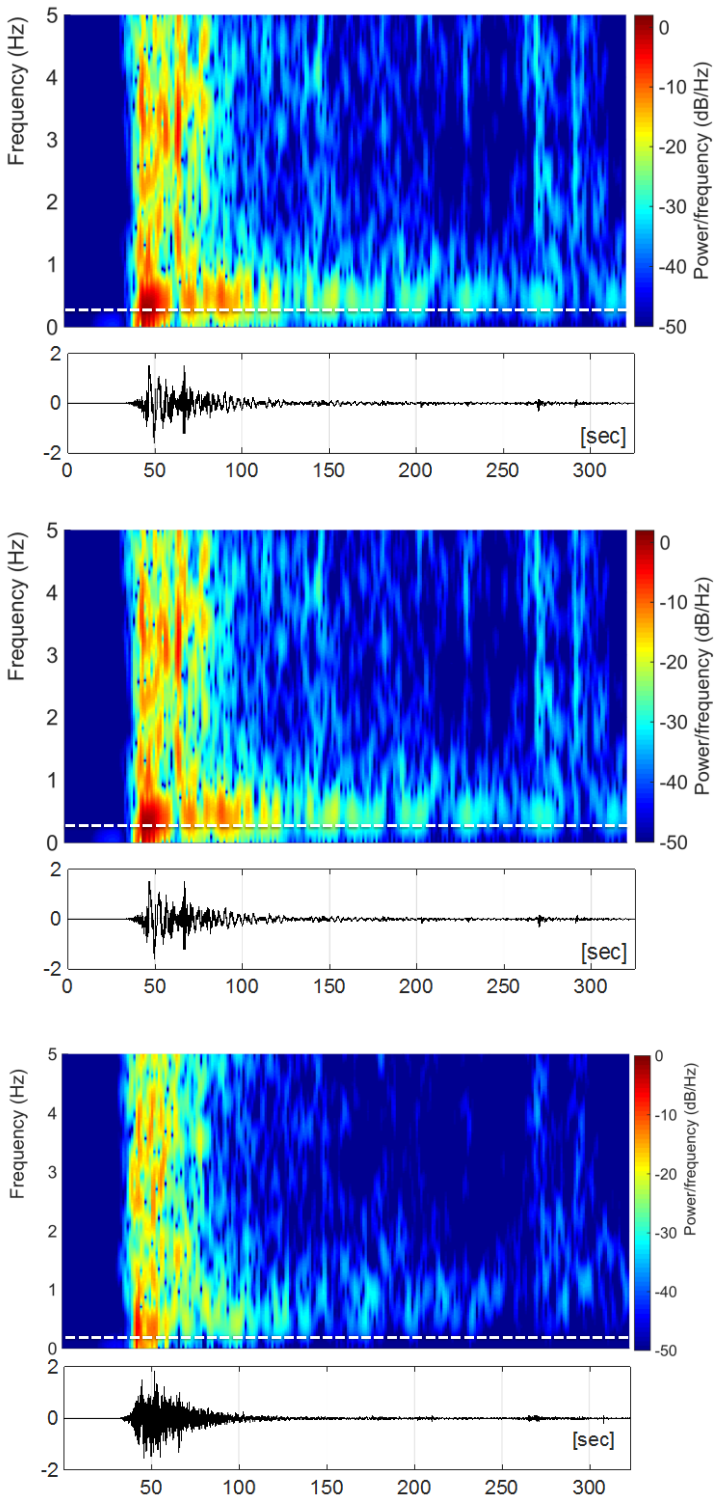

Figure 3-10 EW, NS and UD component spectrogram of the 04/25/2015 M7.8 Gorkha mainshock at KATNP.

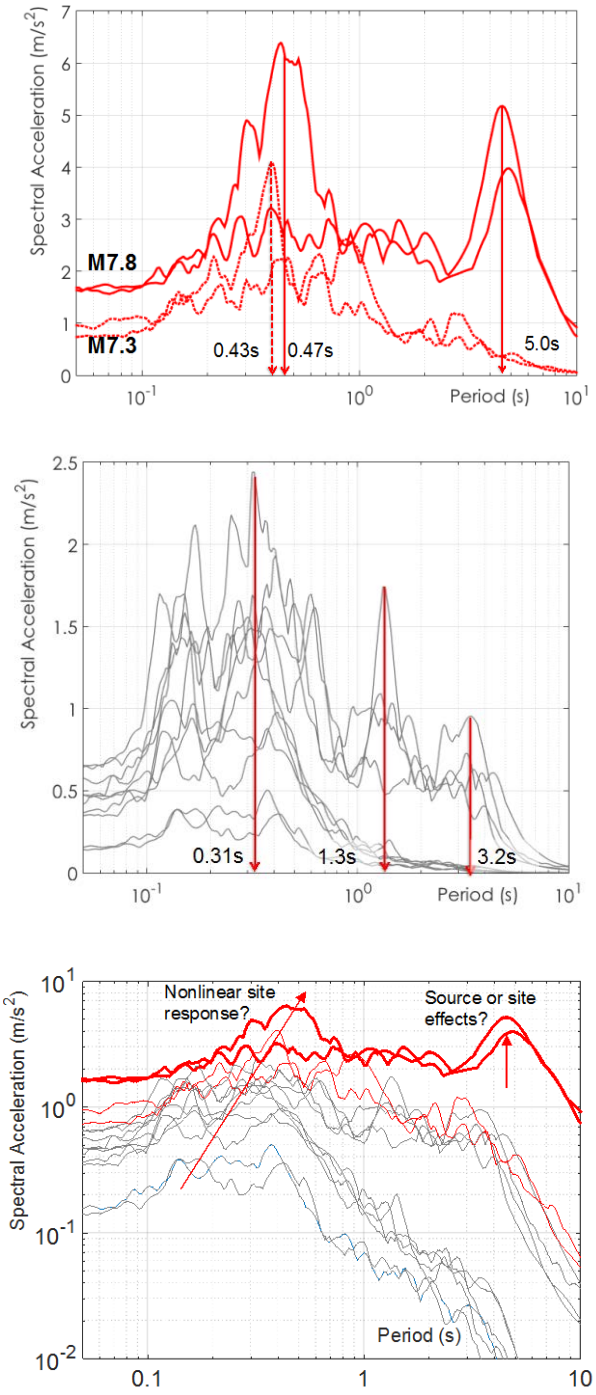

Figure 3-11 Response spectra of mainshock and 7 strongest aftershocks of the 04/25/2015 M7.8 Gorkha mainshock sequence recorded at KATNP.

It is interesting to compare the records of stations KKN4, KATNP and NAST, located 68, 77, and 82 km from the epicenter respectively. KKN4 is situated in the western hills outside of Kathmandu basin (Figure 3.6), and KATNP and NAST are situated within the basin. KKN4 and NAST are 5 Hz GPS time series processed from ALOS-2 data (Galetzka et al., 2015). The raw GPS data is provided by the Nepal Geodetic Array run by the California Institute of Technology, and the Department of Mines and Geology (Nepal). The Scripps Permanent Array and Observation Center (SOPAC) processed the raw GPS data to displacement time histories, which is included in ascii format in the appendix of this report. Station KATNP is the USGS strong motion station at Kathmandu discussed previously. Figure 3.11 compares the three

component velocity records from the three sites. Station KKN4 has the simplest and lowest amplitude waveforms, consisting of the pulse-like S-wave with a duration of 5-6 seconds. The other stations show amplification and extension of the duration due to the low velocity sediments of the Kathmandu basin. KATNP shows secondary pulses that are basin generated surface waves, that judging from the lack of similar motions on the vertical components are Love waves, although the particle motions in the horizontal plane are not linearly polarized indicating complex 3D propagation of the basin generated surface waves. At station NAST, at the southern edge of the basin the surface wave duration lasts more than 40 seconds with a predominant period of approximately 4 seconds. There are 5 cycles with motions at or above 50 cm/s. There is a second packet of surface wave energy that likely comes from interactions of the wavefield with the edges of the basin.

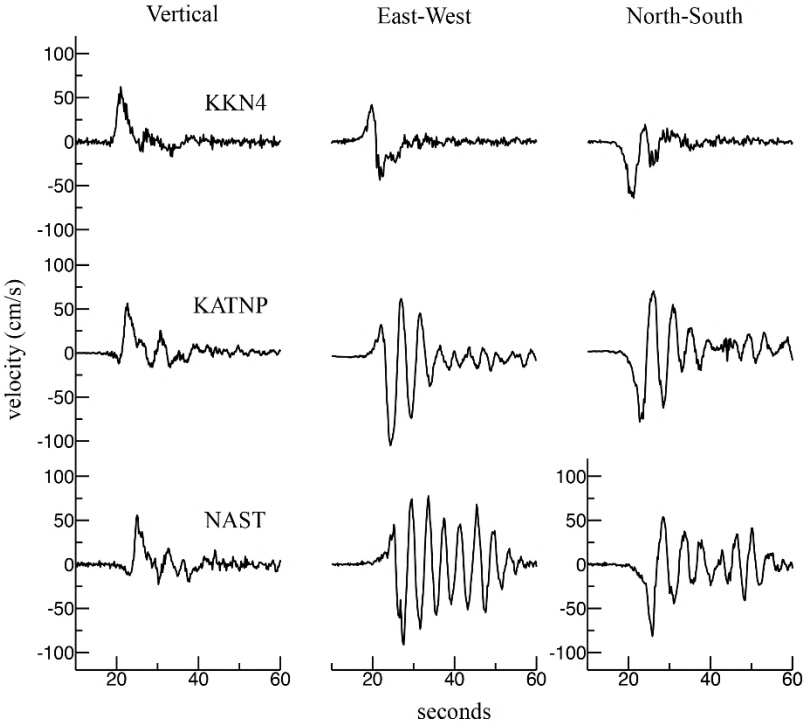

Figure 3-12 Comparison of three component velocity records for the sites outside and within the Kathmandu basin. Strong Love wave signals are generated by basin edge effects and 3D propagation within the basin sediments.

As the three Kathmandu sites are located approximately 10 km from the rupture plane the long-period displacement records are complicated through the interference of near-, intermediate- and far-field waves. As shown in Figure 3-12 the later long-period reverberations are likely surface waves propagating in the basin. In displacement all sites exhibit large static deformation, including the accelerometer site KATNP although recovery of the static is difficult due to the double integration. Figure 3-13 compares the three-component KKN4 displacement time series from 5 Hz GPS observations. The horizontal records have been rotated into fault parallel (FP, azi=295) and fault normal (FN, azi=25) components. All three components show large static offsets in displacement. The static displacement is controlled by the intermediate-field term, which is proportional to the moment time history, or the slip time history on the fault. From the vertical and FN components the slip rise time may be directly determined from the initiation of the development of the static offset to the time that the stable offset is achieved. The dashed lines show the inferred rise time, which also correlates with the beginning and end of the vertical component velocity pulse. From these records the slip rise time is estimated to

be approximately 7.4 seconds. A minimum estimate can be inferred from the times that vertical velocity pulse rises from and falls to zero. The measured rise time is consistent with the interpretation that the long-period energy observed in the mainshock response spectra is primarily due to source.

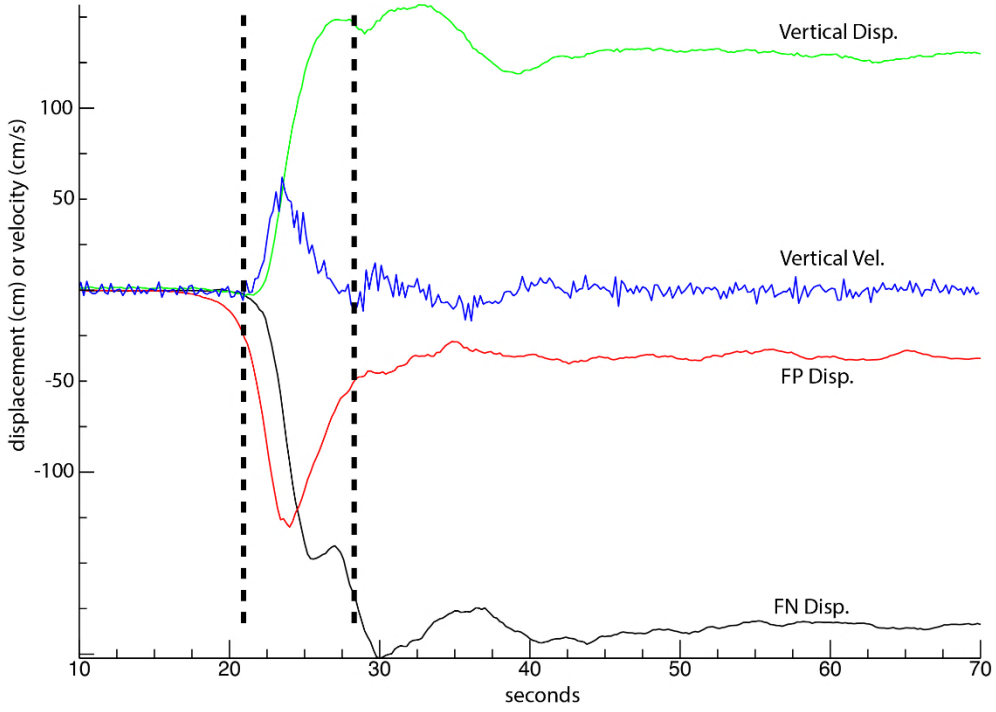

Figure 3-13 Comparison of 5 Hz GPS vertical, fault-normal (FN) and fault-parallel (FP) displacement time histories. The blue trace compares the vertical component of velocity. The dashed lines show the inferred slip rise time from zero to static offset.

The long-period slip velocity pulse in of itself is not an explanation for the low shorter period ground motions at KATNP (Figure 3-11) though it does explain the high long-period response. The short-period motions could be low for a variety of reasons including; 1) the aforementioned subdued nature of directivity focusing in dip-slip earthquakes; 2) the possibility of a relatively smooth rupture process leading to weak radiation at short-periods; and 3) seismic attenuation properties of the region. Future work is needed to reconcile these possibilities.

3.7 Fault Rupture

The M_w 7.8 and subsequent aftershocks produced no observed surface fault rupture. Extensive field investigations were conducted by members of the GEER Team as well as by other researchers and the consensus is that the slip at depth did not propagate to the surface.

The 1934 Bihar-Nepal earthquake is believed to have ruptured at depth on the MFT to the southeast of Kathmandu. Recent work by Bollinger et al. (2014) and others have documented evidence that the 1934 and 1255 earthquakes both ruptured the ground surface. Although seismological evidence suggests the hypocenter of the 2015 Gorkha earthquake was located along or near the MFT fault plane, no similar evidence of surface ground rupture or ground deformation (i.e., folding or warping) was identified following the 2015 Gorkha earthquake or aftershocks. This trend is consistent with the magnitude-dependence of surface rupture for events in this region: surface rupture resulted from the M > 8 (e.g., 1255, 1934) events but not the M < 8 events (e.g., 1803, 1833, 1905).

These observations are consistent with the Moss et al. (2013) model for surface fault rupture of reverse mechanisms. Using mapped estimates of V_S30 as an indication of near surface stiffness where the MFT plane projects to the ground surface, the model gives a 55% probability of surface rupture for the M_w 7.8 event, but a larger 62% probability of surface rupture for the M 8.1 event. Even for large magnitude events, the compressional nature of reverse events often results in the displacements at depth being partially or fully mitigated before reaching the ground surface.

3.8 References

Aagaard, B., J. Hall, and T. V. Heaton (2004), Effects of fault dip and slip rake angles on near-source ground motions: Why rupture directivity was minimal in the 1999 Chi-Chi, Taiwan, earthquake, Bull. Seismol. Soc. Am., 94, 155– 170.

Bollinger, L., Sapkota, S.N., Tapponnier, P., Klinger, Y., Rizza, M., Van der Woerd, J., Tiwari, J.R., Pandey, R., Bitri, A., and Bes de Berc, S. (2014). Estimating the return times of great Himalayan earthquakes in eastern Nepal: Evidence from the Patu and Bardibas strands of the Main Frontal Thrust, Journal of Geophysical Research: Solid Earth, 119, 7123-7163, doi:10.1002/2014JB010970.

Donahue, J. L., and N. A. Abrahamson (2014). Simulation-based hanging wall effects, Earthquake Spectra, Vol. 30, No. 3, 1269-1284.

Galetzka, J., D. Melgar, J. F. Genrich, J. Geng., S. Owen, E. O. Lindsey, X. Xu, Y. Bock, J. P. Avouac, L. B. Adhikari, B. N. Upreti, B. Pratt-Sitaula, A. More, K. W. Hudnut, W. Szeliga, J. Normandeau, M. Fend, M. Flouzat, L. Bollinger, P. Shrestha, B. Koirala, U. Gautam, M. Bhatterai, R. Gupta, T. Kandel, C. Timsina, S. N. Sapkota, S. Rajaure, and N. Maharjan (2015). Slip pulse and resonance of Kathmandu basin during the 2015 Mw 7.8 Gorkha earthquake, Nepal imaged with space geodesy, submitted to Science.

Moss, R. E. S., Stanton, K. V., and Buelna, M. (2013). The impact of material stiffness on the likelihood of fault rupture propagating to the ground surface, Seismological Research Letters, 84, 485-488, May/June.

Leonard, M. (2010). Earthquake fault scaling: Self-consistent relating of rupture length, width, average displacement and moment release, Bull. Seism. Soc. Am., Vol. 100, No. 5A, 1971-1988.

Lindsey, E. O., R. Natsuaki, X. Xu, M. Shimada, M. Hashimoto, D. Melgar, and D. T. Sandwell (2015). Line of sight displacement from ALOS-2 Interferometry: M_w7.8 Gorkha earthquake and M_w 7.3 aftershock, *submitted to Geophysics. Res. Lett.*

Moss, R. E. S., Stanton, K. V., and Buelna, M. (2013). The impact of material stiffness on the likelihood of fault rupture propagating to the ground surface, Seismological Research Letters, 84, 485-488, May/June.

Rolandone, F., D. Dreger, M. Murray, and R. Burgmann (2006). Coseismic slip distribution of the 2003 Mw6.6 San Simeon earthquake, California, determined from GPS measurements and seismic waveform data, *Geophys. Res. Lett*., 33, L16315, doi:10.1029/2006GL027079.

U.S. Geological Survey (2015). Significant Event Webpage for the April 25, 2015 Gorkha Earthquake, (http://earthquake.usgs.gov/earthquakes/eventpage/us20002926#general_summary)

4 Ground Response

Given the magnitude of the M7.8 Gorkha earthquake on April 25, 2015, and the epicentral distance of the fault rupture from Kathmandu –that is, approximately zero-- the mainshock ground motion was very atypical: it was characterized by a very long period (5s) predominant pulse that reverberated in the valley for 4-5 cycles before gradually decaying, and a very low high frequency content, which together led to a surprisingly low peak ground acceleration (PGA) of 0.16g. Although the nature of the mainshock strong motions is still poorly understood, it will become clear from the following Chapters that it explains to a large extent the surprisingly low extent of infrastructure damage within the basin, compared to the empirical predictions for a M7.8 earthquake below Kathmandu.

Unfortunately, the earthquake sequence was poorly recorded, since only one strong motion instrument on soft sediments has so far provided acceleration time-series (see Chapter 3). Anecdotal evidence has several more instruments recording ground motions within the basin and on top of rock outcrop, although the data is proprietary and there is no indication on the quality of the records or on their release date. Last, high rate (5Hz) GPS measurements were recorded within the basin and on the surrounding mountain ranges by the network originally installed by Jean-Philippe Avouac (Caltech/Cambridge UK) and now maintained by UNAVCO. Susan Owen at JPL has processed the data through the Caltech/JPL ARIA collaboration, and the double differentiated acceleration time series show remarkable agreement with the KATNP USGS strong motion record at frequencies below 0.5Hz, including the puzzling prevailing frequency of the mainshock at 0.2Hz.

As a consequence, our understanding of site effects, including ground response, basin and topography effects, is mostly based on literature references, observations of damage patterns and single station techniques such as Horizontal to Vertical (H/V) spectral ratios. In the following sections of this chapter, we provide a literature review of documented evidence of site effects within the basin and on the surrounding mountain ranges; we summarize the complex tectonic and geologic setting of the Kathmandu basin, and previous work on ambient noise-based characterization of the basement depth; we analyze the KATNP strong motion records to extract information on the ground response; and we document observational evidence of 3D site effects, namely basin edge and topography effects, through infrastructure damage patterns within the basin and on the surrounding hills and ridge tops.

4.1 Ground motions and site effects in Nepal: Historical evidence

The pattern of devastation reported repeatedly after historical and recent earthquakes listed in Section 3.1 indicates the more severe damage in major cities of Kathmandu Valley such as Kathmandu, Bakhtapur, and Patan after each major earthquake. During the April 25 Gorkha earthquake, these cities once again suffered from severe damage. This repeated pattern of devastation at these cities after each major earthquake further indicates the ground motion amplification due to the site and topographic effects at these locations. Figure 4-1 plots the intensity contours of 1934 Nepal Earthquake (M8.1) from Figure 3-1a together with the USGS ShakeMap of 2015 Gorkha Earthquake (M7.8). Intensity maps from both events indicate higher intensity of shaking in Kathmandu Valley.

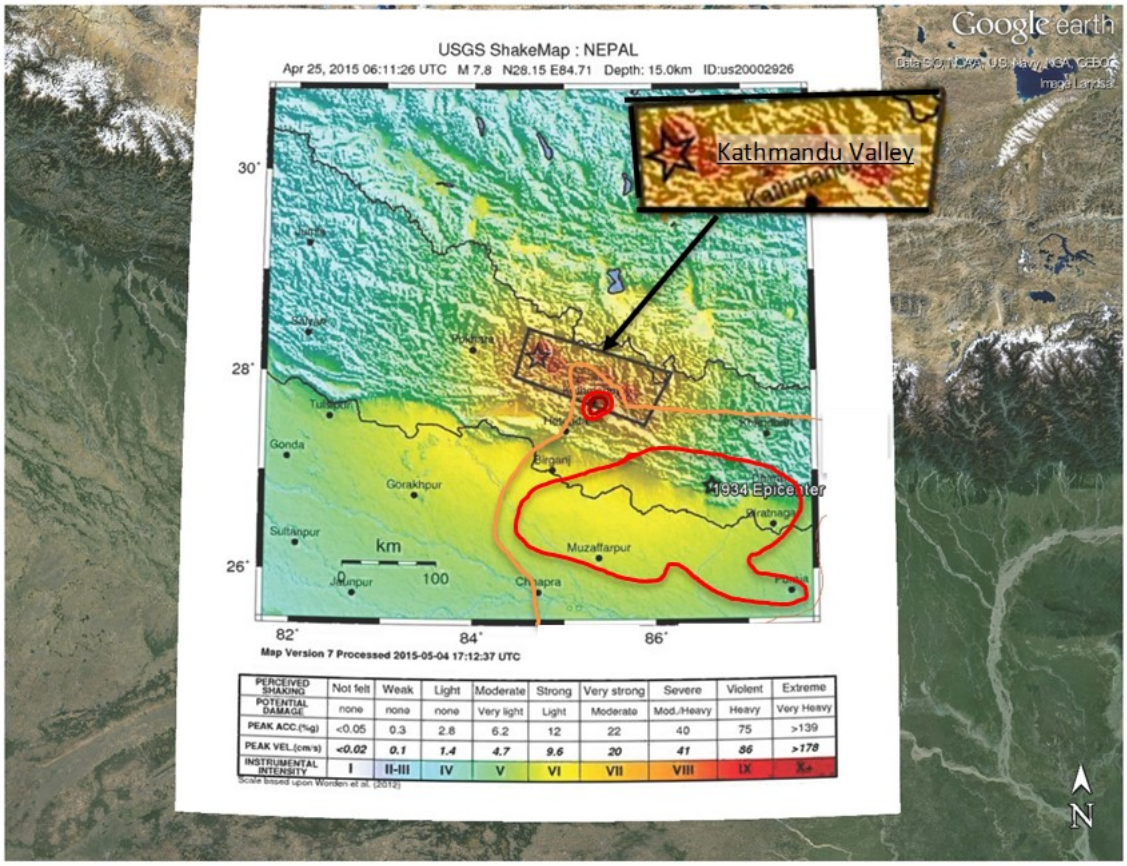

Figure 4-1 Comparison of shaking intensity contours of 1934 Nepal Earthquake (M8.1) with the USGS ShakeMap based intensity distribution of 2015 Gorkha Earthquake (M7.8).

4.2 Geology of the Kathmandu basin

The Kathmandu Basin lies on the Kathmandu Nappe (Hagen, 1969; Upreti, 1999) along the southern slopes of the Himalaya. A lake occupied a large part of the basin from Pliocene to Pleistocene (Yoshida and Igarashi, 1984). The basin is currently filled with a very thick (500–600 m) sequence of fluvio-lacustrine sediments (Moribayashi and Maruo, 1980) and is bounded southwards by a tectonic ridge developed above the Main Boundary Thrust (MBT). The semiconsolidated sediments consist of muds, silts, sandy loams, fine to coarse sands and gravel to pebble conglomerates (Katel et al., 1996). The sedimentary facies (Sakai et al., 2001, 2006) are related to delta plain, delta front and pro-delta environments. Numerous fluctuations of the lake level have been identified by Gajurel (2006) among others, and the classical nomenclature is mainly related to terraces at the top of deltas developed during different stages of the lake extension (Sakai et al., 2006) (Figure 4-2 adapted from Yoshida and Gautam; and enhanced using data from Mugnier et al, 2011). Specifically, the Lukendhol and Boregaon-Pyangaon-Chapagaon formations were deposited between 2.8 and 1 Ma during the older stages of the lake development; the Gokarna formations are related to several stages of the lake development between 1 Ma and 29 kyr (Gautam et al., 2001); the Thimi formation was deposited between ~29 and 19 kyr BP (Yoshida and Igarashi, 1984); the Patan formation is associated to the last stage (19–11 kyr). Outlet of the paleo-lake took place ~10 kyr ago and was followed by river incision resulting in the development of several recent fluvial terraces (Yoshida and Gautam, 1988).

The sedimentation processes in the Kathmandu valley are controlled by the regional fault activity, and the drainage system of the surrounding mountains. According to Sakai et al (2001), the active faults related to the basin sediment formation are, on the southern part of the valley, the Chandragiri Fault and the Chobhar Fault, which run through the colluvial slopes and terraces of the late Pleistocene; and on the North-West of the valley, the Kalphu Khola Fault, which runs through the late Pleistocene gneissic boulder beds (Nakata et al., 1984). The complex tectonic environment surrounding the Kathmandu basin is shown in Figure 4-3. As a consequence of this environment, the geology of the valley is strongly heterogeneous: the southern sediments are predominantly composed by weathered meta-sedimentary rocks from the southern hills such as Chandragiri and Phulchowki, and the northern sediments are composed by weathered gneiss and granites from the northern Shivapuri hills.

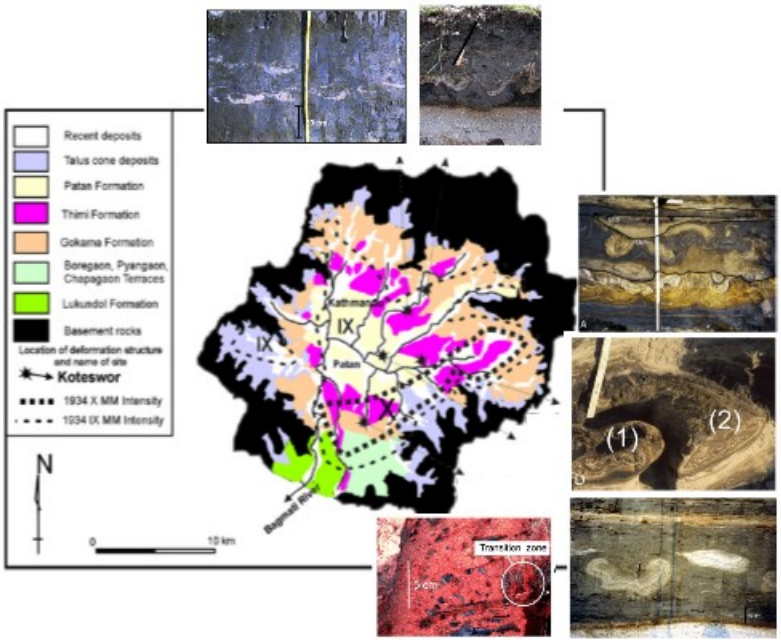

Figure 4-2 Geological map (adapted from Yoshida and Gautam, 1988) of Kathmandu hydrological basin with location of paleo-seismites. Iso-intensity distribution of the1934 earthquake from Dixit et al. (1998). Inserts of typical sedimentary formations revealing the strong tectonic forces the sediments are subjected to are extracted from Mugnier et al (2011).

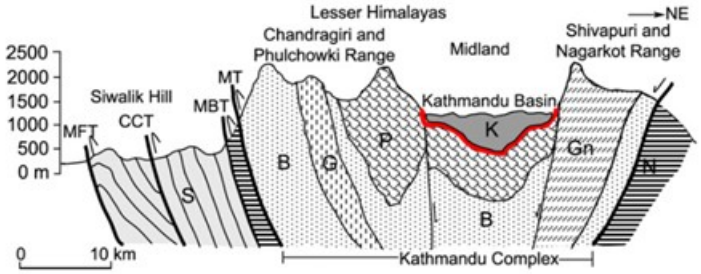

Figure 4-3 A schematic geological cross-section through Central Nepal (after Sakai et al., 2002, and Stöcklin and Bhattarai, 1981). Capital letters correspond to the nomenclature developed by Sakai et al to describe the Kathmandu basin geology: Siwalik Group, B: Bhimphedi Group, P: Phulchowki Group, N: Nawakot Complex, G: Granite, Gn: Gneiss Complex, K: Kathmandu Complex, MFT: Main Frontal Thrust, CCT: Central Churia Thrust, MBT: Main Boundary Thrust, MT: Mahabharat Thrust. Details on the correspondence between the formations in Figure 4-2 and Figure 4-3 can be found in Mugnier et al (2011).

The most recent, unconsolidated sediments of the Kathmandu valley are highly heterogeneous fluvial-lacustrine sequences. On the northern part of the valley, sediments are poorly sorted, thin to medium-bedded highly micaceous coarse sands, gravel and silts interlayered with clays in some places. On the southern part, they consist of a thick sequence of dark grey to black highly plastic clay and silts, usually overlain and underlain by coarse sediments. The black plastic clay (locally called Kalimati or *black cotton soil*) is rich in organic matter, a fact also corroborated by the presence of natural gas within the valley. The age of this clay is placed in the Pliocene to Pleistocene time according to Yoshida and Igarashi (1984). Its thickness is greatest along the central part of the valley starting from Satungal towards Lalitpur and Bhaktapur, with maximum reported depth 300m. Borings show the basin is upwards of 500m deep, primarily filled with soft sediment. The clay thickness also increases quite substantially towards the Bungmati and Harisidhi areas in the South. Furthermore, alluvial deposits in river channels, flood plains, and fans are spread across the valley, which date back in the Holocene age (Yoshida and Igarashi, 1984). Numerous well-developed alluvial fans can also be found along the valley rim, characterized by steep upper slopes that flatten and widen progressively towards the valley (see geological map in Figure 4-2).

All the above information is strongly suggestive of the heterogeneous nature of the basement geometry and stratigraphy of the Kathmandu valley. Piya (2004) synthesized a very detailed 3D geologic model of the valley, using 168 borehole records from a variety of different sources. These include, among others, a report of the Japanese International Cooperation Agency (JICA, 1990) for a ground water management project in Kathmandu Valley, which was obtained from the Library of Nepal Water and Sewerage Corporation (NWSC); a report of the Geological Survey of India (GSI) for groundwater resources of Kathmandu valley (1966); and the reports of the Environmental Geology Project (EGP) of the Department of Mines and Geology (DMG) for hydrogeological conditions and barrier potential sediments (Clay) in the Kathmandu valley (1998).

The deepest borehole that Piya (2004) reports in Kathmandu valley is shown in Figure 4-4. The borehole log reveals the sedimentation history of the basin, starting with 32 m of coarse sediments (coarse sand and gravel beds) that were transported by the proto-Bagmati river system (Hagen, 1968) from the northern Shivapuri hill before the formation of the lake; 27 m of grey clay at the bottom of the lake; 54 m of medium to coarse-grained sand that was deposited as a consequence of fluvial activity, interrupting the clay deposition for a considerable period of time; an additional 18 m of thick clay sediments; followed by 136 m of sand to gravelly sand interlayered with thin clay deposits, which, according to Piya, corresponds to the most turbulent phase of the fluvial activity. The location of all the boreholes used in that study, plan views of the heterogeneous sedimentary formations at various depths, and cross sections revealing the strongly heterogeneous nature of the valley, are shown in Figure 4-5.

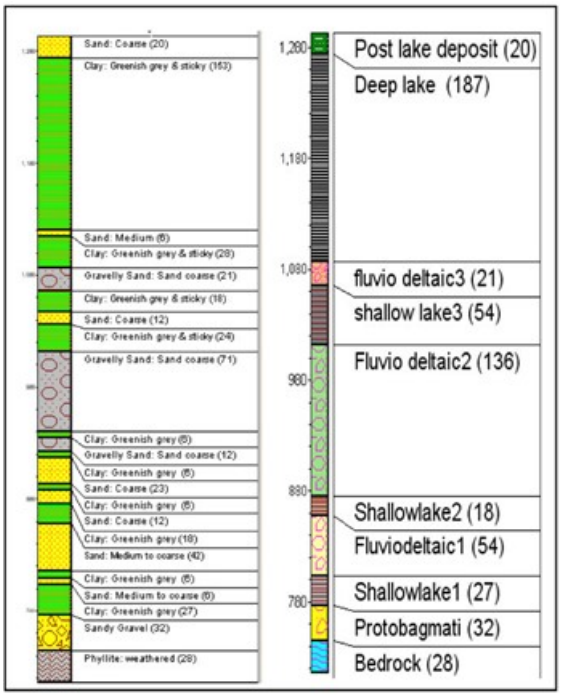

Figure 4-4 The deepest geologic log available in Kathmandu valley (Piya, 2004): (left) Borehole log with lithological information; and (right) borehole log with stratigraphic sequence. The number in bracket indicates thickness of each formation or deposits.

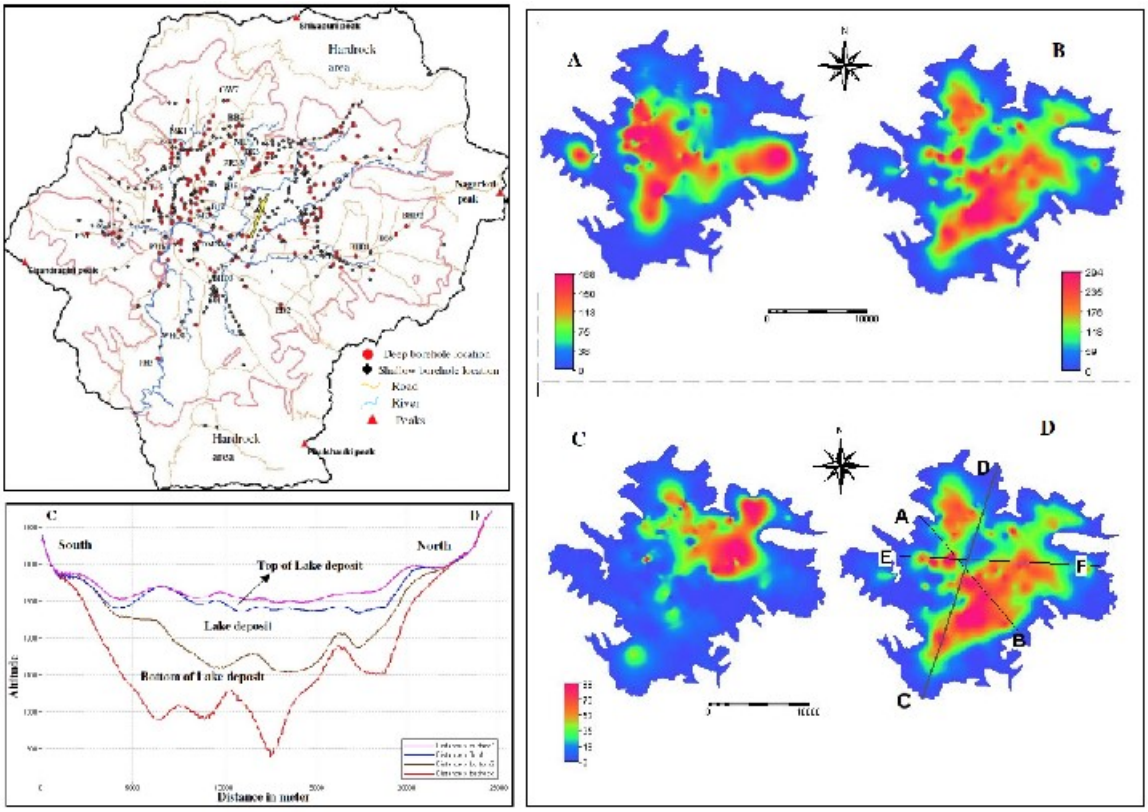

Figure 4-5 (top left) Location of boreholes in the Kathmandu basin; (right) 3D geological model, showing the thickness of the lake deposits (A); pre-lake deposits (B) and post-lake deposits (C); as well as the location of cross section C-D shown on the bottom left (Figure synthesized from Piya, 2004).

4.3 Ground response effects

As mentioned in Chapter 3, the mainshock ground motion frequency and amplitude characteristics are still poorly understood. In this section, we investigate the extent to which local site effects may have contributed to the ground motion characteristics. Due to lack of rock outcrop recordings, we rely primarily on a comparative study between the mainshock and 7 strongest aftershocks recorded at the station, as well as single station methodologies to estimate site response.

Figure 4-6 shows the response spectra of the M_w7.8 mainshock (04/25/2015) and M_w7.3 strongest aftershock (05/12/2015), where we identify the following characteristics: (a) the NS component of the mainshock has two prominent peaks, one at 0.47 s and one at 5 s; (b) both mainshock components have peaks at 5 s whereas the aftershock components do not, possible indication that the 5s pulse was characteristic of the mainshock source, and not related to site effects; and (c) the NS and EW components of the mainshock and aftershock are practically self-similar in the T < 1 s range: the NS have large amplitude at 0.4-0.5s, whereas the EW have a much flatter response in the same period region. The similarities in two orthogonal components could be attributed to similar high frequency radiation mechanisms of the source, or to anisotropy of the local site conditions.

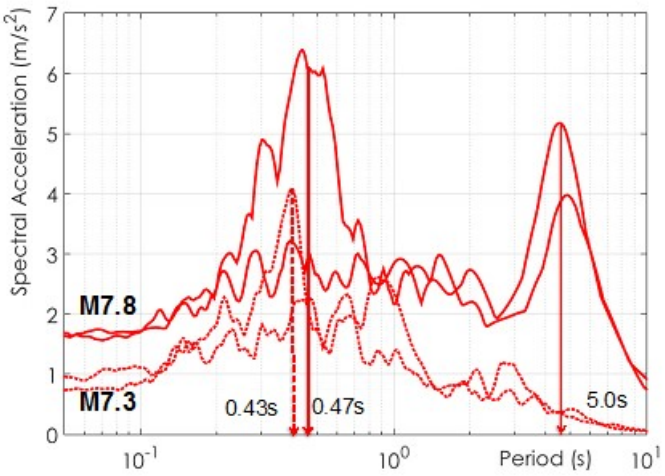

Figure 4-6 Response spectra of the NS and EW components of the M7.8 mainshock (04/25/2015) and M7.3 strongest aftershock (05/12/2015) of the Gorkha earthquake sequence.

To further investigate this question, Figure 4-7 plots the response spectra of the next 6 largest aftershocks of the sequence (to date), which are listed below in order of decreasing moment magnitude. Figure 4-7 shows that all aftershock response spectra have peaks in the 0.31s period range or less, which may be related to the same phenomena that give rise to the slightly more elongated resonant period of the M7.3, T=0.43s, and the even more elongated resonant period of the M7.8 mainshock, T=0.47s. This observation alludes to nonlinear site effects, a possibility that we investigate in the following paragraphs.

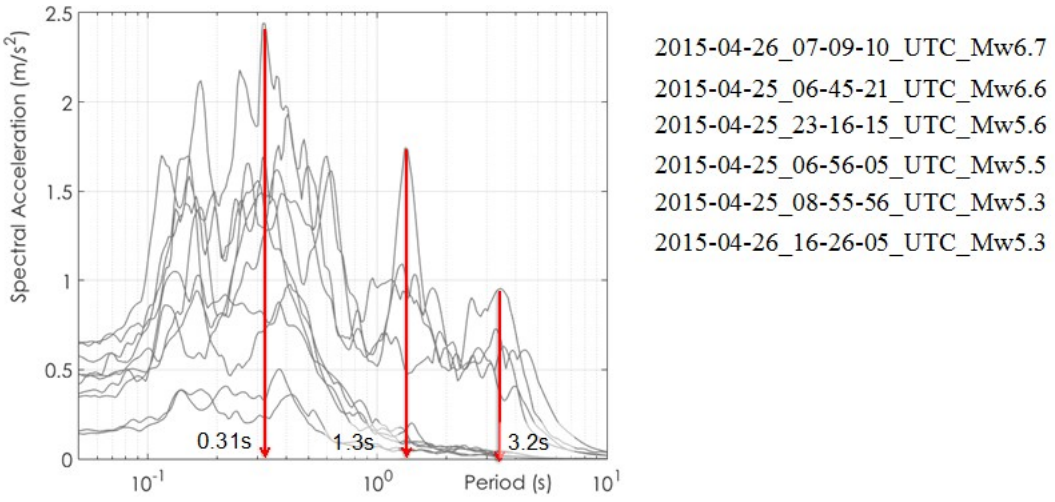

Figure 4-7 Response spectra of the NS and EW components of the six largest aftershocks of the Gorkha earthquake sequence after the 2015-05-12 Mw7.3 plotted in Figure 4-6.

We also observe relatively pronounced amplification of the strongest aftershocks in the vicinity of 1.3 s, which is not evident in the mainshock. The M_w7.3 spectrum on the other hand peaks at a shorter period (0.9 s), which may or may not be related to the same site characteristic; in either case, the shift cannot attributed to nonlinear response because the peak period of the strongest motion is shorter than that of the motion with lower intensity. Last, the same aftershocks also show a less pronounced peak in the vicinity of 3.2 s, similarly to the M_w7.3 aftershock, but have practically no energy in the 5s range where the mainshock has a pronounced peak. The ensemble of response spectra of the two horizontal components from the 8 events described above is plotted on Figure 4-8.

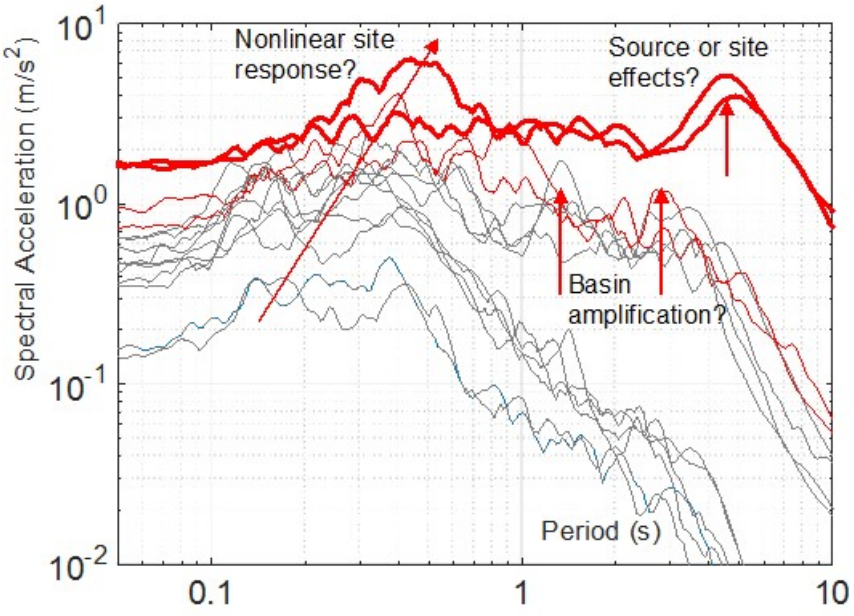

Figure 4-8 Response spectra of EW and NS components of the mainshock and 7 strongest aftershocks recorded at the USGS station KATNP to date.

In absence of strong ground motion recordings, we next implemented single station techniques to evaluate site response. Several methodologies have been developed to estimate site response from single station records. The most prominently used are the horizontal-to-vertical (H/V) ratio proposed by Nakamura (1979) that is based on recorded ambient microtremors, and the H/V receiver function (HVSR), which uses the spectral ratios of the horizontal to the vertical components of an earthquake record instead. Field and Jacob (1995) showed that HVSR of earthquake records within the S-wave window captures the frequency dependence of site response, but not its absolute amplitude. Lachet et al (1995) compared the two approaches (H/V and HVSR), and showed that the agreement between receiver's function, Nakamura's ratios and the traditional soil-to-reference station spectral ratios is satisfactory in the amplified frequency band. They also concluded that the HVSR method provides only partial information on site response, such as the fundamental resonance frequency, and that the H/V ratios systematically under-estimate the amplitude of traditional soil-to-reference rock site spectral ratios. Last, Assimaki et al (2007) came to similar conclusions by comparing HVSR and H/V site response estimations to surface-to-borehole spectral ratios, using records from the Japanese strong motion network KIK-net.

Figure 4-9 shows the HVSRs for the two components of the mainshock (top left), the mainshock compared to the M7.3 aftershock (top right) and the mainshock compared to the 6 next strongest aftershocks (bottom). The most striking observation is that although none of the aftershock response spectra (including the M7.3) showed a peak at 0.2 Hz (5 s) --which initially led us to believe that the predominant pulse of mainshock was related purely to source effects-- all HVSRs show clear amplification in the range 0.2-0.4Hz. This empirical result suggests that the 0.2Hz of the mainshock is also related to site (or *near-surface path*) effects. The plausible scenario that we are currently testing is that the mainshock predominant period is the combination of directivity effects (corroborated by the large PGV>100cm/s) and basin effects (which could explain the reverberations of the pulse recorded at KATNP).

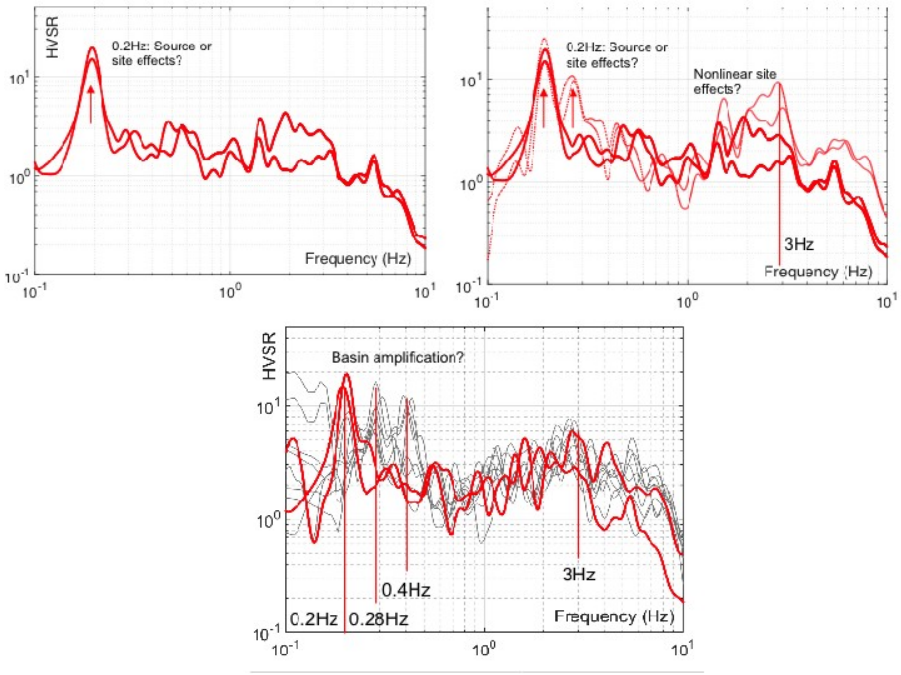

Figure 4-9 HVSRs of mainshock and 7 strongest aftershocks of the M_w7.8 Gorkha earthquake sequence.

The HVSRs have also peaks at higher frequencies, which are typically less reliable than the fundamental mode, but still suggestive of site amplification in the vicinity of 3Hz. Comparing the mainshock to the M7.3 aftershock (top right of Figure 4-9), one could in fact argue that the HVSRs are also revealing nonlinear site effects in this frequency range, since the peak of the M_w7.8 HVSR is at lower frequency and has lower amplitude than the corresponding peak of the M_w7.3 aftershock (although the amplitude of HVSRs is not a reliable estimate of site amplification). However, when we compare the mainshock HVSR to the next 6 strongest aftershocks (bottom of Figure 4-9), which range in PGA from 0.03-0.078g, we find that the peak frequency (and amplitude) of the higher (3Hz) mode of the mainshock is identical to the aftershocks.

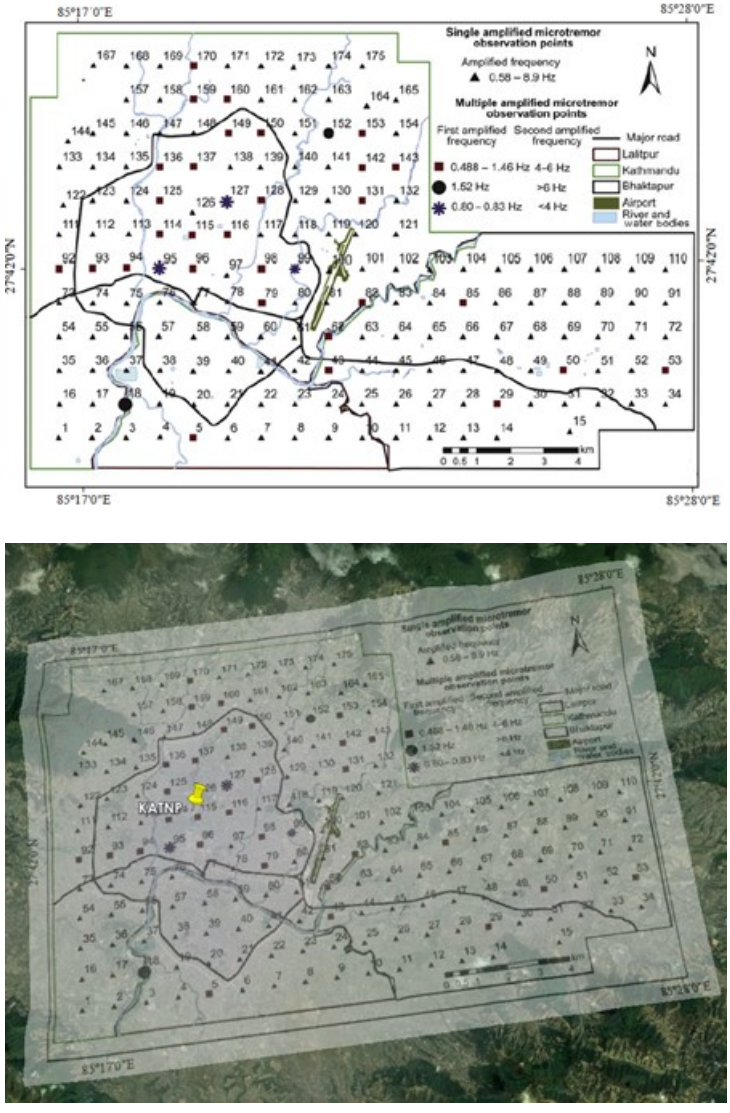

Figure 4-10 (top) Location of microtremor stations in Paudyal et al (2012); (bottom) Map overlay on Google Earth™, and approximate position of strong motion station KATNP.

We next compared our findings from the KATNP station records to a study that used ambient noise H/V ratios to map the bedrock geometry and obtain a first order estimate of the near-surface stratigraphy of the Kathmandu basin. Specifically, Paudyal et al (2012) recorded and processed microtremor observations at 172 nodal points in a 1-km grid covering an area of about 210 km2 in the Kathmandu Valley (see Figure 4-10). According to this study, 80% of the H/V ratios had only one clear peak in the frequency range from 0.58 Hz to 8.9 Hz, whereas the

H/V ratios at the remaining sites showed two amplified frequencies, the first between 0.48 Hz to 1.52 Hz, and the second between 3.1 Hz to 7.5 Hz. We should also note that most of the H/V ratios with two amplified frequencies lie in the center-north parts of the basin, in the broader geographical region of KATNP, which are dominated by the marginal fluvio-deltaic facies (river bed materials) (Sakai, 2001). In Figure 4-10 we also ovelay the Paudyal et al (2012) map of the microtremor site characterization sites on a Google Earth™ map of the Kathmandu basin, and we depict the location of the KATNP strong motion station.

Next, Figure 4-11 shows the recorded microtremor resonant frequencies at the Paudyal et al (2012) stations closest to KATNP (as estimated from our map overlay in Figure 4-10). As can be seen, the first mode measured in the vicinity of KATNP was 0.5 - 0.75 Hz, which is comparable with the observed 0.2 - 0.4 Hz of the receiver functions depicted in Figure 4-9[1]. Similarly, the second mode at 3 – 4 Hz is also comparable to the higher frequency peak shown in the same figure. The H/V ratio that was computed by Paudyal et al at station 95, one of the two stations identified in Figure 4-11, is finally shown in Figure 4-12.

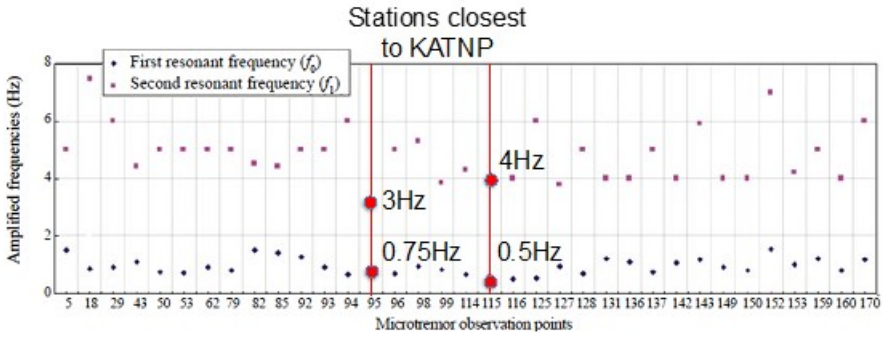

Figure 4-11 Resonant frequencies recorded at microtremor stations 95 and 115, which are the closest to KATNP according to the map overlay shown in Figure 4-10.

Last, we compare the rotation independent response spectral acceleration RotD50 (Boore, 2010) for both the M_w 7.8 mainshock and M_w 7.3 aftershocks against the Boore et al. (2014; BSSA) ground motion prediction equation (GMPE) (Figure 4-13). Although the BSSA equations were developed primarily with ground motions from the Western United States (WUS), it is an approximate analog to Nepal because both are active crustal regions. Additionally, the GMPE selection scheme employed by ShakeMap (Garcia et al., 2012) uses a WUS GMPE for this region. The BSSA equations predict a PGA of 0.49 g for the M_w 7.8, which is much higher than the recorded PGA of 0.16 g. Because of the data paucity, however, the factors that shaped the amplitude and frequency content of the mainshock are still poorly understood.

The low levels of short period shaking in the mainshock could be due to larger crustal attenuation rates in this region, high attenuation in the deep lacustrine sediments of the Kathmandu Basin, or perhaps this earthquake did not generate the high frequencies at the source. However, the observation that the short period energy of the aftershock is well modeled by BSSA is evidence that the lack of short period energy is related to the specific

[1] Although this is arguably higher than the dominant period of the mainshock (0.2Hz), the high frequency noise recorded by Paudyal et al (vehicles, industrial facilities, construction activities etc.) is unlikely to have had enough energy at frequencies much lower than 0.5Hz.

characteristics of the mainshock rather than the properties of the crust or basin. Although the response spectra of the mainshock appears to be rich in energy at long periods, the comparison to BSSA shows that it is not especially large for an earthquake of this size at a soft soil site. For the comparisons in Figure 4-13 we assume the time-averaged shear-wave velocity in the upper 30 m (V_{S30}) is 200 m/s based on horizontal-to-vertical ratios at the KATNP station presented above.

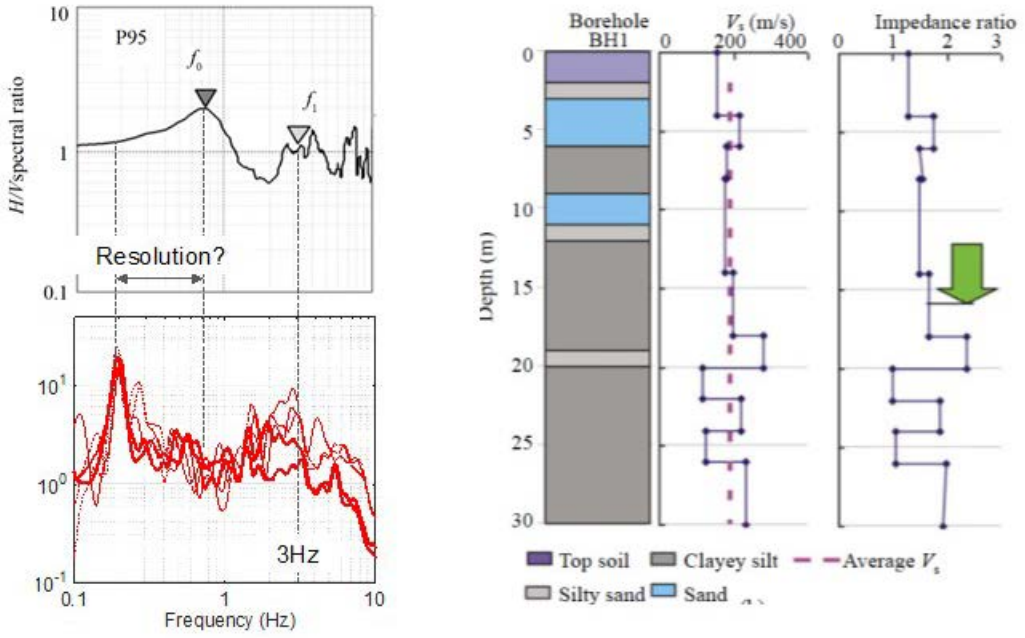

Figure 4-12 (left) Comparison of H/V computed by at Paudyal et al (2012) at microtremor station 95 to the HVSR we computed at KATNP using the EW and NS components of the mainshock and M7.3 aftershock; (right) borehole within 300m from KATNP, showing an estimate of the Vs30 in the area (JICA, 2002).

At this point, our understanding of the role that nonlinear site response has played in modifying the frequency content and amplitude of the mainshock acceleration at KATNP in particular, and across the valley more generally, is limited. Further studies are necessary to obtain velocity profiles, modulus reduction and damping curves of black cotton soil, and rock outcrop records to establish a reference ground motion at higher frequencies.

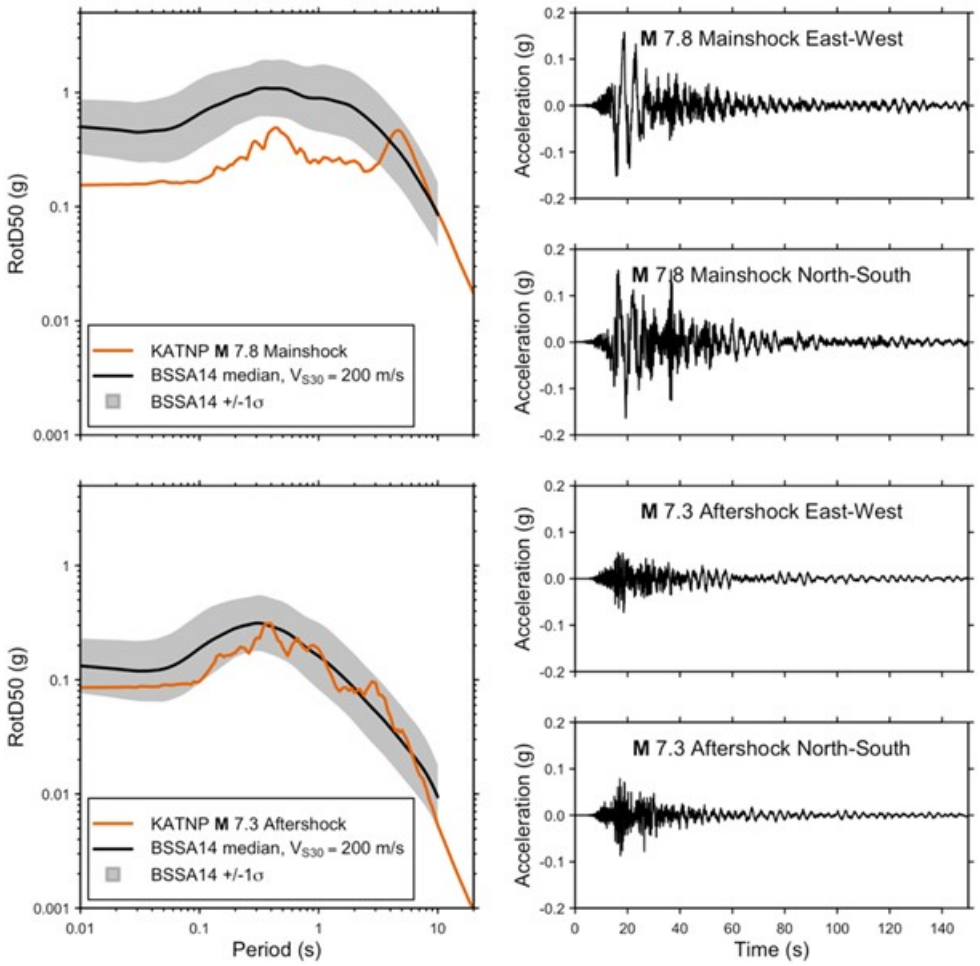

Figure 4-13 Ground shaking of the M_w 7.8 Gorkha earthquake (top row) and the M_w 7.3 aftershock recorded at station KATNP. Left: orientation independent response spectral acceleration (RodD50) compared to the BSSA14 GMPE. Right: horizontal component time histories.

4.4 Basin Effects

Deep sedimentary basins can significantly amplify and lengthen the period of bedrock ground motions, such effect of deep sedimentary basin on the surface ground motion is known as basin effects. Quantification of basin effects on surface ground response usually requires knowledge of the shear wave velocity profiles of the deep sedimentary basins and the underlying bedrock, which can be often obtained from detailed geotechnical information available for the deep sedimentary basin. Such detailed geotechnical information that can be used to estimate the shear wave velocity of the deep sediments of the Kathmandu Valley and its basement rock is not available. To our knowledge, Paudyal et al (2012) is the only available study that estimated the 3D geometry of the basement structure using seismic velocity measurements. Specifically, they used five boreholes where shear wave velocities were measured by the Japan International Cooperation Agency (JICA, 2002) using PS logging to estimate an average Vs_{30} of 246.87 m/s for Kathmandu (JICA, 2002). The profile at the borehole closest to KATNP is shown in Figure 4-12. Successively, using this Vs_{30} and the frequency of the second peak from their microtremor H/V measurements (that ranged from 4 – 6 Hz across all stations), they back calculated the thickness of the uppermost layer of the Kathmandu Valley to be between 10 – 15 m.

In a follow up study, Paudyal et al (2012b) used the first mode (peak) of the microtremor measurements to estimate the depth of the valley basement (Figure 4-14**)**. We should note here that their calculated depth of sediments represents the depth of lake deposits down to a strong impedance contrast, not necessarily to hard rock. Their study showed that the central part of the Kathmandu City, denoted by I in Figure 4-14**,** lies over the main ancient lake of the Kathmandu Basin. Their study also revealed a number of shallower depressions across the basin, and numerous buried ridges which separate/connect the depressions. The strong geometric heterogeneity of the Katmandu basement rock estimated by Paudyal et al (2012b) compares qualitatively well with the work by Piya (2004) presented in Section 4.2.

Finally, Figure 4-15 shows the topographic map of the Katmandu basin basement from Paudyal et al (2012b) as an overlay on Google Earth™ and indicates the location of station KATNP. As can be readily seen, the station appears to be sitting on top of the depression I in Figure 4-14, where the depth of sediments is estimated approximately 250 m.

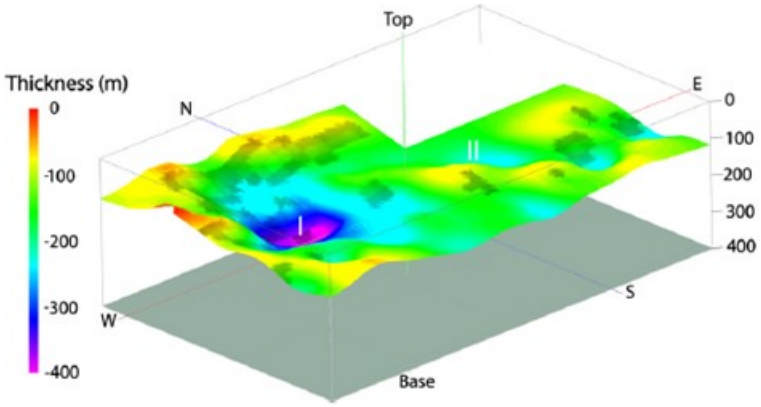

Figure 4-14 Bedrock-soft sediment paleo-topography of the Kathmandu Valley Basin (the vertical scale is 15 times exaggerated). I and II are the depressions with the thickest deposits in the study area (from Paudyal et al, 2012b).

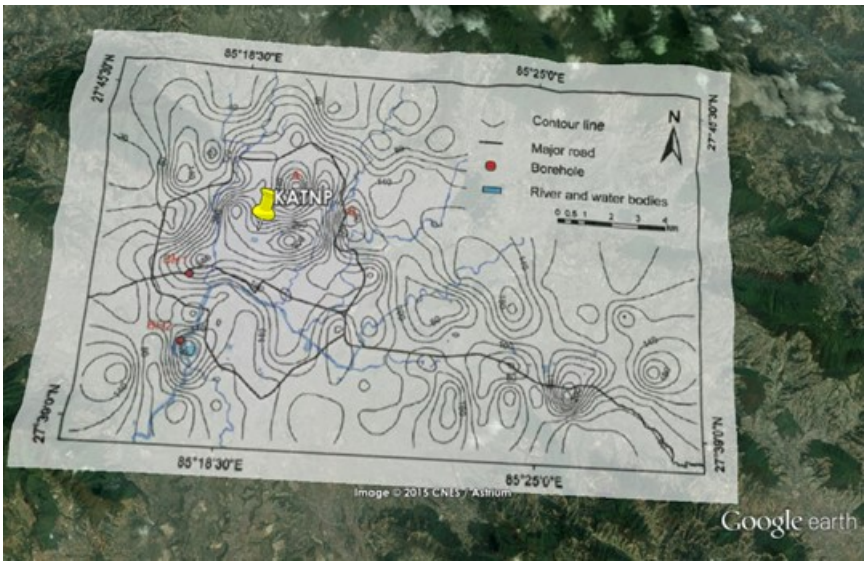

Figure 4-15 Contour map of the basement topography of the Kathmandu Basin and location of station KATNP (from Paudyal et al, 2012b).

The depth of sediments at the station as estimated by Paudyal et al (2012b) doesn't adequately explain the 0.2 s reverberating pulse of the mainshock: assuming Vs_{30} = 200 m/s and a quadratic increase in stiffness with confining pressure, the fundamental mode of the soil column below KATNP is approximately 2 s. Nor could the elongation of the pulse to 5 s be the result of a widespread nonlinear response, since this would require the entire 250 m deep soil column to be subjected to strains large enough to cause yielding. A working hypothesis is that the 5 s pulse corresponds to lateral resonance of the basin, and that the long period waves of the mainshock are primarily surface waves. To test this hypothesis, we use the approximation of Bard and Bouchon (1995) for a 2D sedimentary valley of depth *h* and width 2*l*. In that case, the resonant frequency of reverberating Rayleigh waves is:

$$f_0 = \frac{V_s}{2l}\sqrt{(1 + (2.9 \times h/l)^2} \qquad [1]$$

Assuming Vs_{30} = 200 m/s and a quadratic increase in stiffness with confining pressure, the average Vs of the soil column is approximated as 2000 m/s. Next, based on the overlay of Figure 4-15 the average width of inclusion I is estimated to be approximately 5 km in diameter. Substituting in equation [1], the fundamental mode of the inclusion (with the assumption of 2D conditions) is calculated as f_0= 0.20 Hz or T_0 = 5 s, which corresponds to the mainshock's observed reverberating pulse. Although this result is only a crude approximation of a hypothetical scenario, it is indicative of the potential role of the lateral resonance of the basin on the strong motion recorded at KATNP station. This working hypothesis is being further investigated by members of the reconnaissance team.

Additional three dimensional site effects that were observed in the damage patterns of structures and soil failure include basin edge and topographic effects along the top of ridges. The mechanisms of both phenomena are qualitatively shown in Figure 4-16. With additional strong motion data, particularly from rock sites surrounding the Kathmandu basin, these effects can be better quantified in future studies. Due to lack of such data at the time of writing, we resort to demonstrating these effects by means of site-specific case-studies in the following sections.

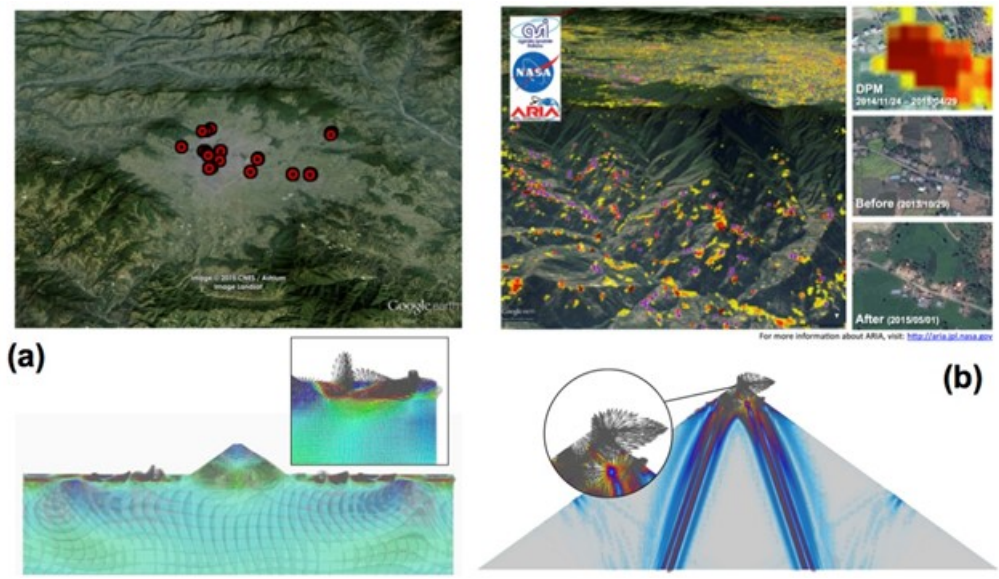

Figure 4-16 Evidence of 3D site effects: (a) Severe damage documented by the GEER team (red dots) near the basin edges, and likely causative mechanism of basin-edge generated surface waves (from Asimaki, 2015); (b) Ridge-top damage interpreted from satellite image decorrelation before and after the mainshock (ARIA, JPL and Caltech), and likely causative mechanism of topographic amplification (from Mohammadi, 2014).

4.5 Basin Edge Effects

Similar to Northridge (1994) and Kobe (1999) earthquake, severe damage has been observed adjacent to basin edges around the Kathmandu Valley after April 25 M7.8 earthquake and subsequent aftershocks. In narrow and deep basins, such as Kathmandu Valley, during earthquakes body waves transform into surface waves creating two dimensional (2D) resonance especially at the basin edges (Iyisan and Hasal, 2011) which may result in significant amplification in the surface ground motion. The severe damage observed along the basin edges of Kathmandu Valley in Bhaktapur, Patan, and Sakhu indicates the potential amplification due to basin edge. Most of the building stock in Sakhu and Bhaktapur either collapsed or suffered severe damage after the Gorkha Earthquake. Figure 4-17a shows the observed damage distribution within the Kathmandu valley. The two main locations where the damage due to ground shaking is concentrated is in the center of the Kathmandu Valley, the damage in the center of the valley is most likely due to site amplification caused by the sedimentary basin. Significant damage has also been observed along the basin edges, especially around Bhaktapur and Sakhu where most of the old structures were collapsed. At these locations the observed damage and higher intensity of the ground shaking (Figure 4-17b) is most probably an indicator of the influence of the basin edge effects.

Figure 4-18 plots the localized liquefaction zones observed in the Kathmandu Valley. Given the liquefaction susceptible nature of the sedimentary basin of the Kathmandu Valley (Piya, 2004), localized liquefaction along the edges of the Kathmandu Valley is another strong indicator of the ground motion amplification as a result of basin edge effects.

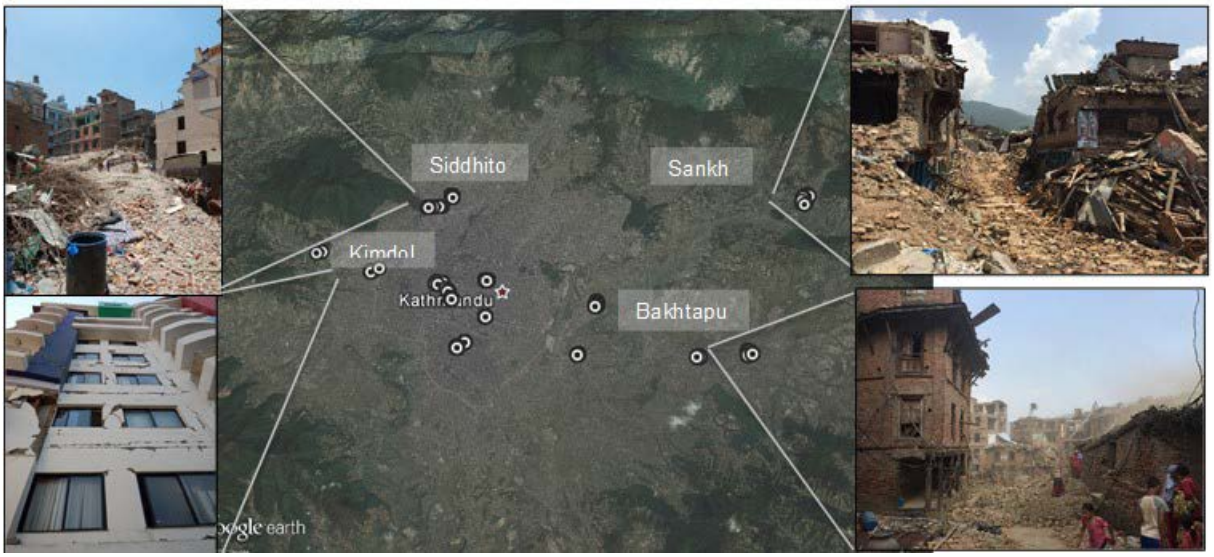

(a) Siddhito: 27°44'7.32"N 85°18'33.81"E, Kimdol: 27°42'35.55"N 85°16'49.09"E, Sakhu: 27 43' 49.5"N 85 27' 52"E, Bakhtapur:27 40' 13.2"N 85 25' 48.8"E.

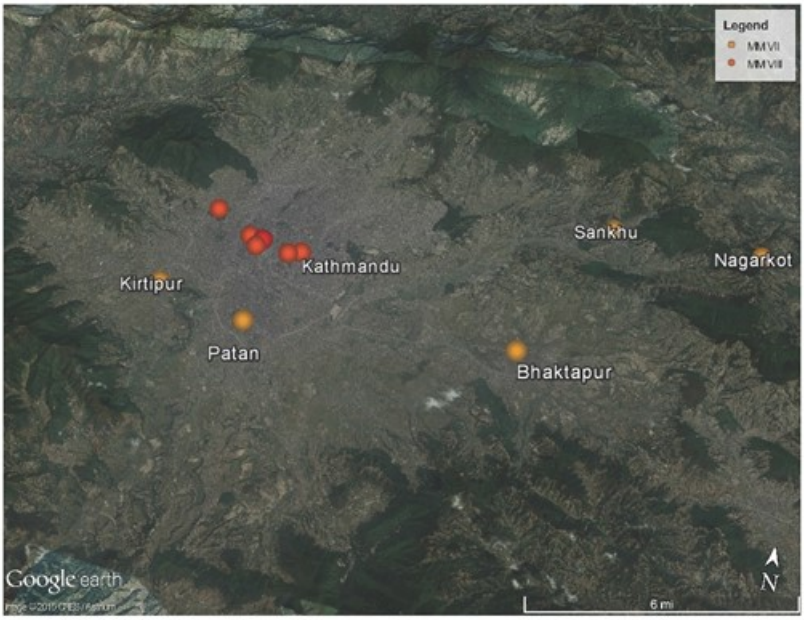

(b) Orange MMI=VII, Red MMI=VIII.

Figure 4-17 Damage distribution in the Kathmandu Valley (a) location of observed building damage, (b) Modified Mercalli Intensities assigned to main cities Kathmandu Valley (GeoNames.org).

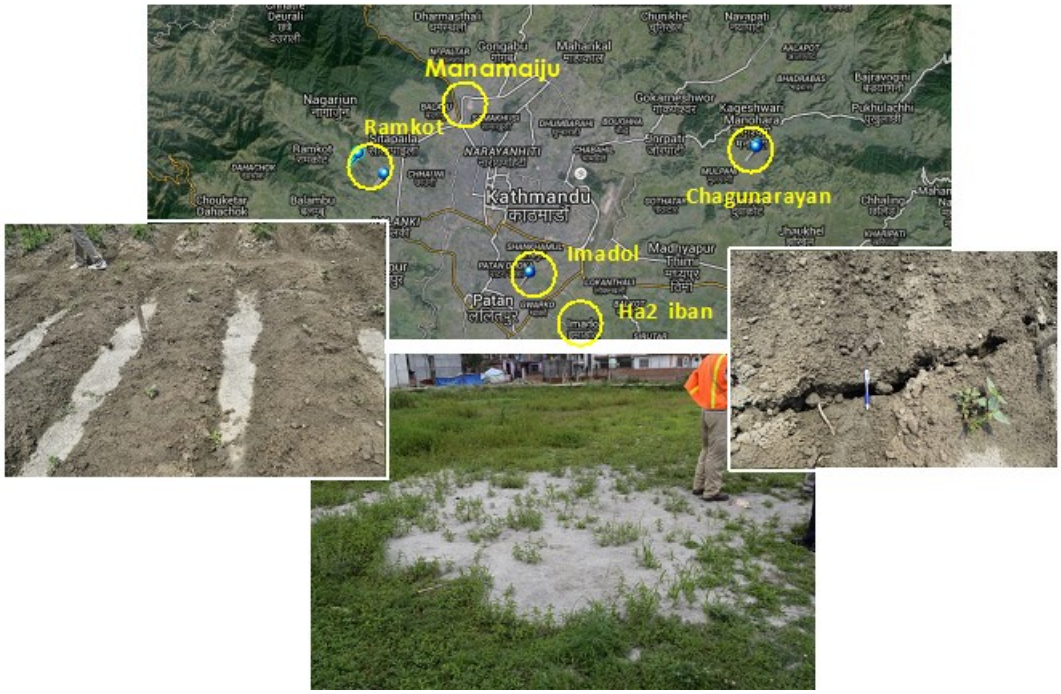

Figure 4-18 Basin edge effects as evidenced by liquefaction

4.6 Topography Effects

Topography effects refer to the modification (frequently amplification) of incident ground motion due to energy focusing effects at convex topographic features (hills, ridges, canyons, cliffs, and slopes), complicated subsurface topography (sedimentary basins, alluvial valleys), and geological lateral discontinuities (e.g., ancient faults, debris zones). These features can significantly alter the intensity, frequency content and duration of ground shaking during earthquakes compared to the shaking that the same site would have experienced, had it been on flat ground. Examples of records and damage observations attributed in part to topographic amplification are the PGA=1.82g recording of the hilltop Tarzana station during the 1994 Northridge Earthquake, the Pacoima Dam (PGA=1.12g) recording during the 1971 San Fernando earthquake, the recent extraordinary ground motion (PGA=2.74g) recorded at KIK-Net station MYG004 during the 2011 Tohoku Earthquake on the crest of a 5m high, steep man-made slope.

Topography effects dominated to a large extent the ground response and ground failure effects observed during the M7.8 Gorkha earthquake sequence, that is the structural damage and ground failure (slope stability failure) distribution patterns. Structural damage was specifically concentrated at the top of isolated hills within the valley such as the one depicted in Figure 4-21, at hilltops within and surrounding the edges of the Kathmandu valley (see Figure 4-19 and Figure 4-20), and at the hilltops and ridge crests of the mountainous country-side (see Figure 4-21 and Figure 4-22). A particular case of note is the total collapse for the historic Duguna Gadhi Fort (Figure 4-23) whereby cracking was observed all around the mountain top and sides and is hence characterized as a shattered ridge. Slope stability failure, on the other hand, was extensive –despite the fact that it was the end of the dry season when slope stability hazard is minimum— that it will be presented separately in Chapter 5.

The damage patterns in Nepal related to topography effects serve as reminders that although regional and site-specific response studies are increasingly relying on simulated ground motions, they are lagging in the understanding, simulation and parameterization of topography

effects: on one end, the majority of seismological models lack resolution and geotechnical input in the frequency range of engineering applications, and on the other, site-specific response analyses have become almost synonymous with the study of flat ground surfaces with horizontal soil stratigraphy. Consequently, seismic code provisions, microzonation studies and ground motion prediction equations do not account for 3D site effects, despite the numerous cases of documented evidence on their role in elevating seismic risk—such as the damage patterns that we observed in Nepal during reconnaissance.

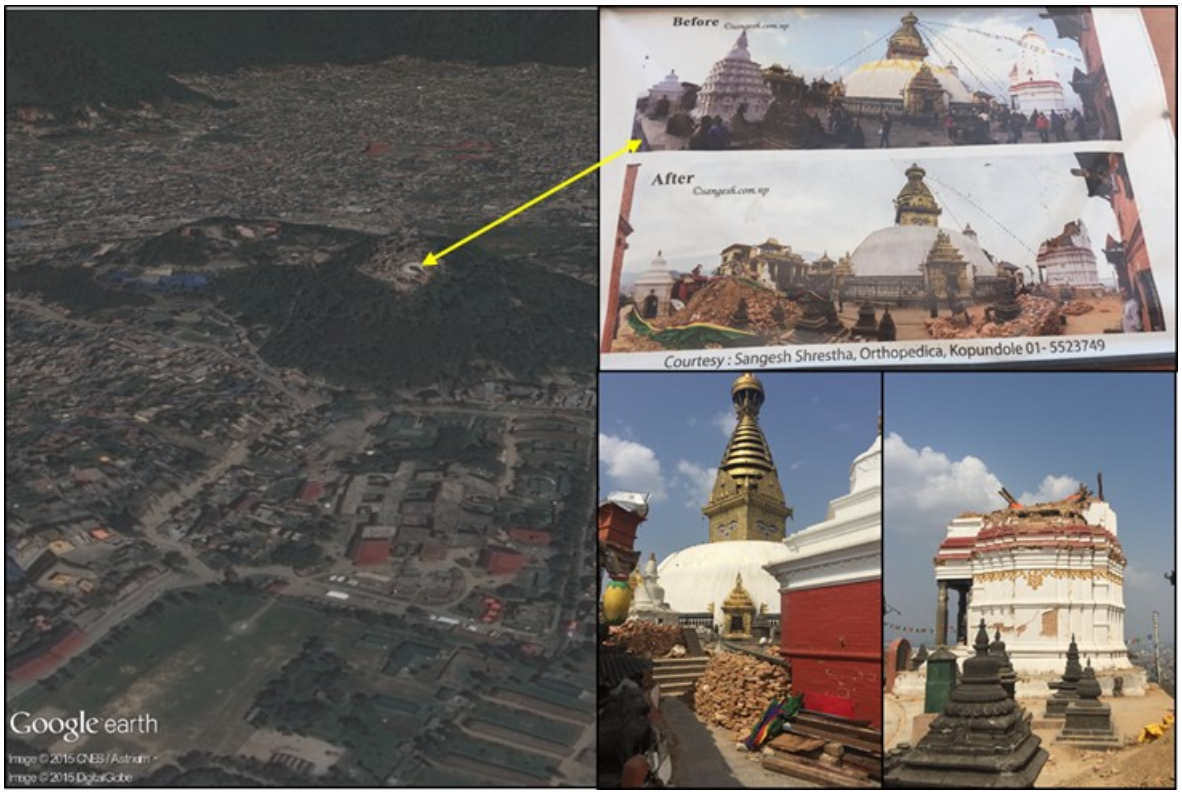

Figure 4-19 Damage in Swayambhu (Monkey) Temple (27.715270 N, 85.290231 E).

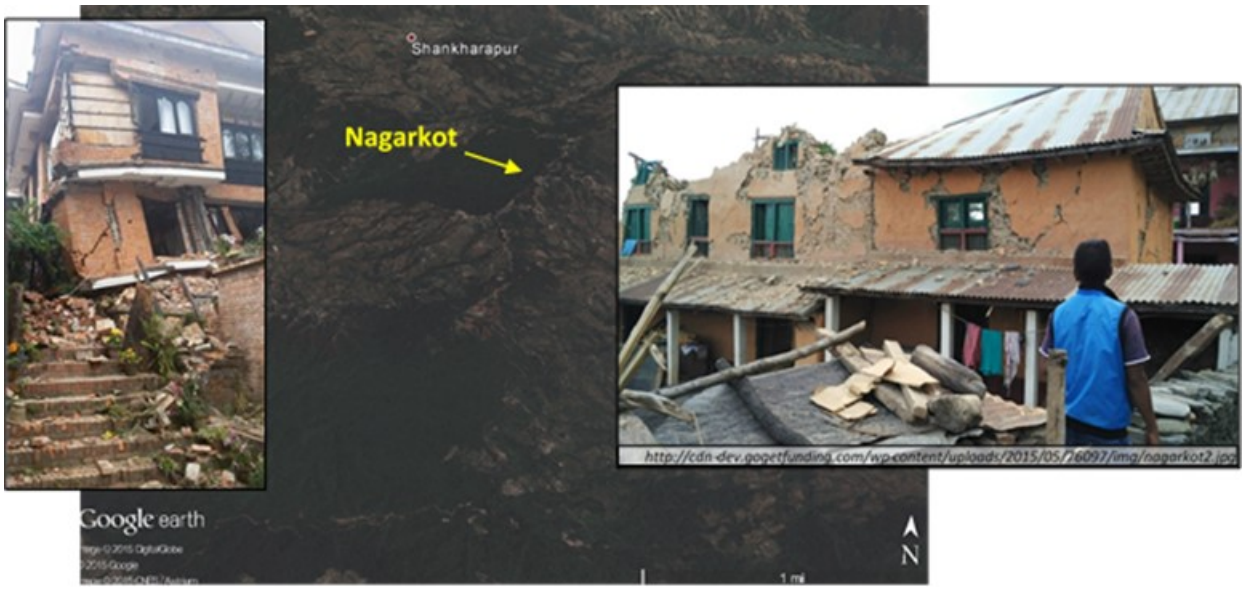

Figure 4-20 Damage in Nagarkot. (27.708109N, 85.510193E).

Figure 4-21 Ridge top damage and school collapse, Simi Gaun, near upper Tamakoshi Dam, (27 52’ 22.5” N, 86 13’ 50.6” E).

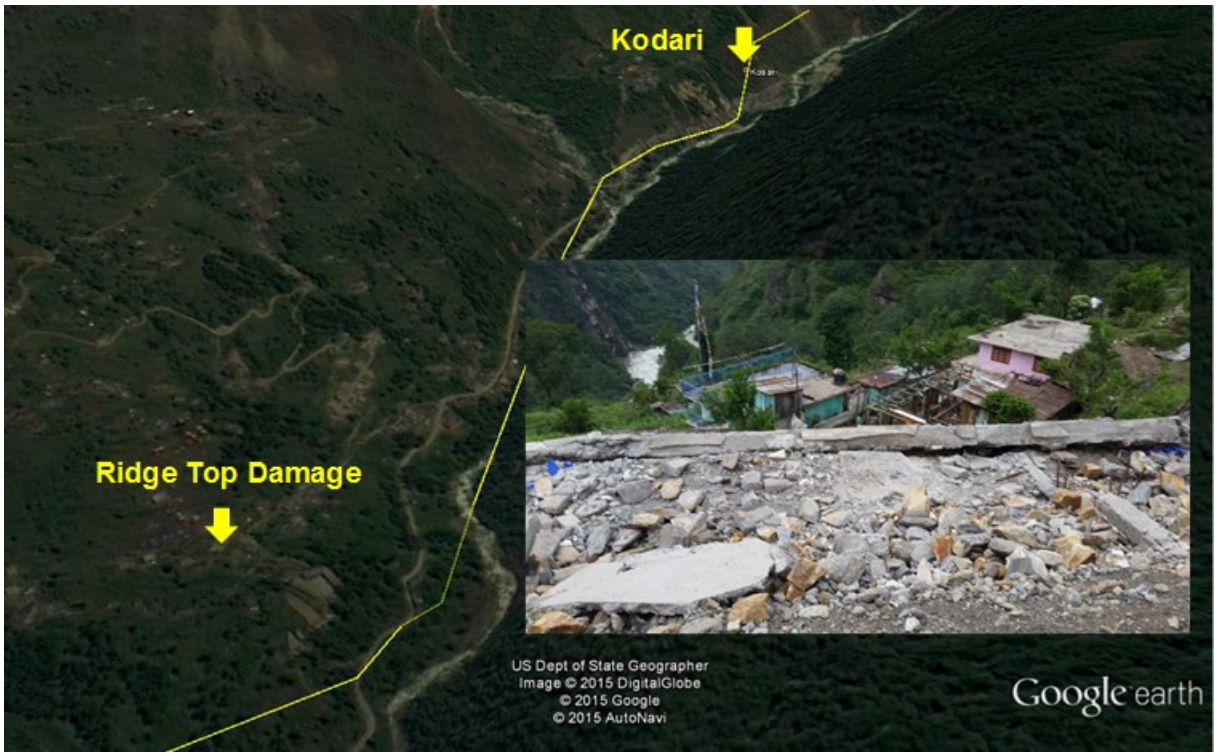

Figure 4-22 Ridge top damage and structure collapse, south of Kodari, near Chinese border (27 57’ 31.9” N, 85 57’ 17.7” E).

Figure 4-23 Shattered Ridge, Duguna Gadhi Fort (27 54’ 59.4” N, 85 55’ 2.38” E).

4.7 References

Ambraseys N and Douglas J (2004). Magnitude Calibration of North Indian Earthquakes, Geophysical Journal International, 159(1): 165–206.

Asimaki, D. (2015). Understanding, simulation and parameterization of 3D topography effects, Seismological Society of America 2015 Annual Meeting, Pasadena, CA, April 29-May 1.

Assimaki, D., Li, W., Steidl, J. H., & Tsuda, K. (2008). Site amplification and attenuation via downhole array seismogram inversion: A comparative study of the 2003 Miyagi-Oki aftershock sequence, Bulletin of the Seismological Society of America, 98(1), 301-330.

Bard, P-Y and M. Bouchon (1995). The two-dimensional resonance of sediment-filled valleys. Bull. Seism. Soc. Am., 75, pp. 519–541. 15

Chitrakar, G.R., Pandey, M.R. (1986). Historical earthquakes of Nepal, Bulletin Geological Society of Nepal 4, 7–8.

Dixit A, Dwelly-Samant L, Nakarmi M, Pradhanang S and Tucker B (1998). The Kathmandu valley Earthquake management plan, Published by National Society for Earthquake Technology-Nepal, pp. 38.

Field, E. H., & Jacob, K. H. (1995). A comparison and test of various site-response estimation techniques, including three that are not reference-site dependent, Bulletin of the seismological society of America, 85(4), 1127-1143.

Hagen, T. (1969). Report on the geological survey of Nepal, Denkschr Schweizerischen Naturforschenden Gesellschaft 81, 185.

JICA (2002), The Study on Earthquake Disaster Mitigation in the Kathmandu Valley Kingdom of Nepal, Japan International Cooperation Agency (JICA) and Ministry of Home Affairs His Majesty's Government of Nepal, Volume I 2002, Summary p. 110, Volume III, Main Report 2/2, Earthquake Disaster Assessment and Data Base System, pp. 76.

Katel, T.P., Upreti, B.N., Pokharel, G.S. (1996). Engineering properties of fine grained soils of Kathmandu Valley Nepal, Journal of Nepal Geological Society 13, 121–138.

Lachet, C., Hatzfeld, D., Bard, P. Y., Theodulidis, N., Papaioannou, C., & Savvaidis, A. (1996). Site effects and microzonation in the city of Thessaloniki (Greece) comparison of different approaches. Bulletin of the Seismological Society of America, 86(6), 1692-1703.

Mohammadi, K. (2014). Scattering of In-Plane Waves by Elastic Wedges, American Geophysical Union 2014 Fall Meeting, San Francisco, CA, December 15-19.

Moribayashi, S., Maruo, Y. (1980). Basement topography of the Kathmandu Valley, Nepal – an application of the gravitational method to the survey of a tectonic basin in the Himalaya. Journal of Japan Society of Engineering Geology 21, 30–37.

Mugnier JL, Huyghe P, Gajurel AP, Upreti BN and Jouanne F (2011). Seismites in the Kathmandu Basin and Seismic Hazard in Central Himalaya, Tectonophysics, 509 (1-2): 33–49.

Nakamura Y (1989). A Method for Dynamic Characteristics Estimation of Subsurface Using Microtremor on the Ground Surface, Quarterly Report of the Railway Technical Research Institute, 30(1): 25–33.

Nakata, T., Kumura, K., Rockwell, T. (1998). First successful paleoseismic trench study on active faults in the Himalayas. Proceedings of AGU 1998 Fall Meeting: Eos, Transactions AGU, 79, p. 45.

Paudyal, Y. R., Yatabe, R., Bhandary, N. P., & Dahal, R. K. (2012). A study of local amplification effect of soil layers on ground motion in the Kathmandu Valley using microtremor analysis. Earthquake Engineering and Engineering Vibration, 11(2), 257-268.

Piya, B. K. (2004). Generation of a geological database for the liquefaction hazard assessment in Kathmandu Valley, Natural Hazard Studies. Enschede, The Netherlands, ITC.

Rana, B.J.B. (1935). Nepal Ko Maha Bhukampa (Great Earthquake of Nepal), Jorganesh Press.

Sakai, H. (2001). Stratigraphic division and sedimentary facies of the Kathmandu Basin Group, central Nepal. Journal of Nepal Geological Society 25, 19–32 (special issue).

Sakai, T., Takagawa, T., Gajurel, A.P., Tabata, H., O'I, N., Upreti, B.N. (2006). Discovery of sediment indicating rapid lake-level fall in the late Pleistocene Gokarna Formation, Kathmandu Valley, Nepal: implication for terrace formation. Quatern. Res. 45, 99–112.

Stöcklin, J., Bhattarai, K.D. (1981). Geology of Kathmandu area and central Mahabharat Range, Nepal Himalaya. United Nations Development Program, Mineral Exploration Nepal (DP/UN/NEP-73-019/3). p. 64.

Upreti, B.N., Yoshida, M. (2009). Seismic Hazard and Mitigation Activities in Nepal, with Emphasis on Kathmandu Valley, Journal of South Asia Disaster Studies 2 (1), 1–19.

Yoshida M and Igarashi Y (1984), Neogene to Quaternary lacustrine sediemnts in the Kathamandu Valley, Nepal, Journal of Nepal Geological Society, 4: 73–100.

5 Slope Stability and Landslides

5.1 Introduction

With elevations in Nepal ranging from 100 to 8,848 m above msl from south to north over a distance of approximately 120 km, topographic relief is exceptional and the characteristically steep slopes and vulnerable to landslides. The average annual human death toll related to landslides over the past 40 years exceeds 110 lives, and approximately 100,000 households are adversely impacted by landslides each year (Nepal Ministry of Home Affairs, 2014). The average annual property loss due to landslides was reported to be over US$1,000,000 (Nepal Ministry of Home Affairs, 2014). In the past, isolated landslides have killed over 100 people in a single landslide. As an example, the Jure Landslide occurred on August 5, 2014 in response to heavy rainfall and blocked the Sun Koshi River and resulted in more than 168 deaths. Although landslides in Nepal typically occur during the monsoon season, significant earthquake-induced landslides have occurred in the past, including the Okharpauwa, Tigaun, and Ilam landslides (Tiwari and Marui, 1998). The April 25, 2015 earthquake and its related aftershocks triggered significant landsliding that killed hundreds of people, blocked several roads, buried villages, and dammed natural rivers. However, considering that the 2015 Gorkha earthquake occurred in a dry climatic period (two months prior to the monsoon season) the extent of landsliding is much less than expected for the worst-case condition of saturated ground conditions and high antecedent moisture conditions.

Interpretation of satellite imagery taken prior and subsequent to the earthquake by the GEER team indicate that the earthquake triggered more than 6,000 new or reactivated landslides within the Sindhupalchok District alone (Ziselsberger, 2016). An example of pre-and-post earthquake satellite imagery is shown in Figure 5-1, and the preliminary landslide inventory map in the Sindhupalchok District is depicted in Figure 5-2.

Figure 5-1 Satellite imagery from December 2014 (left) and May 2015 (right), 27°52'3.57"N, 85°39'5.41"E. Light scars in right image indicate areas of earthquake-induced landsliding.

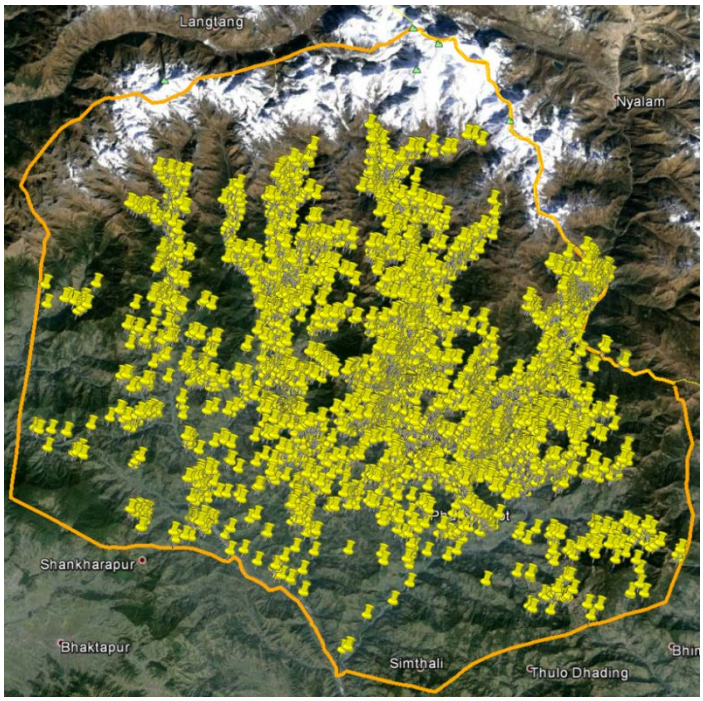

Figure 5-2 New and reactivated landslides in the Sindhupalchok District resulting from the 2015 Gorkha Earthquake and related aftershock sequence. Orange line indicates boundary of Sindhupalchok District and pin marks indicated locations of individual landslides (from Ziselsberger, 2016)

Detailed descriptions of significant earthquake-induced landslides observed by the GEER team in the field are enumerated below. The landslides discussed here have been presented by route (land/air) or by specific slide location. A more comprehensive description of the landslides from this event can be found in Collins and Jibson (2015).

5.2 Damage along the Prithvi Highway

Along the Prithivi Highway only localized instances of earthquake-induced landsliding were observed (Figure 5-3). Figure 5-4 depicts the Krishnabhir Landslide, which existed prior to the earthquake but was not reactivated during the 2015 Gorkha Earthquake.

Check dams constructed to retain landslide debris adjacent to the Marshyandgi Hydropower project generally performed well (Figure 5-5); however, minor rockfalls along a road cut were observed (Figure 5-6). Additionally, irrigation channels were locally affected by earthquake induced landslides (Figure 5-7). The landslides mainly involved near-surface regolith and weathered bedrock, and appear to have mobilized primarily as raveling failures, rock slides, and rock falls.

Figure 5-3 Typical landslides observed along Prithivi Highway alignment.

Figure 5-4 Pre-exisitng Krishnabhir Landslide, which performed well during the 2015 earthquake.

Figure 5-5 Check dams near the powerhouse of Marshyangdi Hydropower Project, which performed well during the 2015 earthquake (27°52.5'0"N 84°32.4'0"E).

Figure 5-6 Rockslides observed at the Marshyangdi Hydropower Project dam site during the 2015 earthquake mainshock.

Figure 5-7 An irrigation channel alignment affected by rockslide.

5.3 Araniko Highway

The Araniko Highway extending east from Kathmandu to the Nepal-China border at Kodari suffered severe landslide damage and was among the most adversely affected highways. Along the road sector from Panchkhal through the Sindhupalchok District along the Sunkoshi River to Kodari in eastern Nepal, landslide effects became progressively severe with increasing elevation northward. Translational block slides and rock falls rendered the highway impassible in numerous locations between Kilometer marker zero and the Indrawati River Bridge. Several river bank failures downslope of the highway threatened to undermine the roadway. The majority of prior landslide mitigation works such as gabion baskets and subsurface drainage improvements appeared to have functioned well, although select structures were affected by fresh landslide activity.

As the Araniko Highway traverses north along the Sunkoshi River, the roadway was increasingly damaged by rock slides emanating from steeper and higher slopes along the roadway. Severe damage as a result of landsliding was evident in nearly all the towns and villages along the Sunkoshi River. The majority of observed landslides were rockfall and rock slides resulting from blocks sliding and releasing along joint planes. A very significant landslide that blocked the Sunkoshi River at Naglwitz in December, 2014 did not reactivate during the 2015 Gorkha Earthquake. The Sunkoshi River was blocked for a short period of time by an earthquake-induced landslide dam near the village of Listikot (Figure 5-9). The landslide dam was about 20 m high and 30 m wide, made of poorly sorted rock and soil debris, and was the result of a large rock slide that released from joint surfaces within a near-vertical 200 m high slope adjacent to the river. The landslide dam was breached prior to GEER observations. No apparent damage was attributed to the landslide dam.

Landsliding and rock fall damage along the Araniko Highway was nearly continuous within several kilometers of Kodari and the Nepal-China border. The bridges that crossed the Sunkoshi River near Kodari, including the “Friendship Bridge” at the Nepal-China border, were mostly undamaged. The town of Kodari was destroyed by large rock falls from the near vertical slopes that resulted in boulders up to 4 m in diameter impacting buildings (Figure 5-9) and automobiles (Figure 5-10) along the narrow roadway.

The road sector from Panchkhal to Tatopani was impacted significantly by new and reactivated landslides (Figure 5-11 through Figure 5-15). The majority of the landslide mitigation works such as gabion baskets and subsurface drainage improvements appeared to be functioning well (Figure 5-16) although localized damage to such structures was observed (Figure 5-17), together with shallow failure of roadside embankment fill, (Figure 5-18). Identified significant concern along this road sector relates to the potential for future large landslides and slope failures triggered high above the roadway. Such landslides may not only block and damage the road but, also potentially block the natural flow of Sunkoshi River (Figure 5-19). Additionally, several potential landslides appear to threaten the existing villages along the highway (Figure 5-20).

Figure 5-8 Landslide dam near the village of Listikot on the Sunkoshi River adjacent to the Araniko Highway (27° 52' 43.22" N; 85° 54' 12.17" E).

Figure 5-9 Destroyed building along Araniko Highway in Kodari (27° 58' 17.61" N; 85° 57' 43.51" E).

Figure 5-10 Destroyed vehicles along Araniko Highway in Kodari (27° 58' 21.55" N; 85° 57' 46.18" E)

The road sector from Panchkhal to Tatopani was significantly affected by rockslides at multiple locations, landslides along the highway, and reactivation of old landslides (Figure 5-11 through Figure 5-15). Majority of the landslide prevention works such as gabion retaining walls and subsurface drainage networks implemented in previously triggered landslide sites appear to have functioned well (Figure 5-16) although a few of those structures got affected (Figure 5-17) by fresh landslides and road side fissures (Figure 5-18) created by the ground shaking. The major issue identified in this road sector is the potential for the initiation of large landslides and slope failures triggered on top of the ridge that may not only block and damage the road but also have the potential to block the natural flow of Sunkoshi River (Figure 5-19). Moreover,

several such potential landslides threaten the current settlement along the highway (Figure 5-20).

Figure 5-11 Typical landslide observed at the Panchkhal-Dolalghat sector of the Araniko Highway.

Figure 5-12 Extent of the landslides observed a few kilometers ahead of Dolalghat at Araniko Highway.

Figure 5-13 Typical rockslide mass observed along the Dolalghat-Lamo Sangu Sector of the Araniko Highway.

Figure 5-14 Reactivation of an existing landslide along the Araniko Highway that was triggered due to stream undercutting (27°44.7'0"N 85°47.5'0"E).

Figure 5-15 Landslide observed along the Dolaldhat – Lamosangu sector of the Araniko Highway.

Figure 5-16 A subsurface drainage work installed at a landslide site along the Araniko Highway performed well during the earthquake.

Figure 5-17 Gabion Retaining wall implemented as the landslide prevention work for existing landslide tilted after the 2015 earthquake.

Figure 5-18 Typical road fill settlement observed along the Araniko Highway.

Figure 5-19 Typical cracks observed on the ridge of the mountain which has potential to trigger large scale landslides and block the Sunkoshi River.

Figure 5-20 Residential area along the Araniko Highway near Lamosangu exposed to potential landslides.

5.4 Lamosangu- Manthali Highway

Due to the close proximity of the Lamosangu-Manthali Highway to the epicenter of the Mw7.3 aftershock, this highway was significantly affected by ground shaking. The characteristics of landslides were similar to those observed in other areas – rock falls that blocked several sections of the road (Figure 5-21 and Figure 5-22), raveling, and ground fissures and sloughing inducing settlement of road fills.

Figure 5-21 Typical rockfall observed along Lamosangu – Manthali Road

Figure 5-22 Boulder that rolled down from a ridge onto the road.

5.5 Melamchi Water Supply Project Access Road

The Melamchi Water Supply Project access road was also affected by many landslides. Landslide characteristics were similar to other areas, including raveling failures (Figure 5-23 and Figure 5-24), and rock falls (Figure 5-25). Earthquake shaking induced sloughing of roadside fill materials (Figure 5-26). At several locations, loose boulders were observed near the head scarp of the landslide mass (Figure 5-27). Although many retaining structures were effective in retaining landslide debris (Figure 5-28), several such structures were damaged due to sloughing of road fill materials (Figure 5-29). Cracks were observed along the bank of the river near a bridge abutment, which can potentially result in further slope movement in future (Figure 5-30). A large scale rockslide observed could potentially block the river in future, considering that its head scarp extends several hundred meters above the roadway (Figure 5-31). This rock slide was still active during the field visit on May 16, 2015 (Figure 5-32).

Figure 5-23 Typical rockfall source observed along the Melamchi Water Supply Project Access Road.

Figure 5-24 Dense landslides along the alignment of Melamchi Water Supply Project Access Road (27°49.8'0"N 85°34.5'0"E).

Figure 5-25 Boulder that rolled down a slope after the mainshock.

Figure 5-26 Settlement crack along the roadway.

Figure 5-27 Loose boulders on top of a slope.

Figure 5-28 Walls performed well during ground shaking.

Figure 5-29 Damage to retaining wall due to excessive settlement and ground shaking.

Figure 5-30 Settlement cracks observed along a bridge abutment.

Figure 5-31 A rockslide that poses a potential hazard to the roadway and below.

Figure 5-32 Rockfall, as evidenced by the dust, observed during field reconnaissance (27°58.5'0"N 85°33.9'0"E).

5.6 Ramkot Area, Kathmandu Valley

A landslide fissure was observed at the ridge of Ramkot Village, which is located at the edge of the Kathmandu Valley (Figure 5-33). The extensive fissure is more than 15 cm wide (Figure 5-34).

Figure 5-33 Head scarp observed on the ridge of the slope triggered by the 2015 earthquake.

Figure 5-34 Head scarp crack was wider than 15 cm.

5.7 Kathmandu - Lama Bagar Air Route

Several landslides were observed along the roads and river banks on the aerial reconnaissance route from Kathmandu to Lama Bagar (Figure 5-35) and along the river terrace slopes which might predated the earthquake (Figure 5-36). Several rural roads were affected by seismic induced landslides (Figure 5-37 through Figure 5-39). Ridge lines along the

Sunkoshi River are locally highly fractured (Figure 5-40 through Figure 5-44) and may potentially experience additional significant activity during the monsoon season. Some of these landslide deposits contain large boulders (Figure 5-45 and Figure 5-46) can potentially be destabilized during the monsoon season or future seismic events.

The access road to the Upper Tamakoshi Hydro Power project, in particular the Singati-Lama Bagar Sector (Figure 5-47 through Figure 5-52) is amongst the most heavily affected areas. The majority of the road alignment was rendered impassable due to landslide activity. The road is narrow and was constructed across very steep topography, exacerbating the impacts of the recent earthquake. Although gabion retaining walls generally performed well, with localized incidents of damage. Both the upstream and downstream areas from the dam site of the Hydro Power Project were affected by multiple rock fall events (Figure 5-53 through Figure 5-55). The boulder sizes, having travelled a distance of over 100 m, indicate high levels of ground shaking (Figure 5-56 and Figure 5-57). However, no ground motion observation data was available in the area.

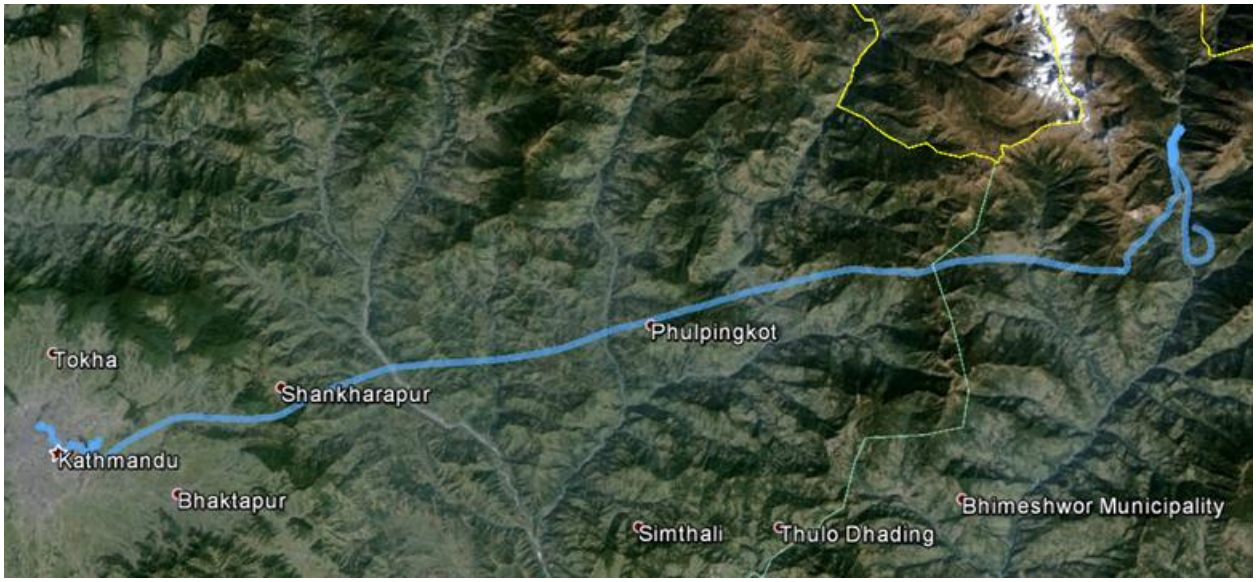

Figure 5-35 Helicopter route from Kathmandu to Lamabagar.

Figure 5-36 Landslide along the river bank at Indrayani, near Kathmandu Valley.

Figure 5-37 Mountain roads that have been affected by landslide triggered by the 2015 Earthquake.

Figure 5-38 Landslides that have affected several mountain roads along the air-route.

Figure 5-39 Small landslide triggered by the earthquake affected a road and a village along the air-route to Lamabagar.

Figure 5-40 Fissures created on the ridge of mountain due to the earthquake shaking.

Figure 5-41 Seismically triggered landslide on a ridge.

Figure 5-42 Slope vulnerable to post-earthquake rainfall induced landslides that could potentially block the natural stream.

Figure 5-43 Settlement at along a bank near a potential landslide.

Figure 5-44 Landslide fissures triggered by the recent earthquake along the hillslope.

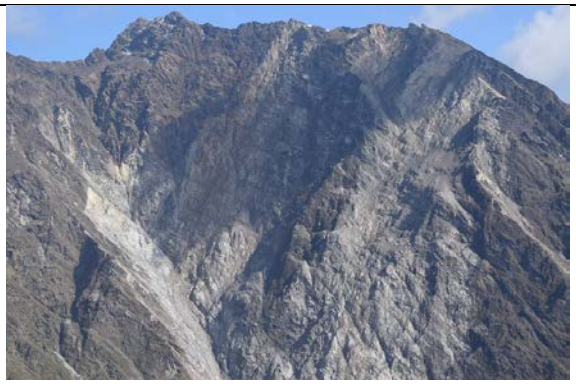

Figure 5-45 Potential large debris flow source during rainy season.

Figure 5-46 Source of landslide.

Figure 5-47 Locations with large scale landslide potential along the Charikot-Lamabagar Road.

Figure 5-48 Charikot-Lamabagar road sector affected by landslides triggered due to the earthquake.

Figure 5-49 Gabion retaining walls that did not perform well along the Charikot-Lamabagar Road.

Figure 5-50 landslides observed along the road alignment constructed along steep terrain.

Figure 5-51.Large scale landslides that affected the Charikot-Lamabagar Road sector

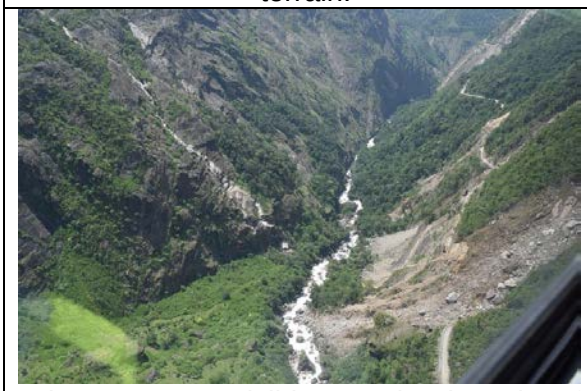

Figure 5-52 Landslide near the dam site of the hydropower project that damaged the road.

Figure 5-53 Landslides observed along dam site of the Upper Tamakoshi Hydropower project

.

Figure 5-54 Rockfall upstream of the hydropower project.

Figure 5-55 Large boulder from the top of the slope near the dam site.

Figure 5-56 Local shop destroyed by the boulder.

5.8 Kathmandu – Duipipal – Tupche – Dhunche – Langtang Khola – Syaprubesi – Rasuwagadi Aerial Route

This area of Nepal (Figure 5-57) was also significantly affected by earthquake triggered landslides. In particular, the region between Nuwakot and Rasuwagadi exibited many dry, raveling-type landslides (Figure 5-58 through Figure 5-60). Several of these landslides blocked the Trishuli River and its tributaries (Figure 5-61 through Figure 5-71) and also affected villages. Several hydropower projects, including the Chilime, Rasuwagadi and Trishuli were adversely impacted by the landslides (Figure 5-72 through Figure 5-74). Access roads to these hydropower projects and majority of the gabion retaining walls constructed along them were damaged by the landslides. Villages situated both above and below the landslides may be at risk due to the potential for landslide reactivation during the monsoon season or future ground shaking (Figure 5-75 through Figure 5-81). Large perched and precarious boulders were also observed above the villages. At several locations along the Trishuli River up to the Nepal - Chinaborder, massive landslides completely or partially blocked the Trishuli River (Figure 5-82).

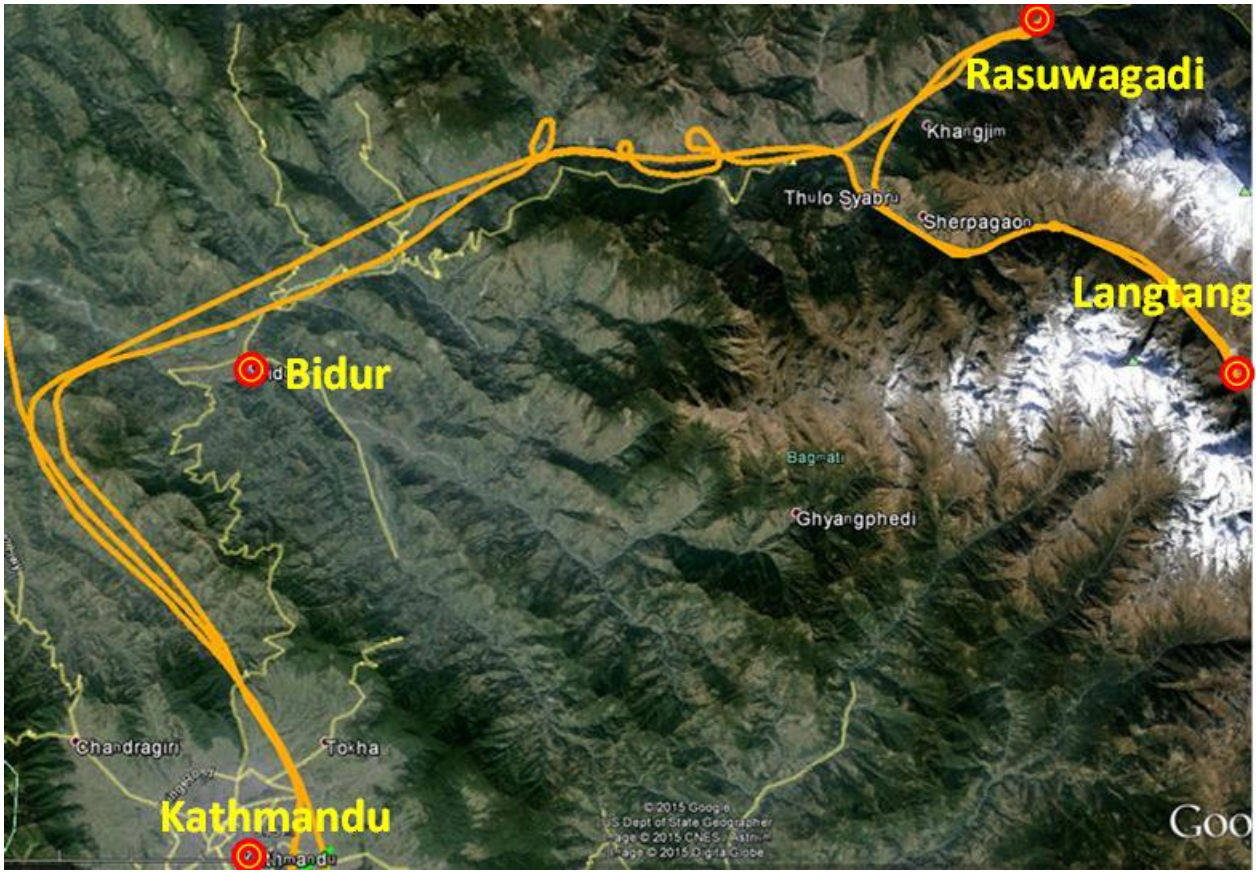

Figure 5-57 Air route Kathmandu - Langtang – Rasuwagadi – Kathmandu.

Figure 5-58 Landslides triggered by the earthquake along steep slope along the Trishuli-Dhunche Road.

Figure 5-59 Local feeder road to the Trishuli-Rashuwagadi Road impacted by the landslide.

Figure 5-60 Gabion retaining walls on the feeder road to the Trishuli-Rasuwagadi Road damaged by the earthquake.

Figure 5-61 Access road to a Hydropower project being affected by the earthquake induced landslides.

Figure 5-62 Tributary of the Trishuli Rivers partially blocked by the earthquake induced landslide debris.

Figure 5-63 Slopes along both banks of the Trishuli River being affected by the seismically triggered landslides.

Figure 5-64 Large landslide along the Trishuli River.

Figure 5-65 Landslide debris partially blocks the Trishuli River near a hydropower project.

Figure 5-66 Landslide debris adjacent to the Trishuli River.

Figure 5-67 Tributary of the Trishuli River partially blocked by the landslides triggered on both sides.

Figure 5-68 A large scale seismically induced landslide that partially blocked the Trishuli River.

Figure 5-69 Water inundation along Trishuli River due to landslide induced natural dam formation.

Figure 5-70 A large scale landslide not only blocked Trishuli River, note the village above the headscarp.

Figure 5-71 Closer view of the landslide dam at the Trishuli River (28°14.9'0"N 85°27.6'0"E)

Figure 5-72 A hydropower project with multiple landslide on its upstream side.

Figure 5-73 Upstream side of a hydropower project affected by large scale landslides.

Figure 5-74 Landslides damaging the desilting basin area of a hydropower project.

Figure 5-75 Regular road sector of the Trishuli-Rasuwagadi Road affected by landslides.

Figure 5-76 Boulders above villages.

Figure 5-77 Villages below a large pre-existing landslides.

Figure 5-78 A village close to a large landslide site that could potentially block the Trishuli River.

Figure 5-79 Access road sector of a hydropower project affected by an earthquake induced landslide.

Figure 5-80 A village near Dhunche heavily damaged by the landslide debris originating from a slope above the village.

Figure 5-81 A village above a large scale landslide that has potential to block the Trishuli River.

Figure 5-82 Trishuli River near the Chinese border at Rasuwagadi partially blocked by large landslides.

Landslides were also observed along both sides of the Langtang River (Figure 5-83 through Figure 5-87). A significant amount of loose sediments originating from slope failures were observed along the headwaters of the Langtang River and the mountains near Kyamgjon Kharka and Yala Peak (Figure 5-88 through Figure 5-90). Several ground fissures, possibly related to lateral spreading, were also observed bordering a morain (glacier) lake above Kyamgjong Kharka (Figure 5-91 and Figure 5-92). Additionally, loose sediment debris was observed along the tributaries of the Langtang River, particularly at or near the mountain peaks throughout Langtang and Kyamgjong Kharka (Figure 5-93 and Figure 5-94).

Figure 5-83 A large seismically induced landslide mass narrowing the width of Langtang River.

Figure 5-84 Another location where Langtang River is blocked by landslide debris.

Figure 5-85 Several large scale landslides along the bank of the Langtang River.

Figure 5-86 Typical loose debris observed along a slope in the Langtang Valley.

Figure 5-87 Upstream of the Langtang River with sediments from loose debris mass that slid after the earthquake.

Figure 5-88 Langtang River blocked by landslide debris at multiple locations.

Figure 5-89 Debris fan observed at the upstream of Langtang River near Kyamgjon Kharka (28°12.2'0"N 85°35.2'0"E).

Figure 5-90 Langtang River blocked at multiple locations (28°12.5'0"N 85°35.1'0"E).

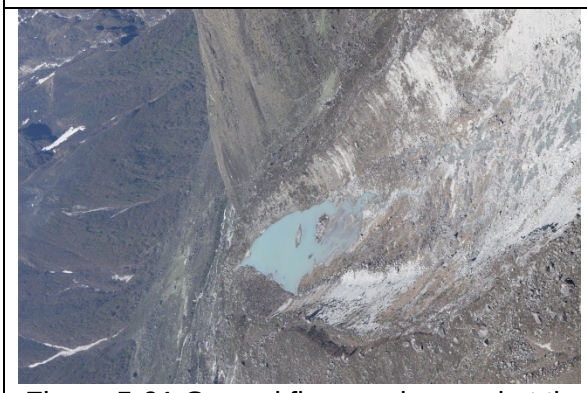

Figure 5-91 Ground fissure observed at the edge of a glacier lake above Kyamgjon Kharka.

Figure 5-92 Kyamgjon Kharka village downstream the glaciar lake (28°12.7'0"N 85°34.1'0"E).

Figure 5-93 Loose sediments observed along mountain slopes.

Figure 5-94 Loose sediments observed near the glacier lake.

5.9 Langtang Debris Avalanche

Within days of the M_w7.8 Gorkha Earthquake, a large debris avalanche buried over 200 people in the Langtang Village located at the Latitude of 28^o 12' 55.43"N; Long – 85^o 30' 8.95"E; Alt 3297 m above msl. Google Earth images of the debris avalance area prior to and after the avalanche are depicted in Figure 5-95 and Figure 5-96, respectively. Although Langtang Village is not clearly visible in the Google Earth image, higher resolution images are presented in Figure 5-97 through Figure 5-99, and a detailed view of the village area is shown in Figure 5-98. The estimated length and width of the debris is 400 m x 900 m, respectively. Based on an average estimated depth of about 5m, the overall debris avalanche volume is estimated at about 2 million m^3.The source of the debris mass is estimated to be 2 km from the current debris deposit, representing a relief on the order of 1,600m (Figure 5-97 and Figure 5-98). Part of Langtang Village was buried under the landslide debris, with the remainder destroyed by associated air blast effects. The air blast flattened forested areas along the left bank of the river (Figure 5-101).Structures beyond the distal reaches of the debris avalanche also succumbed to violent air blast (Figure 5-102 and Figure 5-103). Where the debris mass completely blocked the Langtang River channel, the river passed under the debris mass and thus avoided ponding of surface water (Figure 5-104). The debris materials were very loose and wet at the time of visit (Figure 5-105). More than 95% of the debris materials were finer than 0.5m (Figure 5-106).

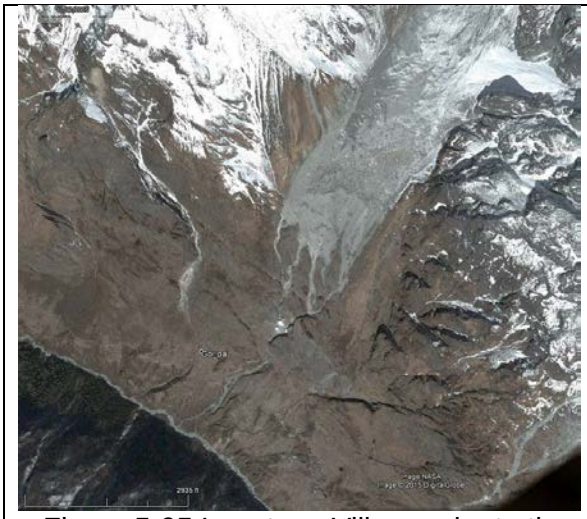

Figure 5-95 Langtang Village prior to the debris avalanche captured from the google earth.

Figure 5-96 Langtang Village after the 2015 debris avalanche captured from the Google Earth.

Figure 5-97 Aerial view of the debris avalanche (28°12.7'0"N 85°34.1'0"E).

Figure 5-98 Aerial view of the source area of the debris avalanche (28°12.5'0"N 85°32.1'0"E).

Figure 5-99 Overall view of the debris flow area from Langtang Village (28°12.5'0"N 85°31.8'0"E).

Figure 5-100 Foot of the debris shoot (a 3 story building on the middle left was the only building undamaged in the area.

Figure 5-101 Flattened trees on the left bank of the river (28°13'0"N 85°30.2'0"E).

Figure 5-102 Aerial view of Langtang Village that was destroyed by the debris avalanche air blast.

Figure 5-103 Closeup view of the d Langtang Valley. The buildings were flattened towards the direction of air blast induced by the avalanche.

Figure 5-104 Langtang River blocked by the debris avalanche.

Figure 5-105 Typical sizes of the debris avalanche mass materials (28°13'0"N 85°30.2'0"E).

Figure 5-106 Few large sized boulders observed in the area.

5.10 Kathmandu – Dhawa – Baluwa – Barpak Air Route

The geographic area observed during this portion of the aerial reconnaissance is shown in Figure 5-107. Many large scale landslides were observed along the Tributaries of Marshyangdi River, including Daraudi River, that have the potential not only to dam the river, but also impact hydropower facilities (Figure 5-108). Several of these landslides blocked the river near Barpak (Figure 5-109), located near the epicenter of the April 25, 2015 Mw7.8 earthquake. Landslide scarps were observed at the north-east edge of Barpak village (Figure 5-110 and Figure 5-111) and along the southwest edge of the village.

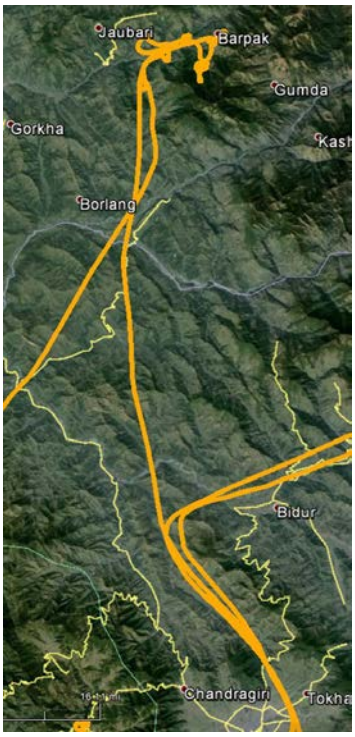

Figure 5-107 Aerial view of the Kathmandu – Barpak air route

Figure 5-108 Dam site of a hydropower station near Barpak is vulnerable to potential landslide in the next rainy season or earthquake event.

Figure 5-109 Seismically induced landslides near Barpak blocked the natural flow of a stream.

Figure 5-110 Main scarp of a seismically induced landslide observed at the north east edge of the Barpak Village, epicenter of the April 2015 Gorkha earthquake.

Figure 5-111 Aerial view of the landslide scarp.

5.11 Kathmandu – Kalyanpani – Arughat – Besisahar – Manang - Prok Area

The aerial route covered in this section is shown in Figure 5-112. The Manang area, especially at elevations higher than Chame, is composed of very loose sediment and weathered materials (Figure 5-113). The 2015 Gorkha Earthquake destabilized the sediments locally and and dammed the Marshayngdi River a few kilometers downstream of Higde Airport (Figure 5-114). Very loose debris masses that have potential to slide down and block the Marshangdi River were observed extending to Lake Tilicho (Figure 5-115). Many landslides were also observed along the banks of Budi Gandaki River in the direction of Prok (Figure 5-116). Those landslides partially blocked the river and damaged the road connecting Arughat to Arukhet at several locations (Figure 5-117). There were many large scale landslides between Arukhet and Prok that partially blocked the Budi Gandaki River (Figure 5-118). A tributary of Budi Gandaki River near Prok was also blocked at several locations due to earthquake induced landsliding.

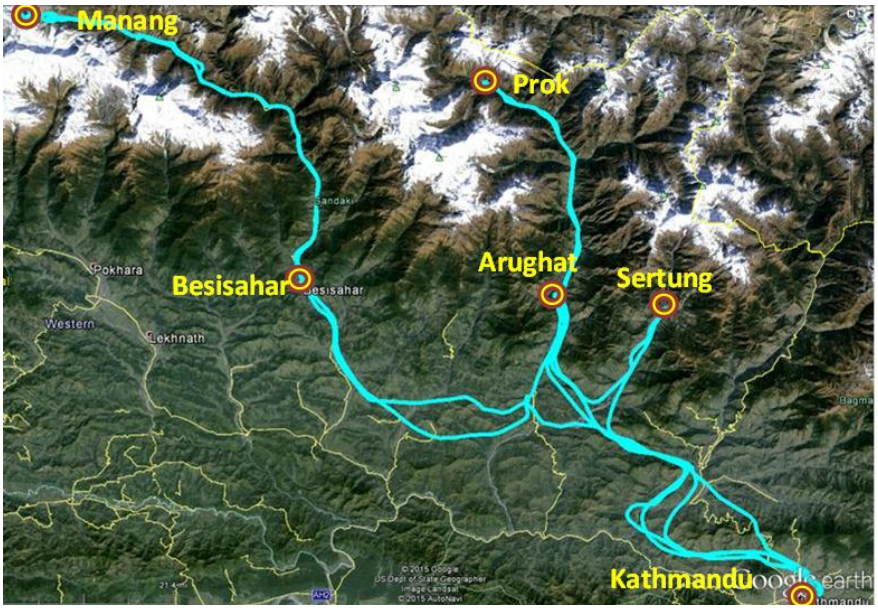

Figure 5-112 Aerial route of the Kathmandu – Manang – Prok Area.

Figure 5-113 View of Manang.

Figure 5-114 A landslide that blocked Marshangdi River temporarily right after the 2015 Gorkha Earthquake.

Figure 5-115 Loose sediment mass along the trekking route from Manang to Lake Tilicho (28°4.97'0"N 85°13.8'0"E).

Figure 5-116 Landslides that damaged the road along Arughat-Arukhet road sector.

Figure 5-117 A landslide along the bank of Budi Gandaki River.

Figure 5-118 Multiple landslide observed along a tributary of Budi Gandaki River near Prok right after the 2015 Gorkha Earthquake.

5.12 Pandise Landslide Dam

A landslide dam was observed at Pandise, located in the Sertung Village Development Committee of the Dhading District (Figure 5-119). The landslide occurred at Ankhu Khola, a tributary of the Budi Gandaki River. The slope gradient of the tributary was approximately 30-35^{o}, and large boulders traveled down the tributary of Ankhu Khola, blocking the river channel for about a week (Figure 5-120). The landslide dam was breached naturally.

Figure 5-119 A landslide dam at the tributary of Ankhu Khola right after the 2015 Gorkha earthquake main shock (28°40.6'0"N 83°59.8'0"E).

Figure 5-120 Debris mass from the left bank of the river that caused the landslide damming.

5.13 Kali Gandaki Landslide

Figure 5-121 Kali Gandaki Landslide

A significant landslide occurred in the early morning of May 24, 2015 on Kali Gandaki River in the Myagdi District, which is located to the northwest of Kathmandu. The Kali Gandaki landslide is a dry, raveling-type landslide that was presumably weakened by the April 25 main shock and subsequent aftershocks. The landslide buried a village with 25 houses but did not cause any human casualties, as the area had already been evacuated before the landslide. Rock's toppling in the day before the landslide and observations of surface cracks at the top of the slope after the April 25, 2015 M_w7.8 main shock and subsequent aftershocks provided sufficient warning to evacuate the village below the landslide.. The massive landslide blocked the Kali Gandaki River forming an artificial earth dam. The water level rose rapidly behind the landslide dam and formed lake upstream of the dam. According to local reports, the lake extended approximately 1 to 3 km upstream within 12 hours of the landslide dam formation.

Warnings were provided by local radio and government officials to people living upstream and downstream of the artificial dam to stay alert and to move higher ground. The Nepal Electricity Authority suspended operations in their 144 MW Kali Gandaki Hydropower project, located 45 km downstream of the landslide area, due to the potential risk of flooding. Water started overflowing the dam 16 hours after the landslide, around 5:30 pm local time according to Nepalese Army technicians (Nepal Republica Media). After overflowing the dam, the water kept a steady flow without causing major damage or casualties in the downstream towns.

Figure 5-122 (a) Location of the Kaligandaki Slide.(b) Landslide was the top news in the local newspaper

Figure 5-123 The landslide blocked the Kali Gandaki River forming approximately 2 km long and 150 m deep artificial lake, 28 24' 8.48"N 83 35' 47.5"E.

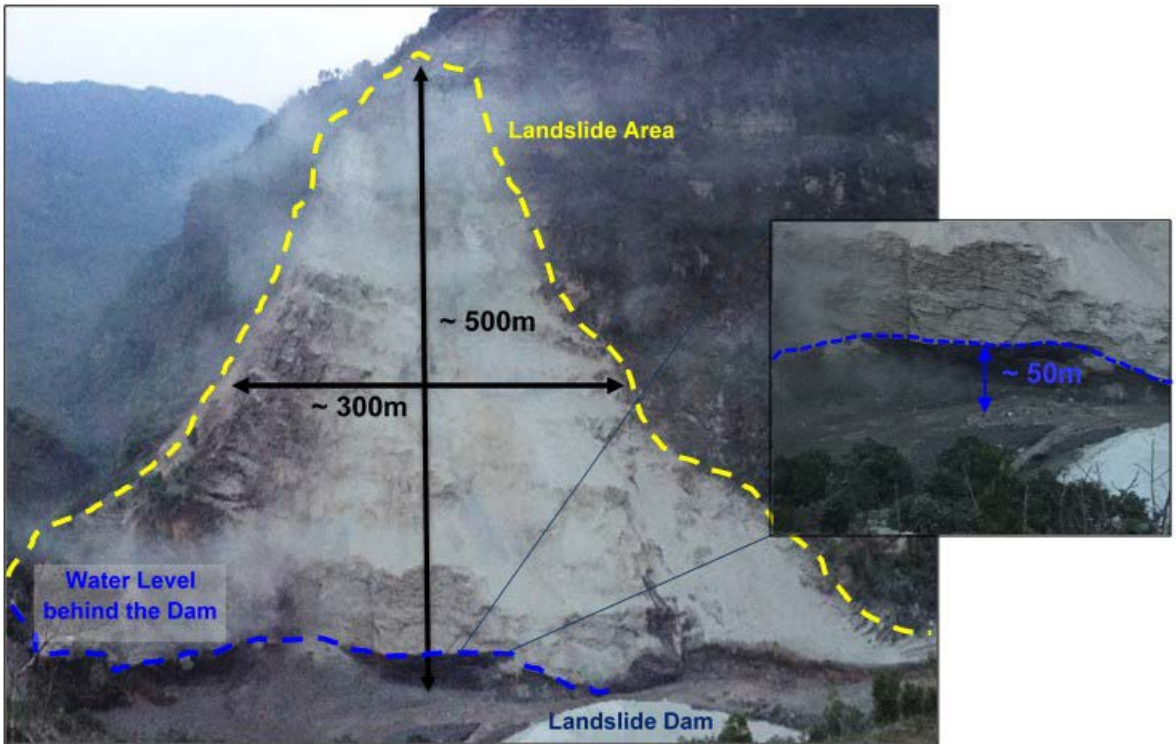

Figure 5-124 Kali Gandaki landlside, 28 24' 8.48"N 83 35' 47.5"E.

5.14 References

Collins, B.D., and Jibson, R.W., 2015, Assessment of Existing and Potential Landslide Hazards Resulting from the April 25, 2015 Gorkha, Nepal Earthquake Sequence: U.S. Geological Survey Open-File Report 2015–1142, 50 p., http://dx.doi.org/10.3133/ofr20151142.

Nepal Ministry of Home Affairs, 2014. Nepal Disaster Report 2013.

Tiwari, B., and Marui, H. 1998. Landslide investigation and prevention practice in Nepal. Annual report of Research Institute for Hazards in Snowy Areas, 20, 37-55. Nepal Ministry of Home Affairs. 2014. Nepal Disaster Report 2013.

Tiwari, B., Juis, S., Cohelho, M. (2015) Landslides triggered by Mw7.8 Nepal earthquake, Poster presented at Brazilian Science Mobility Program Research Workshop, California State University Fullerton, July 2015.

Ziselsberger, M., 2016. Inventory of Earthquake-Induced Landslides in the Sindulpalchok District of Nepal Resulting from the M7.8 Gorkha Earthquake and Related Aftershock Sequence. M.S. Thesis, Insitute of Applied Geosciences, Graz University of Technology (in preparation).

6 Liquefaction and cyclic soil failures

6.1 Introduction

Ground failure due to the Nepal earthquakes was dominated by landslides, coming in many different forms of seismic induced mass movement. Because of the ongoing tectonic uplift and the steep nature of the terrain, landsliding is to be expected. There are, however, a few valleys in Nepal that geomorphically lend towards other types of ground failure common in soft or loose soils. The Kathmandu Valley contains lake and river sediments that, when shaken, can deform due to either cyclic failure or liquefaction. This chapter of the GEER report documents these forms of ground failure. The GEER team covered broad regions of the country, but found ground failure due to weak soils almost exclusively in the Kathmandu Valley.

The weak soils that caused ground damage ranged from fine sands to silty sands to silty clays. In some locations, the ejecta indicated clear evidence of liquefaction as the controlling failure mechanism. However, in other locations, the controlling failure mechanism was not clear even after trenching and sampling, because of complex layering, variable water table depth, driving shear stresses, and complex deformations patterns. In this section we have carefully documented our field observations, what is known, and what has yet to be determined. The most interesting and informative sites are covered in detail, with other sites mentioned for completeness.

Further ground failure research is warranted both for Nepal and the broader earthquake community. Further research is predicated on the existence of strong motion recordings of the main M7.8, the M6.7 aftershock, and the M7.3 subsequent event. If the strong motion data is of sufficient quality and close enough to the sites to be used as loading, then penetration measurements using local SPT and possibly imported CPT could then be mobilized to fully document the soil resistance. SPT measurements exist for some of these sites and obtaining access would be invaluable.

6.2 Quaternary Geomorphic Setting of the Kathmandu Valley

The greater Kathmandu region is structurally defined by thrust faulting on the north and the south (see Figure 6-1). The Main Central Thrust (MCT) bounds the north side and the Main Boundary Thrust (MBT) the south side, creates a structural basin that defines the Kathmandu Valley. This valley is filled with deep sediments, on the order of 500 m thick, and has experienced long geologic periods where a lake dominated the depositional environment. The lake deposits are variable in thickness and in lateral extent and consist mainly of interbedded clays and silts with some sands and gravels (Piya 2004).

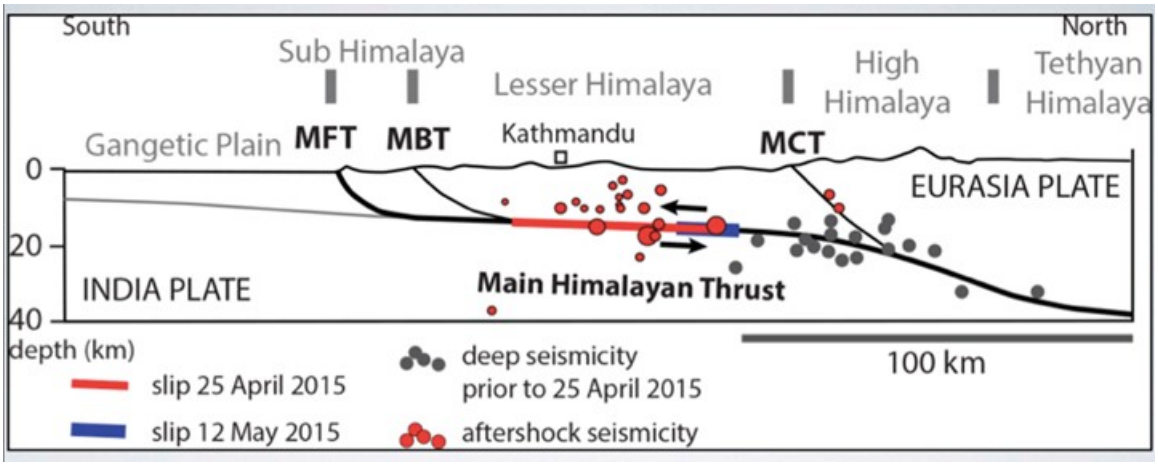

Figure 6-1. Tectonic structures of the central Nepal region. Kathmandu Valley lies between the MCT and MBT (USGS, 2015).

The lacustrine environment shifted around 10 to 11 thousand years ago (Sakai, 2001a) giving way to a fluvial environment that deposited primarily sands and gravels in the many river channels and flood plains which drain the basin. Figure 6-2 shows the Holocene river systems. The shift from a lake to a river-dominated landscape at the end of the last ice age has been attributed to fault movement (Sakai, 2001b), but has not been definitively investigated. The shift is also embedded in local belief systems; Hindu's believe lord Krishna drained the lake by cutting a gorge with his weapon at the South end of the Katmandu Valley, and Buddhists believe that Bodhisattva Manjushri cut the mountains at Chobhar with his sword and drained the lake (Piya, 2004). The shift from lacustrine to fluvial environments has precedent in other parts of the world. Most familiar is the draining of glacial Lake Missoula at the end of the ice age due to a breach (or repeated breaches) of an ice dam that released the lake in a quick and catastrophic manner onto the Columbia Plateau. Accordingly, the Pacific Northwest of the United States has similar tectonic and depositional characteristics as Nepal.

The water table in the Kathmandu valley is generally shallow, ranging from 0.5 to 9 m in most locations. DMG (1998) found, based on 82 representative wells, that the north-eastern part of the Valley had water tables between 5 to 9 meters and in the southern part of the Valley water tables were around 1 m.

Figure 6-2 Katmandu Valley and Regional Map (from Piya, 2004) showing Holocene Rivers systems.

The river systems that dominate the Kathmandu Valley landscape today are seen in the survey map from 1803 prior to twentieth century development (Figure 6-3).

Figure 6-3. Map of Kathmandu Valley circa 1802 (Crawford 1803).

6.3 Ground Failure Observations

The liquefaction hazard thesis by Piya (2004) forecast liquefaction in many areas of the Kathmandu Valley; the general characteristics of soils that are susceptible to liquefaction are clearly present: young sandy sediments at shallow depths that coincide with a shallow ground water table. However, there are a number of factors that may have led lessened the extent of damage due to liquefaction in this event. Due to the monsoon, there is likely a strong seasonal dependence of the depth to the ground water table, which could substantially affect the susceptibility of the soils, decreasing susceptibility in the dry season. Additionally, the ground shaking appears to have less high frequency energy than would be expected for an event of the same magnitude, yielding a relatively low peak ground acceleration of about 0.16 g at the KATNP strong motion station in central Kathmandu. The reasons for the unusual ground motion frequency content are difficult to discern because of the limited number of recordings near the fault (both within and outside the valley) that are available at this time and will be addressed in more detail in other chapters of this report.

Regardless of the reason, the single recording that is currently available within the Kathmandu Valley (station KATNP) indicates that the ground motions that resulted from the April 25 mainshock were not strong enough to fully weaken liquefiable materials and in most cases incipient or “marginal” liquefaction was observed. This makes the observations potentially valuable except for the fact that the loading has been so poorly quantified. Cyclic failure of the silty clays in the Valley is not a hazard that has been analyzed before and appears to be a very interesting effect from the strong ground shaking.

The following map shows rough locations of the ground failure sites investigated by Teams A and B throughout the reconnaissance effort and are discussed in the next sections.

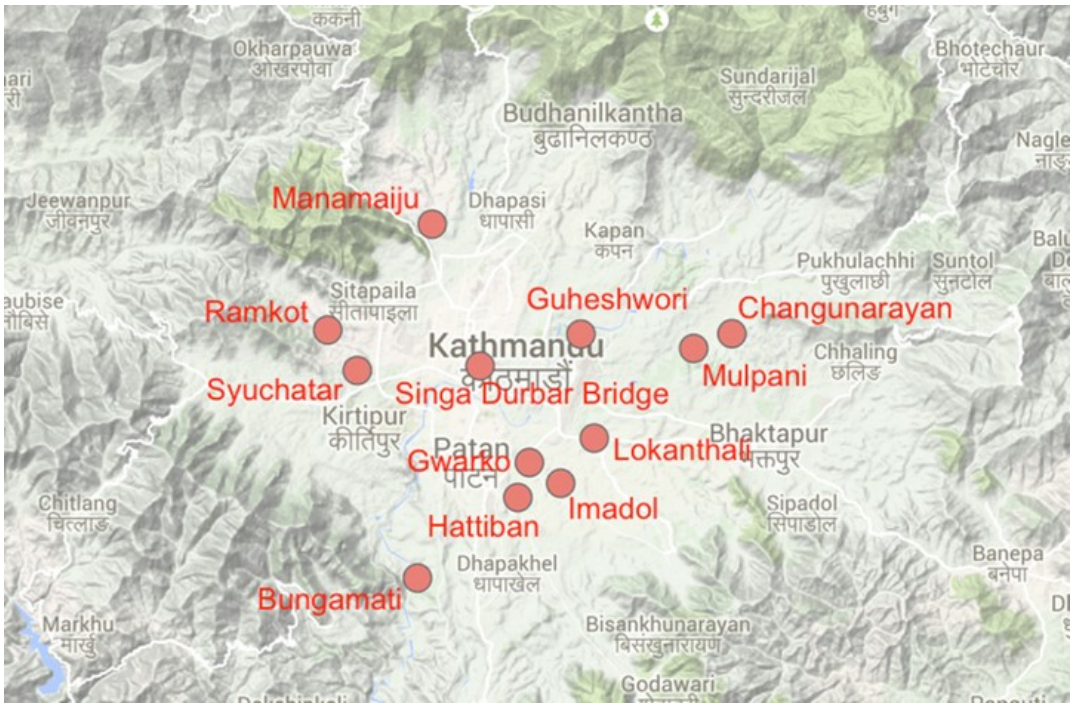

Figure 6-4. Ground Failure sites visited by Team A and B.

6.4 Ramkot

Ramkot is located on the western edge of the Kathmandu Valley. Liquefaction of very fine material was observed on steep terraces (Figure 6-5 and Figure 6-6). No lateral deformation of terraces was found. Ejecta located in the terraces and on lower fields was confined to a narrow swath of the hillside (see Figure 6-5). Similar features were found down by the creek (Figure 6-6), but the biggest sand boils were on the steep (20 degree) slopes. Locals reported that the boils issued for 2+ hours following the M7.8 earthquake. Foundation damage of two small poorly constructed houses correlated with this narrow swath of liquefaction. Other taller more modern structures experienced no damage. Increased driving stress due to taller building may have inhibited liquefaction by locking up the soil. Slope failures were observed in the surrounding hills but were not associated with liquefaction. Structural damage was heavy in the town of Ramkot but not associated with liquefaction.

Figure 6-5. Liquefaction ejecta on steep terraced slopes (27.711025° N 085.262290° E). No lateral movement was observed. No damage to the building in the background.

Figure 6-6. Liquefaction ejecta in agricultural field. Material was very fine, primarily silt with some sand. No damage to the building in the background (27.711025°N, 085.262290°E).

Sand boils were observed in an empty plot of land (Figure 6-6). This site is located about 90 m northeast of a meandering river; it is elevated above the floodplain. According to the locals, the ground flooded during the earthquake and remained flooded for two days. Locals also claimed that other plots in the vicinity liquefied, but we could not find surface effects of liquefaction elsewhere. After auguring on this site, we found that the soil profile generally

consists of interbedded layers of loose find sand and silt up to 2.5m depth. The water table was located ~3m below the ground surface.

6.5 Singa Durbar Bridge

One bridge case history of interest is the Singa Durbar Bridge in the center of Kathmandu (Figure 6-7). This bridge was undamaged after the M7.8 and first aftershock, but sustained damage in the M7.3 event. There appears to be a soft soil failure that aligns with the width of the creek deposits under the bridge. Lateral cracks in the raised concrete sidewalk sections run on both sides of the bridge parallel to the creek and are separated by roughly 100m along the length of the bridge. Talking with a local who is currently building a deep foundation in the affected area, he says the subsurface conditions are fill over “black cotton” silty clays, the same lake deposit found throughout the Kathmandu valley. It is anticipated that there are underlying sandy soils as well but currently there are not subsurface investigations to confirm this. The mode of soil failure, liquefaction or cyclic failure, at this site is undetermined at this moment.

Figure 6-7. Singa Durbar Bridge (27.698793°N, 85.320060° E). To the right of the bridge can be seen the deep foundation that is currently being installed for a building.

Figure 6-8. Cracking in concrete section of bridge (27.698793° 85.320060°). Cracks on both sides of the bridge line up with the creek below. No cracking in the asphalt over fill section, it behaved in a ductile manner

Figure 6-9. Creek below the bridge (27.698793° 85.320060°). The flood plain of this creek defines the extent of the cracking, with the cracks parallel to the creek alignment.

6.6 Manamaiju

Liquefaction was observed in free field conditions as well as under building foundations at Manamaiju (Figure 6-10 and Figure 6-11). The location is an old abandoned river channel. There were sand boils of fine micaceous sand (see lab tests, Figure 6-12), some minor building tilting/punching, and a possible incipient lateral spread along a free face. Locals stated that sand boils ejected material up to 1 m above the ground surface. Here liquefaction was triggered but not enough shaking occurred to get large displacements. This would be called a "marginal" liquefaction site in Seed et al. (1985) terminology, and if the ground shaking can be properly quantified at this site, it would provide a datapoint right near the triggering threshold. A bag sample of ejecta was collected and tested at Tribhuvan Univeristy for FC, gradation, and PI. Follow up studies should include acquiring any existing bore logs from nearby site, make detailed measurements of the free face, make more detailed measurements of foundation settlement (on the order of a few cm) and building tilt (less than 2 degrees), and arrange for some penetration measurements (preferably CPT).

The recent history of this site is also interesting. The locals said that the surface soil was originally sand, which was removed and used for the construction of new buildings. Then fill was brought into the area. The original level of the natural ground surface is evident at the edges of the valley, and is about 1 m above the current ground level. Hand augering indicates that the current surface layer (likely fill) is about 1 m of silty clay/clayey silt mixed with occasional larger grains. We encountered the water table at 0.8 m, and at 1.1 m observed a micaceous sand with minor amounts of gravel-sized grains. The grain sizes generally increased with depth to about 1.3 m where we saw gains as large as 50 mm.

Figure 6-10. Large sand boil in a field at Manamaiju. The ejecta was a micaceous silty fine sand. (27.745523° N, 85.302223° E).

Figure 6-11. Tilt of left building away from right building, measured at roughly 2 degrees (27.745523° N, 85.302223° E).

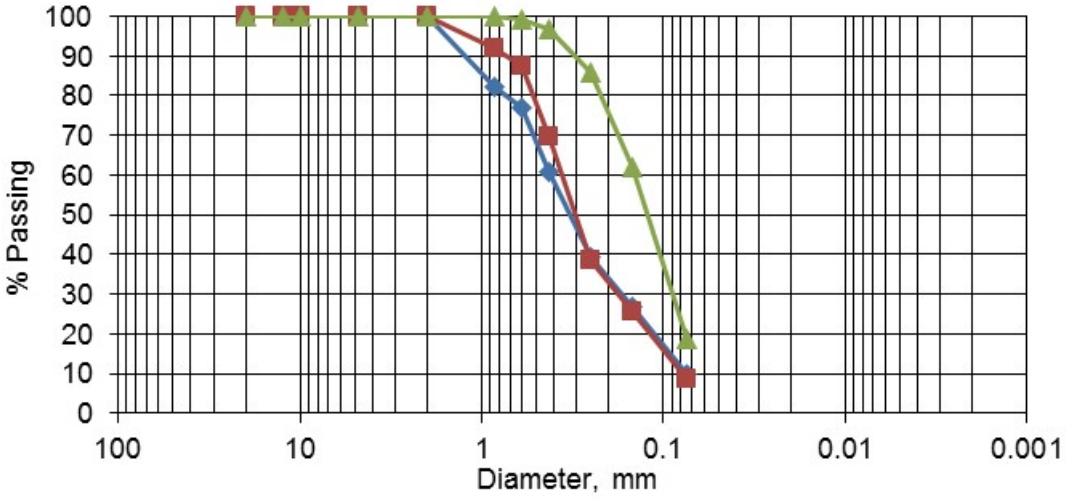

Figure 6-12 Grain size distribution for soil samples from Manmaiju. Depth of 1m, FC = 9 to 10%, Clay Fraction (<0.005) = 0%, => Fine Sand with Silt.

6.7 Guheshwori

We would not have been able to identify Guheshwori as a location that liquefied if the locals had not described that sand and water had spouted out of the ground and the area had flooded during and after the earthquake shaking (27.709253 N 85.357553 E). It is similar to Manamaiju in that it is on a floodplain where the top layer of sand had been removed for use in construction. There also did not appear to be substantial structural damage resulting from the liquefaction here (although there were only a few structures in the vicinity; see Figure 6-13). Local residents informed us that water jetted approximately one meter above the ground

surface for one to two minutes, and that the site was flooded for a couple of hours following the April 25 earthquake.

Figure 6-13. Location of liquefaction at Guheshwori (27.709253 N, 85.357553 E).

6.8 Lokanthali

Lokanthali is a highly interesting case history of soil failure from the Nepal earthquakes (27.674816° N, 85.362646° E) and surrounding region) in the Kathmandu Basin. Large lateral cracks with 2 m deep fissures and up to 1.2 m of nearly vertical offset have occurred over a large area on or near sloping ground. Observations were made by Teams A and B over the span of several weeks. Investigations include detailed mapping of the cracks, disturbed sampling of the material at the bottom of the fissures, hand trenching and block sampling with depth, hand augering and hand vane testing with depth, and trenching with a backhoe to map the subsurface structure.

At one location a silty clay with low PI (see lab tests), was sampled with a (bamboo) sampler at the bottom of the fissures. At a nearby location a 2 m deep hand-dug trench within one of the fissures was excavated to acquire bulk samples of the same soil. Adjacent to the trench buildings had experienced 0.75 m vertical displacement and bulk samples of the silty clay were acquired from the excavated foundation. The deformations were reported by the home owners as co-seismic with small displacements from the main M_w7.8 and then the bulk of the displacements due to the first aftershock that was M_w6.7.

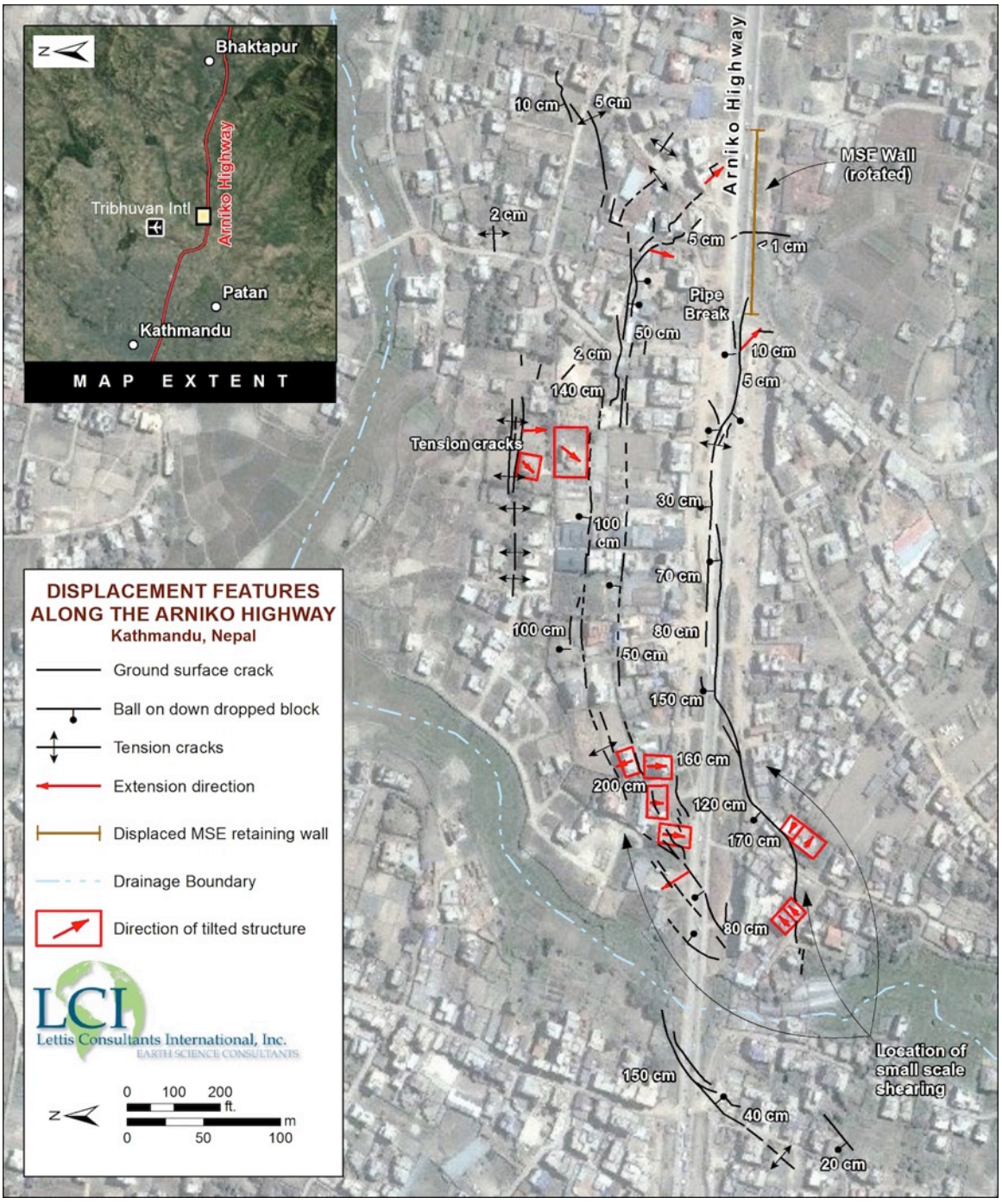

Figure 6-14. Cracks mapped at Lokanthali site (27.674816° 85.362646° and surrounding region). Vertical displacements on the order of 1m, horizontal displacements on the order of 0.5m, with fissure roughly 2 m deep.

Figure 6-15 Cracks near the top of the rise in Lokanthali (27.674816° 85.362646° and surrounding region). Depth of cracks 2 to 3 m deep. Most of the deformation was reported to have occurred during the first aftershock, with only a small amount of deformation from the mainshock.

Figure 6-16. Bamboo sample of silty clay soil called “black cotton” in the Kathmandu Valley. (27.674816° 85.362646°).

Figure 6-17. Bottom of crack at 2m depth where the “black cotton soil” was sampled. (27.674816° N, 85.362646° E).

Figure 6-18. Hand trench to 2m depth to acquire bulk sample of "black cotton" silty clay. Depth coincides with slip surface of nearby houses that experienced vertical deformation of up to 0.75 m. Here the trench is dug into the hanging wall of the crack (27.674316° N, 85.362654° E).

Figure 6-19. House on the hanging wall of the crack. The ground pulled away from the structure dropping upwards of 3/4 m and moving laterally 1/2 m. Before the earthquake the brick foundation was completely below the ground surface.

Initial investigations observed that the failure planes entered a silty clay/clayey silt with low PI. Near the location of maximum slip (27.67439 N, 85.36267 E) we dug a pit about 2 m deep (depending on which side of the scarp is considered the ground surface). We used the shear vane to measure the peak shear strength of 150 kPa and residual shear strength of 112 kPa at 1 m below the base of the trench (sensitivity of about 1.3). However, these values should be used with caution since we could not confirm that the silty clay at this depth was fully saturated. Based on the observations described above, as well as the length of the fissures and local accounts that the failures progressed slowly, the failure mechanism was initially attributed to cyclic failure in the clay.

Figure 6-20. Cross section of failure plane on wall of trench at EMT04. Horizontal string is separated vertically by 0.5 m (27.67439 N, 85.36267 E).

Subsequently, we found an empty lot (27.675524 N, 85.363083 E) with space for a backhoe to dig a large trench a little over 2.25 m deep. The ground is dipping here at about 4 degrees toward the river. The excavation revealed more complex failure planes than were evident on the surface or from the previous trenching efforts. A well in an adjacent house showed that the

water table is at about 13 ft. The trench did not reach the water table, but it did reveal liquefaction escape structures that were capped by the clay/fill layers. We augered from the base of the trench and reached the saturated sand. The water table was 1.8 m below the bottom of the trench (or about 4 m depth) which is consistent with the adjacent well. The slip surfaces in the top layer of clay/silt terminated in the sand that was brought up to the base of the clay. The cracks continue past the sand layers but shift to different paths. Offset beds forming a graben are evident at depths greater than 2 m. Interestingly, the slip between blocks of the graben have created large voids that have not caved in at the time of the trenching. These features were only evident at the base of the trench so it was difficult to determine the full extent of the voids.

Figure 6-21. Cross section perpendicular to scarp at EMT09. Horizontal and vertical spacing of the string is 0.5 m and 1.0 m, respectively (27.675524 N, 85.363083 E).

Large fissures and ground cracks extending for long distance over shallow ridge. Samples taken from the bottom of fissures from hand trench, from excavated foundation, and with bamboo sampler.

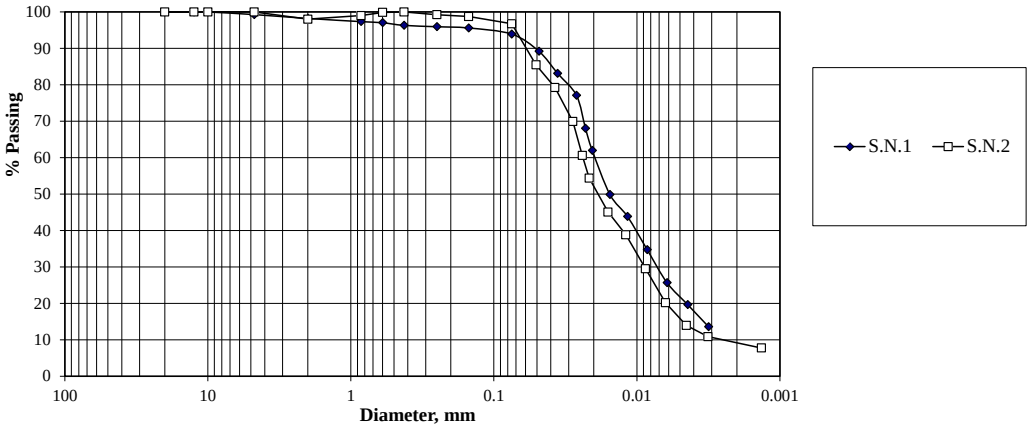

Figure 6-22 Laboratory test results on hand trench samples from Lokanthali, water content 30 to 38%, FC=97%, LL=30.8, PL=22.7, PI=8.1, => CL (S.N.1), LL=27, PL=20.8, PI=6.8, => CL (S.N.2), LL=32.5, PL=22.6, PI=9.9, => CL (house), Direct shear = 30 ± 0.5 degrees

Bamboo samples (remolded): water content 30 to 38%, FC=84%, Direct shear fully softened friction angle= 16.7 degrees, LL=29, PL=22, PI=7, => CL

The hand trench samples of the "black cotton" CL were block samples and undisturbed. The bamboo samples were highly disturbed due to the crude sampling process. If the bamboo samples are interpreted as remolded for the direct shear tests then this CL has a peak to residual friction angle of 1.9, which can be used as an indicator of sensitivity (St) even though these are not typical undrained strengths used for estimating sensitivity. The Liquidity Index (LI), is found to be in the range of roughly 1.0 to 2.3.

St ~ 1.9

LI ~ 1.0 to 2.3

These limited lab tests the "black cotton" CL indicates moderate sensitivity and a liquidity index higher than one (Holtz, Kovacs and Sheahan, 2011). This means that once the structure is broken the soil can be mobilized at a lower strength and behave in a more viscous manner thereby resulting in deformations. With the addition of the driving shear stresses from the sloping ground and from the building-induced stresses, this lends to cyclic failure (Idriss and Boulanger, 2004) as a possible failure mode for some of the locations at Lokanthali. the Lokanthali case is interesting with its "black cotton" silty clay. Note that the PI is 7 to 9 and the wc/LL is > 1, so it could also be cyclic mobility as per Bray and Sancio (2006). Whether it developed pore pressures and underwent cyclic mobility or was a structural breakdown of a sensitive clay and hence cyclic failure, it caused significant ground cracking. It would be useful to mobilize additional follow up investigations to resolve the underlying soil behavior,

6.9 Syuchatar

The fissures at Syuchatar (27.69723 N, 85.27408 E) are very similar to those at Lokanthali. The fissures are very long (greater than about 1 km) although the offset is relatively small compared to Lokanthali. We augered down to about 3 m depth in a handful of spots. In most cases we found a silty clay/clayey silt with orange oxidation staining. At larger depths we found small lenses of fine sand. At one site (27.69794 N, 85.27374 E) we encountered the fine sand near the surface and could not auger through it (sampled the sand at depths from 0.5-1.1 m). Here, the sand was saturated, although in other locations the water table was not reached until

depths of 2-3 m. The variability of the soil and water table is difficult to reconcile with the length and simplicity of the surface expression of the fissure. It is likely that the crack is controlled by structure that is deeper than we could reach at this time.

The hand vane gave generally smaller strength values in the clay than at Lokanthali. The following table gives the values at two sites where we were confident that the measurements were at depths below the water table:

Table 6-1 Hand vane test values at Lokanthali

Site	Depth(m)	Peak (kPa)	Residual (kPa)
EMT05	3	68	50
EMT05	4	80	50
EMT07	2.8	92	32
EMT07	3.25	120	40

6.10 Bungamati

Sand boils occurred on the floodplain about 200 m from the Bagmati River (Figure 6-23). The ground water table was measured at about 1.3 m. We hand augered to get the stratigraphy along a 23 m long transect. The stratigraphy was relatively consistent: 0.5 m of micaceous brown silty clay topsoil, followed by Black Cotton Clay to about 1.5 m, followed by fine sand that coarsened with depth. It is likely that this saturated sand layer liquefied, but of course we are unable to determine what is present at greater depths. The local residents told us that water ejected from the ground surface approximately 1 m in height for 30 minutes after strong shaking had ceased, and that the flooding lasted 2 to 3 days. In addition, residents mentioned that nearby agricultural fields along the Bagmati River had also shown surficial signs of liquefaction after the April 25 earthquake. The land owner mentioned that the Nepal Government plans to build a super highway through this site within the next 25 years.

Figure 6-23. Sand boils in Bungamati (photo courtesy of Dewakur Khadka, 27.62863 N, 85.29665 E).

6.11 Changu Narayan

This is another site with clear liquefaction as indicated by sand boils. The site is located about 300 m from the river on the floodplain (Figure 6-24). As with Bungamati, we hand augered in a number of locations. The soil profile is relatively similar consisting of micaceous silty clay top soil, which transitions into a gray silt with orange oxidation staining down to about 0.9 m, and then a fine sand at 1.1-1.2 m. While the clay becomes progressively wetter with depth, we were not able to reach the water table at this site. Given the location on the floodplain, proximity to the river, and oxidation of the clay particles, we suspect that the water table is very shallow and exhibits large seasonal fluctuations, often being much shallower.

Figure 6-24. Sand boils in Changu Narayan (27.70943 N, 85.41397 E).

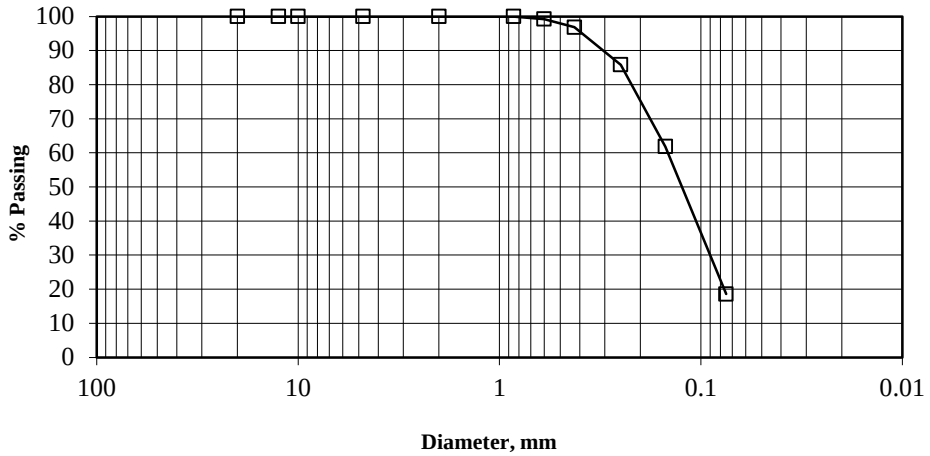

Figure 6-25 Grain size distribution curve, FC = 18%, => Sand, Chagu Narayan (locally known as Duwakot).

6.12 Mulpani

The liquefaction site near Mulpani is located on the same floodplain as Changu Narayan, but about 1.5 km southeast (Figure 6-26). Upon arrival we noticed that a lot of the children were eating raw carrots and that a lot of carrots were lying on the ground in seemingly random locations. We met with the owner of the land and he said that the entire area around the river liquefied, stating that water spouted out of the ground all around them. We asked if the carrots were brought out of the ground during the earthquake shaking and he said that it had. He also noted that he knew of other farms where potatoes had been removed from the ground due to the earthquake shaking.

Figure 6-26. Carrots that were ejected out of the ground due to liquefaction in Mulpani, 27.704575 N, 85.399617 E.

6.13 Gwarko/Imadol

We observed sandboils in cropfields near Gwarko (27.666782 N, 85.338346 E). Although the ground clearly liquefied here, there did not appear to be any related structural damage.

6.14 Hattiban

Numerous sand boils were observed at the Hattiban site. Unlike other liquefaction sites that the GEER team visited, this site was not a borrow pit for sand. We performed an auger (Figure 6-27). At the auger location, about 25 mm of fine sand ejecta was on the surface. Below the ejecta, we found that the site was characterized by a low plasticity silt or silty clay in the top 1.9 m. Dykes of fine sand were found in the auger samples from approximately 0.9 to 1.6 m. Below the silt and silty clay layers was a 0.5 m thick layer of black cotton clay. Below the black cotton layer was a fine sand layer, and the groundwater table was found at 2.5 m below the ground surface.

Figure 6-27. Hand augering a sand boil in Hattiban, 85.33441 N, 27.65567 E.

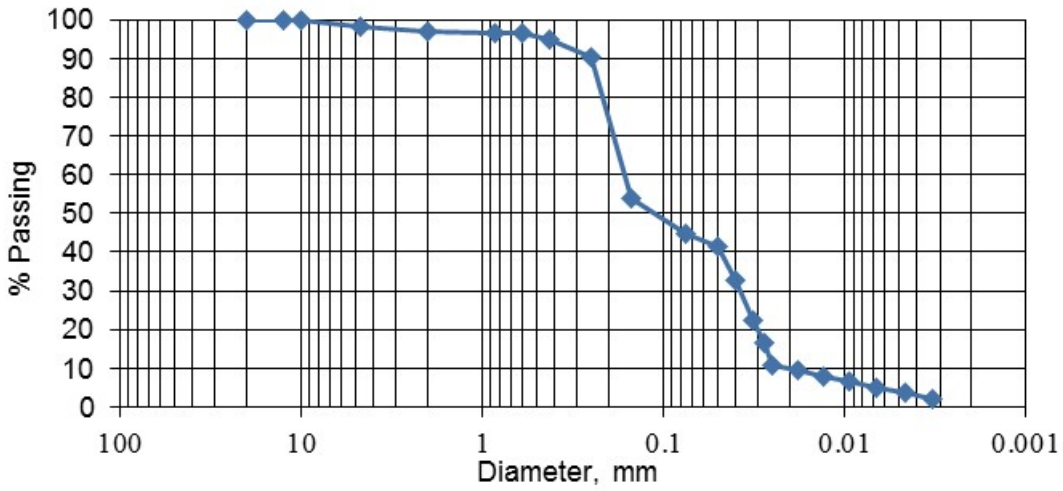

FC = 45%, Clay fraction (<0.005) = 4%, => Silt

Figure 6-28 Grain size distribution curve, Hattiban.

6.15 Kamalvinayak, Bhaktapur

On May 23, 2015, after getting leads from local resident, GEER team went to Kamalvinayak in Bhaktapur, East of Kathamandu valley to observe exposed surface cracks (Figure 6-29). The cracks were formed along the edge of flood plain and the gentle hill, ~5m above the flood plain. The team has traced the crack upto 250m long and according to local resident the cracks appears to be propagated further. The cracks were upto 0.8m wide and upto 1.5m deep (Figure 6-30). A small creek with flowing water was found near the one end of the crack. Probably the cracks were developed due to lateral spreading that may have occurred as a result of liquefaction in underlying ground. The cracks near the buildings were already filled by locals in order to prevent further failure of the ground due to rain water filling up the cracks. The team has observed damage on a reinforced concrete building wall due to the lateral spreading and cracks passing through the foundation of the building (Figure 6-31a). However, no major damages were observed on the building lateral load resisting system. Furthermore, no damages were observed on a building within the same location as cracks could not passes through the foundation (Figure 6-31b). According to local residents, few mud mortar-brick buildings located on the hill were collapsed.

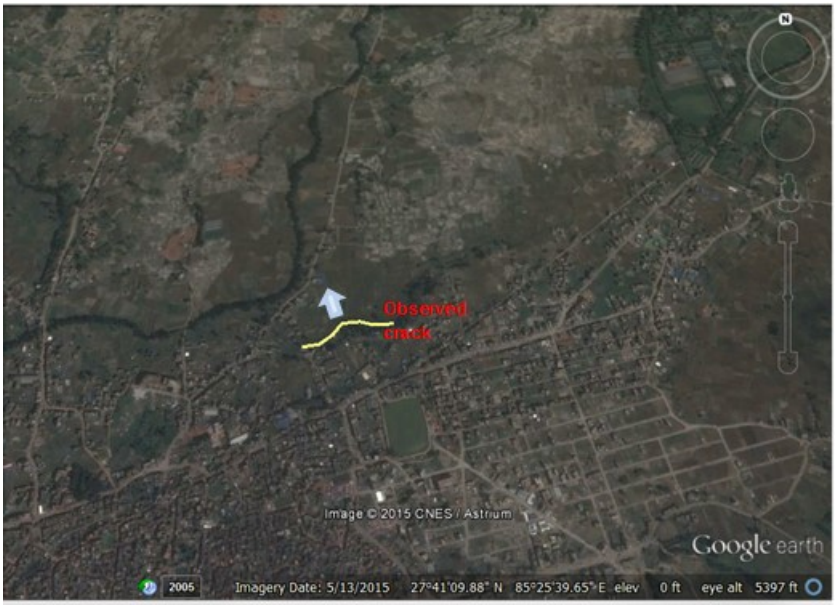

Figure 6-29 Map of observed surface crack in Kamalvinayak in Bhaktapur, Nepal

Figure 6-30 Observed surface cracks ~250m long, up to 0.8m wide, and up to 1.5m deep (Location: 27˚40’42.20” N, 85˚26’13.12” E)

Figure 6-31 (a) Observed cracked in the wall of a RC building due to lateral deformation of ground (b) no damage on a building within the same location as cracks could not passes through the foundation (Location: 27˚40’43.22” N, 85˚26’10.52” E)

6.16 Nagarjun and Syuchatar

On May 22, 2015, local news in Kathmandu, Nepal mentioned a 3 km surface crack that was reported around the Northwest portion of the Kathmandu Valley. As the location of the mentioned 3 km crack was not clearly stated, a subgroup of the GEER Reconnaissance Team visited two different sites with exposed surface rupture on May 23, 2015 that are located around Nagarjun and Syuchatar that are to the West of Kathmandu City, respectively (Figure 6-32). Neither of the surface cracks observed in these locations was found to be 3 km long. The surface crack in Nagarjun is most likely due to a slope stability problem, whereas the

surface crack in Syuchatar is most caused by lateral spreading. To better understand the mechanism behind the observed surface crack in the second location, GEER team revisited the second site on May 27, 2015 and collected samples at three different locations along the observed surface crack in collaboration with the United States Geological Survey (USGS) team. Soil samples collected in each of these three location indicated presence of a sandy layer that might have liquefied during the April 25, 2015 main shock causing observed surface crack due to lateral spreading.

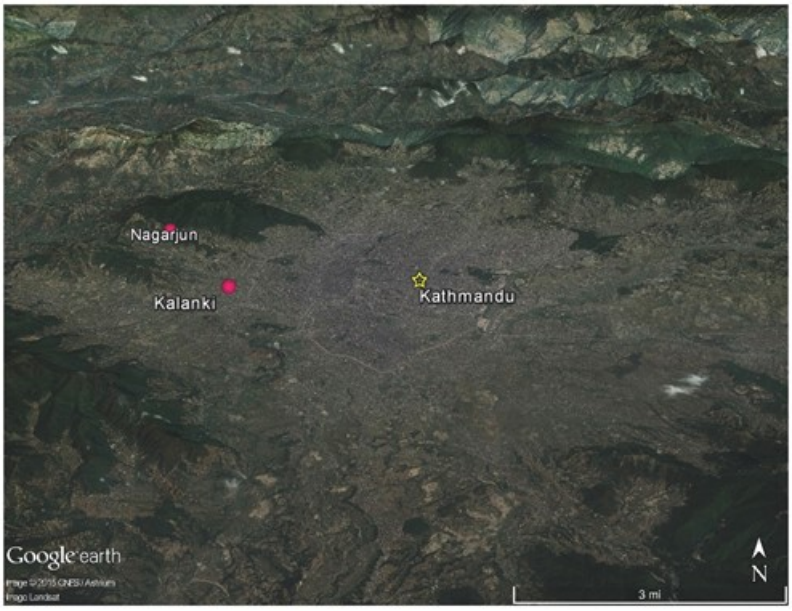

Figure 6-32 Locations of observed surface cracks

GEER team first visited the surface crack observed in Nagarjun/Ramkot. The local people living in the area directed the GEER team to the observed surface crack that was located on the slope of a hill. The surface crack was located on a slightly at a higher elevation on the sloping hill. The surface crack of approximately 5 inches around the hill as shown in Figure 6-33. The length of the crack was approximately 170 ft, in most of the parts the surface crack was already filled with mud by the locals as a preventive measure before the monsoons against possible landslide and slope failure that might be triggered with rain-water filling up the surface cracks (Figure 6-33). Although the area was not highly occupied, few collapsed mud-mortar type of single to two story houses were observed on the hill side in addition to the few slightly damaged reinforced concrete frame structures (Figure 6-34). Temporary shelter were being built in the area.

Figure 6-33 Observed surface 170 ft. long, 5 inch wide surface crack in Nagarjun

Figure 6-34 Building damage around the surface crack observed in Nagarjun

The second site visited by the GEER Team was at Syuchatar. The team walked along the exposed surface crack following the directions of the locals living in the vicinity. The surface crack is found to be on a mildly sloping hill that is occupied by few one to two story, mostly reinforced concrete frame structures (Figure 6-35). Some of the mud-mortar and masonry concrete houses in the area were damaged, however most of the reinforced concrete frame structures did not experience major damage (Figure 6-36). At some locations where the surface crack crosses through the structure a crack on the foundation slab and on the walls were observed (Figure 6-37). The surface crack at this location is estimated to be approximately 1800 ft long, at some locations the depth of the crack is observed to be up to 14 ft. and width of the crack is overserved to be up to to 1 ft. wide (Figure 6-35). The mechanism of the failure is predicted to be lateral spreading. In order to better understand the subsurface soil conditions, GEER Team returned to the site to collect samples and perform in-situ shear strength tests. At three different locations along the crack, team collected soil samples using hand-auguring and performed strength test using in-situ vane shear in collaboration with USGS (Figure 6-38). Collected samples has shown presence of silty sand layer that might have liquefied and caused lateral spreading.

Figure 6-35 Observed surface ~1800 ft. long, ~1 ft. wide, 14ft. deep surface crack in Syuchatar.

Figure 6-36 Building damage around the surface crack observed in Syuchatar.

Figure 6-37 Cracks on the floor and walls due to lateral spreading in Syuchatar.

Figure 6-38 Soil sampling and field strength testing performed in Syuchatar.

6.17 Lateral Spreading at Tsho Lorpa Glacial Lake Dam, El 14,500 ft

The Tsho Lorpa glacial lake dam is a natural lake located at an El 14,500 (4,535m, Figure 6-39). A spillway was built to control the water level in the lake and prevent overtopping and possible breaching of the natural dam. The site was visited by helicopter to examine the integrity of the natural dam material around the lake, Figure 6-40, as well as the spillway, Figure 6-41. The natural dam material showed now cracking or slumping. At the spillway lateral spreading was observed on the lake side. Significant lateral and vertical displacement, Figure 6-42, are observed in excess of a total of about 1.5 m laterally and about 0.5 m vertically.

Figure 6-39 Plan view of Tsho Lorpa Glacial Lake Dam (27^0 52’ 9.57”N, 86^0 27’ 44”E).

Figure 6-40 Glacial Lake (27^0 52’ 9.57”N, 86^0 27’ 44”E).

Figure 6-41 Spillway of Glacial Lake (27^0 52’ 9.57”N, 86^0 27’ 44”E).

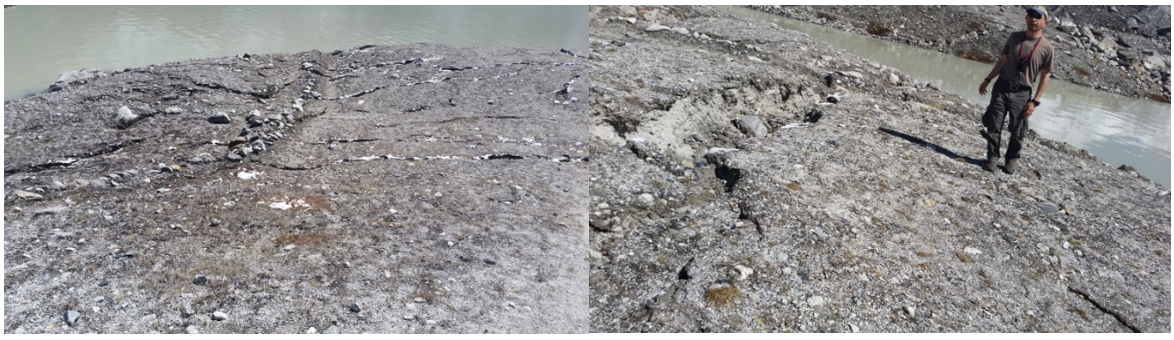

Figure 6-42 Lateral Spreading along the upstream side of the spillway (27^0 52’ 9.57”N, 86^0 27’ 44”E).

6.18 Summary and Recommendations for Future Research

The M7.8 and aftershocks caused soil failure in a number of locations around the greater Katmandu Valley. Because the loading was not very intense (low amplitude high frequency energy) the soil failure resulted in small to medium deformations in most cases. This is often termed "marginal" or "incipient" liquefaction. Follow-up research on these sites would be warranted if the ground shaking can be better characterized that it currently is with the single strong motion recording. "Marginal" sites are particularly useful case histories because they define the boundary or threshold of soil failure.

The Lokanthali site presents the most interesting soil failure case history from this event. The large spatial extent of ground cracking and the large deformations associated with these cracks have been mapped in some detail here. Limited trenching and sampling to date has indicated that weak sandy soils and weak clayey soils are present. As mentioned already follow-up research would be predicated on acquiring better loading information in the form of more and

closer strong motion recordings, or calibrated site response analysis. Follow-up research could include:

- acquiring existing and new penetration resistance measurements (preferably CPT) to characterize the cyclic resistance of these soils.
- assessing the contribution of static driving shear stresses from slopes and buildings to the crack patterns
- analyzing how the main shock and aftershocks effected the weak soils individually and collectively
- evaluating foundation type and performance when subjected to deformations from ground cracking

6.19 References

Bray, Jonathan D., and Rodolfo B. Sancio. "Assessment of the liquefaction susceptibility of fine-grained soils." Journal of geotechnical and geoenvironmental engineering 132.9 (2006): 1165-1177.

DMG (1998). Engineering and Environmental Geology Map of the Kathmandu Valley. Department of Mines and Geology, Kathmandu (Nepal).

Idriss, I. M., and R. W. Boulanger. "Semi-empirical procedures for evaluating liquefaction potential during earthquakes." Soil Dynamics and Earthquake Engineering 26.2 (2006): 115-130.

Piya, B. K. (2004). Generation of a Geological database for the Liquefaction hazard assessment in Kathmandu valley. Thesis in partial fulfillment of MS, International Institute for Geo-Information Science and Earth Observation, Enschede, The Netherlands, March.

Sapkota, S. N., Bollinger, L., Klinger, Y., Tapponnier, P., Gaudemer, Y., & Tiwari, D. (2013). Primary surface ruptures of the great Himalayan earthquakes in 1934 and 1255. Nature Geoscience, 6(1), 71-76. Sakai, H. (2001a). The Kathmandu Basin as archive of Himalayan uplift and past monsoon climate, Jour. Nepal Geol. Soc., v 25 (sp. Issue), pp.1-7.

Sakai, H. (2001b). Danuwargaun Fault as a trigger for draining of the Palaeo-Kathmandu Lake, Central Nepal, Jour. Nepal Geol. Soc., v 25 (sp. Issue), pp.89-92.

Bolton Seed, H., Tokimatsu, K., Harder, L. F., & Chung, R. M. (1985). Influence of SPT procedures in soil liquefaction resistance evaluations. Journal of Geotechnical Engineering, 111(12 Boulanger, R. W., & Idriss, I. M. (2004). Evaluating the potential for liquefaction or cyclic failure of silts and clays (p. 131). Center for Geotechnical Modeling.

Holtz, R.D., Kovacs, W.D. & Sheahan, T.C. 2011. An Introduction to Geotechnical Engineering, 2nd Ed. Pearson Education, NJ.

7 Performance of Dams and Hydropower Facilities

7.1 Introduction

The April 25th mainshock and May 12th aftershock damaged six projects of the Nepal Hydroelectric Authority, totaling approximately 190 Megawatts (MW) of generating capacity, and 10 projects by independent power producers, totaling over 80 MW of capacity (http://www.hydroworld.com/articles/2015/05/nepal-s-456-mw-upper-tamakoshi-hydroelectric-project-suffers-settlement.html). Given the importance of the hydropower plants in the country and upcoming large-scale hydropower projects it is important to understand the type damage observed in the existing hydropower facilities. This section summarizes the GEER team reconnaissance study on the performance of dams and hydropower facilities.

With its steep mountainous topography and around 6000 rivers, rivulets, and tributaries, Nepal has the world's second largest hydropower resources, with a potential to generate 42,000 MW of hydropower. Despite this huge potential, the country was producing only 800 MW through 20 major hydropower plants and a number of small micro hydropower plants before the April 2015 earthquake and its aftershocks. The production rate of 800 MW is not enough to meet the current 1,400 MW demand electricity, which is growing by 9% annually. Due to this big difference between the demand and the supply, only 40% of the Nepalese population has access to the electricity (www.ippan.org.np). Nepalese people experience 12 to 18 hours energy cuts daily.

Hydropower development in Nepal began with the development of the 500 kW Pharping power plant in 1911. Until 1990, hydropower development was under the control of the Nepal Electricity Authority. In 1992, hydropower sector was opened to the private sector. Today private power producers contribute 148 MW of power production. In recent years, many international organizations and countries began supporting projects to help increase the energy production in the area. One of these projects is the South Asia Sub-regional Economic Cooperation (SASEC) Power Expansion Project that seeks to build new transmission infrastructure to increase hydropower investment to increase energy capacity and to help overcome the power shortages (http://www.norway.org.np/Norway_and_Nepal/News_and_events/Increasing-energy-capacity-and-network/#.VavzCflViko). In 2015, the Nepal Electricity Authority proposed the Nepal Power Sector Reform and Sustainable Hydropower Development Project (PSRSHDP) that intends to provide technical and analytical studies as a preparation for the upcoming transmission lines and large-scale private and public investment in hydropower. As of February 2015, Nepalese authorities signed project development agreements for 900 MW Upper Karnali with GMR-India, 900 MW Arun-3 with SJVNL, 600 MW Upper Marsyangdi, 750 MW West Seti with Three Gorges-China, and 880 MW Tamakosi III with SN Power (Rajbhandari, 2015).

GEER team personnel conducted two campaigns to visit damaged hydropower sites by road, where accessible, supplemented by aerial helicopter surveys. Between May 26 and 28 a group of the team members visited projects along the Trishuli River near the mainshock epicenter, including Rasawagadhi near the Chinese border, Chilime, Upper Trishuli 3A and Trishuli. Between May 29 and 30 a group of the team members visited projects in the aftershock area along the Sunkoshi River, including Upper Bhotekoshi, Sunkoshi, and Sanima. A group of GEER team members also visited the Upper Tamakoshi Project by helicopter on May 27.

Figure 7-1 shows the hydropower plants visited by the GEER Team B together with the surface tracks of the team.

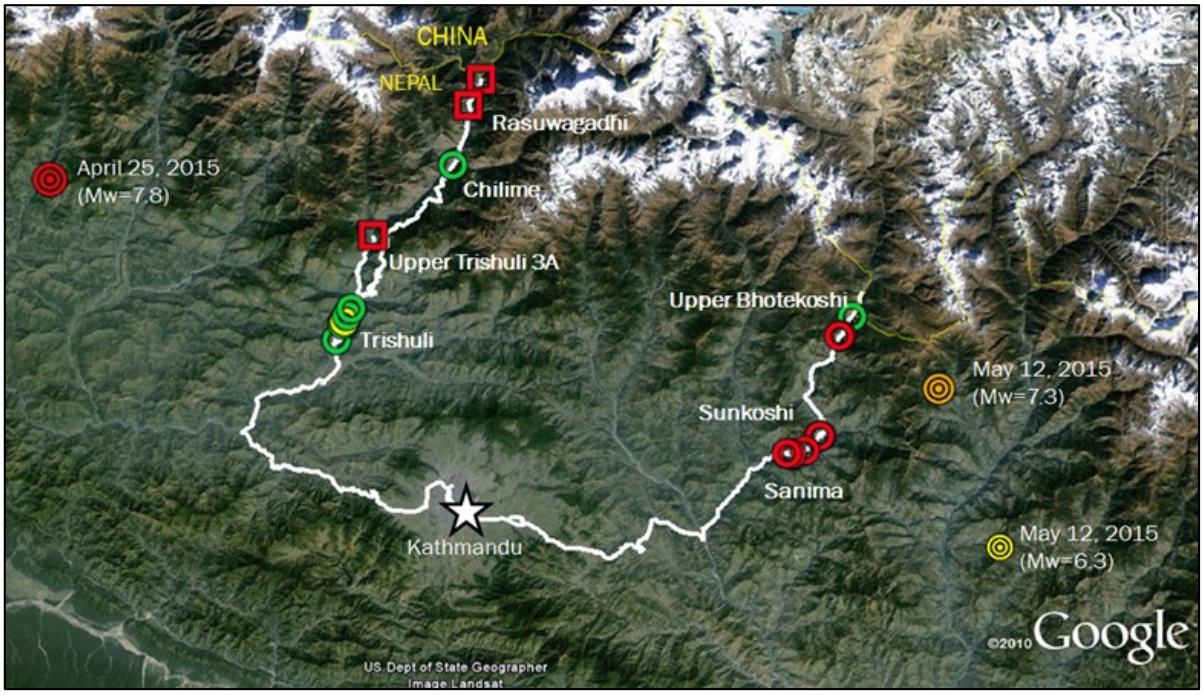

Figure 7-1 Hydroelectric plants visited by the GEER Team B. Squares indicate projects under construction. Circles mark completed projects. Red marks projects that sustained damage during the earthquake or were not operational due to earthquake damage, ongoing construction, or other issues. White marks the surface tracks of the GEER Hydro Assessment Team. The western track follows the Trishuli River and the eastern track follows the Sunkoshi River.

7.2 Trishuli River Projects

Between May 26 and 28 some of the team members visited projects along the Trishuli River near the mainshock epicenter, including Rasawagadhi near the Chinese border, Chilime, Upper Trishuli 3A and Trishuli. Table 7-1 summarizes the site conditions for projects along the Trishuli River. 111 MW Rasuwagadi and 60 MW Upper Trishuli 3A that were not in operation during the time of earthquakes but suffered major damages and still under continuous risks.

7.2.1 Rasuwagadhi

The 111 MW Rasuwagadhi project is located where the Trishuli River cuts through the high Himalaya just south of the Chinese border. The project site is located in a narrow gorge composed of gneissic and quartzitic bedrock. From upstream to downstream, the GEER team visited the headworks area near the border, the new workers colony site, the dam offices, and the powerhouse access tunnel. The project is currently under construction.

In the project area, shaking from the mainshock caused abundant rockfalls sourced from high on the canyon walls, with more localized slope failures occurring in fluvial and colluvial deposits mantling the lower canyon walls. Damage was caused primarily by rockfall impact.

In the headworks area, several rockfalls on the north side of the river damaged construction equipment, including a crane (Figure 7-2). A large rockfall on the south side of the river buried the road to the border and diverted channel flow causing a breach in a temporary coffer dam

and inundating portions of the headwork construction area downstream (Figure 7-2). The same rockfall buried the Nepal welcome center at the Nepal/Chinese border, reportedly killing over 20 people.

Table 7-1 Hydropower projects along the Trishuli River.

Project	In operation at time of EQ	Rockfall, landslide	Debris flow	Settlement	Tension cracks	Damage to structure	Damage to tunnels, canals or penstocks	Damage to equipment	Damage to site roads	Damage to access roads	Resumed Operation	Remaining Risks	Comments
Rasuwagadhi		x	x		x	x	x	x	x			x	Under construction. Temporary coffer dam breached by rockfall, inundating dam construction area. Minor rockfall in unlined tunnel section.
Chilime	x	x				x					x		Rocks fell through roof of secondary structures.
Upper Trishuli 3A								x	x	x		x	Under construction. Access roads covered by rockfalls. Large rocks impacted equipment yard, hydro camp, and sand catcher.
Trishuli	x			x			x				x		Settlement of fill caused minor cracking of secondary structures at headworks. Settlement of canal walls caused cracking of liner and piping.

Figure 7-2 Site access roads, infrastructure and equipment including a crane in the Rasawugadhi headworks area were damaged by rockfalls. A temporary coffer dam was damaged by the rockfalls and then breached when flow of the river was diverted around the rockfall, directly toward the dam, causing overtopping and erosion (28°16'27.03" N, 85°22'41.59" E).

Downstream of the headworks, near the dam office and powerhouse access tunnel, roads and fluvial terraces above oversteepened slopes locally exhibited tension cracks (Figure 7-3). The access road to the surge chamber was blocked by small accumulations of rock debris shed from roadcuts upslope. Rockfalls continued throughout the project area during our site visit.

Figure 7-3 Tension cracks were observed along roads built on cut-fill slopes near the powerhouse access tunnel. Rockfall debris locally blocked access roads to this area, especially on steepened slopes. (a) 28°14'23.91" N, 85°21'28.67" E, (b) 28°14'28.46" N, 85°21'30.18" E

Although many portions of the hydro project are not directly in the path of rockfalls, some areas are directly below debris chutes, such as the new site for the dam workers colony that is currently under construction (Figure 7-4).

Figure 7-4 New hydro camp buildings located between the headworks and powerhouse have been impacted by some rock fall debris from above (28°15'55.10" N, 85°22'30.11" E).

Dam infrastructure generally performed well with only minor cracking observed in walls of the dam offices. Inspection of the powerhouse access tunnel showed no rockfalls in areas where

the tunnel was lined. One area where the lining had not been completed experienced failure of several small blocks near the crown at joint/foliation intersections.

Rockfalls will continue to be a concern for the Rasuwagadhi project due to the high volume of material loosened by rockfalls and shaking that remains perched on the canyon walls above the site. A debris flow sourced from a rockfall debris chute in the headworks area was mobilized during heavy rains on the evening of our arrival at the site, underscoring the potential for high sediment flux during the coming monsoon. Damage and ongoing hazards increase the potential for construction delays for the project.

7.2.2 Chilime

The 22 MW Chilime hydropower project sustained minimal damage from the earthquake and was operational at the time of our visit. The GEER team visited the underground powerhouse on the right bank of the river in the town of Chilime and the powerhouse yard. The powerhouse was operating during our visit. Storage buildings housing the backup diesel generator and other equipment sustained localized cracking from shaking and holes in their roofs where individual rocks measuring up to 0.25 m or more fell from overlying cliffs (Figure 7-5).

Figure 7-5 Secondary buildings at Chilime exhibited minor shaking. Damage was limited to cracks in infill walls and holes in the roofs of some structures. (a) 28°9'27.30" N, 85°16'54.38" E, (b) 28°9'27.30" N, 85°19'54.38" E

7.2.3 Upper Trishuli 3A

The Upper Trishuli 3A Project is under construction and will have a generating capacity of 60 MW when completed. At the time of the GEER team visit, access to the site was cut off where several kilometers of rockfall debris covered over the main access road to the site (Figure 7-6). GEER personnel accessed the site on foot and surveyed, from upstream to downstream, the headworks area, tunnel portal, workers colony, and concrete batching plant.

Figure 7-6 Continuous rockfalls block the main access road to the Upper Trishuli 3A headworks. The large pile of boulders on the right marks the location of the road. A walking path has been worn into the rockfall debris by villagers and dam workers. Tallus slopes in the background are all from fresh rockfalls. Vegetated debris cones on the left side provide evidence for previous rockfalls that were not reactivated during the 2015 earthquake. View is to the southwest (28°2'53.76" N, 85°12'4.27" E).

The project is located in a narrow canyon composed of medium to high grade metamorphic bedrock including phylite, slate, schist, and metagranites, locally with gneissic texture. The lower canyon walls are nearly vertical for up to several hundred meters. Debris chutes channel rockfall debris down the steep walls. Vegetated talus cones at the base of the chutes are evidence for past rockfalls in the area.

The Upper Trishuli area exhibited the most extensive rockfalls of any of the hydro projects that we visited. Rockfalls occurred primarily on the southeast side of the river, and were typically sourced where steep canyon walls met lower gradient slopes high above the site. The largest rockfalls occurred in areas of hard granitic augen gneiss, with large resistant blocks, typically several meters in diameter mantling the lower slopes of the canyon in the order of 10 to 100s of meters above the river. Although not as extensive as to the southwest, localized rockfalls also blocked access roads in the headworks areas (Figure 7-7). Infrastructure in the headworks area sustained minimal damage, with the diversion dam, sand catcher and canal structures mostly unaffected (Figure 7-8). Rock impacts to the sand catcher, for example, produced small (<1 m diameter, < 0.25 m deep) impact craters in the outermost concrete (Figure 7-9).

Figure 7-7 Road blocked by rockfalls through the headworks area (28°3'47.21" N, 85°12'23.25" E).

Figure 7-8 View downstream of the Upper Trishuli 3A headworks. Two of the gates are open, two closed. Due to damage to equipment and lack of vehicle access to the site, the remaining two gates cannot be opened before monsoon, which will likely lead to additional damage to the site. Flooding is also expected at the workers colony downstream (28°3'52.35" N, 85°12'20.86" E).

Figure 7-9 Sand trap under construction downstream of the headworks diversion dam were impacted by rockfall from above. Damaged observed was not consequential. (a) 28°3'41.77" N, 85°12'24.74" E, (b) 28°3'40.03" N, 85°12'23.69" E

Slope stabilization measures in the headworks area performed effectively during the earthquake. On the right abutment of the diversion dam, a near-vertical 25 m high cut in colluvium (older rockfall debris) had been benched into four 6-foot high flights. The entire wall was covered in shotcrete, with rock bolts placed in the upper three walls. Despite spalling of shotcrete from the lowest unbolted wall, the slope remained stable.

The GEER team observed little to no rockfall from the crown or ribs within 30 m of the upstream portal of the water conveyance tunnel to the powerhouse (Figure 7-10). The presence of loose blocks perched on the cliffs above the portal rockfalls, suggests that falling rocks will continue to be a hazard in this area in the upcoming months and perhaps years.

Figure 7-10 Scattered rockfall debris observed outside portal entrance with risk of continued rock fall evident. View is upstream toward dam (not shown) (28°3'36.20" N, 85°12'24.21" E).

7.2.4 Trishuli

The 24 MW Trishuli Project is located downstream of the gorges that define the upper Trishuli River in a broad river valley marked by flights of fluvial terraces. The GEER team visited the headworks and powerhouse areas, and selected sections of the open canal system that connects the two areas.

At the headworks, a concrete diversion dam extends from the right bank to the mid-point of the river. The dam control room and a gate rack sit on a fill pad adjacent to the right dam abutment. Although the team did not observe significant cracks or other damage to the dam, slight settling of the fill pad during the earthquake produced several centimeters of gap between the concrete pad beneath the gate rack and the dam abutment (Figure 7-11). Movement of the fill also produced a crack in a retaining wall at the edge of the fill. Shaking from the earthquake produced localized cracking in the walls of the dam control room focused around the support columns (Figure 7-12).

(a) (b)

Figure 7-11 Minor damage observed from settling of fill platform adjacent to right abutment of Trishuli diversion dam. (a) foundation of the gate rack structure built on the fill pad (27°57'48.01" N, 85°10'12.52" E) and (b) Several centimeters of dilational cracking between the dam abutment, showing cracking at the edge of a retaining wall at the edge of the fill pad and the gate rack in the background (27°57'47.96" N, 85°10'13.34" E)

(a) (b)

Figure 7-12 Shaking damage in walls of dam control room. (a) 27°57'48.55" N, 85°10'14.49" E, (b) 27°57'48.55" N, 85°10'14.49" E

Dam personnel took the team to a section of the canal where several instances of cracking of the canal liner, and in one case piping of water from slopes beneath the canal had been observed. Cracking occurred along the edges of two large settling ponds, one lined and the other unlined. Cracks in the lined settling pond were patched with pitch. Cracks in the walls of unlined pond were patched with mud likely derived from the silt and clay caps on older terrace deposits in the vicinity. The unlined settling pond also experienced lateral spreading (Figure 7-13).

Figure 7-13 Lateral spreading around a settling pond along the canal system between the Trishuli headworks and powerhouse (27°56'15.18" N, 85°9'22.28" E).

Another section of canal upstream of the settling ponds had cracks in the liner where water escaped and flowed out of the terrace riser below. The leaks stopped when the cracks were patched with pitch. The close proximity of landslide headscarps below the canal wall in this area suggests that the cracking may have been caused by lateral movement of the area adjacent to the canal (Figure 7-14). This area will require monitoring during the monsoon season to assess whether cracks reappear along this section of the canal. The powerhouse and penstocks for the Trishuli Project were not damaged by the earthquake.

Figure 7-14 Section of Trishuli canal that leaked after the April 25th earthquake. Fresh head scarps (hummocky vegetated area left of power lines) along the outer edge of the fluvial terrace to the right of the canal suggest that this area is unstable and may have mobilized during the earthquake, possibly causing extension along cold joints in the canal liner (27°56'49.48"N, 85° 9'37.79"E).

7.3 Sunkoshi River Projects

Between May 29 and 30 a group of the GEER team members visited projects in the aftershock area along the Sunkoshi River, including Upper Bhotekoshi, Sunkoshi, and Sanima. Table 7-2 summarizes the site conditions for projects along the Sunkoshi River. Damage observed at all three hydropower projects visited by the GEER team along the Sunkoshi River.

Table 7-2 Summary of site conditions for projects along the Sunkoshi River.

Project	In operation at time of EQ	Rockfall, landslide	Debris flow	Settlement	Tension cracks	Damage to structure	Damage to tunnels, canals or penstocks	Damage to equipment	Damage to site roads	Damage to access roads	Resumed operation	Remaining risks	Comments
Upper Bhotekoshi	x	x	x			x	x	x	x			x	Headworks: Minor rockfall impact damage to handrails and surficial damage to the concrete gravel catcher structure. Penstock/PowerHouse: Rockfall impact to penstocks above powerhouse causing leak. Resulting debris flow damaged hydro camp buildings, scoured the penstock liner and inundated powerhouse area.
Sunkoshi	?					x	x						Significant damage to headworks from June 2014 landslide and subsequent landslide dam breach during last monsoon season. Some additional structural shaking damage observed and expected to be from recent earthquake events. Damage to canal also noted from recent earthquakes.
Sanima	?					x							Micro hydro powerhouse damaged by shaking mostly. Infill wall collapsed.

7.3.1 Upper Bhotekoshi

The 45 MW Upper Bhotekoshi Project is located where the Sunkoshi River cuts through narrow gorges south of the Chinese border. Bedrock consists of medium to high grade metamorphic rock including phylite, schist, gneiss and quartzite and is highly resistant, forming near vertical cliffs in the project area.

The GEER team inspected the headworks, powerhouse and penstock above the powerhouse. A tunnel extending between the headworks and powerhouse on the left side of the river was not accessible for inspection.

The diversion dam at the headworks was in good condition. The earthquake dislodged only small scattered rocks from the cliffs above the left abutment of the dam, with only railings and light installations damaged by rock impacts (Figure 7-15).

(a) (b)

Figure 7-15 The Upper Bhotekoshi Headworks - Handrail damage, surficial debris impact and debris inundation from rock fall was observed at the gravel catchers. Remaining risks of damage and danger to life safety in this area are remaining risks. (a) 27°56'17.80" N, 85°56'42.88" E, (b) 27°56'17.39" N, 85°56'43.10" E

Larger rockfalls affected the powerhouse area, causing significant damage. On the left (southeast) side of the canyon, scattered blocks rained down on the penstock where it exited the canyon wall above the powerhouse. A direct hit by one of these blocks ruptured the penstock at a seam (Figure 7-16).

Figure 7-16 Penstock punctured by rock fall (a) 27°54'48.89" N, 85°55'38.25" E, (b) 27°54'46.11" N, 85°55' 38.28" E.

Mobilization of rockfall debris by water from the burst penstock created a debris flow that inundated the workers colony, scoured the penstock liner and inundated buildings and electrical equipment on the upstream side of the powerhouse (Figure 7-17). Fine rockfall debris from the other side of the river also impacted the powerhouse area, possibly blowing out powerhouse windows (Figure 7-18).

Figure 7-17 (a) Debris flow damage (27°54'45.77" N, 85°55'38.00" E), (b) Debris flow damage the workers colony (27°54'44.47" N, 85°55'32.87" E), (c) powerhouse, showing debris that has accumulated to the top of doorways in the powerhouse area (27°54'45.67"N, 85°55'28.23"E), (d) penstock liner (27°54'45.32" N, 85°55'27.15" E)

Figure 7-18 A debris plume and water from the impact of the rock fall across the river is hypothesized to have broken windows and resulted in the silt coating on river-facing walls of the powerhouse (contrast blue walls facing away from river with brown, silt coated walls

facing river). Silt was also observed piled on the sills of the topmost windows. (a) 27°54'46.80" N, 85°55'26.52" E, (b) 27°54'45.44" N, 85°55'26.88" E

7.3.2 Sunkoshi

The 10 MW Sunkoshi Project is located at the transition from narrow gorges upstream to a wider river valley downstream. Bedrock consists of foliated low to medium grade metamorphic rock including phylite and schist that is significantly weaker than upstream, resulting in large slope failures and earthflows in the vicinity of the project. The 2014 Jure landslide, with a length of over a kilometer is representative of this type of slope failure. The landslide created a dam that breached sending a wave of water of the Sunkoshi headworks.

The GEER team evaluated earthquake effects to the dam, the powerhouse and open canal connecting the two structures. Despite experiencing the breaching of the Jure landslide and two significant earthquakes the 10.05 MW Sunkoshi Dam is in relatively good condition, with relatively little structural damage (Figure 7-19).

Figure 7-19 (a) Headworks damaged by June 2014 landslide and the 2015 earthquake (27°45'30.24" N, 85°52'5.39" E), (b) Concrete spalling expected to be as a result of earthquake induced shaking (27°45'26.85" N, 85°52'3.33" E), and (c) Headworks structure shifted to the right) on top of the beam column base structure (27°45'29.40" N, 85°52'3.25" E)

The canal was dry at the time of the GEER inspection due to a breach in the liner at the bottom of the canal (Figure 7-20). The breach occurred where a crack extended through the liner for over 60 m long. The penstock intake structure and powerhouse both suffered structural cracking but do not appear to be in danger of collapse (Figure 7-21, Figure 7-22).

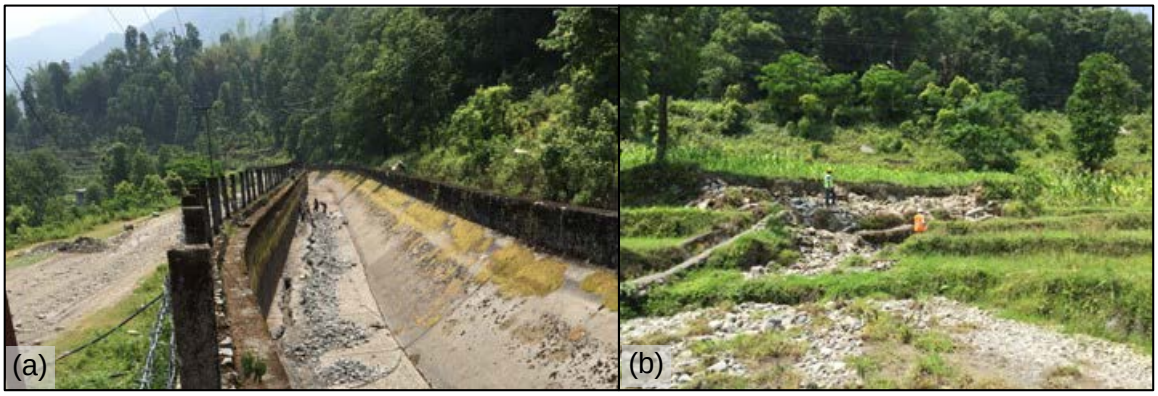

Figure 7-20 Cracking observed in canal (left). Water from cracked canal is expected to have saturated soil and contributed to slope failure downslope of the canal. The photo at the right shows where canal water drained out of the hillside below the canal. (a) 27°45'11.01"N, 85°50'44.07"E, (b) 27°45'11.94" N, 85°50'47.58" E

Figure 7-21 Structural damage observed in the intake structure of Sunkoshi powerhouse. Significant shear cracks were observed in the upper structure after the May 12th M 7.3 aftershocks. No significant damage was observed in the penstock (27°45'10.66" N, 85°50'17.70" E).

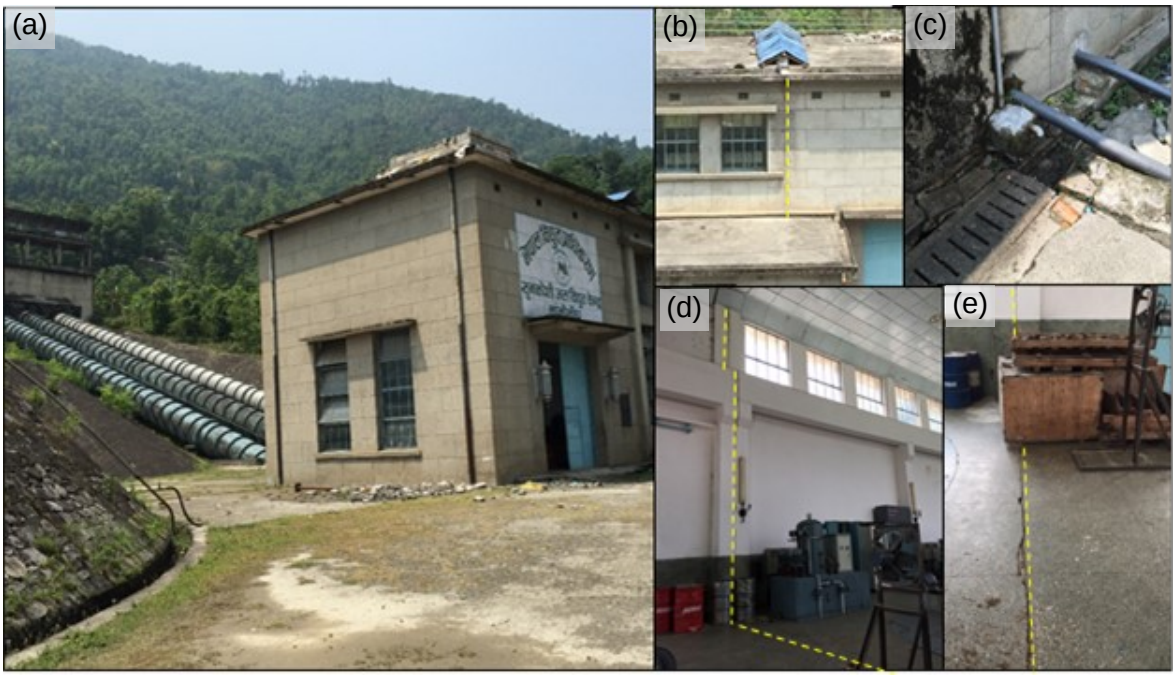

Figure 7-22 A continuous crack running through the walls and the floor is observed in the powerhouse structure. This observed crack can be potentially due to the differential settlement across the power plant structure, which can be further supported by the cracks and slight vertical offset observed in the pavement shown on the upper left side (7-21 27°45'13.96"N, 85°50'17.26"E).

7.3.3 Sanima

The 2.5 MW Sanima Project is a micro hydro project along the Sanima River which is a tributary of the Sunkoshi River. We inspected the penstock system and powerhouse which sits on a young alluvial fan at the mouth of the Sanima River where it drains into the Sunkoshi River.

The powerhouse sustained heavy shaking damage from the May 12 aftershock after having reportedly survived the April 25th mainshock relatively unscathed. Shaking from the aftershock caused the infill walls to collapse (Figure 7-23). This may have been caused by amplification of shaking in the young, poorly consolidated alluvium on which the powerhouse was constructed.

Figure 7-23 Shaking damage to powerhouse building observed. Infill walls collapsed. Concrete reinforced frame appeared to suffer little damage. Some liquefaction also evident in the area around the structure. (27°46'36.05" N, 85°53'25.62" E)

7.4 Upper Tamakoshi Power Plant

The 456 MW Upper Tamakoshi Power plant was considered the national priority project, since upon completion, it will be the largest hydroelectric project in Nepal. The earthquake induced ground shaking caused excessive settlement in the headworks and resulting in an interruption in the construction schedule.

According to the Upper Tamakoshi Power plant authorities, the four cm of settlement occurred a M5 earthquake on December 18, 2014. Settlement increased to 12 cm and 18 cm after the April 25 mainshock and the May 12 aftershock, respectively (Figure 7-24b). On April 27 a landslide induced by the April 25, 2015 earthquake closed the access road to the headworks. The earthquake also toppled a gabion wall used as a cofferdam/diversion structure (Figure 7-24c). Rockfalls were observed in the headworks area. (Figure 7-24-d). The very steep left and right abutments may create further landslide hazard at the site (Figure 7-24e). The construction work at the Upper Tamakoshi Plant is currently stopped.

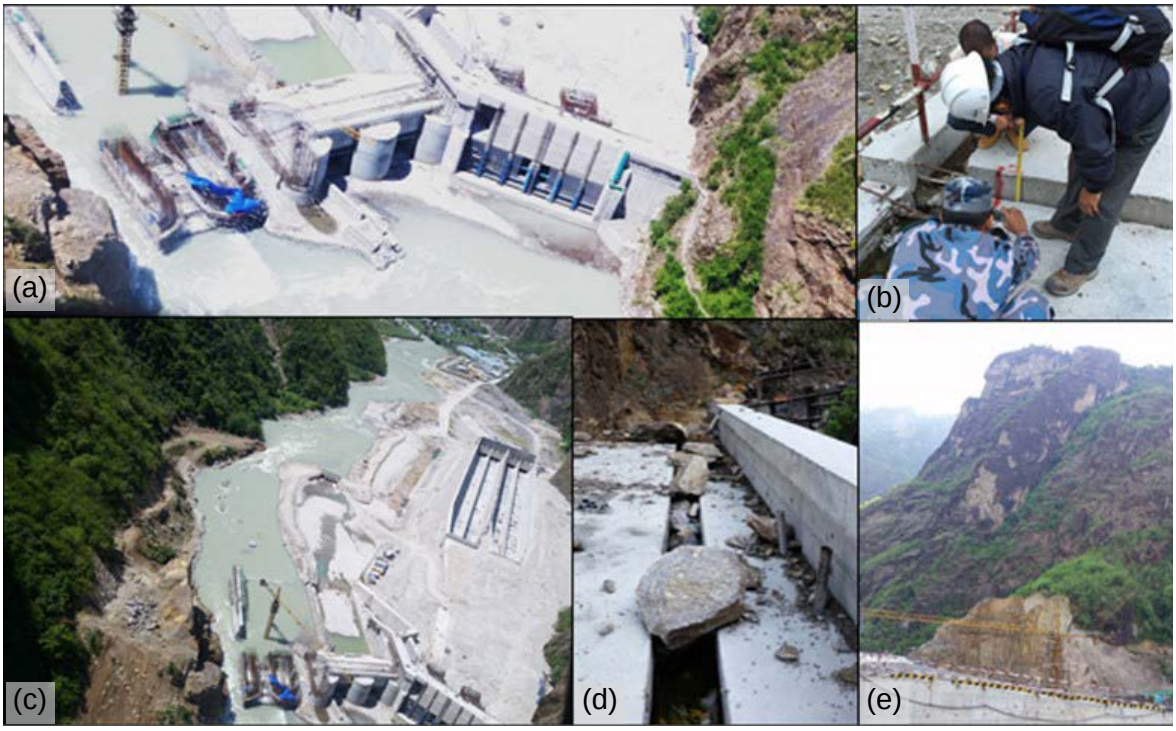

Figure 7-24 Damages observed at the Upper Tamakoshi Powerplant. (a) Aerial image of the headworks, (b) the settlement at the headworks, (c) breached cofferdam, (d) rockfalls, (e) steep slopes at the abutments.(27 55’ 29.8’’ N, 86 12’ 46.4’’ E)

7.5 Conclusions

Hydro projects along both the Trishuli and Sunkoshi showed similar patterns of earthquake response. In the steep, narrow upper reaches of each drainage, projects were impacted primarily by rockfalls. Roads, penstocks and secondary structures received the brunt of damage from these slope failures. In the lower reaches of the drainages, where river valleys open up and water is typically transmitted via open canals, shaking-related impacts such as settlement and structural damage to structures was more common. Projects along the Sunkoshi River appeared to be in worse condition than similar projects on the Trishuli River, perhaps due to the “one-two punch” of the mainshock and large aftershock.

The significant amount of rockfall debris still mantling the steep walled upper reaches of the rivers near the epicentral areas poses a continued rockfall hazard that will impact roads and hydropower infrastructure far into the future. As this material is washed into rivers, increased sediment flux could become a significant issue within the hydropower system.

7.6 References

Nepal Electricity Authority, “Environmental and social management framework (ESMF) for project sector reform and sustainable hydropower development project (PSRSHDP)”, January 2015

Rajbhandari S., “Recent developments in Nepal power sector including the status of D-M 400Kv CBLT”, Third meeting of taskforce 2, February 25-26, 2015, Colombo, Srilanka. (http://www.sari-energy.org/PageFiles/What_We_Do/activities/Advancement_of_Transmission_Systems_Interconnection_2015/Presentations/Cross-Border-Interconnection.pdf)

8 Performance of Roadways, Bridges and Retaining Structures

8.1 Highways & Roads

The total length of roadways in Nepal is approximately 12,493.94 km based on 2013/2014 Strategic Road Network Report of Nepal Department of Roads. There are three type of roads across the country: (i) blacktop, (ii) gravel, and (iii) earthen roads. Nepal government classify these roads in four main categories: (i) national highway, (ii) major and minor feeder roads, (iii) mid-hill roads, and (iv) postal roads. Table 8-1 presents the distribution of the road network in Nepal based on road type and class. According to Table 8-1, more than half of the road network consists of blacktop roads and the major feeder roads constitute approximately the 54 % of the total length of the total length of strategic road network in Nepal. Figure 8-1 maps the strategic road network of Nepal for 2013-2014 showing the roadways are more concentrated in the southern part of the country, along the Indian border due to geographic difficulties associated with the northern, where the surface elevation increase significantly due to the Himalayan Mountains. Figure 8-1 also shows that more than 40% of the road network is located in the central region of Nepal, where the Kathmandu Valley is located.

Table 8-1.Distribution of Road Network in Nepal

Type of Roads	Length (km)
Black Top	6368.98
Gravel	1735.49
Earthen	4389.47
Total	12493.94

Road Class	Length (km)
National Highways	3101.56
Feeder Roads (Major/Minor)	2869.74/194.98
Mid-hill Roads	79
Postal Roads	123.70
Total	12493.94

April 25, 2015 M_w 7.8 earthquake and the aftershocks has caused significant damage to road network of Nepal. Ministry of Physical Infrastructure and Transport (MoPIT) has calculated the loss and damage of roads and other official infrastructures in current rates at around 23.5 million dollars based on the preliminary studies. The expected final cost for the repair and rehabilitation work for the strategic road network to be around 4.7 million dollars. Most of the damage was observed in the areas that experienced high shaking intensity such as Gorkha, Sindhupalchowk, Dolakha, Rasuwa, and Makawanpur.

Landslides induced by the April 25 main shock and the aftershocks caused significant damage and interruptions in the roadways (Figure 8-2). In Gorkha, Sindhupalhowk, and Dolaka portions of the roads were swept away by the landslides. Based on MoPIT data, Barhabise-Tatopani section of the Arniko highway, a section in Ramche in Pasang Lhamu Highway, different setions of Narayanghat-Muglig road, Dolakha-Singati-Lamabagar road, Zero Kilo-Melamchi road, Gorkha-Barpak road, and Beni-Jamsom road were damaged after the main shock. May 12 M_w 7.3 aftershock caused additional damage in the road network where Ratame of the East

West Highway, Bhaise of Tribhuvan Highway, Lumle of Baglung-Pokhara road and several different sections in Krishnabhir-Jogimara road were damaged (The Himalayan Times, 2015). Fast approaching monsoon seasons increases the concerns for additional landslide damage due to weakened slopes after the April 25 ground shaking and following aftershocks as the landslides are already one of the major challenge the road network of Nepal faces each year due to the heavy rainfall during monsoons season. Often 60% of the road infrastructure gets damaged and become unusable during and after monsoon season.

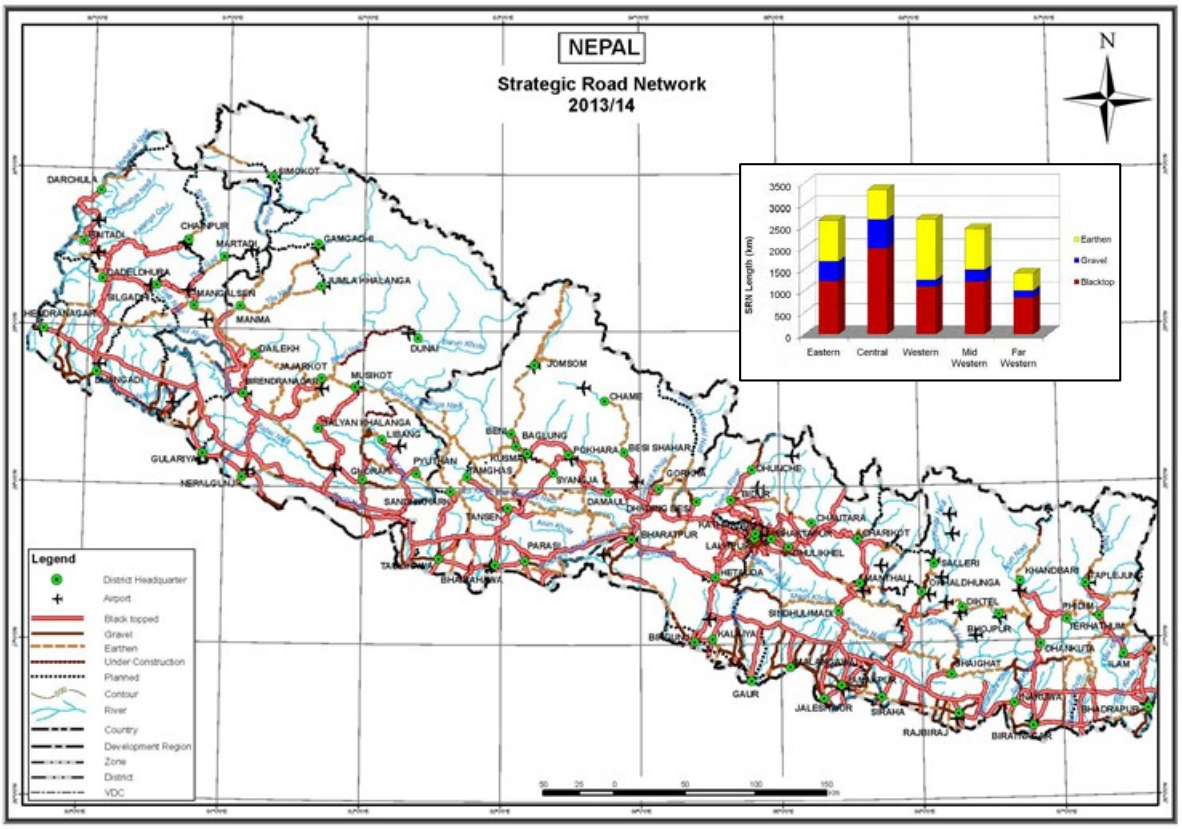

Figure 8-1 Strategic Road Network of Nepal (Ref: SSRN 2013/14, Nepal Department of Roads)

Rock falls after the mainshock and aftershocks caused interruption and damage in road network especially on the Eastern portion of the country, in areas closer to the Chinese border. Figure 8-2 shows the damage in the Arniko Highway due to the rock falls in Sindhupalchok, which is located close to the Chinese Border.

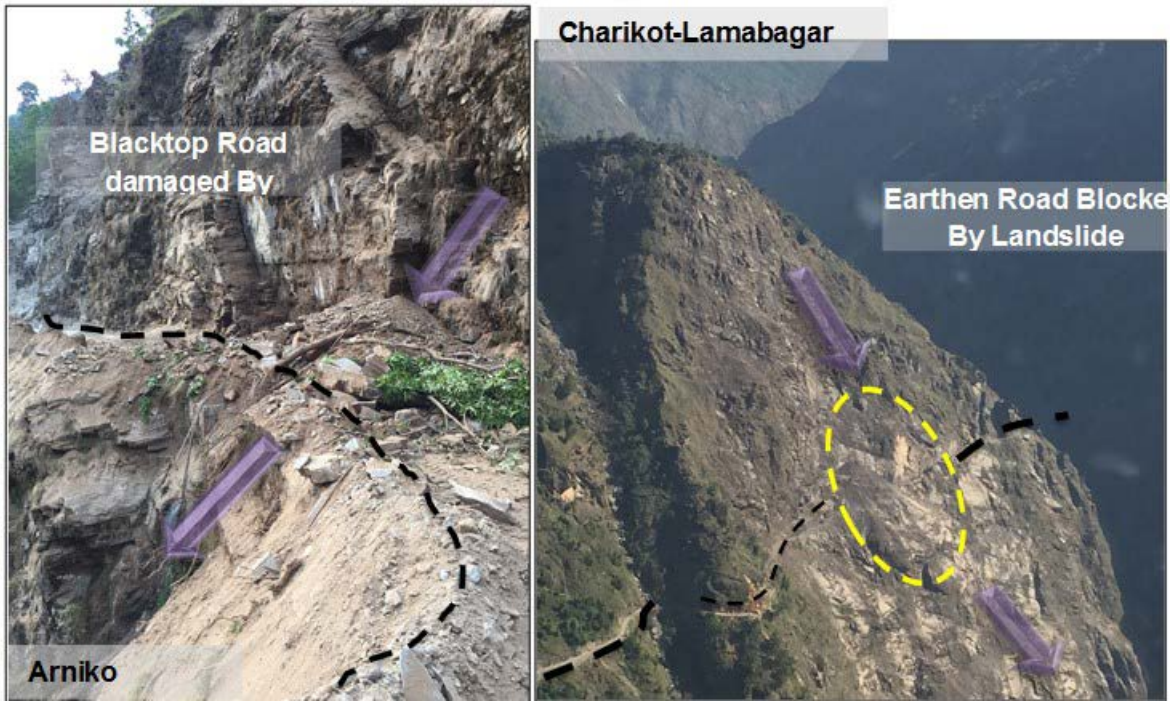

(a) (b)

Figure 8-2 Interruptions and damage on roadways caused by the earthquake-induced landslides, (a) 27 52' 15.9"N 85 53' 15.9"E, (b) 27 52' 19.1"N 86 13' 20.7"E.

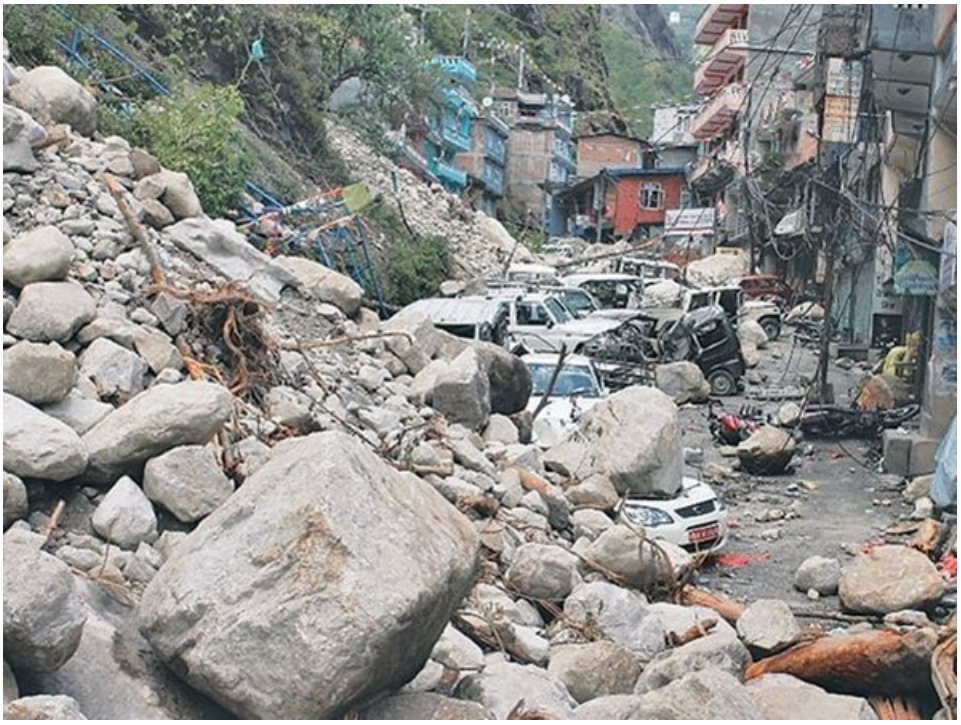

Figure 8-3 Rock falls triggered by the earthquake interrupted transportation along the Arniko Highway in Sindhupalchock. (*Ref: http://www.ekantipur.com/*)

In the Kathmandu Valley, Arniko Highway suffered from earthquake-induced damage in the Lokanthali area, where large lateral cracks with vertical offset has been observed as described in Chapter 6. Figure 6-14 plots the displacement features observed along the Arniko Highway and clearly illustrates significant vertical and horizontal offset observed in the area. Figure 8-4

presents pictures of observed lateral cracks and associated vertical offset along the Arniko Highway. Figure 8-4a shows the lateral cracks and associated vertical offset towards the sloping ground, while Figure 8-4b shows the significant vertical offset along the highway.

Figure 8-4 Road damage due to liquefaction induced ground failure in Arniko Highway in Lokanthali, 27°40'29.06"N 85°21'36.77"E.

Figure 8-5 Lateral cracks observed on Blacktop roads.

The B.P. Koirala Highway, often referred to as the Japanese Highway as it was built by a Japanese contractor and funded with Japanese grant money, is a vitally important roadway for the safe evacuation of Nepal. It is the only major eastbound exit to the south from the highly populated Kathmandu Valley. The 160 km B.P. Koirala Highway was prioritized for construction by the Nepalese government and was completed in sections over the last 15 years. The highway traverses very steep and challenging topography and extensive concrete retaining walls and drainage systems were constructed to support the Highway. These mitigation structures performed very well following the Gorkha earthquake with no significant damage observed along the entire length of the highway.

Figure 8-6 The B.P. Koirala Highway winding over the challenging topography near Sindhuli (27° 15’ 52.92” N; 85° 56’ 11.28” E).

Figure 8-7 Extensive concrete retaining walls and drainage systems of the B.P. Koirala Highway performed very well during the Gorkha earthquake (27° 16’ 05.98” N; 85° 56’ 40.56” E).

8.2 Bridges

Major bridges in Nepal are constructed and maintained either by the Department of Roads or the Department of Local Infrastructure Development and Agricultural Roads, majority of the

bridges are managed by the former. According to the database published by the Department of Roads, Nepal, DOR maintains 1709 number of highway bridges. Length of these bridges range from 6 m to 1149 m. Among those bridges, 19, 35, 27, 11, 15, 7, 46, 8, 10, 21, 40, and 22 numbers of bridges are located in the districts affected by the 2015 Gorkha Earthquake such as Kaski, Tanahu, Dhading, Gorkha, Nuwakot, Rasuwa, Kathmandu, Lalitpur, Bhaktapur, Kavre, Sindhupalchowk, and Dolakha, respectively. The GEER team was able to drive over many of those bridges during reconnaissance. These bridges performed well during the 2015 Gorkha earthquake and its aftershock sequences mainly due to the low intensity ground shaking this event produced and the good construction quality of the bridges. Damage to any of those bridges could have easily caused a serious transportation break and impacted the rescue operation as well as transportation of goods and people in and out of Kathmandu Valley. Although liquefaction induced sand boiling was observed in the flat area along the old river terrace of Manohara River at Duwakot area in Chagu Narayan, the bridge across the river performed well except a few bridge stoppers sustaining minor cracks (Figure 8-8). Likewise, a 370 m long 9 span steel composite bridge (Figure 8-9) over Madi Khola of Tanahu along the Prithvi Highway also performed well despite a few gabion river bank protection retaining wall that toppled due to stream under cutting (Figure 8-10). A close observation of a 62.6 m long 3 span steel composite deck bridge along Kumle Khola at Prithivi Highway shows that this bridge also performed well (Figure 8-11). Other bridges that the team observed exhibited similar performance level. Despite the fact the bridges performed well, several bridges, such as the one along the access road of Melamchi Water Supply Project (Figure 8-12) have been threatened by the seismically induced settlement of the approach road filling material and potential landslides along the river bank (Figure 8-13).

Figure 8-8 Manahara Bridge at Duwakot. This bridge performed well despite of several liquefaction induced sand boils evidenced near the bridge (27°40'23.1"N, 85°20'30.6"E & 27°42'49.584"N 85°24’42.26"E).

Figure 8-9 Bridge over Madi Khola along Prithvi Highway (27°40'23.1"N 85°20'30.6"E).

Figure 8-10 Collapse of gabion bank protection retaining wall along Madi Khola due to river bank erosion

Figure 8-11 Bridge over Kumle Khola at Prithivi Highway (28°1'44.022"N 84°5'22.182"E).

Figure 8-12 Bridge along the access road of Melamchi Water Supply Project being threatened by potential landslides along river banks and seismic settlement of road fill materials (27°55'38.43"N 85°33’14.510"E).

Figure 8-13 Potential landslides along the river bank that are endangering the bridge approach road (27°55'38.988"N 85°33’14.598"E).

8.3 Retaining structures

Previous major earthquakes has demonstrated that earth retaining structures generally behave well under strong ground shaking. Similarly, after the April 25 main-shock and the proceeding aftershocks in Nepal, the retaining structures generally performed well (Figure 8-14) and did not experience major damage or catastrophic failures. At few locations, some damage in the retaining walls were observed mainly due to the earthquake-induced slope stability failures (Figure 8-15 and Figure 8-16). Similarly, some cracks were observed on the retaining walls in the areas with potential site and topographic amplification effects (Figure 8-17). Figure 8-17 illustrates the cracks observed on the earth retaining wall on a ridge, located to the west of Kathmandu basin around the basin edge. The reason of the observed results and cracks can be potentially due to the poor/design and construction. Figure 8-18 shows the lost diversion wall in the Upper Tamakoshi Hydropower Plant after April 25 Mw7.8 main-shock.

Figure 8-14 Retaining walls generally behaved well during after the April 25 mainshock and aftershocks with limited cracking (a) 27 54’ 59.2”N 85 55’ 48.4”E, (b) 27 41’20.1”N 85 19’ 51.2”.

Figure 8-15 Damage in retaining walls due to the slope failures (a) 27 45’ 22.2”N 85 51’ 8.18”E

Figure 8-16 Damaged Retaining Wall (a) 27 57’ 36.4”N 85 57’ 24.2”E, (b) 27 56’ 57.2”N 85 57’ 8.28”E.

Figure 8-17 Retaining wall damage observed at the ridges (a) around Monkey Temple, Kathmandu (27 42’ 54”N 85 17’ 23.5”E) (b) around western basin edge of Kathmandu valley (27 42’ 51.5”N, 85 11’ 59.7”E).

Figure 8-18 Lost diversion wall at Upper Tamakoshi Hydropower Plant (27 55’29.1”N, 86 12’47.26”E)

9 Performance of Building Structures

Temples and historical monuments such as the Bhimshen Tower (Figure 9-1) suffered heavy earthquake damage. Many cultural heritages sites, especially temples in Kathmandu, Lalitpur and Bhaktapur were significantly damaged, along with many of the government office buildings that were constructed during the Rana Regime (such as Sinha). The primary reasons for structural damage appear to include relatively weak and brittle construction materials. The GEER team visited various sites witin Kathmandu Valley, Gorkha, Barpak, Pokhara, Melamchi (Sindhupalchowk), Dolakha, Manang, and Rasuwa to observe the effect of earthquake shaking on building structures. Observations are presented below according to geographic location.

Figure 9-1 Seven story tall Bhimshen Tower collapsed due to earthquake shaking (27°42’ 2.23” N, 85°18’43.11” E).

9.1 Kathmandu Basin/Valley

The Kathmandu basin includes Kathmandu, Lalitpur, and Bhaktapur with an aerial dimension of approximately 14 km x 18 km (Figure 9-2). The team reconnaissance included a large portion of the Kathmandu basin. In general, building damage was rather isolated and sporadic, rather than exhibiting strong geographic patterns and trends. The isolated occurrence of damage may be due to foundation or structural design details, and possibly construction quality issues. Although building design codes have been implemented in many municipalities of the country (including all municipalities in Kathmandu basin), based on the team’s conversation with local geotechnical and structural engineers, the design code does not take soil/rock site effects into consideration and the code has not been strictly enforced. As enumerated below, the effects of the earthquake in Kathmandu basin are divided into: a) basin margins, b) high rise buildings, and c) geotechnical effects.

9.1.1 Basin Margins

Severe damage was observed at the basin edges in the areas of Kapan, Balaju, Sitapaila and Ramkot. As presented in Figure 9-3 and Figure 9-4, more than 50 people died due to the collapse of two buildings at Kapan. As other buildings in the area were not seriously affected by the earthquake, this suggests the two collapses are isolated cases of the seismic effect on structures.

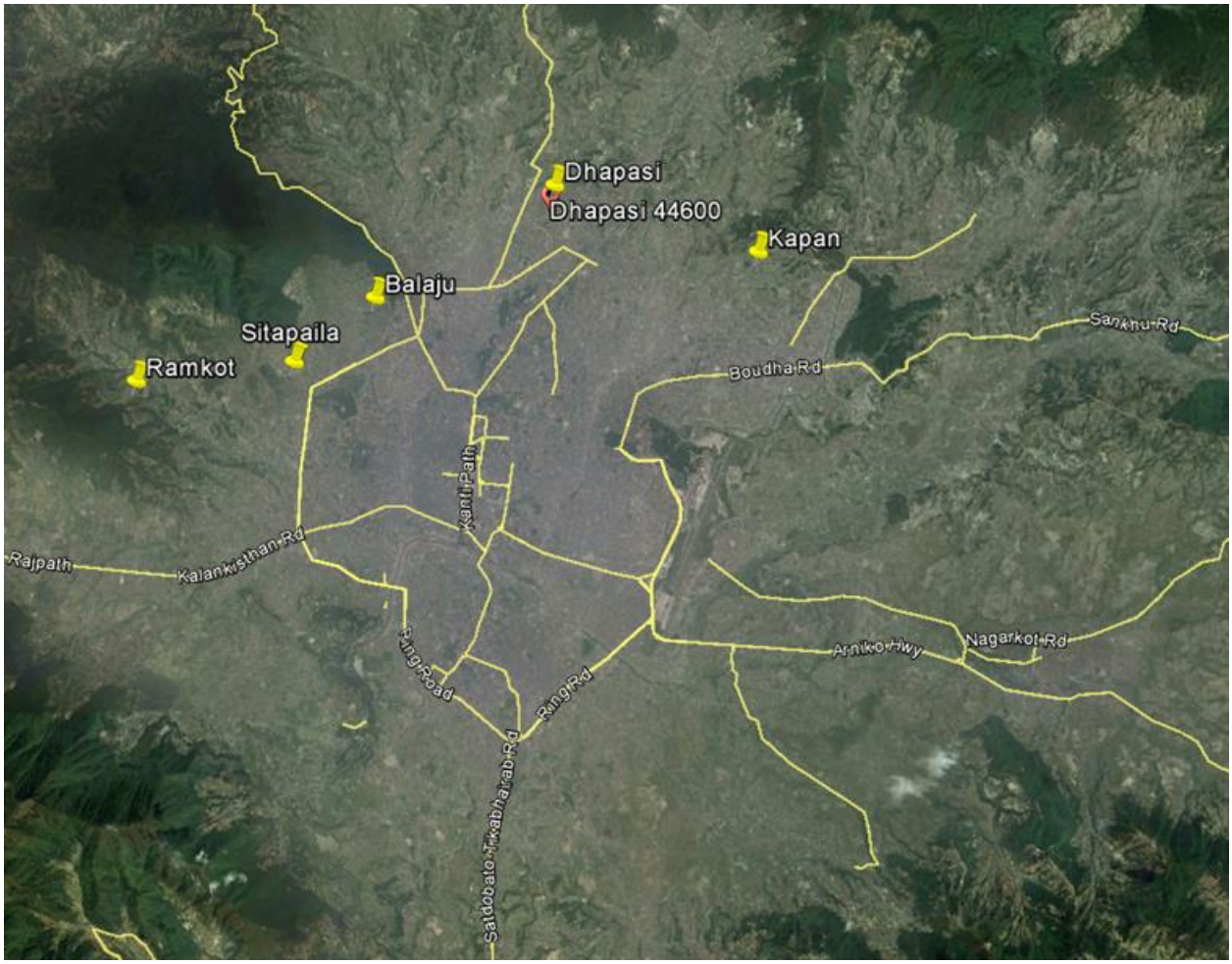

Figure 9-2 Major structural damage observed at Kathmandu Valley

Figure 9-3 A 5.5 story building collapsed at Kapan after the ground shaking due to the M_w7.8 Gorkha Earthquake. A total of 11 people died at this building (27^{0}43'30.0" N, 85^{0}21'54.89" E).

Figure 9-4 A 7 story building collapsed at Kapan after the ground shaking due to the M_w7.8 Gorkha Earthquake. A total of 40 people died at this building (27^{O}43'26.15" N, 85^{O}2'"30.75" E).

Several buildings in Balaju area (and Gogabu area, which is close to Balaju) collapsed during the earthquake. The majority of these buildings (such as Figure 9-6 through Figure 9-9) have an open ground floor level, and failure might have occurred due to the lack of shear walls. However, a detailed study is required to understand the actual cause of the damage. The cause for the collapse of a six story school building (Figure 9-6) is still unknown.

Figure 9-5 Soft-story collapse of a five story building at Gogabu area (27^{O}44’2” N, 85^{O}18’42” E).

Figure 9-6 Soft story collapse of a six-story school building during the earthquake shaking (27^{O}44’15.5” N, 85^{O}18’33.8” E).

Figure 9-7 Structural damage of a RCC frame structure at Gogabu Bus Park near Balaju (27^{O}44’7” N, 85^{O}18’29” E).

Figure 9-8 Soft story collapse of a six story building near Gogabu Bus Park. Three buildings were completely damaged in the neighborhood that killed over 20 people (27^{O}44’06” N, 85^{O}18’32” E).

Figure 9-9 Collapse of a six-story lodge at Balaju killed more than 20 people (27^{O}44’06” N, 85^{O}18’20”).

At the ridge of Balaju (known as the Bashara area), several buildings collapsed in a row (Figure 9-10). This could possibly be due to basin edge amplification effects, although detailed investigation is required to confirm this. One RCC frame structure under construction at that area sustained only minor damage (Figure 9-11).

Figure 9-10 Building damage pattern at the ridge of Balaju Baisdhara area. This area is considered a rock site (27^{O}44’6.71” N, 85^{O}18’11.51” E).

Figure 9-11 Building under construction at Balaju Baisdhara area (27^{O}44’8.28” N, 85^{O}18’6.91” E).

The collapse of several buildings in close proximity to each other was observed in the Sitapaila area. The pattern of existing buildings in this area is presented in Figure 9-12. However, several buildings along the ridge, especially between Swayambhunath and Sitapaila, had collapsed. Within Sitapaila Height and near the Ring Road, more than five buildings (Figure 9-13) collapsed in row, and several recently constructed buildings were severely damaged (Figure 9-14). Along the opposite side of the Ring Road and in the same geographic area (Figure 9-15 and Figure 9-16), more than five buildings collapsed, killing over 20 people. These damages appear to be attributable to basin edge effects; however, further detailed study is required to confirm the actual cause.

Figure 9-12 Building pattern at Sitapaila area (27°42.1’0” N, 85°16.1’0” E)

Figure 9-13 Five buildings collapsed along the ridge line at Sitapaila area near Ring Road at Swayambhunath. One building at the rightmost part of the picture was not damaged (27°42.7’0” N, 85°17’0” E).

Figure 9-14 Recently constructed buildings at Sitapaila height also sustained significant damage although did not collapse (27^{O}42’51” N, 85^{O}16’58” E).

Figure 9-15 Collapse of two multi story buildings at Sitapaila killed over 20 people (27°42.7’0”N, 85°17’0”E).

Figure 9-16 More than 5 buildings were collapsed near this building at Sitapaila area (next to the building shown in Figure 9-15).

Several buildings also collapsed in the area of Ramkot. Many of the collapsed structures were constructed of unreinforced brick masonry and mud mortar. However, several modern

RCC buildings were also severely damaged (Figure 9-17). This area could have also experienced basin edge effects.

Figure 9-17 Typical modern building collapse patter at Ramkot, Kathmandu.

9.1.2 High Rise Buildings

High rise apartment construction commenced in Kathmandu approximately 15 years ago. Several high rise apartment buildings with less than 26 stories were observed throughout the Kathmandu basin. The structural and geotechnical design of such buildings are supervised by the Department of Housing. A few structures, such as the Park Horizon Apartment at Dhapasi suffered serious damage (Figure 9-18 through Figure 9-21), whereas others appeared to have suffered little to no damage. The typical damage pattern includes shear cracks in the exterior walls and significant cracking of plaster surfaces (Figure 9-12 through Figure 9-27).Evaluation of the damage pattern in these apartment building could provide important insight regarding the ground shaking level and spectral response of high rise buildings.

Figure 9-18 Structural damage to the park Horizon Apartment Building at Dhapasi due to the strong ground motion. Eye witness said that the buildings were pounding due to story drift due to ground shaking.

Figure 9-19 Close view of the structural damage (27°44.4’0”N, 85°19.4’0”E).

Figure 9-20 None of the other 3-4 story buildings in the area were damaged by the ground shaking.

Figure 9-21 Aerial view of the apartment complex.

Figure 9-22 A high rise apartment building at Hattiban, Lalitpur. This building also sustained some major damage due to the earthquake.

Figure 9-23 High rise apartment complex at Hattiban that sustained some damage due to earthquake shaking (27^{O}38’59” N, 85^{O}19’46” E).

Figure 9-24 Aerial view of the apartment complexes at Hattiban (27^{O}38’58”N, 85^{O}19”45” E).

Figure 9-25 Damage observed at an apartment complex in Kalikasthan (27^{O}42’13” N, 85^{O}19’38.3” E).

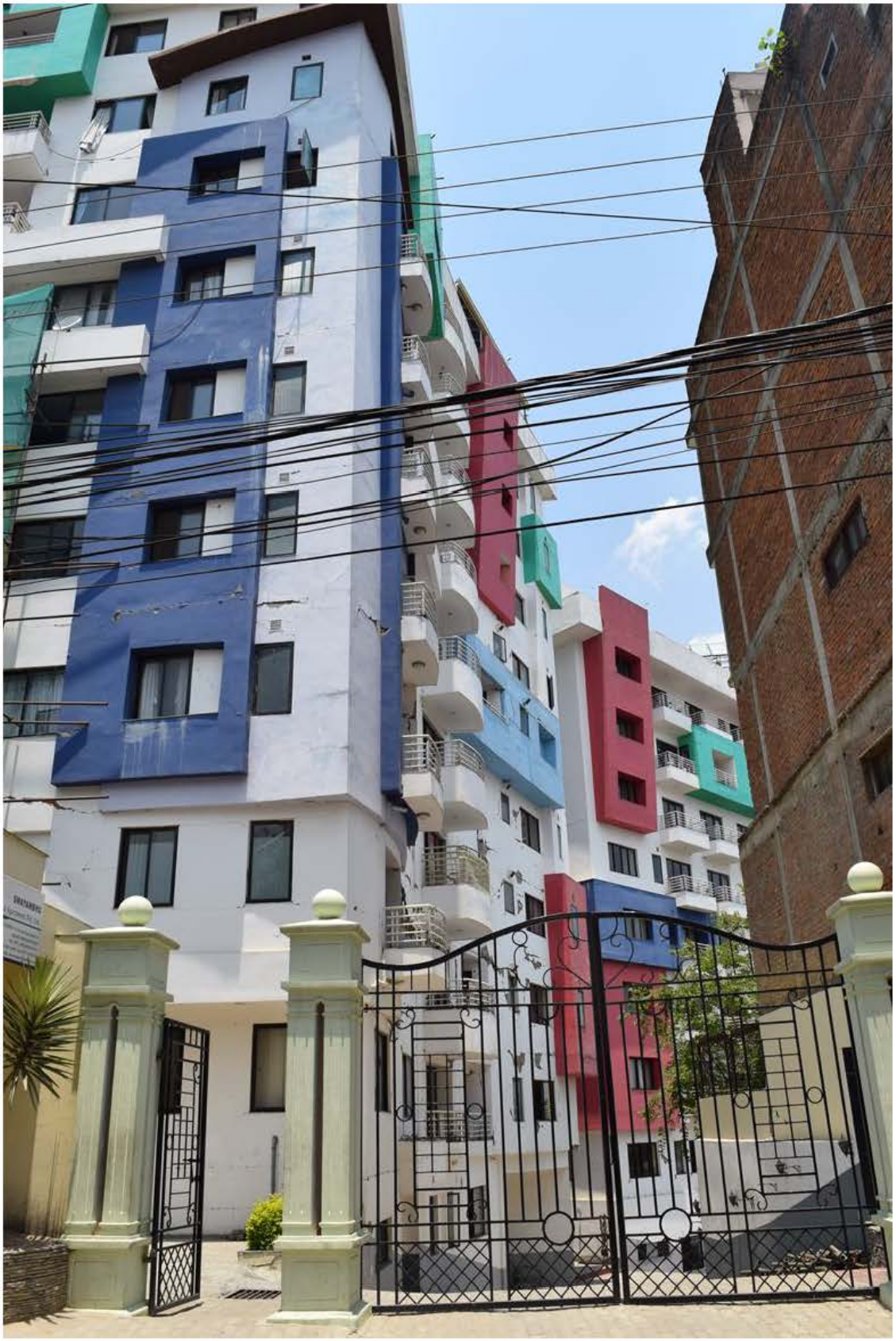

Figure 9-26 Damage observed at an apartment complex in Sitapaila

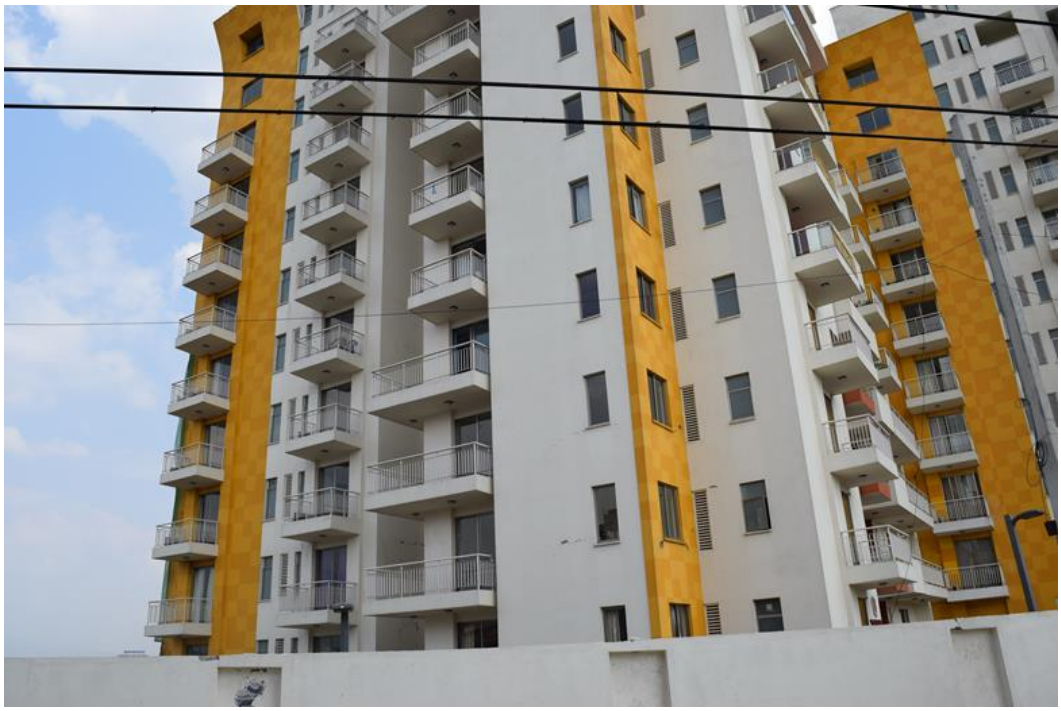

Figure 9-27 Minor damage sustained by an apartment complex at Bishal Nagar (27^{O}43’40”N, 85^{O}20’05” E).

9.1.3 Damage due to Geotechnical Effects

There were some locations where buildings were damaged due to geotechnical effects such as ground failure or foundation failure. One example of such failure are the buildings damaged at Lokanthali due to the liquefaction induced lateral spreading (Figure 9-28 and Figure 9-29).

Figure 9-28 House tilted at Lokanthali area due to the lateral spread (27^{O}40’29.28” N, 85^{O}21’49” E).

Figure 9-29 Buildings tilted at Lokanthali area (opposite side of the one presented in Figure 9-28) due to ground failure (27^{O}40’25.83” N, 85^{O}21’44.3” E).

In the north-eastern part of the basin, extensive structural damage was not noted (Figure 9-30). Stupas sustained less damage compared to temples. Many old buildings with unreinforced brick masonry in mud mortar and temples in Bhaktapur sustained serious damage due to the strong ground motion (Figure 9-31 and Figure 9-32). The majority of modern buildings showed only a small extent of damage. There were several isolated cases in Kathmandu where multi-story buildings collapsed (Figure 9-33). The team visited Indrayani village, which is loacated along a broad ridge, and observed similar damage patterns as in Bhaktapur (where old buildings collapsed and the RCC buildings sustained less damage) (Figure 9-34).

Figure 9-30 Aerial view of north-eastern part of Kathmandu near Bouddhanath temple.

Figure 9-31 Aerial view of damage in Bhaktapur

Figure 9-32 Unreinforced brick masonry in mud mortar at Bhaktapur collapsed due to ground shaking whereas the modern RCC structures did not sustain much damage (27^{O}40’33.64” N, 85^{O}24’26.18” E).

Figure 9-33 A four and half story RCC frame structure collapsed at Samakoshi, Kathmandu (27^{O}43’49” N, 85^{O}18’52” E).

Figure 9-34 Old buildings with unreinforced brick masonry at Indrayeni Village got damaged due to ground shaking (27°43.7'0" N, 85°26.2'0" E).

9.2 Bhaktapur

The historic town of Bhaktapur, located along the eastern margin of the Kathmandu valley, was severely damaged. Bhaktapur was visited on May 11, 2015 and on May 12 following the M_w 7.3 aftershock on that same day. The historic districts of Bhaktapur, including Durbar Square, were built between the 15th and 18th centuries and have experienced several large magnitude earthquakes. Structural damage was extensive to the mostly unreinforced brick structures, and numerous casualties resulted. The Gorkha earthquake caused numerous heavy brick facades to collapse into the narrow alleys within the historic areas of Bhaktapur. The M_w 7.3 aftershock on May 12, 2015 was located approximately 40 km east of Bhaktapur and caused significant additional damage to already weakened structures.

Figure 9-35 Collapsed unreinforced masonry building in Bhaktapur following the Gorkha earthquake (27° 40’ 21.64” N; 85° 25’ 58.24” E).

Figure 9-36 Distressed unreinforced masonry building and façade following the May 12, 2015, M_w 7.3 aftershock (27° 40’ 19.45” N; 85° 25’ 40.80” E).

Figure 9-37 Photos on left taken May 11, 2015 and photo on right taken after the May 12, 2015 M_w 7.3 aftershock. Already damaged unreinforced masonry building experienced additional collapse (27° 40' 21.15" N; 85° 25' 56.23" E).

9.3 Pokhara

Buildings in Pokhara sustained less damage compared to those in Kathmandu due to the comparatively lower levels of ground shaking in Pokhara (Figure 9-38). However, several buildings exhibited structural cracks (Figure 9-39 and Figure 9-40).

Figure 9-38 Typical building pattern in Pokhara. Majority of these buildings performed well.

Figure 9-39 Structural damaged observed in a high school building at Pokhara.

Figure 9-40 Damage to stone masonry walls under heavy roof at the staff quarter of Western Region Campus of the Institute of Engineering.

9.4 Gorkha

Although the town Gorkha is close to the Mw 7.8 epicenter, only a few damaged buildings were noted in the area of the Gorkha Bazar (Figure 9-41 and Figure 9-42). The majority of RCC structures performed well, although several houses in Gorkha showed minor cracks in load bearing and partition walls. Additionally, significant damage was observed in the retaining walls and exterior walls of the Gorakhnath Temple (Figure 9-43 and Figure 9-44). As the temple is located at high altitude and along a ridge, topographic amplification may have influenced shaking intensity at this location.

Figure 9-41 Modern buildings in Gorkha Bazar did not sustain massive damage due to the ground shaking.

Figure 9-42 Modern buildings in Gorkha Bazar that did not sustain much damage due to earthquake shaking.

Figure 9-43 Retaining walls of Gorkhnath Temple/Gorkha Palace showing shear cracks.

Figure 9-44 Damage to Gorakhnath Tample walls due to the earthquake shaking (28°0.217'0" N, 84°38.3'0" E).

9.5 Barpak Epicentral Village

Barpak village is located at the epicenter of the Mw 7.8 earthquake. The majority of buildings are constructed of stone rubble, and the remainder are constructed of RCC, unreinforced stone masonry, or wood framing with metal siding. Nearly all of the stone rubble structures suffered complete collapse (Figure 9-45 through Figure 9-48). In stark contrast, with few exceptions both RCC and wood framed structures with metal siding suffered no damage (Figure 9-49 and

Figure 9-50). Unfortunately, with the limited available local resources and urgency to provide shelter through the monsoon and winter, Barpak is being actively rebuilt with highly vulnerable stone rubble structures (Figure 9-51)

Figure 9-45 An aerial view of seismic damage at Barpak Village.

Figure 9-46 A closer look at the damage pattern in Barpak Village.

Figure 9-47 A few RCC building at Barpak Village standing well after the earthquake.

Figure 9-48 Closer look at the earthquake damage to stone masonry and RCC buildings.

Figure 9-49 Typical condition of RCC structures in Barpak.

Figure 9-50 The school building of Barpak (wood framing with metal sheet siding).

Figure 9-51 Rebuilding Barpak with stone rubble.

9.6 Other Areas

The reconnaissance included other areas that were either accessed via ground transportation or surveyed from a helicopter.Within the Gajuri of Dhading District, along the Prithivi Highway (Figure 9-52) several buildings exhibited structural damage. Along both the Arniko Highway and Melamchi Access Road, modern RCC buildings performed well, while unreinforced masonry structures sustained severe damage (Figure 9-53 through Figure 9-56). Additionally, potential topographic effects were observed at several villages within the Sindhupalchowk District, along the aerial route from Kathmandu to Lama Bagar (Figure 9-57 through Figure 9-59). The villages shown in these figures were completely destroyed by the earthquake.

Figure 9-52 Structural damage pattern at a building in Gajuri, Dhading.

Figure 9-53 Old unreinforced masonry buildings sustained massive damage while modern buildings performed relatively better at Dolalghat, Kavre District, along Araniko Highway.

Figure 9-54 Several old unreinforced masonry buildings collapsed in Mude, Dolakha.

Figure 9-55 Comparison of performance of unreinforced and reinforced buildings in Melamchi, Sindhupalchowk.

Figure 9-56 Another example of comparative performance of unreinforced and reinforced buildings in Melamchi, Sindhupalchowk.

Figure 9-57 Aerial view of building damage at a ridge in Sindhupalchowk – aerial way to Lamabagar.

Figure 9-58 An entire village flattened in Sindhupalchowk due to strong ground shaking.

Figure 9-59 Another example of entire village flattened due to earthquake shaking in Sindhupalchowk.

Along the Langtang Trekking Route, almost all small trekking villages and lodges had collapsed. Modern RCC structures performed well whereas the unreinforced stone rubble masonry structures collapsed (Figure 9-60). Within the Rasuwa district along the catchment of Trishuli River near Rasuwagadi, several villages with buildings constructed of unreinforced masonry sustained severe damage or collapsed (Figure 9-61 and Figure 9-62). However, modern RCC buildings in Dhunche performed well (Figure 9-63). As can be observed in

Figure 9-64 through Figure 9-66, villages located to the west of the epicenter did not exhibit significant building damage; however, near epicenter, observed structural damage was high for unreinforced masonry and low for RCC structures (Figure 9-67 through Figure 9-69).

Figure 9-60 RCC structures at Kangjun Gumba, Langtang Trekking Route performed well whereas the unreinforced stone masonry walls flattened due to seismic shaking (28°12.7'0" N, 85°34.1'0" E).

Figure 9-61 Building damage due to seismic shaking near Rasuwagadi of Rasuwa district.

Figure 9-62 Building damage at a village near Rasuwagadi in Rasuwa District due to earthquake shaking and earthquake induced landslides.

Figure 9-63 Several modern RCC structures at Dhunche of Rasuwa District performed well during the earthquake.

Figure 9-64 Many of the modern RCC structures in Sundarbazar of Lamjung District performed well during the earthquake.

Figure 9-65 Villages near Sundarbazar did not show similar extent of damage as was observed in Rasuwa and Sindhupalchowk.

Figure 9-66 Manang village had minimum damage compared to other places (28°36.8’0” N, 84°8.99’0” E).

Figure 9-67 Modern RCC structures in Arughat of Gorkha showed more limited damage compared to unreinforced masonry.

Figure 9-68 Buildings shattered at Machhigaon of Gorkha, which is close to the epicenter.

Figure 9-69 A village near Prok of Gorkha was devastated due to the seismic induced damage of unreinforced masonry structures.

9.7 Damage to Brick Kilns

Brick is a primary construction material in Nepal and is produced in kilns located across the country. These kilns have also been a dominant source of air pollution in the Kathmandu Valley. Many kilns stopped operation after the earthquake due to damage to their smokestacks (Figure 9-70). This resulted in likely temporary improvement in air quality however resulting in shortage in building material necessary for reconstruction.

Figure 9-70 Damaged smokestack at a brick kiln in the Kathmandu Valley southeast of Bhaktapur (27^{O} 29’ 52.9” N, 85^{O} 26’ 52.9” E).

10 Summary and Conclusions

The overall distribution of seismically triggered damage resulting from the M_w 7.8 April 25, 2015 Gorkha Earthquake is asymmetrical with respect to the epicenter, with pronounced damage to the east and comparatively little damage to the west. The asymmetric damage pattern indicates significant regional directivity effects. The major earthquake effects include infrastructure and building losses, landsliding, and ground failures including liquefaction, lateral spreading, and cyclic failure of silty clay. Observed damage was not only related to the main shock but also to numerous aftershocks and in one case to a foreshock in Dec 2014.

In the Kathmandu Basin, recorded strong ground motion data suggest that directivity in combination with deep basin effects resulted in significant amplification at a period of approximately five seconds. Modern buildings constructed within the basin generally performed well; however, local occurrences of heavily damaged and collapsed reinforced concrete structures were observed.

Along the margins of Kathmandu Basin, the occurrence of structural damage and ground failures is more pronounced than in the basin interior, indicating possible ground motion amplification along the basin edges. Ground failures within the basin and along its margins include cyclic failure of silty clay, lateral spreading and liquefaction.

Significant landsliding was triggered over a broad area, with concentrated activity east of the April 25, 2015 epicenter and between Kathmandu and the Nepal-China border. For example, pre-and-post earthquake satellite imagery indicates that within the Sindulpalchok District alone, over 6,000 landslides were triggered by the earthquake. The asymmetric distribution of concentrated landsliding with respect to the epicenter partially reflects the directivity in ground motion. Many incipient landslides were generated by the earthquake, and there are countless instances of precarious slopes that suffered partial collapse. These slopes will be particularly vulnerable to renewed instability during monsoon rains and future seismic activity.

Several occurrences of significant damage to hydropower facilities were observed, together with damage to roadways, bridges and retaining structures. The majority of infrastructure damage was related to rock falls and landslide activity. Greater infrastructure damage was concentrated along steep hillsides, ridges and mountain peaks, indicating the occurrence of topographic amplification.

In remote village areas that experienced intense ground shaking, such as the epicentral village of Barpak, building damage is highly correlated to construction methods. Nearly all buildings constructed of stone rubble suffered complete collapse. However, modern reinforced concrete structures and wood-frame structures having thin sheet metal siding typically survived the earthquake shaking with minimal damage. It is important that these behavioral tendencies be understood and incorporated into the overall rebuilding strategy of remote villages.

The lack of available strong motion records has severely limited the GEER team's ability to understand how strong motions were distributed and how they correlate to distributions of landsliding, ground failure and infrastructure damage. It is imperative that the engineering and scientific community continues to install strong motion stations so that such data is available for future earthquake events to gain insight to damage thresholds and expected future ground motions. Such information will benefit the people of Nepal through improved approaches to earthquake resilient design.

Appendix A: Team Itinerary

TEAM A AGENDA

May 06, 2015:
Arrivals: Scott Kieffer (SK), Binod Tiwari (BT), Kevin Clahan (KC), Maja Bitenc (MB), Mirjam Ziselsberger (MZ)
Departures:
Day Activities: Team separated into 1 group.
Group 1: SK, MB, MZ
Group 1 visited Structural damage areas in Kathmandu Valley and Lokanthali Ground Fissure

May 07, 2015:
Arrivals:
Departures:
Day Activities: Team separated into 2 groups after initial meeting with collaborators in Tribhuvan University.
Group 1: SK, MB, MZ, KC, Basanta Adhikari (BA), Surendra Awasthi (SA)
Group 1 visited Lokanthali Ground Fissure and mapped the fissures
Group 2: BT, Indra Acharya (IA), Vijay Mahato (VM), Monika Maharjan (MM), Sangita Rai (SR), Sanjeeb Basnet (SB)
Group 2 visited Lokanthali and liquefaction areas at Imadol and structural damages in Kathmandu Valley.

May 08, 2015:
Arrivals: Robb Moss
Departures:
Day Activities: Team separated into 3 groups.
Group 1: SK, MB, MZ, SA
Group 1 visited Kathmandu-Trishuli Road landslides.
Group 2: KC, BA
Group 2 visited Araniko Highway up to Kodari to see landslides and damage to infrastructure.
Group 3: BT, IA, VM, MM, SR, SB
Group 3 visited Chagu Narayan Liquefaction area, structural damage at Indrayani village, and structural damage in Kathmandu Valley

May 09, 2015:
Arrivals:
Departures:
Day Activities: Team separated into 3 groups.
Group 1: SK, MB, MZ, SA
Group 1 visited landslides along Prithvi Highway from Kathmandu to Abu Khaireni and Gorkha.
Group 2: KC, BA
Group 2 visited landslides along Prithivi Highway from Kathmandu to Abu Khaireni and Gorkha; structural damage in Gorkha
Group 3: BT, RM, IA, VM, MM, SR, SB
Group 3 visited landslides along Prithivi Highway from Kathmandu to Abu Khaireni and Gorkha; structural damage in Gorkha

May 10, 2015:
Arrivals:
Departures:
Day Activities: Team separated into 3 groups.
Group 1: SK, MB, MZ, SA
Group 1 visited landslides along Baluwa-Barpak road and structural damage in Barpak.

Group 2: KC, BA, SB
Group 2 visited Hetauda and Bardibas along the HFT to explore fault rupture surface
Group 3: BT, RM, IA, MM, SR
Group 3 visited landslides along Prithivi Highway from Abu Khaireni to Pokhara, hydropower station, bridges and structural damage in Pokhara

May 11, 2015:

Arrivals:
Departures:
Day Activities: Team separated into 3 groups.
Group 1: SK, MB, MZ, SA
Group 1 structural damage in Barpak, and returned back to Kathmandu
Group 2: KC, BA, SB
Group 2 visited Bardibas and BP Koirala Highway and returned to Kathmandu
Group 3: BT, RM, IA, MM, SR
Group 3 visited Ramkot liquefaction site and structural damage at Ramkot.

May 12, 2015:

Arrivals:
Departures:
Day Activities: Team separated into 3 groups.
Aftershock of Mw7.3 hit on this day
Group 1: SK, MB, MZ, SA
Group 1 Prepared reports
Group 2: KC
Group 2 visited Hetauda and observed landslides along Tribhuvan Highway
Group 3: BT, RM, SR
Group 3 visited Lokanthali rupture surface and observed landslides and structural damage along Kathmandu – Lamosangu road and Lamosangu-Jiri Road. Returned back to Kathmandu from Mude (close to the epicenter of Mw7.3 aftershock)

May 13, 2015:

Arrivals:
Departures:
Day Activities: Team separated into 2 groups.
Group 1: SK, MB, MZ, SA, KC
Group 1 Mapped crack at Lokanthali area
Group 2: BT, RM, IA, VM, MM, SR
Group 2 visited Manamaiju liquefaction site and collected soil samples from Lokanthali ground fissure.

May 14, 2015:

Arrivals:
Departures:
Day Activities: Team separated into 2 groups.
Group 1: SK, MB, SA, KC
Group 1 prepared report and mapped Lokanthali area
Group 2: BT, RM, IA, MM, MZ, SR
Group 2 visited Hattiban liquefaction site

May 15, 2015:

Arrivals:
Departures: SK, MM, MZ, KC, SA
Day Activities: Team separated into 2 groups after debrief at Tribhuvan University
Group 1: SK, MB, MZ, KC
Group 1 observed damages in Kathmandu
Group 2: BT, RM, MM, SR
Group 2 visited Sinha durbar bridge, discussed at Nepal Geotechnical Society

May 16, 2015:

Arrivals:
Departures: RM

Day Activities: Team separated into 1 group
Group 1: BT, RM, MM, SR
Group 2 visited Melamchi Water Supply Project in Sindhupalchowk to investigate landslides and damage to infrastructure.

May 17, 2015:
Arrivals:
Departures:
Day Activities:
Group 1: BT
Group 1 observed structural damage in Kathmandu, ground fissure at Syuchatar

May 18, 2015:
Arrivals:
Departures:
Day Activities:
Group 1: BT
Group 1 observed structural damage in Kathmandu

May 19, 2015:
Arrivals:
Departures:
Day Activities:
Group 1: BT
Group 1 observed structural damage in Kathmandu and coordinated Team B activities

May 20, 2015:
Arrivals:
Departures:
Day Activities:
Group 1: BT
Group 1 observed structural damage in Kathmandu

May 21, 2015:
Arrivals:
Departures:
Day Activities:
Group 1: BT
Group 1 observed structural damage in Kathmandu

May 22, 2015:
Arrivals:
Departures:
Day Activities:
Group 1: BT
Group 1 observed structural damage in Kathmandu and coordinated activities for team B.

TEAM B AGENDA

May 22, 2015:

Arrivals: Youssef Hashash (YH), Deepak Rayamajhi (DR)

Departures: -

Day Activities: Team coordination meeting with Binod Tiwari

May 23, 2015:

Arrivals: Menzer Pehlivan (MP), Amy MacDonald (AM), Sital Uperty (SU),

Departures: -

Day Activities: Team separated into two groups.

Group 1: YH, MP, BT, SR

Group 1 went to investigate the 3km crack that was reported in the news. Group 1 visited two different locations around the Kathmandu Basin where lateral cracks were observed.

Group 2: DR, AM, SA and Sachindra Dahal (SD)

Group 2 visited Arniko Highway and Bakhtapur investigated the damage.

May 24, 2015:

Arrivals: -

Departures: -

Day Activities: Team separated into three groups.

Group 1: YH, MP, SU, BA

Group 1 headed northwest to investigate the Kaligandaki landslide that happened overnight on May 24, 2015. Group stayed in Pokhara overnight

Group 2: AM, DR, SA, SD

Group 2 headed east to investigate the May 12, 2015 Mw 7.3 aftershock epicenter area.

Group 3: BT

Group 3 coordinated hydropower authorities to get access.

May 25, 2015:

Arrivals: Eric Thompson (ET), Chris Madugo (CM), Brian Collins (BC), Randall Jibson (RJ)

Departures: -

Day Activities: Team separated into three groups.

Group 1: YH, MP, SU

Group 1 drove back to Kathmandu. Met with BT and had a meeting with the Upper Tamokoshi hydropower plant officials

Group 2: CM, AM, DR, SA

Group 2 headed northeast towards Chinese border to investigate the damaged hydropower plants

Group 3: ET, SD, Diwakar Khadka (DK), Indra Acharya (IA)

Group 3 performed sampling and trenching in Lokantali, around Arniko Highway

May 26, 2014:

Arrivals: -

Departures: -

Day Activities: Team separated into three groups.

Group 1: MP, YH, BT

Group 1 went to inspect the damage in Upper Tamokoshi Hydropower Plant

Group 2: CM, AM, DR

Group 2 continued inspection of hydropower plants in northeastern Nepal.

Group 3: ET, SU, DK

Group 3 continued trenching, sampling, and field testing in the Arniko Highway

May 27, 2015

Arrivals: Ben Mason (BM)

Departures: -

Day Activities: Team separated into three groups.

Group 1: MP, BT, ET

Group 1 went to Kalanki area to collect samples and perform field testing along the observed surface crack.

Group 2: CM, AM, DR

Group 2 continued inspection of hydropower plants in northeastern Nepal.

Group 3: BC, RJ, YH

Group 3 performed helicopter reconnaissance investigating slope failures in Central Nepal

May 28, 2015

Arrivals: -

Departures: YH

Day Activities: Team separated into four groups.

Group 1: MP, YH, SU

Group 1 went to Sakhu to investigate the damage extent in the area and visited Bakhtapur and Monkey Temple to investigate possible topographic effects

Group 2: CM, AM, DR, SA

Group 2 continued inspection of hydropower plants in northeastern Nepal and returned to Kathmandu.

Group 3: ET, BM

Group 3 performed trenching, sampling, and field testing in the areas with observed ground failures

Group 4: BM, RJ, BT

Group 4 continued with helicopter reconnaissance investigating slope failures in Western and Central Nepal.

May 29, 2015

Arrivals: -

Departures: -

Day Activities: Team separated into three groups.

Group 1: CM, AM, MP, SA

Group 1 headed East towards Chinese boarder for the inspection of hydropower plants in eastern Nepal.

Group 2: ET, BM, DR

Group 2 performed trenching, sampling, and field testing in the areas with observed ground failures

Group 3: BC, RJ, BT

Group 3 continued with helicopter reconnaissance investigating slope failures in Western and Central Nepal.

May 30, 2015

Arrivals: -

Departures: -

Day Activities: Team separated into three groups.

Group 1: CM, AM, MP

Group 1 continued with the inspection of hydropower plants in eastern Nepal and returned back to Kathmandu.

Group 2: ET, BM, DR

Group 2 performed trenching, sampling, and field testing in the areas with observed ground failures

Group 3: BM, RJ, BT

Group 3 continued with helicopter reconnaissance investigating slope failures in Western and Central Nepal.

May 31, 2015

Arrivals: -

Departures: BT, MP

Day Activities: Team separated into three groups a debriefing at Tribhuvan University..

Group 1: AM, CM

Prepare presentation for debriefing at Tribhuvan University

Group 2: ET, BM, DR

Group 2 performed trenching, sampling, and field testing in the areas with observed ground failures

Group 3: BC, RJ

Compiled data of helicopter survey

June 01, 2015

Arrivals: -

Departures: AM

Day Activities: Team separated into three groups.

Group 1: --

Group 2: ET, BM, DR

Group 2 performed trenching, sampling, and field testing in the areas with observed ground failures

Group 3: BM, RJ, CM

Group 3 continued with helicopter reconnaissance investigating slope failures in Western and Central Nepal.

June 02, 2015

Arrivals: -

Departures: -

Day Activities: One group consisting of ET, BM, DR, and CM performed trenching, sampling and field testing in areas with observed ground ruptures.

June 03, 2015

Arrivals: -

Departures: ET, BM

Appendix B: GPS Station Data

GPS station CHLM

```
# Data provided by the Nepal Geodetic Array run by the California
Institute of Technology
# and the Departement of Mines and Geology (Nepal).
#
# Raw data processed by the Scripps Permanent Array and Observation
Center (SOPAC).
#
# If you use this data please cite:
#
# Galetzka et al.(2015), Slip pulse and resonance of Kathmandu basin
during the 2015
# Mw 7.8 Gorkha earthquake, Nepal imaged with space geodesy,
Science.
#
# GPS station CHLM
# 28.20727 N Latitude 85.314073 E Longitude
# First sample is at 2015-04-25T06:11:26.600000Z
#
# Time(s)  North(m)     East(m)      Up(m)
  0.00         0.0000     0.0000     0.0000
  0.20        -0.0009    -0.0012     0.0019
  0.40        -0.0006    -0.0011    -0.0009
  0.60         0.0006    -0.0005    -0.0014
  0.80         0.0016     0.0002    -0.0002
  1.00         0.0000    -0.0015    -0.0044
  1.20         0.0005    -0.0022    -0.0031
  1.40        -0.0015    -0.0008     0.0020
  1.60         0.0026    -0.0037    -0.0026
  1.80         0.0001     0.0011    -0.0039
  2.00         0.0017    -0.0007    -0.0002
  2.20         0.0012    -0.0023    -0.0026
  2.40         0.0006    -0.0014    -0.0003
  2.60        -0.0003    -0.0021    -0.0015
  2.80         0.0009    -0.0030     0.0037
  3.00        -0.0003    -0.0029     0.0009
  3.20         0.0021    -0.0024    -0.0015
  3.40         0.0017    -0.0047    -0.0050
  3.60         0.0022    -0.0031    -0.0017
  3.80         0.0017    -0.0033    -0.0002
  4.00         0.0013    -0.0043    -0.0044
  4.20         0.0032    -0.0060    -0.0091
  4.40         0.0026    -0.0020    -0.0079
  4.60         0.0044    -0.0013     0.0014
  4.80         0.0034    -0.0013    -0.0105
  5.00         0.0020     0.0008    -0.0039
  5.20         0.0007    -0.0027    -0.0074
  5.40         0.0008    -0.0019    -0.0065
  5.60         0.0004    -0.0026    -0.0053
  5.80         0.0015    -0.0048    -0.0102
  6.00         0.0004    -0.0043    -0.0055
  6.20         0.0017    -0.0021    -0.0105
  6.40         0.0004    -0.0013    -0.0058
  6.60         0.0012    -0.0004    -0.0055
```

6.80	0.0004	-0.0017	-0.0020
7.00	0.0021	-0.0006	0.0172
7.20	-0.0002	-0.0047	-0.0013
7.40	-0.0006	-0.0035	-0.0010
7.60	-0.0005	-0.0043	-0.0008
7.80	0.0006	-0.0031	-0.0018
8.00	0.0007	-0.0013	0.0033
8.20	0.0002	-0.0035	0.0013
8.40	0.0014	-0.0049	-0.0020
8.60	0.0015	-0.0026	0.0006
8.80	0.0022	-0.0055	-0.0015
9.00	0.0019	-0.0021	-0.0018
9.20	-0.0007	-0.0009	0.0060
9.40	0.0027	-0.0030	-0.0056
9.60	0.0024	-0.0021	0.0023
9.80	0.0025	-0.0008	-0.0009
10.00	0.0030	-0.0005	0.0001
10.20	0.0020	-0.0016	0.0027
10.40	0.0030	-0.0029	-0.0076
10.60	0.0028	-0.0022	-0.0010
10.80	0.0017	-0.0045	-0.0057
11.00	0.0024	-0.0033	0.0035
11.20	0.0025	-0.0053	0.0018
11.40	0.0021	-0.0054	-0.0036
11.60	0.0025	-0.0028	-0.0015
11.80	0.0005	-0.0050	0.0023
12.00	0.0027	-0.0075	0.0013
12.20	0.0031	-0.0043	0.0020
12.40	0.0024	-0.0053	-0.0028
12.60	0.0001	-0.0072	0.0032
12.80	0.0030	-0.0037	-0.0033
13.00	0.0027	-0.0046	-0.0019
13.20	0.0011	-0.0066	0.0032
13.40	0.0031	-0.0070	0.0012
13.60	0.0013	-0.0067	0.0056
13.80	0.0039	-0.0056	0.0046
14.00	0.0018	-0.0078	0.0046
14.20	0.0010	-0.0042	0.0016
14.40	0.0015	-0.0115	0.0013
14.60	0.0011	-0.0066	-0.0003
14.80	0.0027	-0.0090	-0.0023
15.00	0.0018	-0.0083	0.0018
15.20	-0.0005	-0.0107	0.0031
15.40	0.0035	-0.0141	0.0033
15.60	0.0008	-0.0109	0.0017
15.80	-0.0007	-0.0130	0.0003
16.00	0.0004	-0.0143	0.0021
16.20	-0.0011	-0.0121	0.0077
16.40	-0.0018	-0.0147	-0.0040
16.60	-0.0018	-0.0163	0.0019
16.80	0.0015	-0.0174	0.0053
17.00	-0.0007	-0.0201	0.0047
17.20	-0.0030	-0.0192	-0.0037
17.40	-0.0025	-0.0209	0.0020
17.60	-0.0068	-0.0259	0.0059
17.80	-0.0058	-0.0341	0.0007
18.00	-0.0048	-0.0355	-0.0003

18.20	-0.0069	-0.0341	0.0058
18.40	-0.0121	-0.0437	0.0030
18.60	-0.0168	-0.0488	-0.0009
18.80	-0.0139	-0.0480	0.0062
19.00	-0.0194	-0.0525	0.0040
19.20	-0.0242	-0.0619	0.0105
19.40	-0.0273	-0.0681	0.0067
19.60	-0.0314	-0.0703	0.0156
19.80	-0.0355	-0.0811	0.0097
20.00	-0.0458	-0.0907	0.0082
20.20	-0.0464	-0.1010	0.0140
20.40	-0.0551	-0.1080	0.0152
20.60	-0.0635	-0.1283	0.0148
20.80	-0.0719	-0.1361	0.0155
21.00	-0.0861	-0.1509	0.0273
21.20	-0.0999	-0.1677	0.0313
21.40	-0.1069	-0.1908	0.0311
21.60	-0.1154	-0.1919	0.0334
21.80	-0.1246	-0.2139	0.0415
22.00	-0.1447	-0.2425	0.0338
22.20	-0.1662	-0.2668	0.0282
22.40	-0.1927	-0.3012	0.0185
22.60	-0.2102	-0.3324	0.0162
22.80	-0.2202	-0.3424	0.0160
23.00	-0.2652	-0.3567	-0.0129
23.20	-0.2847	-0.3734	-0.0216
23.40	-0.3419	-0.3800	-0.0334
23.60	-0.3631	-0.4068	-0.0639
23.80	-0.4094	-0.4604	-0.1016
24.00	-0.4560	-0.4439	-0.1374
24.20	-0.4801	-0.4031	-0.1622
24.40	-0.5182	-0.4131	-0.2074
24.60	-0.5631	-0.4327	-0.2501
24.80	-0.6564	-0.3976	-0.2656
25.00	-0.6754	-0.3291	-0.2667
25.20	-0.6651	-0.3523	-0.2923
25.40	-0.6671	-0.4323	-0.3275
25.60	-0.6668	-0.4820	-0.3429
25.80	-0.7414	-0.4731	-0.3645
26.00	-0.8362	-0.5234	-0.4247
26.20	-0.9299	-0.5906	-0.4787
26.40	-1.0467	-0.5776	-0.4988
26.60	-1.1027	-0.5234	-0.5206
26.80	-1.1498	-0.5191	-0.5618
27.00	-1.1543	-0.5320	-0.5738
27.20	-1.1409	-0.5499	-0.5942
27.40	-1.1714	-0.5457	-0.5982
27.60	-1.2298	-0.5178	-0.6315
27.80	-1.2593	-0.4696	-0.6314
28.00	-1.2741	-0.4131	-0.6376
28.20	-1.2811	-0.3433	-0.6300
28.40	-1.3125	-0.2847	-0.6206
28.60	-1.3169	-0.2605	-0.6159
28.80	-1.3426	-0.2840	-0.6508
29.00	-1.3208	-0.3379	-0.6693
29.20	-1.3101	-0.3358	-0.6521
29.40	-1.3191	-0.3076	-0.6284

29.60	-1.3358	-0.2926	-0.6288
29.80	-1.3715	-0.3219	-0.6720
30.00	-1.3835	-0.3715	-0.7119
30.20	-1.3676	-0.3553	-0.7211
30.40	-1.3314	-0.2714	-0.7223
30.60	-1.2748	-0.1983	-0.7117
30.80	-1.2335	-0.1897	-0.7025
31.00	-1.1958	-0.1658	-0.6616
31.20	-1.1873	-0.1453	-0.6401
31.40	-1.1871	-0.1475	-0.6430
31.60	-1.2324	-0.2162	-0.6675
31.80	-1.2901	-0.2725	-0.6882
32.00	-1.3238	-0.2984	-0.6890
32.20	-1.3347	-0.2783	-0.6838
32.40	-1.3435	-0.2577	-0.6740
32.60	-1.2921	-0.2706	-0.6586
32.80	-1.2492	-0.2527	-0.6264
33.00	-1.2269	-0.2538	-0.5940
33.20	-1.2273	-0.2603	-0.5779
33.40	-1.2321	-0.2614	-0.5749
33.60	-1.2692	-0.2860	-0.5897
33.80	-1.2733	-0.2852	-0.6082
34.00	-1.2744	-0.2830	-0.6034
34.20	-1.2774	-0.2662	-0.6088
34.40	-1.2732	-0.2607	-0.6234
34.60	-1.2796	-0.2627	-0.6324
34.80	-1.2739	-0.2564	-0.6442
35.00	-1.2861	-0.2450	-0.6465
35.20	-1.2915	-0.2354	-0.6566
35.40	-1.2763	-0.2284	-0.6501
35.60	-1.2577	-0.2041	-0.6365
35.80	-1.2516	-0.1759	-0.6235
36.00	-1.2685	-0.1679	-0.6131
36.20	-1.2892	-0.1626	-0.5996
36.40	-1.3258	-0.1778	-0.6051
36.60	-1.3468	-0.2037	-0.6094
36.80	-1.3511	-0.2141	-0.6094
37.00	-1.3686	-0.2095	-0.6078
37.20	-1.3629	-0.2031	-0.5870
37.40	-1.3676	-0.1659	-0.5782
37.60	-1.3903	-0.1481	-0.5696
37.80	-1.4008	-0.1789	-0.5915
38.00	-1.4332	-0.1821	-0.5989
38.20	-1.4788	-0.1879	-0.5931
38.40	-1.5144	-0.1863	-0.6184
38.60	-1.5257	-0.1835	-0.6342
38.80	-1.5493	-0.1742	-0.6495
39.00	-1.5590	-0.1688	-0.6549
39.20	-1.5501	-0.1316	-0.6564
39.40	-1.5263	-0.1018	-0.6546
39.60	-1.4791	-0.0740	-0.6616
39.80	-1.4348	-0.0793	-0.6630
40.00	-1.4091	-0.1286	-0.6478
40.20	-1.4160	-0.2219	-0.6489
40.40	-1.4391	-0.2971	-0.6486
40.60	-1.4441	-0.3132	-0.6423
40.80	-1.4200	-0.2656	-0.6441

41.00	-1.3907	-0.1874	-0.6458
41.20	-1.3817	-0.1205	-0.6280
41.40	-1.3585	-0.0986	-0.6098
41.60	-1.3542	-0.0946	-0.5944
41.80	-1.3838	-0.1667	-0.6167
42.00	-1.3991	-0.2349	-0.6132
42.20	-1.3974	-0.2236	-0.6093
42.40	-1.4098	-0.2072	-0.6109
42.60	-1.3998	-0.2191	-0.6093
42.80	-1.3841	-0.1997	-0.5906
43.00	-1.3907	-0.1937	-0.5867
43.20	-1.3870	-0.2027	-0.5819
43.40	-1.3720	-0.2033	-0.5840
43.60	-1.3648	-0.2021	-0.5834
43.80	-1.3724	-0.1870	-0.5704
44.00	-1.3821	-0.1757	-0.5714
44.20	-1.3928	-0.1733	-0.5757
44.40	-1.4065	-0.1808	-0.5781
44.60	-1.4173	-0.1977	-0.5820
44.80	-1.4183	-0.2322	-0.5891
45.00	-1.4173	-0.2463	-0.5874
45.20	-1.4181	-0.2309	-0.5942
45.40	-1.4170	-0.2031	-0.5982
45.60	-1.4151	-0.1775	-0.5922
45.80	-1.4233	-0.1654	-0.5939
46.00	-1.4284	-0.1757	-0.6024
46.20	-1.4324	-0.1915	-0.5997
46.40	-1.4343	-0.2044	-0.5949
46.60	-1.4298	-0.2071	-0.5849
46.80	-1.4255	-0.2021	-0.5800
47.00	-1.4247	-0.1957	-0.5748
47.20	-1.4290	-0.1983	-0.5825
47.40	-1.4477	-0.2005	-0.5905
47.60	-1.4610	-0.1931	-0.5964
47.80	-1.4701	-0.1785	-0.5930
48.00	-1.4661	-0.1851	-0.5974
48.20	-1.4595	-0.1732	-0.5953
48.40	-1.4556	-0.1737	-0.5956
48.60	-1.4500	-0.1802	-0.5968
48.80	-1.4364	-0.1847	-0.6019
49.00	-1.4293	-0.1979	-0.5986
49.20	-1.4119	-0.2008	-0.5934
49.40	-1.3960	-0.2070	-0.5982
49.60	-1.3949	-0.2148	-0.5909
49.80	-1.3944	-0.2168	-0.5889
50.00	-1.4047	-0.2153	-0.5876
50.20	-1.4161	-0.2120	-0.5973
50.40	-1.4188	-0.2155	-0.6013
50.60	-1.4179	-0.2220	-0.6108
50.80	-1.4197	-0.2167	-0.6057
51.00	-1.4203	-0.2134	-0.6024
51.20	-1.4224	-0.2128	-0.6120
51.40	-1.4216	-0.2160	-0.6132
51.60	-1.4191	-0.2171	-0.6161
51.80	-1.4192	-0.2205	-0.6122
52.00	-1.4232	-0.2243	-0.6134
52.20	-1.4276	-0.2211	-0.6182

52.40	-1.4321	-0.2256	-0.6249
52.60	-1.4232	-0.2278	-0.6291
52.80	-1.4201	-0.2195	-0.6233
53.00	-1.4119	-0.2082	-0.6199
53.20	-1.4010	-0.2022	-0.6292
53.40	-1.3882	-0.1972	-0.6147
53.60	-1.3910	-0.2087	-0.6088
53.80	-1.3960	-0.2175	-0.6111
54.00	-1.3962	-0.2308	-0.6172
54.20	-1.3969	-0.2357	-0.6069
54.40	-1.3920	-0.2459	-0.6165
54.60	-1.3864	-0.2313	-0.6173
54.80	-1.3866	-0.2267	-0.6115
55.00	-1.3872	-0.2238	-0.6182
55.20	-1.3862	-0.2184	-0.6192
55.40	-1.3822	-0.2132	-0.6163
55.60	-1.3841	-0.2073	-0.6189
55.80	-1.3781	-0.2050	-0.6128
56.00	-1.3768	-0.2157	-0.6063
56.20	-1.3773	-0.2271	-0.6054
56.40	-1.3811	-0.2372	-0.6150
56.60	-1.3672	-0.2481	-0.6125
56.80	-1.3805	-0.2399	-0.6062
57.00	-1.3776	-0.2416	-0.5996
57.20	-1.3924	-0.2364	-0.6029
57.40	-1.3935	-0.2350	-0.5953
57.60	-1.3953	-0.2370	-0.6108
57.80	-1.3971	-0.2302	-0.6039
58.00	-1.4142	-0.2221	-0.6054
58.20	-1.4004	-0.2247	-0.5982
58.40	-1.3954	-0.2107	-0.5953
58.60	-1.3951	-0.2001	-0.5969
58.80	-1.3968	-0.1976	-0.5897
59.00	-1.3996	-0.2005	-0.5876
59.20	-1.4064	-0.2135	-0.5897
59.40	-1.4158	-0.2126	-0.5938
59.60	-1.4175	-0.2281	-0.5954
59.80	-1.4194	-0.2260	-0.5967
60.00	-1.4147	-0.2131	-0.6002
60.20	-1.4046	-0.2265	-0.5942
60.40	-1.4053	-0.2507	-0.5986
60.60	-1.4170	-0.2655	-0.6054
60.80	-1.4248	-0.2684	-0.6027
61.00	-1.4281	-0.2650	-0.6065
61.20	-1.4164	-0.2623	-0.6046
61.40	-1.4104	-0.2496	-0.5937
61.60	-1.4013	-0.2418	-0.5943
61.80	-1.3965	-0.2340	-0.5887
62.00	-1.3894	-0.2477	-0.5936
62.20	-1.3878	-0.2376	-0.5879
62.40	-1.3852	-0.2292	-0.5822
62.60	-1.3784	-0.2107	-0.5773
62.80	-1.3731	-0.2025	-0.5871
63.00	-1.3657	-0.2015	-0.5831
63.20	-1.3654	-0.1987	-0.5883
63.40	-1.3695	-0.1962	-0.5961
63.60	-1.3705	-0.2140	-0.5940

63.80	-1.3678	-0.1959	-0.5874
64.00	-1.3639	-0.1942	-0.5871
64.20	-1.3622	-0.1794	-0.5908
64.40	-1.3679	-0.1769	-0.5949
64.60	-1.3719	-0.1783	-0.6077
64.80	-1.3793	-0.1795	-0.6142
65.00	-1.3837	-0.1804	-0.6184
65.20	-1.3830	-0.1854	-0.6212
65.40	-1.3788	-0.1999	-0.6239
65.60	-1.3789	-0.2091	-0.6267
65.80	-1.3829	-0.2193	-0.6312
66.00	-1.3758	-0.2225	-0.6209
66.20	-1.3702	-0.2319	-0.6208
66.40	-1.3649	-0.2293	-0.6243
66.60	-1.3625	-0.2266	-0.6213
66.80	-1.3605	-0.2239	-0.6130
67.00	-1.3527	-0.2266	-0.6151
67.20	-1.3561	-0.2306	-0.6115
67.40	-1.3537	-0.2287	-0.6047
67.60	-1.3605	-0.2259	-0.6060
67.80	-1.3578	-0.2292	-0.6072
68.00	-1.3560	-0.2241	-0.6012
68.20	-1.3562	-0.2178	-0.6020
68.40	-1.3586	-0.2133	-0.5962
68.60	-1.3574	-0.2185	-0.5944
68.80	-1.3529	-0.2217	-0.5895
69.00	-1.3528	-0.2297	-0.5871
69.20	-1.3570	-0.2284	-0.5881
69.40	-1.3595	-0.2218	-0.5768
69.60	-1.3643	-0.2216	-0.5808
69.80	-1.3656	-0.2305	-0.5804
70.00	-1.3679	-0.2365	-0.5863

GPS station KKN4

```
# Data provided by the Nepal Geodetic Array run by the California
Institute of Technology
# and the Departement of Mines and Geology (Nepal).
#
# Raw data processed by the Scripps Permanent Array and Observation
Center (SOPAC).
#
# If you use this data please cite:
#
# Galetzka et al.(2015), Slip pulse and resonance of Kathmandu basin
during the 2015
# Mw 7.8 Gorkha earthquake, Nepal imaged with space geodesy,
Science.
#
# GPS station KKN4
# 27.80075 N Latitude 85.278802 E Longitude
# First sample is at 2015-04-25T06:11:28.000000Z
#
# Time(s)  North(m)     East(m)      Up(m)
  0.00         0.0000     0.0000     0.0000
  0.20        -0.0015    -0.0039     0.0030
  0.40         0.0004    -0.0011     0.0013
  0.60        -0.0016     0.0019     0.0056
  0.80        -0.0012    -0.0022     0.0098
  1.00        -0.0018     0.0023    -0.0034
  1.20        -0.0026    -0.0019     0.0059
  1.40        -0.0030    -0.0004     0.0086
  1.60        -0.0019     0.0011     0.0054
  1.80        -0.0011     0.0015     0.0005
  2.00        -0.0019    -0.0019     0.0027
  2.20        -0.0030    -0.0008     0.0088
  2.40        -0.0032     0.0004     0.0049
  2.60        -0.0015     0.0010     0.0041
  2.80         0.0004    -0.0011     0.0056
  3.00        -0.0042    -0.0011     0.0086
  3.20        -0.0035    -0.0014     0.0078
  3.40        -0.0038    -0.0011     0.0049
  3.60        -0.0014    -0.0016     0.0078
  3.80        -0.0037    -0.0008     0.0005
  4.00        -0.0026    -0.0037     0.0105
  4.20        -0.0023     0.0012     0.0113
  4.40        -0.0012     0.0001     0.0027
  4.60        -0.0045    -0.0023     0.0083
  4.80        -0.0017     0.0005     0.0054
  5.00        -0.0018    -0.0017     0.0007
  5.20        -0.0046     0.0014     0.0072
  5.40        -0.0032    -0.0005     0.0092
  5.60        -0.0023     0.0030     0.0064
  5.80        -0.0005    -0.0040     0.0083
  6.00        -0.0025    -0.0021     0.0091
  6.20        -0.0029    -0.0052     0.0115
  6.40        -0.0027    -0.0016     0.0145
  6.60        -0.0021    -0.0001     0.0150
  6.80        -0.0031    -0.0028     0.0116
```

7.00	-0.0027	-0.0026	0.0158
7.20	-0.0031	0.0005	0.0091
7.40	-0.0021	-0.0020	0.0078
7.60	-0.0026	-0.0009	0.0102
7.80	-0.0006	0.0006	0.0070
8.00	-0.0044	-0.0016	0.0144
8.20	-0.0018	0.0008	0.0057
8.40	-0.0038	-0.0026	0.0142
8.60	-0.0001	-0.0014	0.0045
8.80	-0.0047	-0.0024	0.0142
9.00	-0.0027	-0.0038	0.0131
9.20	-0.0011	0.0000	0.0130
9.40	-0.0021	0.0002	0.0068
9.60	-0.0024	-0.0002	0.0109
9.80	-0.0026	-0.0017	0.0094
10.00	-0.0012	0.0015	0.0061
10.20	-0.0012	-0.0007	0.0147
10.40	-0.0020	0.0011	0.0087
10.60	-0.0035	0.0036	0.0185
10.80	-0.0047	0.0001	0.0169
11.00	-0.0020	-0.0007	0.0130
11.20	-0.0035	-0.0005	0.0096
11.40	-0.0023	0.0004	0.0092
11.60	-0.0024	0.0003	0.0157
11.80	-0.0033	0.0017	0.0133
12.00	-0.0025	0.0003	0.0089
12.20	-0.0051	-0.0001	0.0162
12.40	-0.0031	0.0031	0.0140
12.60	-0.0032	-0.0012	0.0142
12.80	-0.0051	-0.0007	0.0153
13.00	-0.0030	0.0007	0.0094
13.20	-0.0067	-0.0006	0.0089
13.40	-0.0055	0.0010	0.0153
13.60	-0.0039	0.0006	0.0161
13.80	-0.0068	0.0004	0.0113
14.00	-0.0058	0.0031	0.0154
14.20	-0.0047	-0.0007	0.0120
14.40	-0.0032	0.0000	0.0117
14.60	-0.0036	0.0020	0.0079
14.80	-0.0030	0.0039	0.0092
15.00	-0.0049	-0.0004	0.0101
15.20	-0.0060	0.0022	0.0095
15.40	-0.0066	-0.0010	0.0185
15.60	-0.0032	0.0057	0.0106
15.80	-0.0057	0.0002	0.0110
16.00	-0.0052	0.0061	0.0094
16.20	-0.0051	0.0051	0.0092
16.40	-0.0053	0.0042	0.0101
16.60	-0.0065	0.0103	0.0050
16.80	-0.0067	0.0104	0.0093
17.00	-0.0083	0.0133	0.0106
17.20	-0.0085	0.0143	0.0061
17.40	-0.0107	0.0179	0.0102
17.60	-0.0117	0.0179	0.0155
17.80	-0.0139	0.0258	0.0105
18.00	-0.0157	0.0266	0.0074
18.20	-0.0203	0.0334	0.0090

18.40	-0.0230	0.0363	0.0061
18.60	-0.0233	0.0411	0.0017
18.80	-0.0231	0.0461	-0.0010
19.00	-0.0246	0.0539	-0.0030
19.20	-0.0256	0.0592	-0.0030
19.40	-0.0281	0.0689	-0.0096
19.60	-0.0346	0.0776	-0.0079
19.80	-0.0456	0.0898	-0.0079
20.00	-0.0552	0.0999	-0.0039
20.20	-0.0653	0.1160	-0.0115
20.40	-0.0768	0.1361	-0.0185
20.60	-0.0927	0.1616	-0.0191
20.80	-0.1068	0.1928	-0.0214
21.00	-0.1343	0.2274	-0.0327
21.20	-0.1620	0.2515	-0.0223
21.40	-0.1937	0.3004	-0.0248
21.60	-0.2382	0.3583	-0.0269
21.80	-0.2864	0.4261	-0.0145
22.00	-0.3488	0.4931	-0.0011
22.20	-0.4004	0.5735	0.0233
22.40	-0.4792	0.6574	0.0560
22.60	-0.5952	0.7302	0.1127
22.80	-0.6976	0.7940	0.1918
23.00	-0.8154	0.8418	0.2788
23.20	-0.9280	0.8894	0.3869
23.40	-1.0525	0.9009	0.4732
23.60	-1.1673	0.8416	0.5974
23.80	-1.2948	0.8108	0.7058
24.00	-1.4064	0.7806	0.8051
24.20	-1.5014	0.7033	0.9023
24.40	-1.5709	0.6163	0.9712
24.60	-1.6226	0.5590	1.0585
24.80	-1.6750	0.4874	1.1094
25.00	-1.7222	0.4082	1.1947
25.20	-1.7540	0.3305	1.2543
25.40	-1.7597	0.2828	1.2948
25.60	-1.7417	0.2395	1.3444
25.80	-1.7220	0.2090	1.3796
26.00	-1.6982	0.1778	1.3980
26.20	-1.6696	0.1425	1.4199
26.40	-1.6447	0.1037	1.4526
26.60	-1.6058	0.0696	1.4662
26.80	-1.5750	0.0356	1.4786
27.00	-1.5544	0.0111	1.4855
27.20	-1.5529	-0.0315	1.4871
27.40	-1.5579	-0.0705	1.4834
27.60	-1.5875	-0.1003	1.4834
27.80	-1.6448	-0.1423	1.4820
28.00	-1.6975	-0.1879	1.4885
28.20	-1.7187	-0.2355	1.4726
28.40	-1.7452	-0.2750	1.4510
28.60	-1.7988	-0.3122	1.4329
28.80	-1.8480	-0.3357	1.4313
29.00	-1.8958	-0.3648	1.4082
29.20	-1.9146	-0.4014	1.4304
29.40	-1.9405	-0.4148	1.4313
29.60	-1.9853	-0.4261	1.4497

29.80	-2.0197	-0.4389	1.4796
30.00	-2.0257	-0.4410	1.4789
30.20	-2.0176	-0.4457	1.5062
30.40	-2.0136	-0.4300	1.5184
30.60	-2.0051	-0.4349	1.5340
30.80	-2.0000	-0.4379	1.5392
31.00	-1.9741	-0.4345	1.5317
31.20	-1.9548	-0.4479	1.5488
31.40	-1.9466	-0.4479	1.5426
31.60	-1.9481	-0.4530	1.5512
31.80	-1.9447	-0.4611	1.5429
32.00	-1.9145	-0.4732	1.5479
32.20	-1.8985	-0.4836	1.5520
32.40	-1.8940	-0.4875	1.5555
32.60	-1.8941	-0.4820	1.5683
32.80	-1.8863	-0.4802	1.5658
33.00	-1.8633	-0.4689	1.5669
33.20	-1.8383	-0.4671	1.5562
33.40	-1.8257	-0.4515	1.5624
33.60	-1.8066	-0.4420	1.5440
33.80	-1.7903	-0.4571	1.5304
34.00	-1.7813	-0.4530	1.5257
34.20	-1.7692	-0.4693	1.5122
34.40	-1.7513	-0.4813	1.4983
34.60	-1.7365	-0.4858	1.4855
34.80	-1.7261	-0.4927	1.4687
35.00	-1.7170	-0.4869	1.4479
35.20	-1.7171	-0.4866	1.4309
35.40	-1.7297	-0.4790	1.4249
35.60	-1.7371	-0.4604	1.4103
35.80	-1.7331	-0.4607	1.3776
36.00	-1.7425	-0.4484	1.3631
36.20	-1.7359	-0.4383	1.3292
36.40	-1.7191	-0.4436	1.3230
36.60	-1.7241	-0.4360	1.3042
36.80	-1.7342	-0.4329	1.2983
37.00	-1.7281	-0.4241	1.2829
37.20	-1.7418	-0.4366	1.2694
37.40	-1.7551	-0.4462	1.2568
37.60	-1.7763	-0.4435	1.2422
37.80	-1.7819	-0.4433	1.2300
38.00	-1.7960	-0.4563	1.2154
38.20	-1.8090	-0.4456	1.2038
38.40	-1.8275	-0.4527	1.2012
38.60	-1.8343	-0.4563	1.2000
38.80	-1.8437	-0.4568	1.1985
39.00	-1.8547	-0.4598	1.1923
39.20	-1.8518	-0.4629	1.1883
39.40	-1.8559	-0.4651	1.1905
39.60	-1.8657	-0.4692	1.2056
39.80	-1.8732	-0.4794	1.2096
40.00	-1.8857	-0.4881	1.2082
40.20	-1.8930	-0.4937	1.2169
40.40	-1.8974	-0.4942	1.2217
40.60	-1.9094	-0.4875	1.2282
40.80	-1.9112	-0.4871	1.2417
41.00	-1.9097	-0.4788	1.2502

41.20	-1.9091	-0.4736	1.2579
41.40	-1.9032	-0.4670	1.2712
41.60	-1.8993	-0.4643	1.2803
41.80	-1.8957	-0.4665	1.2825
42.00	-1.8976	-0.4624	1.2858
42.20	-1.8984	-0.4512	1.2866
42.40	-1.8948	-0.4479	1.2841
42.60	-1.9041	-0.4407	1.2809
42.80	-1.9018	-0.4501	1.2721
43.00	-1.9027	-0.4564	1.2820
43.20	-1.9138	-0.4562	1.2800
43.40	-1.9115	-0.4659	1.2811
43.60	-1.9172	-0.4631	1.2829
43.80	-1.9274	-0.4696	1.2992
44.00	-1.9162	-0.4768	1.2998
44.20	-1.9064	-0.4787	1.3035
44.40	-1.8979	-0.4745	1.3103
44.60	-1.8828	-0.4756	1.3154
44.80	-1.8782	-0.4698	1.3164
45.00	-1.8824	-0.4676	1.3199
45.20	-1.8793	-0.4676	1.3203
45.40	-1.8833	-0.4590	1.3192
45.60	-1.8778	-0.4537	1.3116
45.80	-1.8747	-0.4561	1.3262
46.00	-1.8639	-0.4575	1.3084
46.20	-1.8601	-0.4545	1.3188
46.40	-1.8603	-0.4609	1.3251
46.60	-1.8632	-0.4592	1.3232
46.80	-1.8625	-0.4614	1.3249
47.00	-1.8667	-0.4613	1.3208
47.20	-1.8621	-0.4666	1.3257
47.40	-1.8602	-0.4705	1.3233
47.60	-1.8616	-0.4743	1.3269
47.80	-1.8570	-0.4756	1.3292
48.00	-1.8502	-0.4704	1.3274
48.20	-1.8401	-0.4687	1.3159
48.40	-1.8452	-0.4583	1.3216
48.60	-1.8430	-0.4533	1.3273
48.80	-1.8453	-0.4587	1.3267
49.00	-1.8445	-0.4612	1.3201
49.20	-1.8432	-0.4555	1.3169
49.40	-1.8455	-0.4615	1.3202
49.60	-1.8526	-0.4571	1.3114
49.80	-1.8582	-0.4516	1.3087
50.00	-1.8635	-0.4524	1.3134
50.20	-1.8683	-0.4518	1.3098
50.40	-1.8645	-0.4546	1.3091
50.60	-1.8740	-0.4498	1.3127
50.80	-1.8670	-0.4448	1.3206
51.00	-1.8621	-0.4441	1.3160
51.20	-1.8658	-0.4435	1.3195
51.40	-1.8588	-0.4407	1.3214
51.60	-1.8457	-0.4493	1.3176
51.80	-1.8343	-0.4501	1.3200
52.00	-1.8321	-0.4488	1.3226
52.20	-1.8273	-0.4567	1.3229
52.40	-1.8331	-0.4586	1.3261

52.60	-1.8377	-0.4575	1.3258
52.80	-1.8347	-0.4533	1.3161
53.00	-1.8266	-0.4641	1.3148
53.20	-1.8206	-0.4628	1.3060
53.40	-1.8167	-0.4649	1.3093
53.60	-1.8137	-0.4694	1.3055
53.80	-1.8105	-0.4731	1.3140
54.00	-1.8073	-0.4660	1.3141
54.20	-1.7982	-0.4651	1.3159
54.40	-1.7947	-0.4698	1.3215
54.60	-1.8000	-0.4599	1.3193
54.80	-1.7976	-0.4529	1.3173
55.00	-1.7935	-0.4619	1.3190
55.20	-1.7901	-0.4608	1.3039
55.40	-1.7896	-0.4649	1.3054
55.60	-1.7917	-0.4740	1.3103
55.80	-1.7944	-0.4750	1.3077
56.00	-1.8026	-0.4805	1.3087
56.20	-1.8035	-0.4824	1.3147
56.40	-1.8095	-0.4793	1.3070
56.60	-1.8118	-0.4754	1.3021
56.80	-1.8159	-0.4750	1.2986
57.00	-1.8130	-0.4687	1.2972
57.20	-1.8088	-0.4636	1.2955
57.40	-1.8061	-0.4662	1.2978
57.60	-1.8074	-0.4570	1.2889
57.80	-1.8025	-0.4477	1.3037
58.00	-1.8071	-0.4400	1.2892
58.20	-1.8068	-0.4342	1.2844
58.40	-1.8109	-0.4292	1.2892
58.60	-1.8123	-0.4280	1.2817
58.80	-1.8189	-0.4309	1.2808
59.00	-1.8104	-0.4351	1.2840
59.20	-1.8072	-0.4404	1.2887
59.40	-1.8089	-0.4379	1.2944
59.60	-1.8097	-0.4397	1.2954
59.80	-1.8085	-0.4402	1.2932
60.00	-1.8098	-0.4376	1.2936
60.20	-1.8094	-0.4438	1.2957
60.40	-1.8091	-0.4382	1.2970
60.60	-1.8137	-0.4328	1.2859
60.80	-1.8173	-0.4318	1.2751
61.00	-1.8180	-0.4247	1.2873
61.20	-1.8208	-0.4280	1.2798
61.40	-1.8205	-0.4283	1.2806
61.60	-1.8232	-0.4272	1.2716
61.80	-1.8210	-0.4251	1.2696
62.00	-1.8199	-0.4283	1.2625
62.20	-1.8179	-0.4302	1.2603
62.40	-1.8236	-0.4262	1.2607
62.60	-1.8248	-0.4274	1.2635
62.80	-1.8290	-0.4305	1.2500
63.00	-1.8377	-0.4352	1.2531
63.20	-1.8423	-0.4385	1.2505
63.40	-1.8424	-0.4411	1.2521
63.60	-1.8402	-0.4466	1.2603
63.80	-1.8410	-0.4516	1.2611

64.00	-1.8348	-0.4587	1.2630
64.20	-1.8307	-0.4607	1.2635
64.40	-1.8337	-0.4677	1.2701
64.60	-1.8329	-0.4737	1.2686
64.80	-1.8279	-0.4801	1.2718
65.00	-1.8220	-0.4834	1.2717
65.20	-1.8222	-0.4838	1.2722
65.40	-1.8248	-0.4806	1.2822
65.60	-1.8234	-0.4811	1.2796
65.80	-1.8327	-0.4770	1.2872
66.00	-1.8315	-0.4719	1.2890
66.20	-1.8388	-0.4687	1.2824
66.40	-1.8389	-0.4684	1.2826
66.60	-1.8388	-0.4631	1.2834
66.80	-1.8379	-0.4550	1.2830
67.00	-1.8349	-0.4510	1.2949
67.20	-1.8314	-0.4506	1.2992
67.40	-1.8277	-0.4470	1.2967
67.60	-1.8219	-0.4432	1.2964
67.80	-1.8241	-0.4405	1.3021
68.00	-1.8237	-0.4349	1.2982
68.20	-1.8230	-0.4349	1.3031
68.40	-1.8229	-0.4361	1.3063
68.60	-1.8242	-0.4359	1.3064
68.80	-1.8239	-0.4343	1.3079
69.00	-1.8225	-0.4318	1.3028
69.20	-1.8209	-0.4302	1.3061
69.40	-1.8244	-0.4349	1.3034
69.60	-1.8230	-0.4357	1.3068
69.80	-1.8180	-0.4348	1.3022
70.00	-1.8230	-0.4363	1.2996

GPS station NAST

```
# Data provided by the Nepal Geodetic Array run by the California
Institute of Technology
# and the Departement of Mines and Geology (Nepal).
#
# Raw data processed by the Scripps Permanent Array and Observation
Center (SOPAC).
#
# If you use this data please cite:
#
# Galetzka et al.(2015), Slip pulse and resonance of Kathmandu basin
during the 2015
# Mw 7.8 Gorkha earthquake, Nepal imaged with space geodesy,
Science.
#
# GPS station NAST
# 27.65672 N Latitude 85.327726 E Longitude
# First sample is at 2015-04-25T06:11:30.400000Z
#
# Time(s)  North(m)     East(m)      Up(m)
  0.00         0.0000     0.0000     0.0000
  0.20        -0.0007     0.0007     0.0023
  0.40        -0.0003    -0.0010     0.0008
  0.60        -0.0007     0.0014    -0.0021
  0.80         0.0004    -0.0017    -0.0012
  1.00         0.0001    -0.0023     0.0022
  1.20        -0.0015    -0.0022    -0.0064
  1.40        -0.0009    -0.0001    -0.0022
  1.60        -0.0023    -0.0011    -0.0018
  1.80        -0.0034    -0.0017    -0.0015
  2.00        -0.0009     0.0009    -0.0108
  2.20        -0.0024     0.0016    -0.0014
  2.40        -0.0022     0.0003    -0.0044
  2.60         0.0003     0.0015    -0.0034
  2.80        -0.0029    -0.0005     0.0009
  3.00        -0.0030     0.0011    -0.0004
  3.20        -0.0016     0.0008    -0.0059
  3.40        -0.0011     0.0015    -0.0026
  3.60        -0.0006     0.0015     0.0091
  3.80        -0.0040    -0.0005    -0.0029
  4.00        -0.0023     0.0014    -0.0027
  4.20        -0.0034     0.0008     0.0027
  4.40        -0.0032     0.0011     0.0056
  4.60        -0.0029     0.0020     0.0058
  4.80         0.0007    -0.0006     0.0023
  5.00        -0.0017     0.0030     0.0068
  5.20        -0.0021    -0.0013     0.0029
  5.40        -0.0006     0.0015     0.0024
  5.60        -0.0037    -0.0007    -0.0009
  5.80        -0.0013     0.0000     0.0041
  6.00        -0.0008     0.0036     0.0096
  6.20        -0.0036     0.0039     0.0053
  6.40        -0.0012     0.0016     0.0063
  6.60        -0.0012     0.0036     0.0085
  6.80        -0.0020     0.0037     0.0083
```

7.00	-0.0013	0.0040	0.0060
7.20	-0.0011	0.0033	0.0077
7.40	-0.0002	0.0023	0.0065
7.60	-0.0023	0.0016	0.0047
7.80	-0.0006	0.0043	0.0076
8.00	-0.0029	0.0030	0.0074
8.20	-0.0016	0.0037	0.0085
8.40	-0.0030	0.0032	0.0135
8.60	-0.0041	0.0030	0.0053
8.80	-0.0038	0.0034	0.0126
9.00	-0.0060	0.0008	0.0085
9.20	-0.0066	-0.0001	0.0117
9.40	-0.0040	0.0013	0.0076
9.60	-0.0053	0.0014	0.0084
9.80	-0.0065	0.0039	0.0079
10.00	-0.0059	0.0022	0.0080
10.20	-0.0061	0.0027	0.0118
10.40	-0.0037	0.0032	0.0103
10.60	-0.0046	0.0026	0.0047
10.80	-0.0041	0.0026	0.0092
11.00	-0.0022	0.0004	0.0087
11.20	-0.0039	0.0007	0.0056
11.40	-0.0072	0.0008	0.0046
11.60	-0.0073	0.0030	0.0093
11.80	-0.0086	-0.0007	0.0130
12.00	-0.0073	0.0005	0.0098
12.20	-0.0079	0.0012	0.0121
12.40	-0.0071	0.0023	0.0116
12.60	-0.0046	0.0024	0.0074
12.80	-0.0068	0.0008	0.0084
13.00	-0.0053	0.0001	0.0107
13.20	-0.0068	0.0007	0.0048
13.40	-0.0055	0.0000	0.0085
13.60	-0.0061	0.0009	0.0080
13.80	-0.0098	0.0014	0.0107
14.00	-0.0074	0.0005	0.0102
14.20	-0.0105	0.0031	0.0088
14.40	-0.0060	0.0036	0.0054
14.60	-0.0089	0.0011	0.0079
14.80	-0.0066	0.0029	0.0059
15.00	-0.0079	0.0035	0.0051
15.20	-0.0087	0.0034	0.0069
15.40	-0.0092	0.0037	0.0073
15.60	-0.0080	0.0018	0.0049
15.80	-0.0084	0.0026	0.0059
16.00	-0.0087	0.0039	0.0140
16.20	-0.0098	0.0023	0.0074
16.40	-0.0080	0.0052	0.0107
16.60	-0.0072	0.0031	0.0102
16.80	-0.0074	0.0050	0.0119
17.00	-0.0060	0.0050	0.0125
17.20	-0.0092	0.0070	0.0091
17.40	-0.0116	0.0069	0.0120
17.60	-0.0133	0.0145	0.0141
17.80	-0.0151	0.0135	0.0140
18.00	-0.0166	0.0175	0.0131
18.20	-0.0197	0.0198	0.0131

18.40	-0.0208	0.0208	0.0160
18.60	-0.0266	0.0239	0.0066
18.80	-0.0292	0.0271	0.0051
19.00	-0.0308	0.0330	0.0060
19.20	-0.0348	0.0370	0.0066
19.40	-0.0398	0.0422	0.0030
19.60	-0.0388	0.0445	0.0094
19.80	-0.0426	0.0468	0.0086
20.00	-0.0441	0.0459	0.0009
20.20	-0.0432	0.0464	-0.0037
20.40	-0.0458	0.0498	-0.0035
20.60	-0.0509	0.0567	-0.0066
20.80	-0.0591	0.0648	-0.0079
21.00	-0.0652	0.0713	-0.0175
21.20	-0.0776	0.0814	-0.0186
21.40	-0.0923	0.0959	-0.0219
21.60	-0.0985	0.1110	-0.0317
21.80	-0.1088	0.1169	-0.0379
22.00	-0.1233	0.1325	-0.0513
22.20	-0.1428	0.1417	-0.0557
22.40	-0.1671	0.1637	-0.0713
22.60	-0.1858	0.1774	-0.0924
22.80	-0.2148	0.1980	-0.1156
23.00	-0.2402	0.2234	-0.1324
23.20	-0.2717	0.2511	-0.1548
23.40	-0.2961	0.2760	-0.1798
23.60	-0.3336	0.3031	-0.1996
23.80	-0.3727	0.3172	-0.2171
24.00	-0.4154	0.3429	-0.2249
24.20	-0.4589	0.3825	-0.2156
24.40	-0.5015	0.4417	-0.2058
24.60	-0.5589	0.5087	-0.1568
24.80	-0.6330	0.5640	-0.0843
25.00	-0.7324	0.6259	0.0197
25.20	-0.8510	0.6954	0.1313
25.40	-0.9788	0.7857	0.2379
25.60	-1.1147	0.8617	0.3078
25.80	-1.2666	0.8756	0.3823
26.00	-1.4304	0.8345	0.4511
26.20	-1.5789	0.7481	0.5125
26.40	-1.6885	0.6339	0.5865
26.60	-1.7395	0.5166	0.6498
26.80	-1.7887	0.3951	0.6906
27.00	-1.8040	0.3142	0.7315
27.20	-1.7869	0.1953	0.7581
27.40	-1.7752	0.0317	0.7742
27.60	-1.7261	-0.1471	0.7847
27.80	-1.6761	-0.3296	0.8127
28.00	-1.6131	-0.4801	0.8347
28.20	-1.5221	-0.5819	0.8565
28.40	-1.4210	-0.6494	0.8678
28.60	-1.3132	-0.6764	0.8808
28.80	-1.2081	-0.6548	0.8724
29.00	-1.1149	-0.5875	0.8685
29.20	-1.0318	-0.4690	0.8725
29.40	-0.9823	-0.3338	0.8757
29.60	-0.9594	-0.1885	0.8893

29.80	-0.9656	-0.0401	0.8798
30.00	-0.9999	0.0726	0.8722
30.20	-1.0659	0.1707	0.8536
30.40	-1.1278	0.2303	0.8082
30.60	-1.1787	0.2307	0.7732
30.80	-1.2471	0.1760	0.7447
31.00	-1.3165	0.0979	0.7219
31.20	-1.4056	-0.0055	0.7220
31.40	-1.4903	-0.1249	0.7039
31.60	-1.5641	-0.2510	0.6995
31.80	-1.6316	-0.3982	0.7198
32.00	-1.6863	-0.5359	0.7206
32.20	-1.7299	-0.6371	0.7415
32.40	-1.7545	-0.7166	0.7692
32.60	-1.7412	-0.7689	0.7948
32.80	-1.7070	-0.7738	0.8315
33.00	-1.6716	-0.7305	0.8656
33.20	-1.6189	-0.6514	0.8892
33.40	-1.5537	-0.5400	0.9077
33.60	-1.5002	-0.4038	0.9155
33.80	-1.4251	-0.2486	0.9205
34.00	-1.3532	-0.1110	0.9189
34.20	-1.2918	-0.0107	0.9107
34.40	-1.2340	0.0716	0.9057
34.60	-1.1835	0.1104	0.8929
34.80	-1.1631	0.0956	0.8771
35.00	-1.1813	0.0620	0.8503
35.20	-1.2157	-0.0125	0.8246
35.40	-1.2582	-0.1195	0.8033
35.60	-1.2928	-0.2316	0.7906
35.80	-1.3305	-0.3468	0.7804
36.00	-1.3751	-0.4423	0.7793
36.20	-1.4055	-0.5351	0.7858
36.40	-1.4440	-0.5903	0.7959
36.60	-1.4623	-0.6042	0.8056
36.80	-1.4688	-0.5974	0.8109
37.00	-1.4504	-0.5494	0.7953
37.20	-1.3998	-0.4697	0.7863
37.40	-1.3531	-0.3851	0.7604
37.60	-1.3057	-0.2801	0.7218
37.80	-1.2693	-0.1800	0.6896
38.00	-1.2141	-0.1114	0.6498
38.20	-1.1742	-0.0647	0.6282
38.40	-1.1367	-0.0591	0.6058
38.60	-1.1081	-0.0794	0.5875
38.80	-1.1002	-0.1324	0.5750
39.00	-1.1033	-0.2115	0.5661
39.20	-1.1115	-0.2908	0.5520
39.40	-1.1288	-0.3817	0.5458
39.60	-1.1509	-0.4551	0.5380
39.80	-1.1719	-0.5207	0.5213
40.00	-1.2037	-0.5725	0.5100
40.20	-1.2521	-0.6072	0.4981
40.40	-1.2916	-0.6225	0.4934
40.60	-1.3295	-0.6059	0.4870
40.80	-1.3596	-0.5619	0.4888
41.00	-1.3807	-0.4886	0.4798

41.20	-1.3901	-0.4039	0.4771
41.40	-1.4013	-0.3172	0.4898
41.60	-1.4063	-0.2259	0.5080
41.80	-1.4117	-0.1484	0.5185
42.00	-1.4121	-0.0848	0.5322
42.20	-1.4013	-0.0486	0.5382
42.40	-1.4020	-0.0466	0.5513
42.60	-1.4016	-0.0788	0.5624
42.80	-1.3819	-0.1420	0.5619
43.00	-1.3490	-0.2208	0.5670
43.20	-1.3220	-0.3098	0.5668
43.40	-1.3113	-0.4128	0.5718
43.60	-1.3121	-0.5053	0.5597
43.80	-1.3327	-0.5878	0.5733
44.00	-1.3655	-0.6544	0.5869
44.20	-1.4042	-0.6936	0.6196
44.40	-1.4486	-0.7151	0.6466
44.60	-1.4734	-0.7129	0.6506
44.80	-1.4920	-0.6850	0.6517
45.00	-1.5291	-0.6331	0.6522
45.20	-1.5378	-0.5515	0.6580
45.40	-1.5440	-0.4480	0.6440
45.60	-1.5130	-0.3120	0.6461
45.80	-1.4663	-0.1896	0.6488
46.00	-1.4285	-0.0962	0.6494
46.20	-1.3730	-0.0190	0.6620
46.40	-1.3121	0.0321	0.6707
46.60	-1.2436	0.0622	0.6643
46.80	-1.1760	0.0573	0.6665
47.00	-1.1341	0.0098	0.6525
47.20	-1.1075	-0.0772	0.6535
47.40	-1.1100	-0.1802	0.6495
47.60	-1.1239	-0.2825	0.6505
47.80	-1.1633	-0.3920	0.6481
48.00	-1.2169	-0.4814	0.6539
48.20	-1.2901	-0.5300	0.6529
48.40	-1.3699	-0.5796	0.6453
48.60	-1.4520	-0.6031	0.6626
48.80	-1.5081	-0.5899	0.6702
49.00	-1.5366	-0.5478	0.6763
49.20	-1.5308	-0.4866	0.6842
49.40	-1.5093	-0.4133	0.6788
49.60	-1.4824	-0.3419	0.6793
49.80	-1.4413	-0.2725	0.6741
50.00	-1.3792	-0.1960	0.6634
50.20	-1.2973	-0.1417	0.6482
50.40	-1.2148	-0.1190	0.6402
50.60	-1.1474	-0.1210	0.6470
50.80	-1.1079	-0.1383	0.6401
51.00	-1.0890	-0.1716	0.6416
51.20	-1.0853	-0.2062	0.6411
51.40	-1.1002	-0.2492	0.6325
51.60	-1.1345	-0.3011	0.6501
51.80	-1.1764	-0.3582	0.6438
52.00	-1.2234	-0.4034	0.6554
52.20	-1.2688	-0.4231	0.6538
52.40	-1.3132	-0.4375	0.6587

52.60	-1.3560	-0.4412	0.6599
52.80	-1.3920	-0.4410	0.6593
53.00	-1.4114	-0.4248	0.6601
53.20	-1.4152	-0.3965	0.6610
53.40	-1.4093	-0.3667	0.6686
53.60	-1.3927	-0.3308	0.6633
53.80	-1.3727	-0.3146	0.6591
54.00	-1.3580	-0.2996	0.6506
54.20	-1.3344	-0.2892	0.6451
54.40	-1.3212	-0.2851	0.6354
54.60	-1.2992	-0.2780	0.6321
54.80	-1.2749	-0.2928	0.6256
55.00	-1.2508	-0.3142	0.6300
55.20	-1.2314	-0.3372	0.6339
55.40	-1.2059	-0.3454	0.6380
55.60	-1.1977	-0.3509	0.6407
55.80	-1.1988	-0.3413	0.6415
56.00	-1.2107	-0.3382	0.6413
56.20	-1.2242	-0.3302	0.6399
56.40	-1.2291	-0.3123	0.6388
56.60	-1.2305	-0.3026	0.6408
56.80	-1.2468	-0.2943	0.6299
57.00	-1.2617	-0.2953	0.6249
57.20	-1.2724	-0.3020	0.6128
57.40	-1.2824	-0.3027	0.6144
57.60	-1.2810	-0.3114	0.6136
57.80	-1.2699	-0.3111	0.6095
58.00	-1.2602	-0.3064	0.6108
58.20	-1.2565	-0.3074	0.6168
58.40	-1.2564	-0.3125	0.6264
58.60	-1.2577	-0.3050	0.6269
58.80	-1.2636	-0.3016	0.6273
59.00	-1.2770	-0.2973	0.6107
59.20	-1.2860	-0.2961	0.5978
59.40	-1.2871	-0.3017	0.5816
59.60	-1.2899	-0.2988	0.5770
59.80	-1.2854	-0.2955	0.5716
60.00	-1.2825	-0.2882	0.5745
60.20	-1.2912	-0.2935	0.5842
60.40	-1.2923	-0.2997	0.5879
60.60	-1.2841	-0.2987	0.5967
60.80	-1.2676	-0.2836	0.5882
61.00	-1.2372	-0.2700	0.6007
61.20	-1.2059	-0.2666	0.5928
61.40	-1.1895	-0.2615	0.5953
61.60	-1.1830	-0.2682	0.5925
61.80	-1.1968	-0.2753	0.5914
62.00	-1.2192	-0.2923	0.5938
62.20	-1.2499	-0.3089	0.5917
62.40	-1.2909	-0.3256	0.5988
62.60	-1.3283	-0.3534	0.5918
62.80	-1.3724	-0.3742	0.5956
63.00	-1.4103	-0.3799	0.5984
63.20	-1.4370	-0.3762	0.6024
63.40	-1.4468	-0.3592	0.5945
63.60	-1.4464	-0.3569	0.6036
63.80	-1.4389	-0.3440	0.5995

64.00	-1.4066	-0.3356	0.6057
64.20	-1.3664	-0.3195	0.6003
64.40	-1.3182	-0.2979	0.6004
64.60	-1.2673	-0.2721	0.5901
64.80	-1.2296	-0.2493	0.5877
65.00	-1.2029	-0.2309	0.5837
65.20	-1.2036	-0.2273	0.5842
65.40	-1.2114	-0.2340	0.5844
65.60	-1.2180	-0.2447	0.5949
65.80	-1.2265	-0.2646	0.6064
66.00	-1.2400	-0.2943	0.6192
66.20	-1.2635	-0.3229	0.6162
66.40	-1.2926	-0.3338	0.6226
66.60	-1.3175	-0.3415	0.6221
66.80	-1.3474	-0.3450	0.6160
67.00	-1.3750	-0.3456	0.6097
67.20	-1.3902	-0.3428	0.6174
67.40	-1.3955	-0.3490	0.6159
67.60	-1.3842	-0.3459	0.6186
67.80	-1.3639	-0.3441	0.6124
68.00	-1.3347	-0.3390	0.6062
68.20	-1.3047	-0.3298	0.6057
68.40	-1.2720	-0.3237	0.6010
68.60	-1.2542	-0.3058	0.5901
68.80	-1.2447	-0.2913	0.5971
69.00	-1.2401	-0.2736	0.5972
69.20	-1.2299	-0.2657	0.6052
69.40	-1.2324	-0.2545	0.6293
69.60	-1.2346	-0.2451	0.6396
69.80	-1.2459	-0.2468	0.6458
70.00	-1.2554	-0.2502	0.6402

GPS station RMTE

```
# Data provided by the Nepal Geodetic Array run by the California
Institute of Technology
# and the Departement of Mines and Geology (Nepal).
#
# Raw data processed by the Scripps Permanent Array and Observation
Center (SOPAC).
#
# If you use this data please cite:
#
# Galetzka et al.(2015), Slip pulse and resonance of Kathmandu basin
during the 2015
# Mw 7.8 Gorkha earthquake, Nepal imaged with space geodesy,
Science.
#
# GPS station RMTE
# 26.99100 N Latitude 86.597062 E Longitude
# First sample is at 2015-04-25T06:12:09.800000Z
#
# Time(s)  North(m)     East(m)      Up(m)
  0.00         0.0000     0.0000     0.0000
  0.20         0.0033    -0.0002     0.0003
  0.40         0.0036    -0.0004    -0.0022
  0.60         0.0059    -0.0005    -0.0019
  0.80         0.0056     0.0020    -0.0042
  1.00         0.0040     0.0008     0.0032
  1.20         0.0040    -0.0016     0.0033
  1.40         0.0043     0.0002     0.0044
  1.60         0.0056     0.0016     0.0001
  1.80         0.0035     0.0012     0.0035
  2.00         0.0033     0.0002    -0.0052
  2.20         0.0047     0.0025     0.0009
  2.40         0.0016     0.0023     0.0033
  2.60         0.0030    -0.0005    -0.0032
  2.80         0.0040    -0.0008     0.0006
  3.00         0.0044     0.0004    -0.0018
  3.20         0.0035     0.0029    -0.0015
  3.40         0.0039    -0.0006     0.0004
  3.60         0.0036    -0.0004    -0.0046
  3.80         0.0041    -0.0005    -0.0050
  4.00         0.0058    -0.0012     0.0012
  4.20         0.0036    -0.0013     0.0007
  4.40         0.0039    -0.0025    -0.0019
  4.60         0.0054    -0.0042    -0.0055
  4.80         0.0035    -0.0019    -0.0029
  5.00         0.0046    -0.0010    -0.0035
  5.20         0.0046    -0.0042    -0.0059
  5.40         0.0057    -0.0003    -0.0052
  5.60         0.0037    -0.0002    -0.0027
  5.80         0.0066    -0.0022    -0.0058
  6.00         0.0048    -0.0016    -0.0003
  6.20         0.0021     0.0007     0.0047
  6.40         0.0007     0.0002     0.0034
  6.60         0.0014     0.0021    -0.0008
  6.80        -0.0015     0.0017    -0.0043
```

7.00	0.0033	0.0008	0.0002
7.20	0.0013	0.0018	0.0033
7.40	0.0016	0.0049	0.0018
7.60	0.0007	0.0048	0.0033
7.80	0.0002	0.0005	0.0023
8.00	0.0006	0.0000	-0.0017
8.20	-0.0005	0.0000	-0.0003
8.40	0.0008	0.0025	0.0017
8.60	-0.0013	0.0025	-0.0039
8.80	-0.0010	0.0005	-0.0038
9.00	0.0016	0.0021	-0.0058
9.20	0.0019	0.0040	0.0027
9.40	0.0016	0.0022	-0.0075
9.60	0.0003	0.0008	-0.0011
9.80	0.0018	0.0009	-0.0045
10.00	0.0030	0.0009	-0.0028
10.20	0.0016	0.0001	-0.0013
10.40	0.0007	-0.0008	-0.0029
10.60	-0.0016	0.0019	-0.0022
10.80	-0.0027	0.0019	-0.0015
11.00	-0.0014	0.0042	0.0008
11.20	-0.0031	0.0032	0.0020
11.40	-0.0048	0.0069	0.0042
11.60	-0.0050	0.0100	0.0029
11.80	-0.0085	0.0080	0.0066
12.00	-0.0076	0.0085	0.0048
12.20	-0.0085	0.0122	0.0088
12.40	-0.0111	0.0111	0.0038
12.60	-0.0128	0.0145	0.0042
12.80	-0.0144	0.0175	0.0083
13.00	-0.0162	0.0167	0.0050
13.20	-0.0150	0.0158	0.0045
13.40	-0.0191	0.0220	0.0062
13.60	-0.0170	0.0226	0.0007
13.80	-0.0153	0.0195	0.0039
14.00	-0.0155	0.0176	0.0025
14.20	-0.0184	0.0198	0.0037
14.40	-0.0139	0.0187	0.0015
14.60	-0.0140	0.0164	-0.0034
14.80	-0.0119	0.0181	-0.0018
15.00	-0.0093	0.0174	-0.0064
15.20	-0.0107	0.0152	-0.0063
15.40	-0.0070	0.0104	-0.0091
15.60	-0.0062	0.0108	-0.0118
15.80	-0.0050	0.0074	-0.0138
16.00	-0.0011	0.0049	-0.0160
16.20	0.0000	0.0071	-0.0153
16.40	0.0015	0.0048	-0.0112
16.60	0.0002	0.0027	-0.0147
16.80	0.0003	-0.0006	-0.0131
17.00	-0.0002	0.0063	-0.0145
17.20	0.0001	0.0005	-0.0179
17.40	-0.0028	0.0040	-0.0103
17.60	-0.0042	0.0048	-0.0092
17.80	-0.0037	0.0092	-0.0079
18.00	-0.0068	0.0063	-0.0114
18.20	-0.0050	0.0063	-0.0099

18.40	-0.0066	0.0085	-0.0104
18.60	-0.0064	0.0139	-0.0134
18.80	-0.0102	0.0129	-0.0085
19.00	-0.0119	0.0150	-0.0067
19.20	-0.0114	0.0151	-0.0077
19.40	-0.0137	0.0177	-0.0062
19.60	-0.0175	0.0189	-0.0078
19.80	-0.0177	0.0231	-0.0046
20.00	-0.0173	0.0228	-0.0094
20.20	-0.0155	0.0233	-0.0116
20.40	-0.0141	0.0239	-0.0141
20.60	-0.0171	0.0250	-0.0088
20.80	-0.0180	0.0178	-0.0105
21.00	-0.0175	0.0211	-0.0121
21.20	-0.0156	0.0241	-0.0130
21.40	-0.0120	0.0196	-0.0166
21.60	-0.0141	0.0212	-0.0161
21.80	-0.0105	0.0210	-0.0179
22.00	-0.0086	0.0210	-0.0192
22.20	-0.0080	0.0161	-0.0194
22.40	-0.0069	0.0142	-0.0204
22.60	-0.0014	0.0157	-0.0275
22.80	-0.0002	0.0142	-0.0196
23.00	0.0036	0.0108	-0.0263
23.20	0.0070	0.0162	-0.0247
23.40	0.0098	0.0164	-0.0217
23.60	0.0180	0.0192	-0.0263
23.80	0.0204	0.0137	-0.0272
24.00	0.0282	0.0187	-0.0267
24.20	0.0320	0.0284	-0.0300
24.40	0.0377	0.0315	-0.0302
24.60	0.0454	0.0323	-0.0282
24.80	0.0471	0.0388	-0.0301
25.00	0.0542	0.0436	-0.0266
25.20	0.0649	0.0540	-0.0293
25.40	0.0696	0.0685	-0.0308
25.60	0.0778	0.0821	-0.0250
25.80	0.0810	0.0804	-0.0273
26.00	0.0842	0.0905	-0.0266
26.20	0.0853	0.0995	-0.0257
26.40	0.0893	0.1069	-0.0218
26.60	0.0897	0.1146	-0.0224
26.80	0.0839	0.1253	-0.0216
27.00	0.0791	0.1206	-0.0209
27.20	0.0752	0.1238	-0.0169
27.40	0.0690	0.1246	-0.0211
27.60	0.0626	0.1198	-0.0222
27.80	0.0503	0.1233	-0.0242
28.00	0.0403	0.1263	-0.0297
28.20	0.0282	0.1286	-0.0279
28.40	0.0190	0.1266	-0.0269
28.60	0.0093	0.1323	-0.0268
28.80	-0.0004	0.1374	-0.0204
29.00	-0.0067	0.1243	-0.0225
29.20	-0.0132	0.1175	-0.0245
29.40	-0.0211	0.1258	-0.0200
29.60	-0.0206	0.1333	-0.0200

29.80	-0.0188	0.1407	-0.0115
30.00	-0.0195	0.1567	-0.0086
30.20	-0.0267	0.1607	-0.0019
30.40	-0.0274	0.1482	-0.0043
30.60	-0.0313	0.1354	-0.0047
30.80	-0.0318	0.1276	-0.0084
31.00	-0.0369	0.1343	-0.0052
31.20	-0.0446	0.1475	-0.0039
31.40	-0.0529	0.1351	-0.0030
31.60	-0.0687	0.1184	-0.0061
31.80	-0.0886	0.1092	-0.0125
32.00	-0.1156	0.1114	-0.0043
32.20	-0.1321	0.1075	0.0120
32.40	-0.1513	0.0909	0.0128
32.60	-0.1666	0.0751	0.0173
32.80	-0.1855	0.0698	0.0280
33.00	-0.2053	0.0709	0.0428
33.20	-0.2137	0.0711	0.0538
33.40	-0.2273	0.0696	0.0683
33.60	-0.2287	0.0515	0.0776
33.80	-0.2218	0.0488	0.0934
34.00	-0.2152	0.0415	0.1074
34.20	-0.2104	0.0576	0.1204
34.40	-0.1953	0.0674	0.1446
34.60	-0.1856	0.0713	0.1624
34.80	-0.1625	0.0703	0.1747
35.00	-0.1344	0.0669	0.1951
35.20	-0.1176	0.0795	0.2140
35.40	-0.0899	0.0769	0.2303
35.60	-0.0591	0.0729	0.2551
35.80	-0.0396	0.0752	0.2722
36.00	-0.0128	0.0829	0.2811
36.20	0.0111	0.0786	0.3003
36.40	0.0445	0.0701	0.3073
36.60	0.0726	0.0545	0.3116
36.80	0.1034	0.0274	0.3142
37.00	0.1295	-0.0096	0.3103
37.20	0.1595	-0.0530	0.3005
37.40	0.1713	-0.0833	0.2879
37.60	0.1862	-0.1227	0.2671
37.80	0.1966	-0.1580	0.2517
38.00	0.2105	-0.1884	0.2283
38.20	0.2202	-0.2176	0.2060
38.40	0.2341	-0.2489	0.1672
38.60	0.2443	-0.2770	0.1386
38.80	0.2508	-0.3007	0.1106
39.00	0.2500	-0.3221	0.0713
39.20	0.2527	-0.3437	0.0345
39.40	0.2459	-0.3562	-0.0061
39.60	0.2330	-0.3640	-0.0436
39.80	0.2156	-0.3703	-0.0800
40.00	0.1990	-0.3693	-0.1171
40.20	0.1767	-0.3569	-0.1509
40.40	0.1531	-0.3400	-0.1781
40.60	0.1345	-0.3308	-0.2099
40.80	0.1039	-0.3018	-0.2306
41.00	0.0786	-0.2632	-0.2551

41.20	0.0553	-0.2198	-0.2586
41.40	0.0343	-0.1773	-0.2644
41.60	0.0151	-0.1456	-0.2612
41.80	-0.0010	-0.1115	-0.2572
42.00	-0.0171	-0.0816	-0.2522
42.20	-0.0234	-0.0540	-0.2349
42.40	-0.0352	-0.0228	-0.2226
42.60	-0.0483	0.0044	-0.2038
42.80	-0.0541	0.0143	-0.1951
43.00	-0.0623	0.0327	-0.1855
43.20	-0.0612	0.0445	-0.1719
43.40	-0.0598	0.0652	-0.1590
43.60	-0.0548	0.0850	-0.1473
43.80	-0.0459	0.0957	-0.1362
44.00	-0.0375	0.0924	-0.1258
44.20	-0.0306	0.0889	-0.1250
44.40	-0.0329	0.0902	-0.1143
44.60	-0.0302	0.0951	-0.1141
44.80	-0.0255	0.1008	-0.1158
45.00	-0.0264	0.1054	-0.1068
45.20	-0.0275	0.1091	-0.0995
45.40	-0.0285	0.1126	-0.0920
45.60	-0.0272	0.1073	-0.0858
45.80	-0.0243	0.1043	-0.0802
46.00	-0.0197	0.0939	-0.0724
46.20	-0.0130	0.0803	-0.0720
46.40	-0.0079	0.0713	-0.0592
46.60	0.0042	0.0583	-0.0594
46.80	0.0160	0.0479	-0.0566
47.00	0.0233	0.0498	-0.0563
47.20	0.0247	0.0538	-0.0530
47.40	0.0278	0.0582	-0.0505
47.60	0.0249	0.0635	-0.0535
47.80	0.0253	0.0630	-0.0559
48.00	0.0228	0.0709	-0.0529
48.20	0.0186	0.0734	-0.0518
48.40	0.0142	0.0702	-0.0481
48.60	0.0010	0.0759	-0.0456
48.80	-0.0030	0.0709	-0.0441
49.00	-0.0081	0.0693	-0.0466
49.20	-0.0191	0.0693	-0.0447
49.40	-0.0252	0.0664	-0.0394
49.60	-0.0329	0.0673	-0.0319
49.80	-0.0409	0.0697	-0.0278
50.00	-0.0452	0.0583	-0.0181
50.20	-0.0482	0.0598	-0.0140
50.40	-0.0536	0.0567	-0.0070
50.60	-0.0507	0.0513	-0.0027
50.80	-0.0550	0.0517	0.0044
51.00	-0.0585	0.0448	0.0051
51.20	-0.0604	0.0373	0.0141
51.40	-0.0621	0.0328	0.0126
51.60	-0.0572	0.0295	0.0172
51.80	-0.0554	0.0318	0.0166
52.00	-0.0521	0.0203	0.0213
52.20	-0.0505	0.0256	0.0251
52.40	-0.0440	0.0249	0.0223

52.60	-0.0425	0.0233	0.0278
52.80	-0.0376	0.0277	0.0285
53.00	-0.0330	0.0279	0.0321
53.20	-0.0268	0.0273	0.0330
53.40	-0.0203	0.0284	0.0335
53.60	-0.0186	0.0285	0.0333
53.80	-0.0154	0.0308	0.0351
54.00	-0.0115	0.0298	0.0408
54.20	-0.0083	0.0348	0.0444
54.40	-0.0034	0.0357	0.0384
54.60	0.0018	0.0348	0.0445
54.80	0.0068	0.0307	0.0407
55.00	0.0103	0.0297	0.0385
55.20	0.0133	0.0244	0.0403
55.40	0.0183	0.0210	0.0362
55.60	0.0214	0.0143	0.0326
55.80	0.0261	0.0121	0.0357
56.00	0.0273	0.0090	0.0300
56.20	0.0325	0.0054	0.0298
56.40	0.0317	0.0016	0.0264
56.60	0.0297	-0.0069	0.0200
56.80	0.0281	-0.0108	0.0125
57.00	0.0265	-0.0153	0.0073
57.20	0.0228	-0.0215	0.0052
57.40	0.0175	-0.0188	0.0019
57.60	0.0147	-0.0219	-0.0039
57.80	0.0127	-0.0176	-0.0025
58.00	0.0135	-0.0155	-0.0027
58.20	0.0068	-0.0127	-0.0089
58.40	0.0010	-0.0104	-0.0052
58.60	-0.0039	-0.0046	-0.0042
58.80	-0.0104	-0.0016	-0.0043
59.00	-0.0135	0.0010	-0.0042
59.20	-0.0199	0.0029	-0.0066
59.40	-0.0210	0.0055	-0.0043
59.60	-0.0250	0.0117	0.0018
59.80	-0.0281	0.0151	0.0034
60.00	-0.0244	0.0141	0.0075
60.20	-0.0221	0.0192	0.0072
60.40	-0.0209	0.0151	0.0074
60.60	-0.0184	0.0200	0.0084
60.80	-0.0129	0.0225	0.0026
61.00	-0.0120	0.0239	-0.0045
61.20	-0.0098	0.0201	0.0046
61.40	-0.0065	0.0183	-0.0004
61.60	0.0004	0.0140	-0.0043
61.80	0.0011	0.0139	-0.0015
62.00	0.0085	0.0152	0.0022
62.20	0.0110	0.0122	-0.0024
62.40	0.0155	0.0136	-0.0034
62.60	0.0192	0.0130	-0.0023
62.80	0.0256	0.0131	0.0019
63.00	0.0286	0.0139	0.0047
63.20	0.0328	0.0179	0.0026
63.40	0.0356	0.0163	-0.0005
63.60	0.0335	0.0139	-0.0003
63.80	0.0338	0.0131	0.0044

64.00	0.0324	0.0136	-0.0025
64.20	0.0366	0.0100	-0.0020
64.40	0.0336	0.0042	-0.0021
64.60	0.0289	0.0047	0.0041
64.80	0.0239	0.0021	0.0062
65.00	0.0216	-0.0014	0.0028
65.20	0.0193	-0.0023	0.0037
65.40	0.0175	-0.0038	0.0011
65.60	0.0118	-0.0047	0.0000
65.80	0.0073	-0.0015	-0.0023
66.00	0.0058	-0.0036	-0.0035
66.20	0.0038	-0.0007	-0.0009
66.40	-0.0005	-0.0022	-0.0047
66.60	-0.0048	-0.0037	-0.0096
66.80	-0.0035	-0.0022	-0.0098
67.00	-0.0025	0.0017	-0.0111
67.20	-0.0035	0.0029	-0.0163
67.40	-0.0005	0.0084	-0.0163
67.60	-0.0007	0.0085	-0.0164
67.80	-0.0027	0.0122	-0.0147
68.00	-0.0026	0.0132	-0.0186
68.20	-0.0028	0.0133	-0.0180
68.40	-0.0038	0.0168	-0.0143
68.60	-0.0053	0.0170	-0.0144
68.80	-0.0024	0.0183	-0.0146
69.00	-0.0033	0.0188	-0.0133
69.20	-0.0017	0.0207	-0.0098
69.40	-0.0055	0.0224	-0.0071
69.60	-0.0038	0.0229	-0.0026
69.80	-0.0013	0.0184	-0.0007
70.00	-0.0007	0.0160	-0.0067

GPS station SNDL

```
# Data provided by the Nepal Geodetic Array run by the California
Institute of Technology
# and the Departement of Mines and Geology (Nepal).
#
# Raw data processed by the Scripps Permanent Array and Observation
Center (SOPAC).
#
# If you use this data please cite:
#
# Galetzka et al.(2015), Slip pulse and resonance of Kathmandu basin
during the 2015
# Mw 7.8 Gorkha earthquake, Nepal imaged with space geodesy,
Science.
#
# GPS station SNDL
# 27.38488 N Latitude 85.798852 E Longitude
# First sample is at 2015-04-25T06:11:38.600000Z
#
# Time(s)  North(m)     East(m)      Up(m)
  0.00         0.0000     0.0000     0.0000
  0.20         0.0013    -0.0026    -0.0015
  0.40         0.0015    -0.0012     0.0010
  0.60        -0.0005    -0.0014    -0.0047
  0.80         0.0005    -0.0002    -0.0008
  1.00        -0.0015    -0.0003    -0.0005
  1.20        -0.0006    -0.0011    -0.0025
  1.40         0.0005    -0.0012    -0.0045
  1.60         0.0026    -0.0016    -0.0030
  1.80        -0.0006    -0.0014    -0.0010
  2.00        -0.0006    -0.0006    -0.0021
  2.20         0.0000    -0.0037    -0.0022
  2.40         0.0008    -0.0013     0.0011
  2.60         0.0014    -0.0030    -0.0003
  2.80         0.0003    -0.0022    -0.0039
  3.00         0.0034    -0.0031    -0.0033
  3.20         0.0024    -0.0034    -0.0012
  3.40         0.0023    -0.0036     0.0016
  3.60         0.0018    -0.0007    -0.0031
  3.80         0.0036    -0.0035    -0.0031
  4.00         0.0007    -0.0032    -0.0053
  4.20         0.0018     0.0010    -0.0023
  4.40         0.0014    -0.0015    -0.0011
  4.60         0.0023    -0.0013    -0.0019
  4.80         0.0009     0.0015     0.0030
  5.00         0.0033    -0.0018    -0.0025
  5.20         0.0030    -0.0018    -0.0022
  5.40         0.0020    -0.0045     0.0034
  5.60         0.0017    -0.0006    -0.0029
  5.80         0.0040    -0.0048    -0.0016
  6.00        -0.0020    -0.0034     0.0025
  6.20         0.0005    -0.0005     0.0024
  6.40         0.0008    -0.0002     0.0040
  6.60        -0.0019    -0.0020    -0.0021
  6.80        -0.0005    -0.0014    -0.0028
```

7.00	-0.0021	0.0003	-0.0004
7.20	0.0000	-0.0008	-0.0011
7.40	-0.0007	-0.0011	-0.0009
7.60	-0.0007	-0.0008	-0.0009
7.80	-0.0010	0.0008	0.0032
8.00	-0.0010	-0.0010	0.0003
8.20	-0.0001	0.0017	0.0044
8.40	0.0004	-0.0016	-0.0013
8.60	0.0008	0.0003	0.0031
8.80	0.0013	-0.0004	0.0014
9.00	0.0013	0.0010	0.0045
9.20	0.0000	-0.0022	-0.0012
9.40	-0.0006	0.0008	0.0026
9.60	-0.0001	-0.0002	0.0037
9.80	0.0021	-0.0009	0.0026
10.00	0.0018	-0.0017	0.0023
10.20	0.0031	-0.0022	0.0049
10.40	0.0031	-0.0007	0.0002
10.60	0.0023	-0.0026	0.0041
10.80	0.0023	-0.0001	-0.0008
11.00	0.0011	-0.0014	0.0023
11.20	0.0016	0.0017	0.0031
11.40	0.0021	-0.0026	-0.0018
11.60	0.0034	0.0014	-0.0006
11.80	0.0026	-0.0006	-0.0006
12.00	0.0014	0.0005	0.0037
12.20	0.0008	0.0003	0.0018
12.40	0.0006	0.0004	0.0018
12.60	0.0018	0.0022	0.0022
12.80	0.0036	0.0033	0.0017
13.00	0.0022	0.0032	0.0053
13.20	0.0031	0.0011	0.0011
13.40	0.0036	0.0031	-0.0040
13.60	0.0033	0.0022	0.0032
13.80	0.0020	0.0017	0.0022
14.00	0.0014	0.0019	0.0038
14.20	-0.0009	-0.0009	0.0012
14.40	0.0005	0.0029	0.0042
14.60	0.0009	0.0032	0.0054
14.80	0.0014	0.0020	0.0053
15.00	-0.0003	-0.0005	0.0031
15.20	-0.0006	0.0013	0.0048
15.40	0.0003	-0.0015	0.0015
15.60	-0.0004	0.0008	0.0089
15.80	0.0016	0.0010	0.0029
16.00	0.0000	-0.0018	0.0078
16.20	0.0023	0.0004	0.0040
16.40	0.0017	-0.0022	0.0073
16.60	0.0014	-0.0019	0.0072
16.80	0.0023	-0.0023	0.0031
17.00	0.0007	0.0010	0.0064
17.20	0.0007	-0.0027	0.0037
17.40	0.0020	-0.0007	0.0023
17.60	0.0011	-0.0005	0.0079
17.80	0.0046	-0.0003	0.0048
18.00	0.0012	-0.0025	0.0067
18.20	0.0031	-0.0031	0.0052

18.40	0.0024	-0.0029	0.0045
18.60	0.0015	-0.0021	0.0027
18.80	0.0017	-0.0005	-0.0037
19.00	0.0009	-0.0033	-0.0007
19.20	0.0012	-0.0020	-0.0005
19.40	0.0007	0.0000	-0.0034
19.60	0.0004	0.0006	0.0005
19.80	-0.0009	0.0011	-0.0020
20.00	-0.0011	0.0031	0.0040
20.20	-0.0046	0.0029	0.0079
20.40	-0.0027	0.0046	0.0032
20.60	-0.0030	0.0061	0.0039
20.80	-0.0052	0.0043	0.0070
21.00	-0.0039	0.0060	-0.0003
21.20	-0.0029	0.0046	0.0007
21.40	-0.0033	0.0057	0.0007
21.60	-0.0016	0.0046	0.0024
21.80	-0.0028	0.0065	-0.0014
22.00	-0.0025	0.0065	-0.0022
22.20	-0.0033	0.0063	0.0028
22.40	-0.0036	0.0075	0.0039
22.60	-0.0038	0.0083	-0.0020
22.80	-0.0083	0.0097	0.0031
23.00	-0.0083	0.0138	0.0038
23.20	-0.0103	0.0160	0.0007
23.40	-0.0138	0.0171	0.0041
23.60	-0.0150	0.0189	0.0041
23.80	-0.0164	0.0239	0.0062
24.00	-0.0190	0.0262	0.0006
24.20	-0.0233	0.0311	0.0062
24.40	-0.0258	0.0325	0.0064
24.60	-0.0271	0.0333	0.0038
24.80	-0.0289	0.0373	-0.0009
25.00	-0.0301	0.0373	0.0017
25.20	-0.0318	0.0391	0.0022
25.40	-0.0313	0.0425	-0.0027
25.60	-0.0332	0.0467	-0.0036
25.80	-0.0343	0.0475	-0.0059
26.00	-0.0350	0.0446	-0.0084
26.20	-0.0321	0.0463	-0.0049
26.40	-0.0352	0.0469	-0.0129
26.60	-0.0354	0.0495	-0.0102
26.80	-0.0377	0.0516	-0.0162
27.00	-0.0406	0.0546	-0.0136
27.20	-0.0396	0.0548	-0.0211
27.40	-0.0416	0.0567	-0.0264
27.60	-0.0448	0.0593	-0.0284
27.80	-0.0508	0.0625	-0.0314
28.00	-0.0515	0.0633	-0.0291
28.20	-0.0546	0.0664	-0.0331
28.40	-0.0621	0.0725	-0.0364
28.60	-0.0653	0.0729	-0.0304
28.80	-0.0720	0.0800	-0.0363
29.00	-0.0799	0.0862	-0.0400
29.20	-0.0865	0.0890	-0.0376
29.40	-0.0922	0.0934	-0.0460
29.60	-0.1005	0.0943	-0.0448

29.80	-0.1038	0.0988	-0.0550
30.00	-0.1077	0.1066	-0.0577
30.20	-0.1091	0.1100	-0.0638
30.40	-0.1099	0.1208	-0.0716
30.60	-0.1135	0.1261	-0.0736
30.80	-0.1137	0.1315	-0.0828
31.00	-0.1121	0.1380	-0.0904
31.20	-0.1029	0.1440	-0.1036
31.40	-0.1066	0.1512	-0.1197
31.60	-0.0855	0.1607	-0.1268
31.80	-0.0866	0.1694	-0.1367
32.00	-0.0874	0.1722	-0.1551
32.20	-0.0765	0.1887	-0.1658
32.40	-0.0875	0.1972	-0.1797
32.60	-0.0908	0.2125	-0.1852
32.80	-0.1085	0.2213	-0.1909
33.00	-0.1325	0.2276	-0.1927
33.20	-0.1386	0.2440	-0.1965
33.40	-0.1727	0.2547	-0.2038
33.60	-0.1923	0.2561	-0.2080
33.80	-0.2168	0.2665	-0.2181
34.00	-0.2460	0.2676	-0.2199
34.20	-0.2928	0.2720	-0.2309
34.40	-0.3230	0.2768	-0.2178
34.60	-0.3655	0.2874	-0.2205
34.80	-0.4135	0.2991	-0.2265
35.00	-0.4716	0.3206	-0.2197
35.20	-0.5200	0.3339	-0.2057
35.40	-0.5762	0.3438	-0.1825
35.60	-0.6328	0.3538	-0.1595
35.80	-0.6785	0.3630	-0.1319
36.00	-0.7197	0.3663	-0.0978
36.20	-0.7400	0.3649	-0.0646
36.40	-0.7808	0.3824	-0.0127
36.60	-0.7725	0.3680	0.0339
36.80	-0.8113	0.3519	0.0826
37.00	-0.8112	0.3294	0.1293
37.20	-0.7963	0.3185	0.1700
37.40	-0.7839	0.2897	0.2127
37.60	-0.7604	0.2707	0.2627
37.80	-0.7055	0.2551	0.2832
38.00	-0.7045	0.2305	0.3303
38.20	-0.6729	0.1968	0.3728
38.40	-0.6410	0.1622	0.4090
38.60	-0.5830	0.1322	0.4455
38.80	-0.5442	0.1102	0.4672
39.00	-0.4975	0.0965	0.4734
39.20	-0.4528	0.0518	0.4820
39.40	-0.4412	0.0351	0.5011
39.60	-0.3701	-0.0064	0.5070
39.80	-0.3471	-0.0227	0.5202
40.00	-0.3095	-0.0409	0.5334
40.20	-0.3068	-0.0568	0.5411
40.40	-0.2897	-0.0764	0.5373
40.60	-0.2472	-0.0980	0.5405
40.80	-0.2424	-0.1215	0.5294
41.00	-0.2244	-0.1478	0.5262

41.20	-0.2001	-0.1632	0.5129
41.40	-0.1694	-0.1837	0.4917
41.60	-0.1541	-0.1918	0.4699
41.80	-0.1532	-0.2065	0.4506
42.00	-0.1496	-0.2249	0.4113
42.20	-0.1347	-0.2517	0.3964
42.40	-0.1155	-0.2458	0.3641
42.60	-0.0911	-0.2457	0.3383
42.80	-0.0622	-0.2332	0.3153
43.00	-0.0356	-0.2385	0.2730
43.20	-0.0250	-0.2288	0.2277
43.40	-0.0103	-0.2240	0.1932
43.60	0.0005	-0.2120	0.1468
43.80	0.0209	-0.1892	0.1263
44.00	0.0107	-0.1761	0.0866
44.20	0.0024	-0.1486	0.0599
44.40	0.0166	-0.1405	0.0421
44.60	-0.0037	-0.1303	0.0052
44.80	0.0040	-0.1171	-0.0120
45.00	-0.0054	-0.0979	-0.0329
45.20	-0.0118	-0.0710	-0.0441
45.40	-0.0470	-0.0669	-0.0565
45.60	-0.0732	-0.0454	-0.0746
45.80	-0.0911	-0.0264	-0.0751
46.00	-0.0987	-0.0053	-0.0855
46.20	-0.1350	-0.0052	-0.0912
46.40	-0.1538	0.0031	-0.0946
46.60	-0.1444	0.0119	-0.0938
46.80	-0.1809	0.0257	-0.1032
47.00	-0.1862	0.0230	-0.0892
47.20	-0.1900	0.0594	-0.0947
47.40	-0.1861	0.0772	-0.0968
47.60	-0.1994	0.0931	-0.0978
47.80	-0.1995	0.1006	-0.1049
48.00	-0.2236	0.1028	-0.0970
48.20	-0.2076	0.1083	-0.0973
48.40	-0.2308	0.1200	-0.0947
48.60	-0.2088	0.1124	-0.0823
48.80	-0.2039	0.1281	-0.0740
49.00	-0.1980	0.1204	-0.0673
49.20	-0.2362	0.1102	-0.0637
49.40	-0.2135	0.1094	-0.0516
49.60	-0.1959	0.1045	-0.0567
49.80	-0.2233	0.0979	-0.0582
50.00	-0.2200	0.1049	-0.0371
50.20	-0.2469	0.0860	-0.0390
50.40	-0.2098	0.0990	-0.0400
50.60	-0.2139	0.0904	-0.0287
50.80	-0.2126	0.0955	-0.0231
51.00	-0.2206	0.0928	-0.0157
51.20	-0.2186	0.0902	-0.0107
51.40	-0.2195	0.0832	-0.0159
51.60	-0.2128	0.0831	-0.0048
51.80	-0.2170	0.0712	0.0069
52.00	-0.1859	0.0663	0.0070
52.20	-0.1762	0.0726	0.0118
52.40	-0.1750	0.0691	0.0060

52.60	-0.1679	0.0721	0.0014
52.80	-0.1588	0.0799	-0.0059
53.00	-0.1579	0.0790	-0.0124
53.20	-0.1474	0.0807	-0.0125
53.40	-0.1611	0.0741	-0.0173
53.60	-0.1597	0.0715	-0.0229
53.80	-0.1576	0.0761	-0.0238
54.00	-0.1547	0.0780	-0.0312
54.20	-0.1660	0.0777	-0.0268
54.40	-0.1566	0.0720	-0.0365
54.60	-0.1554	0.0706	-0.0398
54.80	-0.1617	0.0628	-0.0444
55.00	-0.1604	0.0558	-0.0442
55.20	-0.1654	0.0544	-0.0443
55.40	-0.1569	0.0490	-0.0507
55.60	-0.1587	0.0493	-0.0525
55.80	-0.1576	0.0454	-0.0512
56.00	-0.1693	0.0471	-0.0503
56.20	-0.1762	0.0445	-0.0537
56.40	-0.1859	0.0452	-0.0527
56.60	-0.1980	0.0468	-0.0470
56.80	-0.2039	0.0427	-0.0452
57.00	-0.2106	0.0479	-0.0391
57.20	-0.2228	0.0478	-0.0335
57.40	-0.2354	0.0480	-0.0231
57.60	-0.2431	0.0548	-0.0179
57.80	-0.2549	0.0589	-0.0170
58.00	-0.2586	0.0592	-0.0134
58.20	-0.2694	0.0605	-0.0165
58.40	-0.2626	0.0577	-0.0126
58.60	-0.2636	0.0627	-0.0087
58.80	-0.2648	0.0535	-0.0027
59.00	-0.2548	0.0497	0.0020
59.20	-0.2639	0.0487	0.0041
59.40	-0.2678	0.0491	0.0118
59.60	-0.2652	0.0517	0.0110
59.80	-0.2672	0.0521	0.0126
60.00	-0.2715	0.0532	0.0091
60.20	-0.2694	0.0521	0.0078
60.40	-0.2696	0.0499	0.0075
60.60	-0.2625	0.0574	0.0063
60.80	-0.2595	0.0605	0.0059
61.00	-0.2564	0.0612	0.0050
61.20	-0.2506	0.0601	0.0035
61.40	-0.2492	0.0547	0.0046
61.60	-0.2490	0.0522	0.0085
61.80	-0.2445	0.0442	0.0153
62.00	-0.2409	0.0429	0.0205
62.20	-0.2380	0.0398	0.0171
62.40	-0.2362	0.0382	0.0233
62.60	-0.2302	0.0368	0.0266
62.80	-0.2311	0.0408	0.0319
63.00	-0.2249	0.0381	0.0302
63.20	-0.2189	0.0410	0.0357
63.40	-0.2104	0.0402	0.0418
63.60	-0.2092	0.0486	0.0426
63.80	-0.2079	0.0515	0.0479

64.00	-0.2112	0.0549	0.0521
64.20	-0.2108	0.0567	0.0494
64.40	-0.2148	0.0608	0.0545
64.60	-0.2178	0.0648	0.0527
64.80	-0.2171	0.0665	0.0484
65.00	-0.2201	0.0671	0.0476
65.20	-0.2233	0.0659	0.0524
65.40	-0.2234	0.0685	0.0444
65.60	-0.2267	0.0662	0.0450
65.80	-0.2232	0.0657	0.0519
66.00	-0.2294	0.0650	0.0498
66.20	-0.2292	0.0596	0.0514
66.40	-0.2342	0.0528	0.0465
66.60	-0.2335	0.0494	0.0428
66.80	-0.2340	0.0477	0.0424
67.00	-0.2327	0.0456	0.0401
67.20	-0.2335	0.0462	0.0377
67.40	-0.2273	0.0434	0.0409
67.60	-0.2322	0.0419	0.0423
67.80	-0.2235	0.0426	0.0378
68.00	-0.2251	0.0436	0.0400
68.20	-0.2188	0.0428	0.0380
68.40	-0.2185	0.0467	0.0296
68.60	-0.2172	0.0491	0.0300
68.80	-0.2149	0.0516	0.0270
69.00	-0.2138	0.0552	0.0226
69.20	-0.2182	0.0583	0.0234
69.40	-0.2169	0.0587	0.0206
69.60	-0.2155	0.0608	0.0273
69.80	-0.2161	0.0600	0.0199
70.00	-0.2145	0.0588	0.0204

GPS station SYBC

```
# Data provided by the Nepal Geodetic Array run by the California
Institute of Technology
# and the Departement of Mines and Geology (Nepal).
#
# Raw data processed by the Scripps Permanent Array and Observation
Center (SOPAC).
#
# If you use this data please cite:
#
# Galetzka et al.(2015), Slip pulse and resonance of Kathmandu basin
during the 2015
# Mw 7.8 Gorkha earthquake, Nepal imaged with space geodesy,
Science.
#
# GPS station SYBC
# 27.81428 N Latitude 86.712448 E Longitude
# First sample is at 2015-04-25T06:12:06.400000Z
#
# Time(s)  North(m)     East(m)      Up(m)
  0.00         0.0000     0.0000     0.0000
  0.20        -0.0021     0.0008     0.0081
  0.40        -0.0013     0.0020     0.0042
  0.60        -0.0026     0.0022     0.0010
  0.80        -0.0033     0.0020    -0.0009
  1.00        -0.0013     0.0028     0.0031
  1.20        -0.0015     0.0034     0.0041
  1.40        -0.0032     0.0006     0.0028
  1.60        -0.0031     0.0037     0.0057
  1.80        -0.0028     0.0037     0.0058
  2.00        -0.0060     0.0052     0.0033
  2.20        -0.0030     0.0036     0.0075
  2.40        -0.0047     0.0028     0.0067
  2.60        -0.0032     0.0045     0.0120
  2.80        -0.0048     0.0041     0.0123
  3.00        -0.0023     0.0084     0.0085
  3.20        -0.0043     0.0057     0.0034
  3.40        -0.0048     0.0020     0.0047
  3.60        -0.0048     0.0043     0.0088
  3.80        -0.0023     0.0019     0.0027
  4.00        -0.0041     0.0038     0.0070
  4.20        -0.0049     0.0038     0.0021
  4.40        -0.0037     0.0016     0.0080
  4.60        -0.0025     0.0025     0.0006
  4.80        -0.0042     0.0023     0.0027
  5.00        -0.0035     0.0025     0.0040
  5.20        -0.0029     0.0044     0.0048
  5.40        -0.0029     0.0024    -0.0003
  5.60        -0.0050    -0.0002     0.0025
  5.80        -0.0014     0.0016     0.0051
  6.00        -0.0024     0.0001     0.0031
  6.20        -0.0014     0.0012     0.0078
  6.40        -0.0039     0.0005     0.0048
  6.60        -0.0023    -0.0013     0.0041
  6.80        -0.0021    -0.0026     0.0007
```

7.00	-0.0018	0.0026	-0.0002
7.20	-0.0010	0.0016	0.0078
7.40	0.0002	-0.0011	0.0001
7.60	0.0004	-0.0013	0.0011
7.80	0.0009	-0.0034	0.0016
8.00	0.0005	-0.0037	0.0014
8.20	0.0022	-0.0050	-0.0018
8.40	0.0012	-0.0067	0.0002
8.60	0.0024	-0.0052	-0.0011
8.80	0.0025	-0.0043	0.0001
9.00	0.0048	-0.0008	0.0010
9.20	0.0042	-0.0007	-0.0002
9.40	0.0035	-0.0018	0.0032
9.60	0.0075	-0.0006	0.0024
9.80	0.0064	-0.0029	0.0057
10.00	0.0034	-0.0057	0.0056
10.20	0.0049	-0.0033	0.0097
10.40	0.0066	-0.0016	0.0106
10.60	0.0070	-0.0019	0.0053
10.80	0.0054	-0.0032	0.0046
11.00	0.0060	-0.0028	0.0008
11.20	0.0088	-0.0063	0.0015
11.40	0.0095	-0.0072	0.0010
11.60	0.0073	-0.0066	0.0079
11.80	0.0099	-0.0071	0.0064
12.00	0.0124	-0.0133	0.0019
12.20	0.0113	-0.0147	0.0055
12.40	0.0121	-0.0112	0.0023
12.60	0.0130	-0.0162	0.0059
12.80	0.0131	-0.0139	0.0062
13.00	0.0148	-0.0141	0.0084
13.20	0.0157	-0.0130	0.0051
13.40	0.0191	-0.0132	0.0053
13.60	0.0191	-0.0118	0.0070
13.80	0.0123	-0.0111	0.0096
14.00	0.0140	-0.0120	0.0068
14.20	0.0138	-0.0083	0.0123
14.40	0.0176	-0.0052	0.0071
14.60	0.0190	-0.0015	0.0046
14.80	0.0166	0.0024	0.0062
15.00	0.0160	0.0010	0.0127
15.20	0.0141	0.0042	0.0045
15.40	0.0155	0.0075	0.0085
15.60	0.0158	0.0129	0.0106
15.80	0.0147	0.0106	0.0108
16.00	0.0154	0.0101	0.0071
16.20	0.0111	0.0106	0.0095
16.40	0.0131	0.0094	0.0085
16.60	0.0148	0.0144	0.0096
16.80	0.0152	0.0141	0.0055
17.00	0.0148	0.0167	0.0039
17.20	0.0135	0.0138	0.0049
17.40	0.0134	0.0154	0.0030
17.60	0.0098	0.0126	0.0072
17.80	0.0111	0.0131	0.0119
18.00	0.0163	0.0084	0.0068
18.20	0.0163	0.0110	0.0041

18.40	0.0111	0.0054	0.0119
18.60	0.0081	0.0079	0.0036
18.80	0.0089	0.0075	0.0081
19.00	0.0085	0.0125	0.0148
19.20	0.0129	0.0109	0.0074
19.40	0.0122	0.0104	0.0106
19.60	0.0129	0.0097	0.0102
19.80	0.0070	0.0127	0.0116
20.00	0.0058	0.0130	0.0125
20.20	0.0041	0.0142	0.0186
20.40	0.0076	0.0125	0.0132
20.60	0.0012	0.0191	0.0123
20.80	0.0041	0.0210	0.0183
21.00	0.0041	0.0172	0.0145
21.20	-0.0003	0.0251	0.0128
21.40	0.0000	0.0198	0.0158
21.60	0.0021	0.0237	0.0167
21.80	-0.0008	0.0265	0.0125
22.00	-0.0054	0.0242	0.0160
22.20	-0.0106	0.0249	0.0112
22.40	-0.0161	0.0292	0.0145
22.60	-0.0105	0.0247	0.0140
22.80	-0.0039	0.0256	0.0105
23.00	-0.0061	0.0252	0.0106
23.20	-0.0115	0.0285	0.0056
23.40	-0.0016	0.0398	0.0155
23.60	-0.0025	0.0335	0.0139
23.80	-0.0153	0.0251	0.0156
24.00	-0.0201	0.0337	0.0120
24.20	-0.0039	0.0282	0.0114
24.40	-0.0006	0.0281	0.0099
24.60	0.0143	0.0418	0.0175
24.80	0.0168	0.0278	0.0298
25.00	-0.0203	0.0169	0.0232
25.20	-0.0479	0.0058	0.0302
25.40	-0.0192	0.0279	0.0239
25.60	0.0205	0.0389	0.0261
25.80	0.0004	0.0331	0.0253
26.00	-0.0202	0.0224	0.0371
26.20	-0.0251	0.0060	0.0491
26.40	-0.0359	0.0049	0.0388
26.60	-0.0128	0.0039	0.0403
26.80	-0.0340	0.0030	0.0387
27.00	-0.0607	-0.0063	0.0377
27.20	-0.0822	-0.0378	0.0290
27.40	-0.1091	-0.0617	0.0219
27.60	-0.1483	-0.0473	0.0082
27.80	-0.1582	-0.0408	0.0091
28.00	-0.1252	-0.0154	-0.0071
28.20	-0.1019	-0.0345	0.0057
28.40	-0.0902	-0.0622	-0.0115
28.60	-0.1056	-0.0786	-0.0198
28.80	-0.1181	-0.0923	-0.0458
29.00	-0.1104	-0.0964	-0.0722
29.20	-0.1176	-0.0930	-0.0882
29.40	-0.1164	-0.1180	-0.0918
29.60	-0.0960	-0.1168	-0.1163

29.80	-0.0856	-0.0985	-0.1228
30.00	-0.0619	-0.0818	-0.1276
30.20	-0.0393	-0.0793	-0.1388
30.40	-0.0473	-0.0705	-0.1602
30.60	-0.0647	-0.0489	-0.1808
30.80	-0.0815	-0.0128	-0.1847
31.00	-0.0696	-0.0053	-0.1829
31.20	-0.0434	-0.0093	-0.1729
31.40	-0.0244	-0.0089	-0.1617
31.60	-0.0225	-0.0005	-0.1658
31.80	-0.0402	0.0290	-0.1697
32.00	-0.0458	0.0697	-0.1610
32.20	-0.0623	0.1035	-0.1500
32.40	-0.0738	0.1160	-0.1346
32.60	-0.0844	0.1035	-0.1290
32.80	-0.0941	0.1001	-0.1159
33.00	-0.0919	0.1112	-0.0907
33.20	-0.0632	0.1139	-0.0731
33.40	-0.0438	0.1121	-0.0542
33.60	-0.0466	0.1118	-0.0304
33.80	-0.0437	0.1139	-0.0123
34.00	-0.0545	0.1177	0.0042
34.20	-0.0710	0.1204	0.0248
34.40	-0.0716	0.1120	0.0483
34.60	-0.0593	0.1021	0.0622
34.80	-0.0384	0.0947	0.0787
35.00	-0.0213	0.0771	0.1005
35.20	-0.0140	0.0701	0.1092
35.40	-0.0119	0.0432	0.1171
35.60	-0.0169	0.0151	0.1277
35.80	-0.0226	-0.0079	0.1330
36.00	-0.0318	-0.0231	0.1349
36.20	-0.0434	-0.0381	0.1267
36.40	-0.0551	-0.0459	0.1202
36.60	-0.0510	-0.0576	0.1141
36.80	-0.0260	-0.0617	0.1073
37.00	-0.0115	-0.0720	0.1047
37.20	-0.0140	-0.0782	0.1017
37.40	-0.0367	-0.0816	0.0909
37.60	-0.0661	-0.0864	0.0814
37.80	-0.0890	-0.0939	0.0766
38.00	-0.0950	-0.0961	0.0602
38.20	-0.0859	-0.1005	0.0528
38.40	-0.0754	-0.0978	0.0389
38.60	-0.0672	-0.0879	0.0257
38.80	-0.0555	-0.0785	0.0134
39.00	-0.0527	-0.0751	0.0003
39.20	-0.0541	-0.0679	-0.0109
39.40	-0.0521	-0.0573	-0.0169
39.60	-0.0501	-0.0456	-0.0183
39.80	-0.0562	-0.0423	-0.0148
40.00	-0.0538	-0.0408	-0.0203
40.20	-0.0519	-0.0464	-0.0233
40.40	-0.0373	-0.0404	-0.0336
40.60	-0.0169	-0.0261	-0.0355
40.80	-0.0067	-0.0167	-0.0394
41.00	-0.0069	-0.0104	-0.0400

41.20	-0.0195	-0.0066	-0.0407
41.40	-0.0368	-0.0100	-0.0412
41.60	-0.0385	-0.0055	-0.0348
41.80	-0.0365	0.0023	-0.0401
42.00	-0.0314	0.0089	-0.0323
42.20	-0.0229	0.0115	-0.0320
42.40	-0.0250	0.0029	-0.0315
42.60	-0.0237	-0.0070	-0.0321
42.80	-0.0217	-0.0137	-0.0295
43.00	-0.0219	-0.0132	-0.0265
43.20	-0.0250	-0.0204	-0.0277
43.40	-0.0215	-0.0182	-0.0312
43.60	-0.0175	-0.0126	-0.0245
43.80	-0.0197	-0.0110	-0.0208
44.00	-0.0157	-0.0189	-0.0161
44.20	-0.0113	-0.0242	-0.0185
44.40	-0.0120	-0.0267	-0.0133
44.60	-0.0119	-0.0240	-0.0187
44.80	-0.0078	-0.0171	-0.0216
45.00	-0.0064	-0.0090	-0.0231
45.20	0.0028	-0.0057	-0.0256
45.40	0.0059	-0.0073	-0.0278
45.60	0.0092	-0.0028	-0.0223
45.80	0.0108	-0.0017	-0.0216
46.00	0.0102	-0.0083	-0.0243
46.20	0.0069	-0.0045	-0.0271
46.40	0.0009	-0.0093	-0.0244
46.60	-0.0018	-0.0002	-0.0243
46.80	-0.0022	0.0033	-0.0297
47.00	-0.0056	0.0032	-0.0258
47.20	-0.0053	0.0084	-0.0203
47.40	-0.0020	0.0040	-0.0184
47.60	-0.0033	0.0053	-0.0155
47.80	-0.0031	-0.0024	-0.0122
48.00	-0.0031	-0.0043	-0.0107
48.20	-0.0012	-0.0096	-0.0127
48.40	0.0005	-0.0053	-0.0125
48.60	-0.0018	-0.0004	-0.0129
48.80	-0.0039	0.0041	-0.0081
49.00	-0.0087	-0.0010	-0.0122
49.20	-0.0110	-0.0081	-0.0158
49.40	-0.0199	-0.0050	-0.0161
49.60	-0.0271	0.0024	-0.0183
49.80	-0.0316	0.0097	-0.0175
50.00	-0.0380	0.0118	-0.0210
50.20	-0.0394	0.0139	-0.0188
50.40	-0.0385	0.0157	-0.0094
50.60	-0.0384	0.0165	-0.0131
50.80	-0.0350	0.0148	-0.0054
51.00	-0.0227	0.0100	-0.0091
51.20	-0.0152	0.0099	-0.0043
51.40	-0.0086	0.0076	-0.0051
51.60	-0.0034	0.0078	0.0023
51.80	-0.0020	0.0049	-0.0030
52.00	0.0041	0.0076	-0.0007
52.20	0.0020	0.0075	0.0034
52.40	0.0033	0.0050	0.0038

52.60	0.0042	0.0033	0.0082
52.80	0.0037	-0.0028	0.0090
53.00	0.0070	-0.0065	0.0001
53.20	0.0101	-0.0074	0.0031
53.40	0.0149	-0.0040	0.0064
53.60	0.0104	0.0045	0.0014
53.80	0.0099	0.0069	0.0045
54.00	0.0082	0.0054	0.0022
54.20	0.0082	0.0026	-0.0023
54.40	0.0031	-0.0021	-0.0048
54.60	0.0010	-0.0084	-0.0049
54.80	-0.0081	-0.0085	-0.0084
55.00	-0.0104	-0.0097	-0.0104
55.20	-0.0115	-0.0076	-0.0128
55.40	-0.0126	-0.0058	-0.0134
55.60	-0.0135	-0.0073	-0.0137
55.80	-0.0127	-0.0084	-0.0075
56.00	-0.0140	-0.0093	-0.0100
56.20	-0.0173	-0.0041	-0.0021
56.40	-0.0129	-0.0046	-0.0006
56.60	-0.0092	0.0052	-0.0053
56.80	-0.0089	0.0095	-0.0032
57.00	-0.0095	0.0047	-0.0016
57.20	-0.0166	-0.0009	-0.0043
57.40	-0.0196	-0.0072	-0.0035
57.60	-0.0227	-0.0135	-0.0055
57.80	-0.0226	-0.0162	-0.0080
58.00	-0.0199	-0.0127	-0.0027
58.20	-0.0172	-0.0128	-0.0087
58.40	-0.0127	-0.0130	-0.0105
58.60	-0.0099	-0.0117	-0.0080
58.80	-0.0099	-0.0097	-0.0048
59.00	-0.0103	-0.0094	-0.0139
59.20	-0.0104	-0.0086	-0.0145
59.40	-0.0076	-0.0024	-0.0144
59.60	-0.0076	-0.0002	-0.0142
59.80	-0.0059	-0.0021	-0.0126
60.00	-0.0045	-0.0016	-0.0146
60.20	-0.0040	-0.0014	-0.0097
60.40	-0.0069	-0.0046	-0.0150
60.60	-0.0074	-0.0055	-0.0095
60.80	-0.0129	-0.0108	-0.0101
61.00	-0.0160	-0.0131	-0.0188
61.20	-0.0167	-0.0137	-0.0087
61.40	-0.0130	-0.0127	-0.0085
61.60	-0.0151	-0.0124	-0.0126
61.80	-0.0151	-0.0100	-0.0128
62.00	-0.0155	-0.0068	-0.0149
62.20	-0.0129	-0.0064	-0.0162
62.40	-0.0135	-0.0093	-0.0149
62.60	-0.0143	-0.0079	-0.0108
62.80	-0.0151	-0.0106	-0.0117
63.00	-0.0139	-0.0051	-0.0122
63.20	-0.0160	-0.0005	-0.0066
63.40	-0.0204	0.0007	-0.0106
63.60	-0.0211	0.0002	-0.0105
63.80	-0.0199	0.0033	-0.0167

64.00	-0.0189	0.0003	-0.0193
64.20	-0.0185	0.0029	-0.0163
64.40	-0.0196	0.0063	-0.0170
64.60	-0.0190	0.0081	-0.0145
64.80	-0.0187	0.0062	-0.0173
65.00	-0.0198	0.0051	-0.0191
65.20	-0.0193	0.0027	-0.0210
65.40	-0.0185	0.0079	-0.0140
65.60	-0.0168	0.0054	-0.0175
65.80	-0.0187	0.0057	-0.0161
66.00	-0.0186	0.0071	-0.0149
66.20	-0.0198	0.0070	-0.0128
66.40	-0.0184	0.0071	-0.0156
66.60	-0.0229	0.0067	-0.0140
66.80	-0.0228	0.0022	-0.0193
67.00	-0.0234	-0.0003	-0.0200
67.20	-0.0142	0.0002	-0.0233
67.40	-0.0116	-0.0031	-0.0237
67.60	-0.0110	-0.0010	-0.0199
67.80	-0.0143	-0.0050	-0.0199
68.00	-0.0179	-0.0077	-0.0199
68.20	-0.0184	-0.0047	-0.0178
68.40	-0.0171	-0.0078	-0.0212
68.60	-0.0193	-0.0057	-0.0244
68.80	-0.0200	-0.0059	-0.0263
69.00	-0.0179	-0.0039	-0.0282
69.20	-0.0172	-0.0032	-0.0261
69.40	-0.0185	-0.0034	-0.0245
69.60	-0.0170	-0.0063	-0.0257
69.80	-0.0163	-0.0031	-0.0228
70.00	-0.0143	-0.0051	-0.0270